JAN 24 1957

~~CONFIDENTIAL~~

Copy 1
RM SL57A14

NACA

RESEARCH MEMORANDUM

for the

Bureau of Aeronautics, Department of the Navy

INVESTIGATION OF DRAG AND STATIC LONGITUDINAL AND LATERAL STABILITY AND CONTROL CHARACTERISTICS OF 1/20-SCALE MODEL OF McDONNELL F4H-1 AIRPLANE AT MACH NUMBERS OF 1.57, 1.87, 2.16, AND 2.53

PHASE II MODEL

TED NO. NACA AD 3115

CLASSIFICATION CHANGE

To Unclassified

By authority of DH2 Memo dtd 3-22-71 T3/ by H Maines

Changed by M. Rudei Dated 3-24-71

GROUP 3
Downgraded at 12 year intervals; not automatically declassified

By Melvin M. Carmel and Kenneth L. Turner

Langley Aeronautical Laboratory
Langley Field, Va.

[redacted]

NATIONAL ADVISORY COMMITTEE FOR AERONAUTICS

WASHINGTON

JAN 22 1957

21

~~CONFIDENTIAL~~

ENCLOSURE (1)

 [redacted]

NATIONAL ADVISORY COMMITTEE FOR AERONAUTICS

RESEARCH MEMORANDUM

for the

Bureau of Aeronautics, Department of the Navy

INVESTIGATION OF DRAG AND STATIC LONGITUDINAL AND LATERAL STABILITY AND CONTROL CHARACTERISTICS OF 1/20-SCALE MODEL OF McDONNELL F4H-1 AIRPLANE AT MACH NUMBERS OF 1.57, 1.87, 2.16, AND 2.53

PHASE II MODEL

TED NO. NACA AD 3115

By Melvin M. Carmel and Kenneth L. Turner

SUMMARY

Tests were performed in the Langley Unitary Plan wind tunnel to determine the drag and static longitudinal and lateral stability and control characteristics of a 1/20-scale model of the McDonnell F4H-1 airplane at Mach numbers of 1.57, 1.87, 2.16, and 2.53. This is the second phase in a series of tests performed on this model. The Reynolds numbers for these tests, based on the mean aerodynamic chord of the wing, are 1.406×10^6, 1.269×10^6, 1.116×10^6, and 0.714×10^6 at Mach numbers of 1.57, 1.87, 2.16, and 2.53, respectively. The model had a 12° wing tip dihedral, a larger vertical tail, and a modified duct.

INTRODUCTION

At the request of the Bureau of Aeronautics, Department of the Navy, an investigation of the aerodynamic characteristics of a 1/20-scale model of the McDonnell F4H-1 airplane at supersonic speeds has been undertaken by the National Advisory Committee for Aeronautics. This is the second phase in a series of tests being conducted on this model at the Langley

[redacted]

Unitary Plan wind tunnel. Results of the first phase of tests on this model may be found in reference 1. These results indicated that the airplane directional stability would be marginal and the roll characteristics undesirable; therefore, the model was modified to include 12° of wing tip dihedral and a larger vertical fin and rudder. The current model also had a double-compression ramp (5° to 8°) in place of a single-compression 9° ramp. The exterior contour of the duct was also modified; these modifications are shown in figure 1.

This paper contains results obtained at Mach numbers of 1.57, 1.87, 2.16, and 2.53, for angles of attack from -2° to 32°, and for angles of sideslip from -10° to 16°.

COEFFICIENTS AND SYMBOLS

The results of these tests are presented as coefficients of forces and moments referred to the stability-axes system. All aerodynamic moments were taken about the center of gravity which is longitudinally located at 33 percent of the mean aerodynamic chord of the wing and at a station 0.976 inch above the root chord of the wing. Symbols used in this paper are as follows:

b wing span, in.

$\bar{c}$ mean aerodynamic chord of wing, in.

$\bar{c}_t$ mean aerodynamic chord of stabilator, in.

M_a moment area of aileron, cu ft

M_{a_r} moment area of rudder, cu ft

S wing area (theoretical total), sq ft

S_h stabilator area, sq ft

A_b base axial force, lb

A_c chamber axial force, lb

D_i' internal-duct force along X-axis, lb

F_D' force along X stability axis, lb

L	lift, lb
m	pitching moment, in-lb
l	rolling moment, in-lb
n	yawing moment, in-lb
Y	lateral force, lb
N_t	normal force on stabilator, lb
h_L	left aileron hinge moment, ft-lb
h_R	right aileron hinge moment, ft-lb
h_r	rudder hinge moment, ft-lb
h_t	stabilator hinge moment, in-lb
C'_{D_b}	base-drag coefficient, $-\frac{A_b \cos \alpha}{qS}$
C'_{D_c}	chamber-drag coefficient, $-\frac{A_c \cos \alpha}{qS}$
C'_D	drag coefficient, $\frac{F'_D}{qS}$
C'_{D_i}	internal-duct drag coefficient, $\frac{D'_i}{qS}$
ΔC_D	change in drag coefficient due to fixing transition
C_{D_e}	net external drag coefficient
C_L	lift coefficient, L/qS
C_m	pitching-moment coefficient, $m/qS\bar{c}$
C_l	rolling-moment coefficient, l/qSb
C_{n_b}	yawing-moment coefficient, n/qSb

C_Y lateral-force coefficient, Y/qS

C_{N_t} stabilator normal-force coefficient, $\dfrac{N_t}{qS}$

C_{n_β} slope of yawing-moment curve

C_{h_L} left-aileron hinge-moment coefficient, $\dfrac{h_L}{2qM_a}$

C_{h_R} right-aileron hinge-moment coefficient, $\dfrac{h_R}{2qM_a}$

C_{h_r} rudder hinge-moment coefficient, $\dfrac{h_r}{2M_{a_r}q}$

C_{h_t} stabilator hinge-moment coefficient, $\dfrac{h_t}{q\bar{c}_t S_h}$

C_{l_β} slope of rolling-moment curve

P free-stream static pressure, lb/sq ft

M free-stream Mach number

q free-stream dynamic pressure, lb/sq ft $= 0.7PM^2$

α angle of attack of wing chord, deg

β angle of sideslip of fuselage center line, deg

i_t incidence of stabilator, deg

δ_{a_L} left-aileron deflection angle (positive deflection, trailing edge down), deg

δ_{a_R} right-aileron deflection angle (positive deflection, trailing edge down), deg

δ_F flap-deflection angle, deg

δ_r rudder-deflection angle, deg

δ_Z spoiler-deflection angle (left wing only), deg

m_E mass flow at duct exit

m_1 free-stream mass flow based on inlet area

F.S. fuselage station

B.L. body line

W.L. water line

H.L. hinge line

APPARATUS AND METHODS

The tests were conducted in the low Mach number test section of the Langley Unitary Plan wind tunnel. This tunnel is a variable-pressure, continuous, return-flow type. The test section is 4 feet square and approximately 7 feet long. The nozzle leading to the test section is of the asymmetric sliding-block type. Mach numbers may be continuously varied through the range of approximately 1.57 to 2.80 without tunnel shutdown.

Model and Support System

The 1/20-scale steel model was constructed by the McDonnell Aircraft Corporation. A three-view drawing of the model is presented in figure 2. Missiles were attached to the model for all test configurations except those in which the TX-28 store was used, for which configurations they were considered to be fired. The missiles were tested in a retracted position unless otherwise noted. The right aileron was deflected in conjunction with the left spoiler in all cases in which the spoiler-aileron combination was used. Geometric characteristics of the model are presented in table I. Photographs of the configurations tested are presented in figure 3.

The model was attached to the forward end of an enclosed six component electrical strain-gage balance. This balance was connected to the central-support system of the tunnel by means of a sting. The central-support components consisted of a remotely operated adjustable coupling, a variable-offset coupling, and a 5° bent coupling or a 20° bent coupling. The variable-offset coupling and the 20° bent coupling were means of offsetting the model from the tunnel center line in order to obtain increased angle of attack. The 5° coupling was used to offset the model from the center line in order to obtain increased angle of sideslip. The adjustable coupling was used to change the angle of the model in the vertical plane.

Measurements and Accuracy

Pitch tests were made throughout an angle-of-attack range of approximately -2° to 22°. Sideslip tests were made throughout an angle range of approximately -10° to 16° at angles of attack of approximately 0°, 7°, 13°, and 17°, at Mach numbers of 1.57, 1.87, 2.16, and 2.53. In addition, at a Mach number of 1.87, sideslip tests were also made at angles of attack of approximately 21°, 27°, and 32°. All basic model tests were performed with a stabilator incidence of 0°. The angles of attack and sideslip are corrected for deflection of the sting and balance under load, and the angles are estimated to be accurate within $\pm 0.1^{\circ}$. The maximum deviation of local Mach number in the portion of the tunnel occupied by the model is ± 0.015 from the average values given.

The dewpoint, measured at stagnation pressure, was maintained below -30° F and the stagnation temperature was maintained at approximately 125° F.

The stagnation pressure was maintained at approximately 6.5 pounds per square inch absolute except for the sideslip tests at angles of attack of 21°, 27°, and 32°, when it was held at approximately 5.0 pounds per square inch absolute.

The tunnel has not been completely calibrated and any angularity of flow that might exist in the tunnel has not been determined. The pressure gradients in the region of the model have been determined and are sufficiently small so as not to induce any buoyancy effect on the model.

The accuracy of the force and moment coefficients, based on balance calibration and repeatability of data, is estimated to be within the following limits:

C_L	± 0.002
C_D	± 0.001
C_m	± 0.001
C_l	± 0.0002
C_n	± 0.0005
C_Y	± 0.0015
C_{h_r}	± 0.002
C_{h_L}	± 0.010
C_{h_R}	± 0.010
C_{h_t}	± 0.002
C_{N_t}	± 0.002

The drag data have been adjusted to correspond to zero-balance chamber-drag coefficient $\left(C_{D_c}' = 0\right)$. An example of the variation of measured balance chamber-drag coefficients with angle of attack for all test Mach numbers are presented in figure 4 in order to show the magnitude of these coefficients.

Internal-duct drag and choke base-pressure drag were obtained only for one pitch run at each Mach number. The internal drag was obtained from an average total-pressure measurement from four tubes placed 1/8 inch ahead of the choke location which was at the duct exit. Base-pressure drag of the duct was obtained from measurements of the average static pressure on the duct base. The variation of internal-duct drag and duct base-pressure drag coefficients with angle of attack for all test Mach numbers are also presented in figure 4.

In an attempt to assure turbulent flow over the model, a transition strip was fixed around the model nose one inch rearward of the tip and also on the 10-percent chord of the wing (top and bottom, full span). The transition strips were 1/4 inch wide and consisted of no. 60 carborundum grains imbedded in shellac with approximately 15 grains per 1/4 square inch. The results of these tests are presented in figure 5. In order to obtain net external drag, the drag coefficients shown on the characteristic plots must first be increased by the incremental difference in drag coefficient shown in figure 5 at the same model attitude. This resultant drag must then be reduced by the amount of the internal drag and the choke base drag at the same model attitude $\left(C_{D_e} = C_D' + \Delta C_D - C_{D_i}' - C_{D_b}'\right)$.

Figure 6 presents variation of mass flow ratio with angle of attack at the test Mach numbers.

Schlieren photographs were taken of many of the model configurations and attitudes. Typical examples of the schlieren photographs are presented in figure 7. A study of the force results and tunnel geometry in conjunction with the schlieren photographs indicates wall-reflected shock waves striking the model at $\alpha = -2^{\circ}$ and 22° and at $\beta = 16^{\circ}$ at a Mach number of 1.56.

PRESENTATION OF RESULTS

The results of the data obtained are plotted in figures 8 to 22.

Figure

SUMMARY OF RESULTS

The basic results are presented with minimum analysis, and some general observations relative to the data are as follows:

1. The minimum drag coefficients for the complete model with a tail incidence of 0° are 0.040, 0.039, 0.037, and 0.037 at Mach numbers of 1.57, 1.87, 2.16, and 2.53, respectively. These values of drag coefficient are for net external drag with a turbulent boundary layer and are somewhat greater than those obtained for the phase I model.

2. The results indicate positive static directional stability for the complete model configuration in the Mach number and angle-of-attack range tested except at a Mach number of 1.87 for angles of attack of 26.5° and 31.7° where the model becomes directionally unstable. The directional stability, as expected, decreases with Mach number; for a Mach number of 2.53, the directional stability becomes marginal at the highest angles of attack.

3. A comparison of the rolling-moment derivatives for the current model tests with those for the phase I model tests indicates that incorporating a larger vertical tail and a 12° dihedral in the wing tips produced a more negative C_{l_β}. The effective dihedral for the current model, however, is essentially neutral for angles of attack up to 6° in the test Mach number range.

Langley Aeronautical Laboratory,
National Advisory Committee for Aeronautics,
Langley Field, Va., December 18, 1956.

Melvin M. Carmel
Aeronautical Research Engineer

Kenneth L. Turner
Aeronautical Research Engineer

Approved: Herbert A. Wilson, Jr.
Chief of Unitary Plan Wind Tunnel Division

sam

REFERENCE

1. Carmel, Melvin M., and Gregory, Donald T.: Preliminary Investigation of the Static Longitudinal and Lateral Stability Characteristics of a 1/20-Scale Model of the McDonnell F4H-1 Airplane at Mach Numbers of 1.59, 1.89, and 2.09 - TED No. NACA AD 3115. NACA RM SL56C26, Bur. Aero., 1956.

TABLE I.- GEOMETRIC CHARACTERISTICS OF THE McDONNELL F4H-1 MODEL (PHASE II)

[Fuselage station 0.00 is 8.4 inches rearward of nose (full scale)]

Model scale, percent	5
Center-of-gravity location, percent of mean aerodynamic chord	33
Wing:	
Loading (combat), lb/sq ft	65
Area, sq ft:	
Exposed	0.886
Theoretical	1.325
Span, in.	23.2
Aspect ratio	2.821
Taper ratio	0.167
Sweep angle of quarter-chord line, deg	45
Dihedral, deg	0 inboard, 12 at tip
Incidence, deg	1
Geometric twist, deg	0
Airfoil:	
Root	NACA 0006.4-65 (modified)
Body line 160 (full scale)	NACA 0004.0-64 (modified)
Tip	NACA 0003.0-64 (modified)
Root chord, in.	14.10
Tip chord, in.	2.35
Root-chord location:	
Longitudinal (leading edge)	Fuselage station 7.518
Vertical	Water line 0.574
Mean aerodynamic chord, in.	9.63
Mean-aerodynamic-chord location:	
Longitudinal (leading edge)	Fuselage station 13.054
Lateral	Body line 4.42
Fuselage:	
Length, in.	33.60
Width (maximum), in.	3.375
Depth (maximum), in.	3.730
Overall fineness ratio	8.40
Base area	None
Horizontal tail:	
Area (theoretical), sq ft	0.237
Span, in.	10.626
Aspect ratio	3.310
Taper ratio	0.200
Root chord, in.	5.35
Tip chord, in.	1.07
Mean aerodynamic chord, in.	3.686
Mean-aerodynamic-chord location:	
Longitudinal (leading edge)	Fuselage station 29.16
Lateral	Body line 2.065
Tail length (distance from quarter-chord point of mean aerodynamic chord of wing to quarter-chord point of mean aerodynamic chord of horizontal tail), in.	14.619
Sweep angle of quarter-chord line, deg	35.5
Dihedral, deg	-15
Geometric twist, deg	0
Airfoil:	
Root	NACA 0003.7-64 (modified)
Tip	NACA 0003.0-64 (modified)
Vertical tail:	
Area (theoretical), sq ft	0.197
Span, in.	3.825
Aspect ratio	0.5976
Root-chord length, in.	10.35
Tip-chord length, in.	2.355
Mean aerodynamic chord, in.	7.192
Mean-aerodynamic-chord location:	
Longitudinal (leading edge)	Fuselage station 26.11
Vertical (leading edge)	Water line 4.836
Tail length (distance from quarter-chord point of mean aerodynamic chord of wing to quarter-chord point of mean aerodynamic chord of vertical tail), in.	11.507
Airfoil:	
Root	NACA 0003.2-64 (modified)
Tip	NACA 0002.5-64 (modified)
Duct with double compression ramp (5° to 8°):	
Capture area, sq ft/side	0.011944
Exit, sq ft/side	0.007906

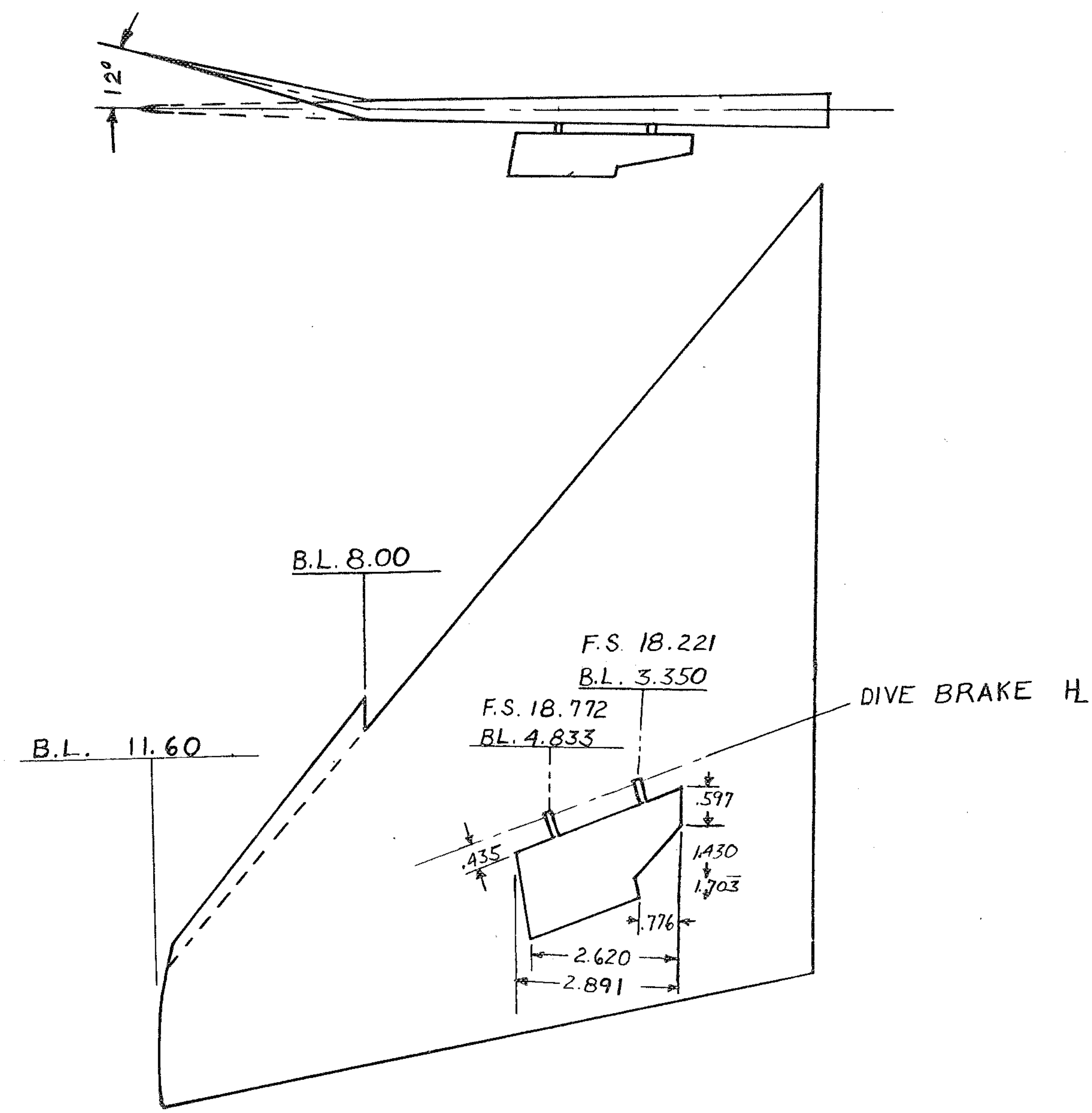

(a) Wing.

Figure 1.- Modifications to model after phase I tests. (Dotted lines indicate phase I model.)

[redacted]

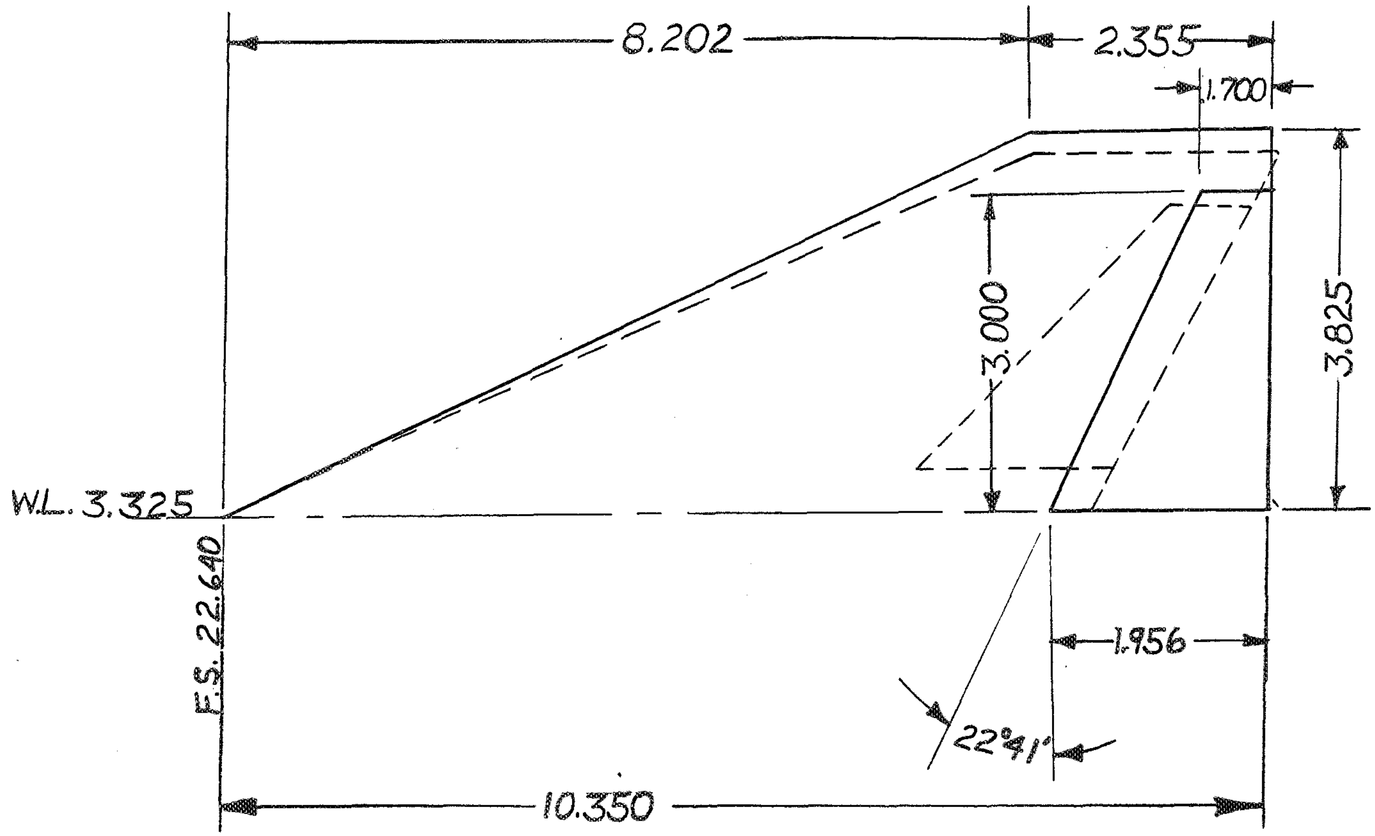

(b) Vertical tail.

Figure 1.- Continued.

[redacted]

~~CONFIDENTIAL~~

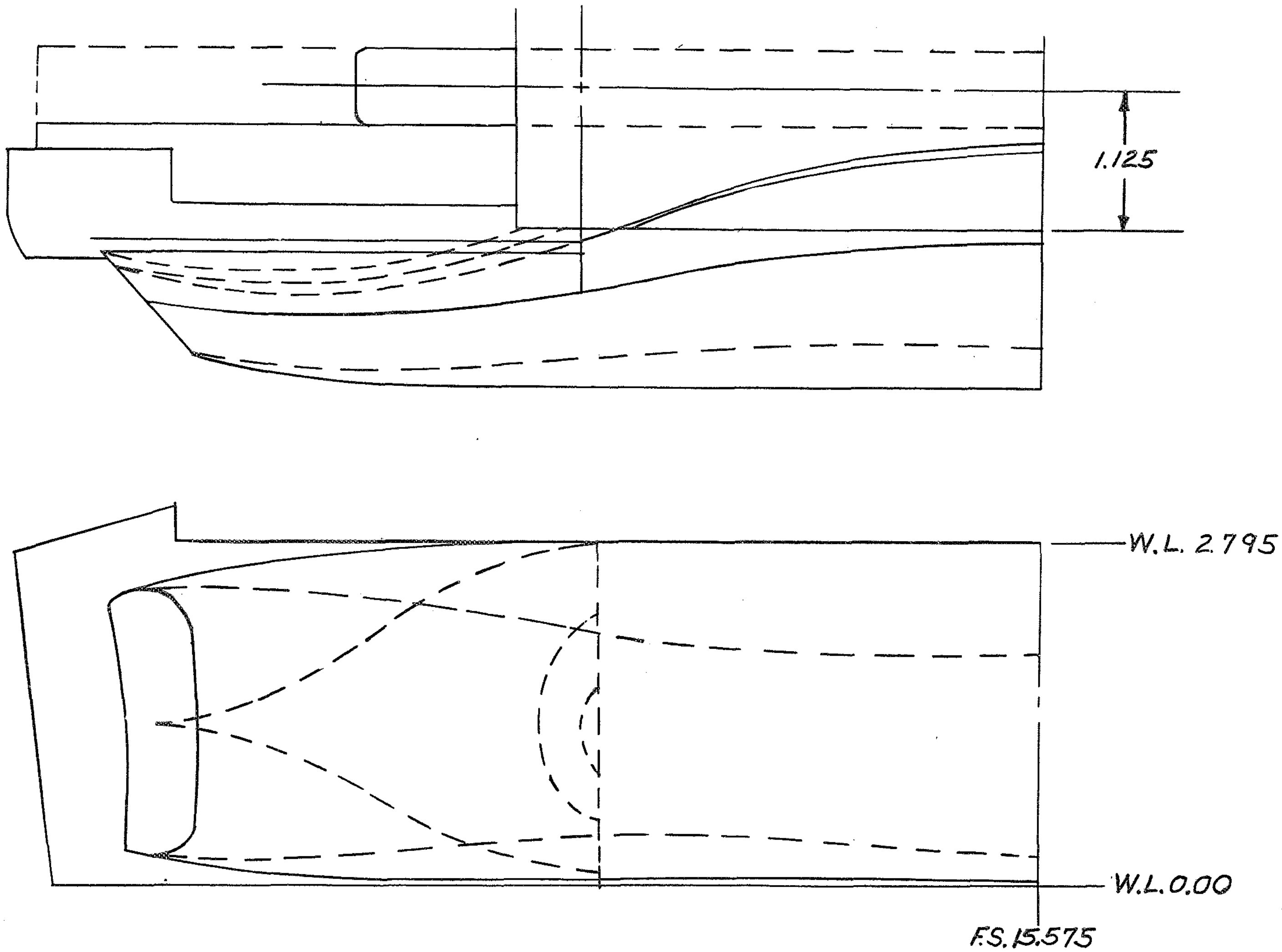

(c) Duct for phase I tests.

Figure 1.- Continued.

~~CONFIDENTIAL~~

[redacted]

~~CONFIDENTIAL~~

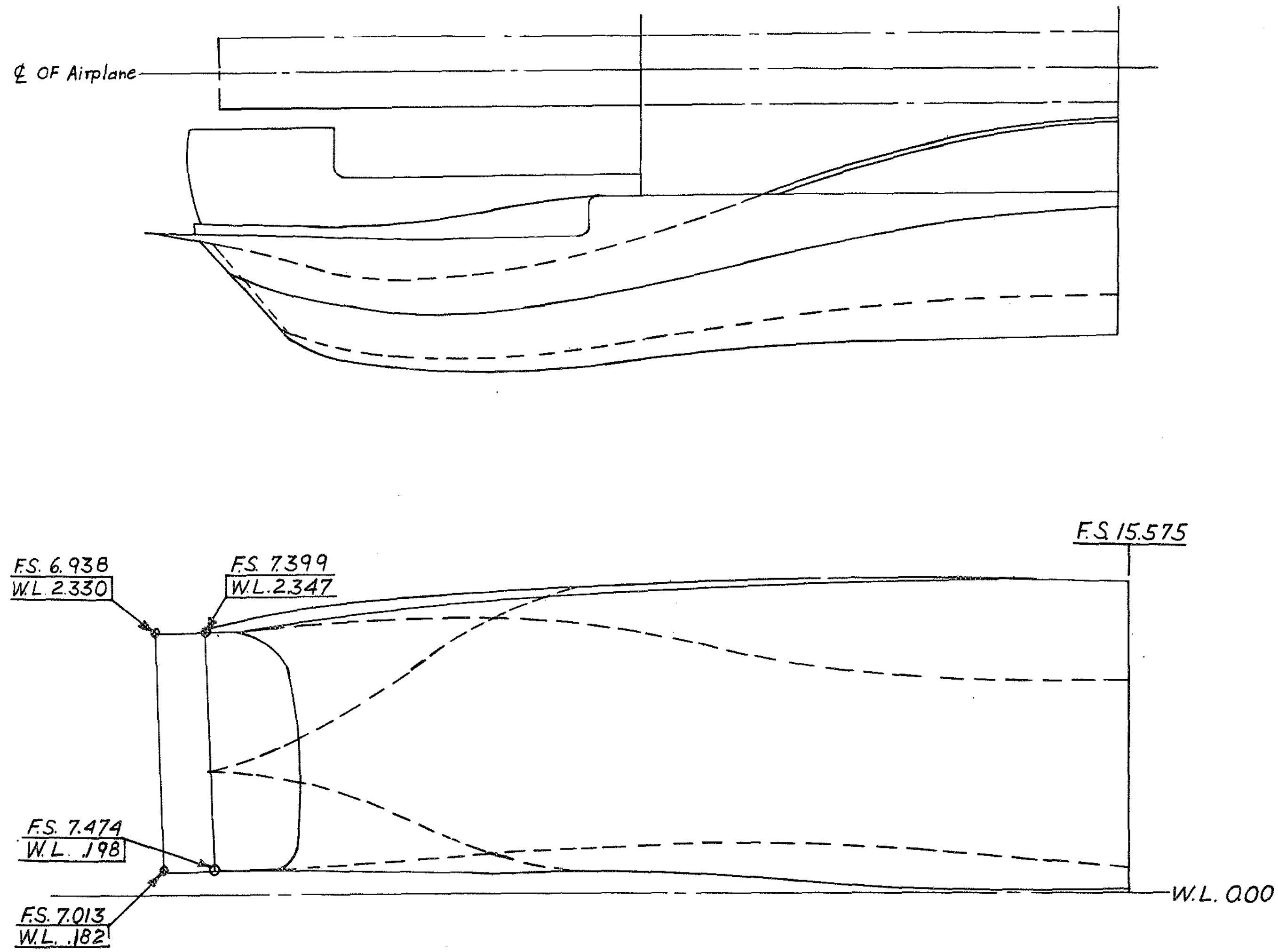

(d) Duct for phase II tests.

Figure 1.- Concluded.

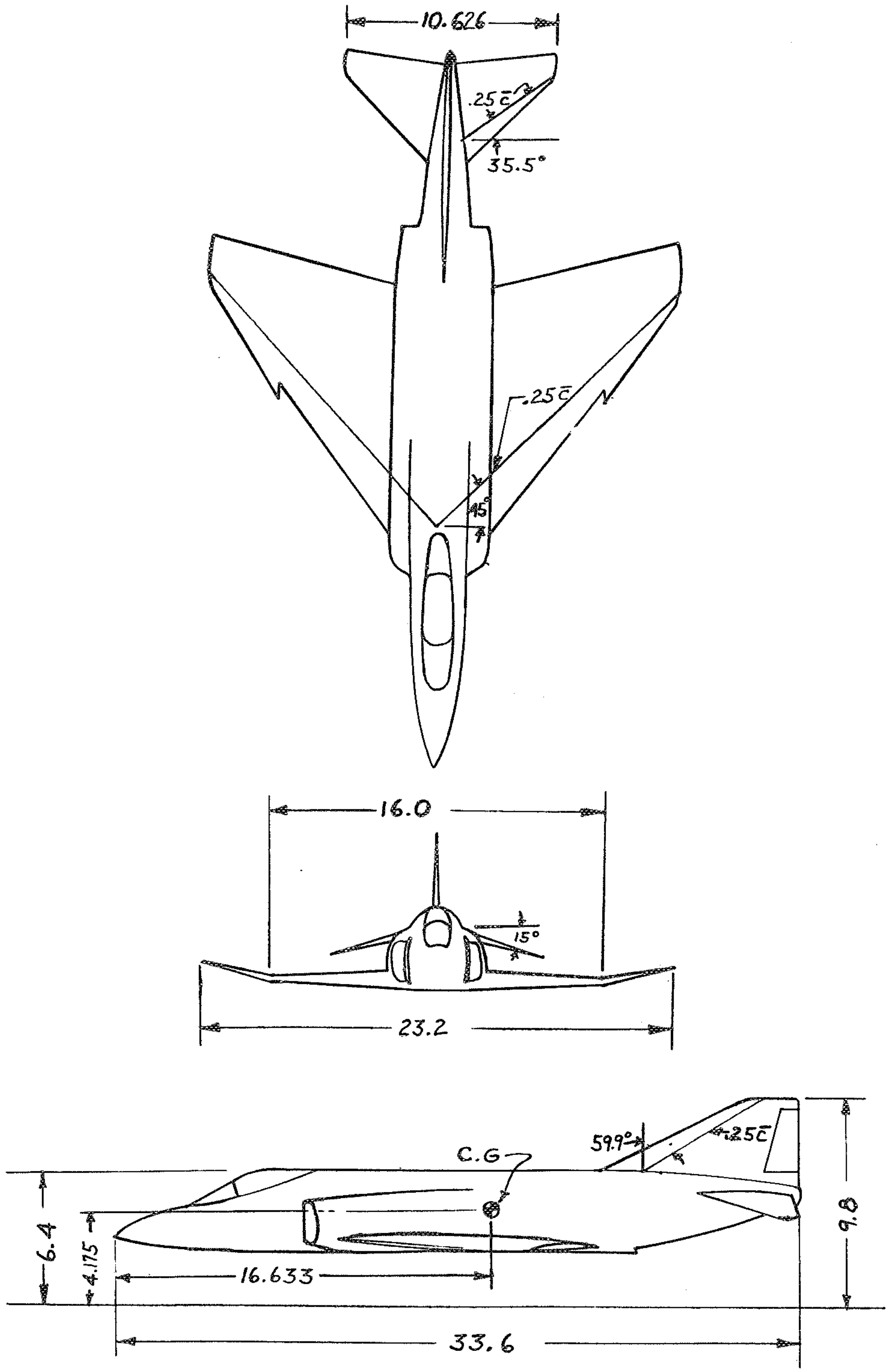

(a) Three-view drawing.

Figure 2.- 1/20-scale model of McDonnell F4H-1 airplane. All dimensions are in inches.

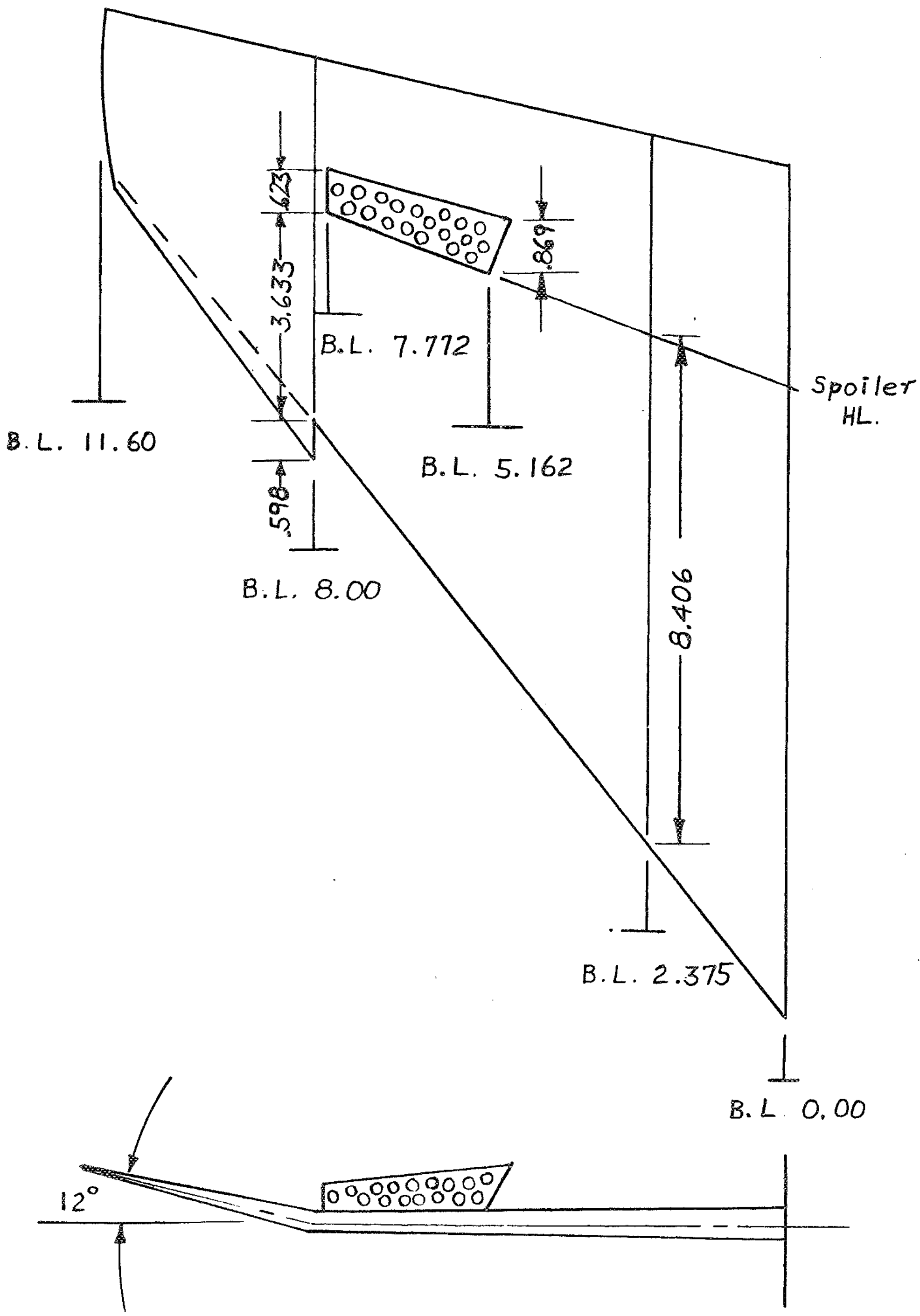

(b) Detail of spoiler (20-percent porosity).

Figure 2.- Concluded.

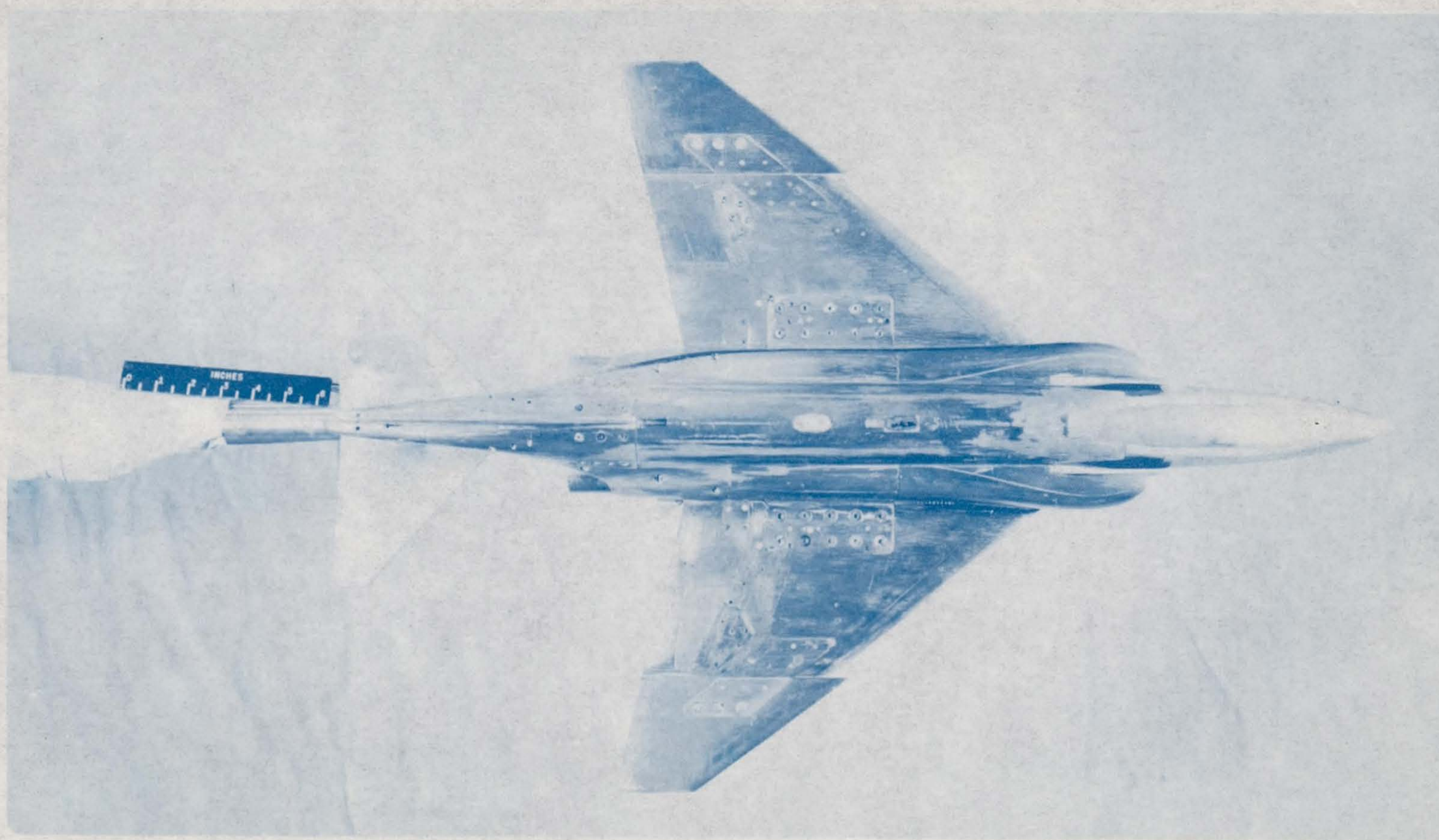

(a) Top view. L-94907

Figure 3.- Photographs of 1/20-scale model of McDonnell F4H-1 airplane.

[redacted]

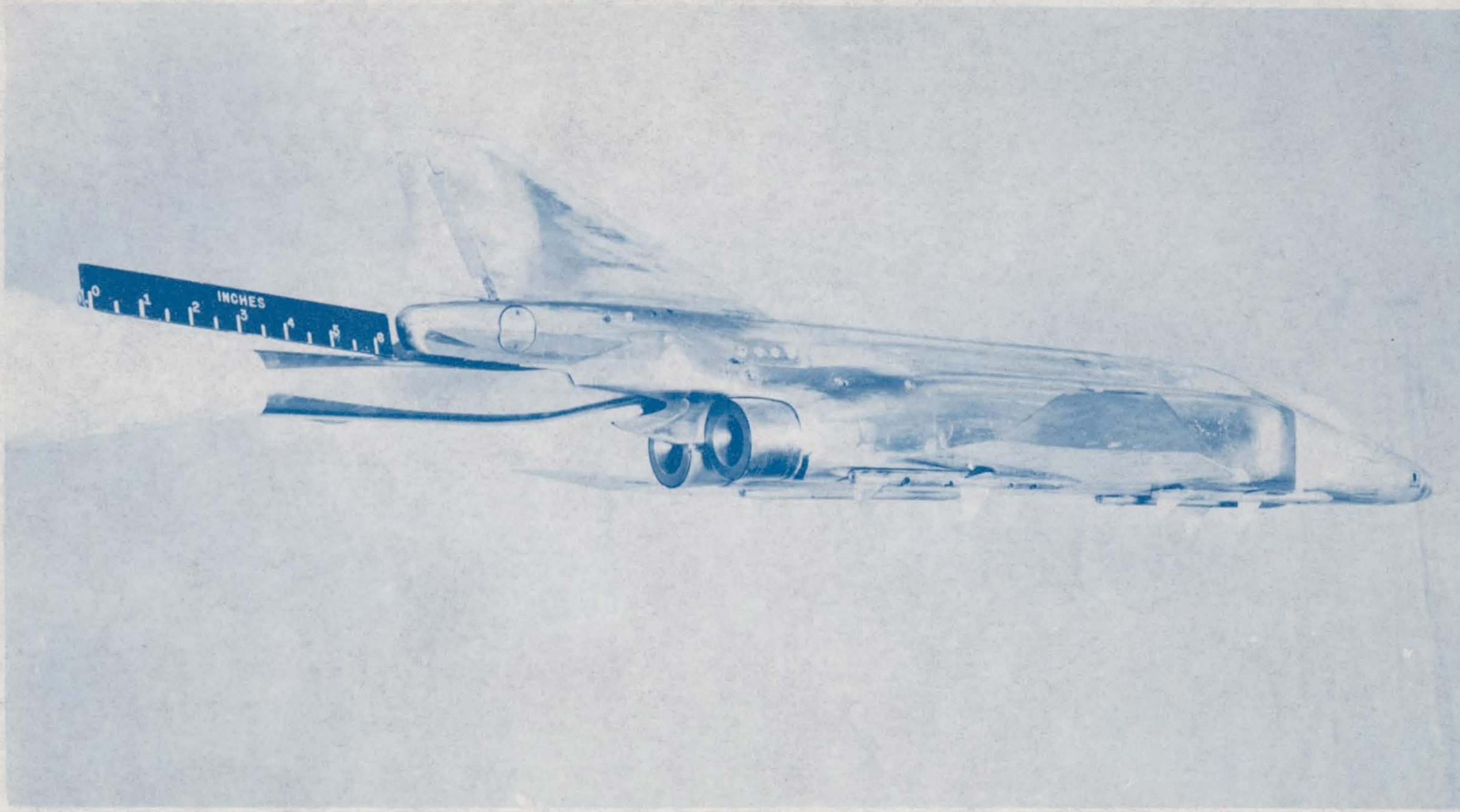

(b) Three-quarter rear view. L-94899

Figure 3.- Continued.

[redacted]

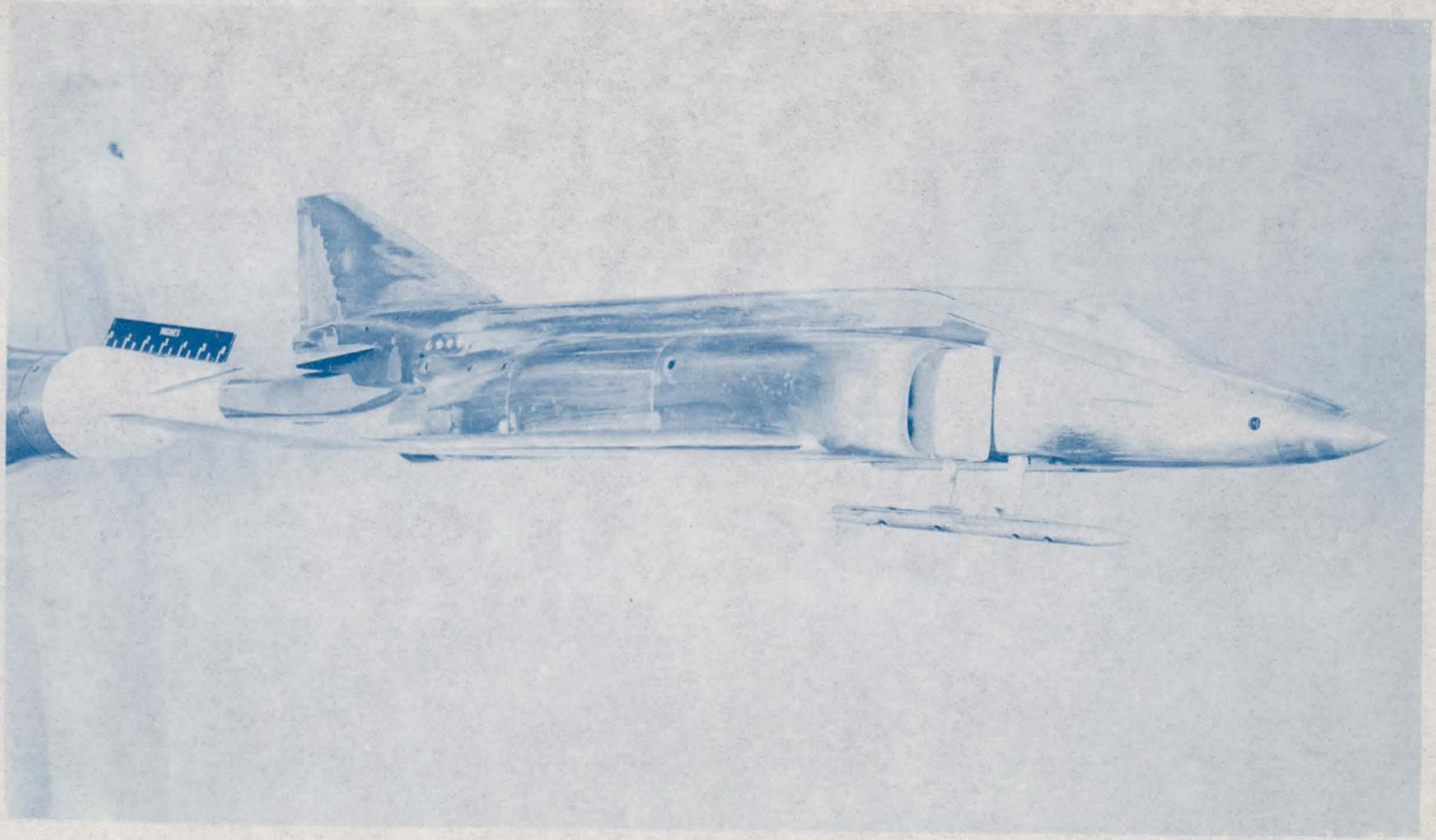

L-94905

(c) Three-quarter front view with forward missile extended.

Figure 3.- Continued.

[redacted]

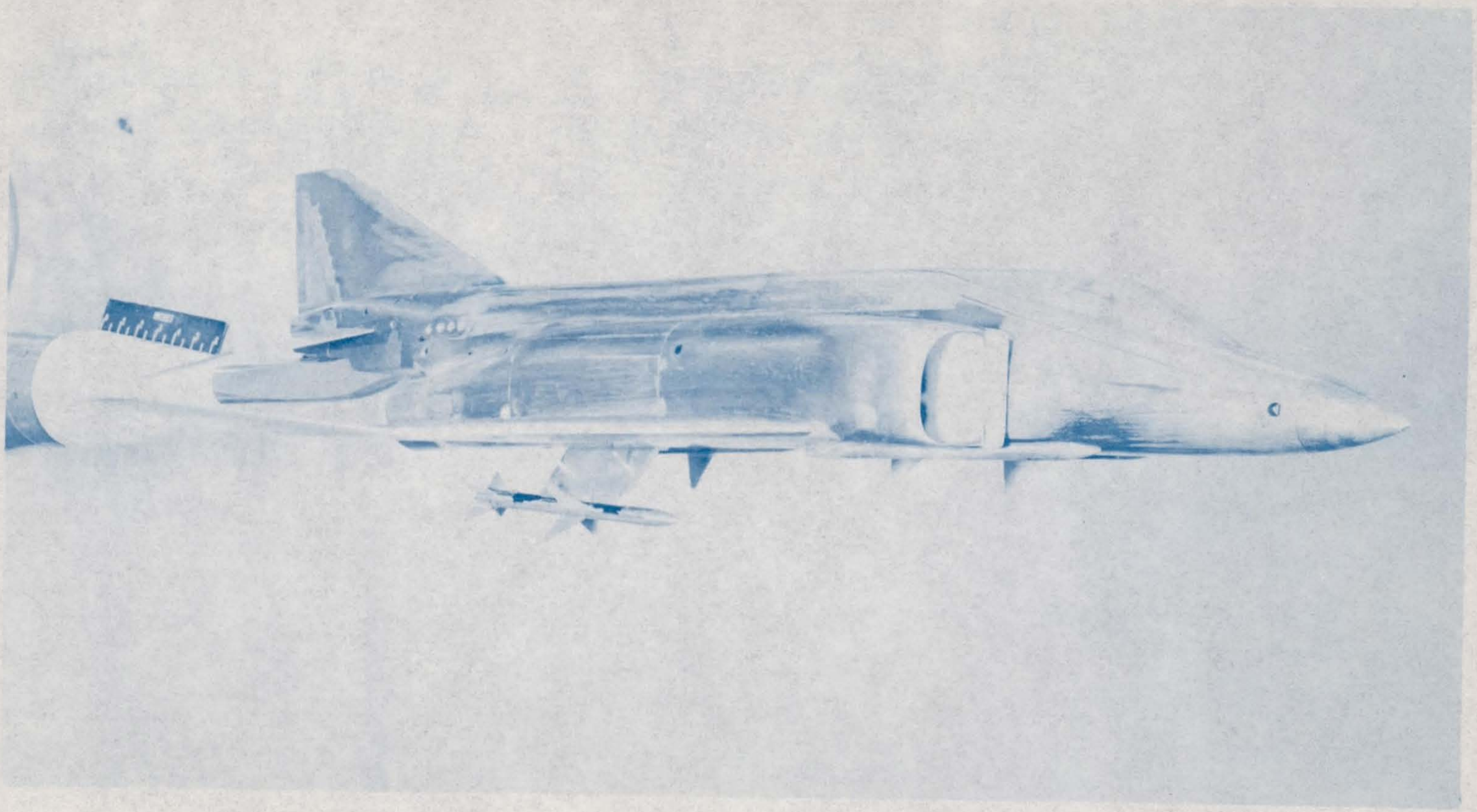

(d) Three-quarter front view with rear missile extended. L-94901

Figure 3.- Continued.

[redacted]

~~CONFIDENTIAL~~

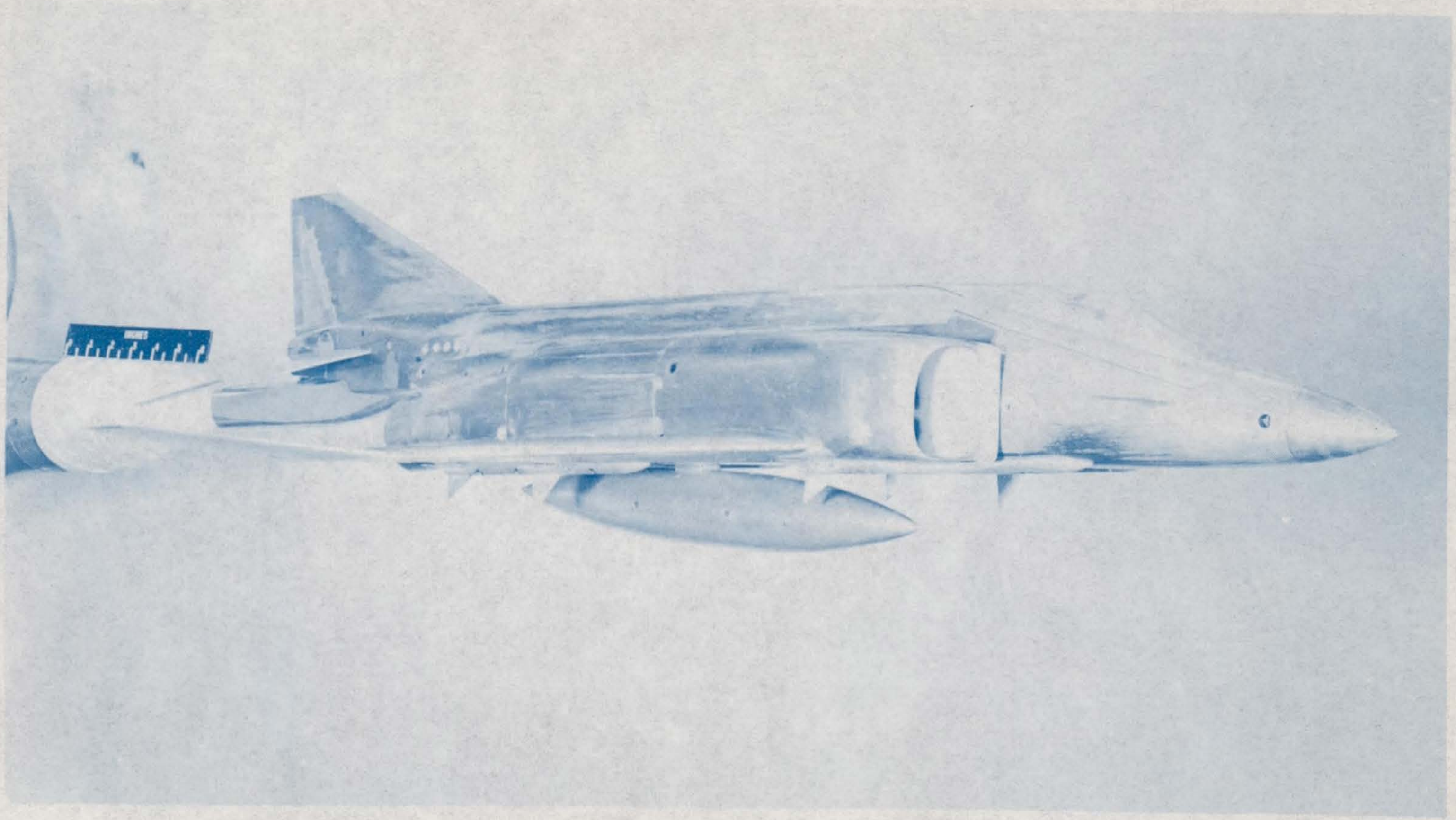

(e) Three-quarter front view with center-line tank. L-94902

Figure 3.- Continued.

~~CONFIDENTIAL~~

~~CONFIDENTIAL~~

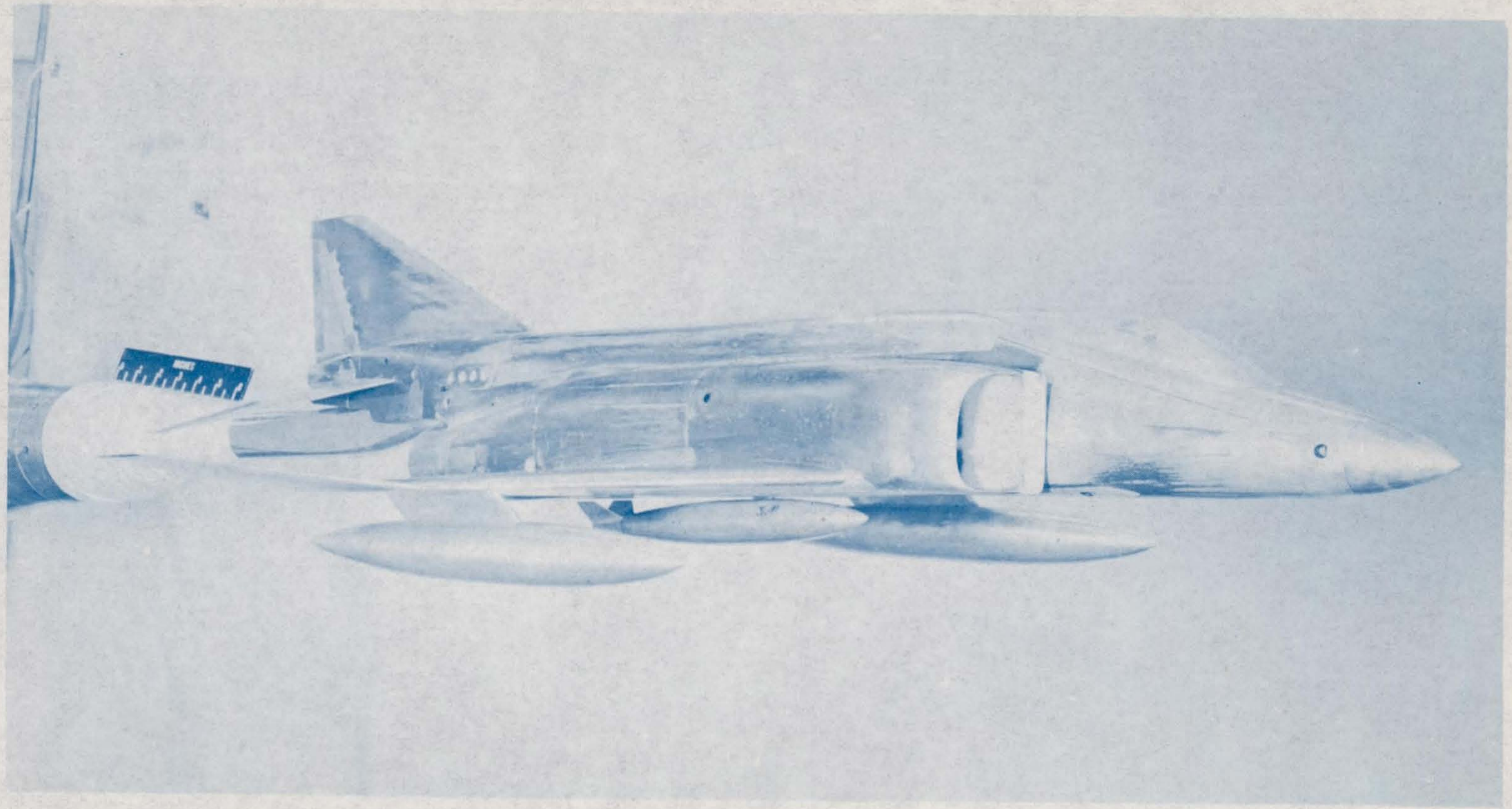

L-94906

(f) Three-quarter front view with wing tanks and TX-28 store.

Figure 3.- Continued.

~~CONFIDENTIAL~~

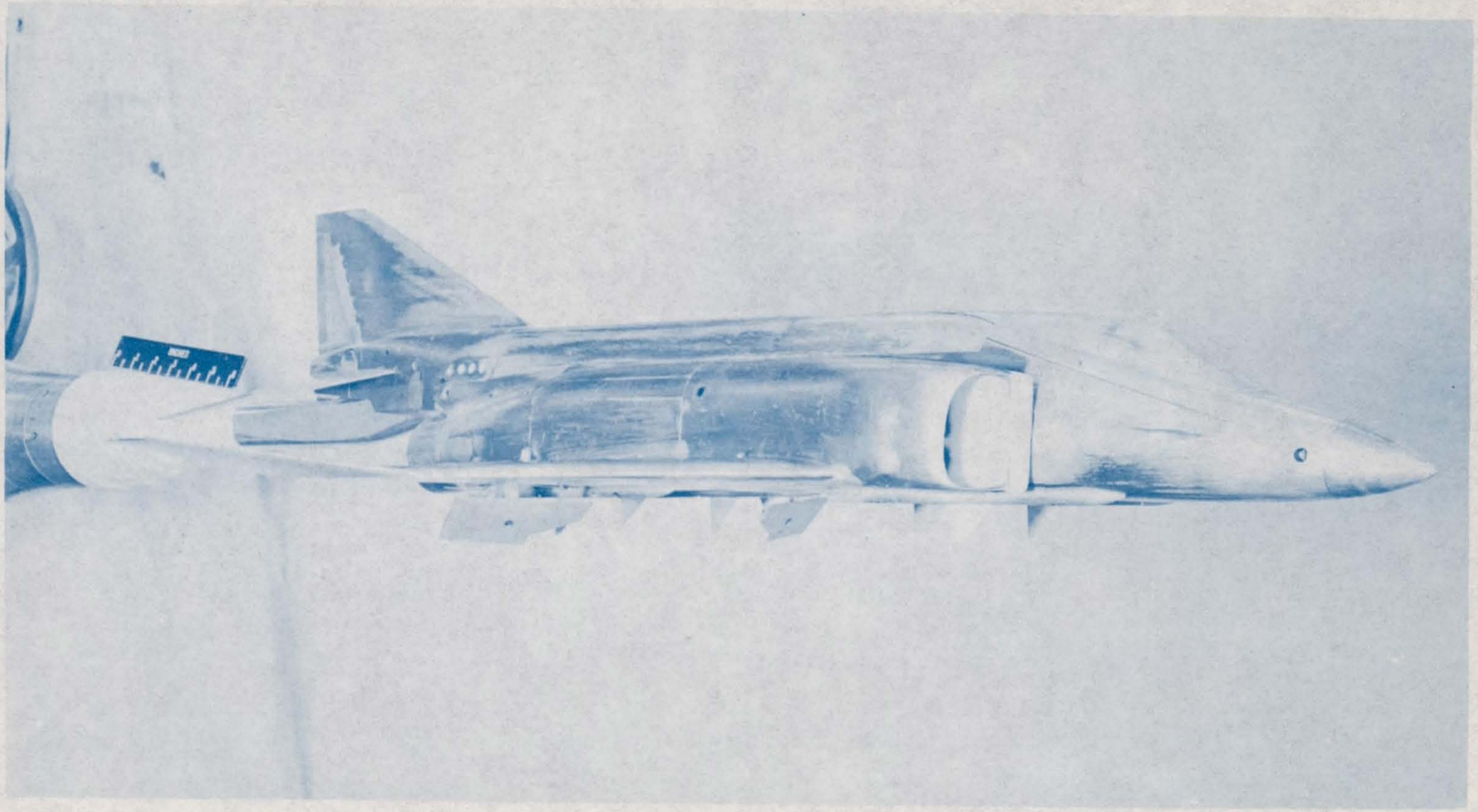

(g) Three-quarter front view with flaps deflected. L-94900

Figure 3.- Concluded.

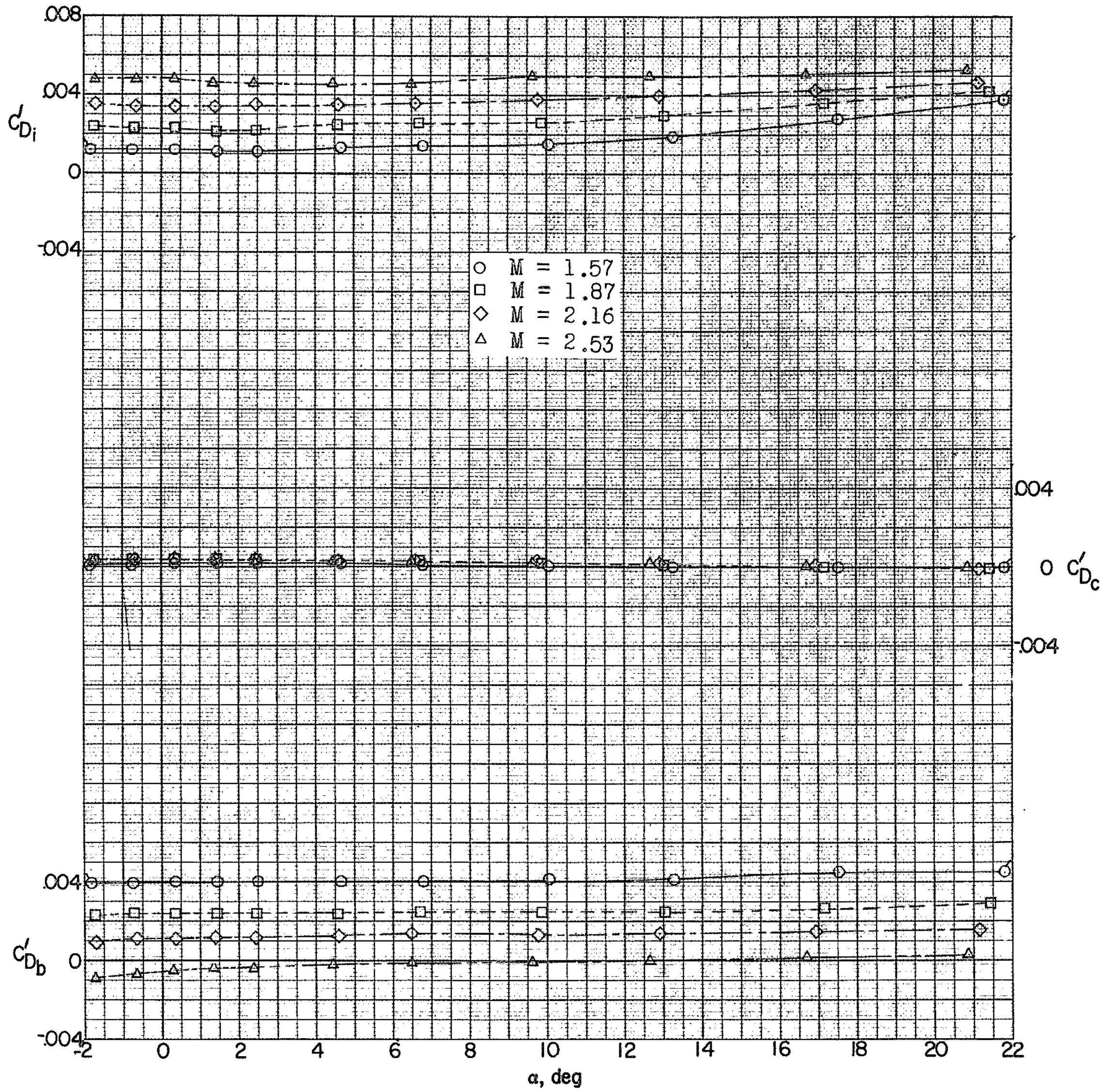

Figure 4.- Variation of internal-, chamber-, and base-drag coefficients with angle of attack. (Flagged symbols denote wall-reflected shock waves striking the tail.)

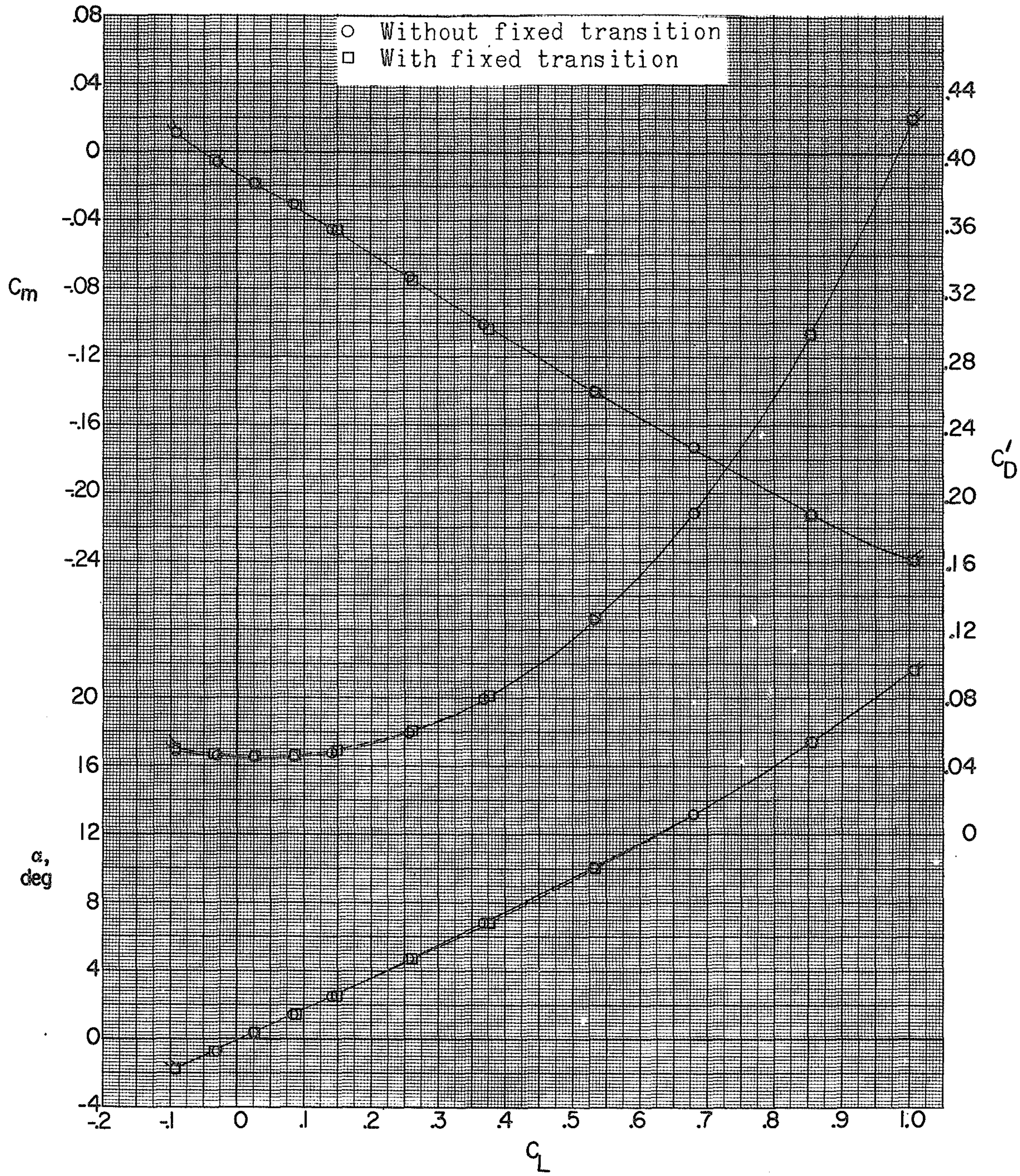

(a) M = 1.57.

Figure 5.- Effect of fixed transition on aerodynamic characteristics in pitch. (Flagged symbols denote wall-reflected shock waves striking the tail.)

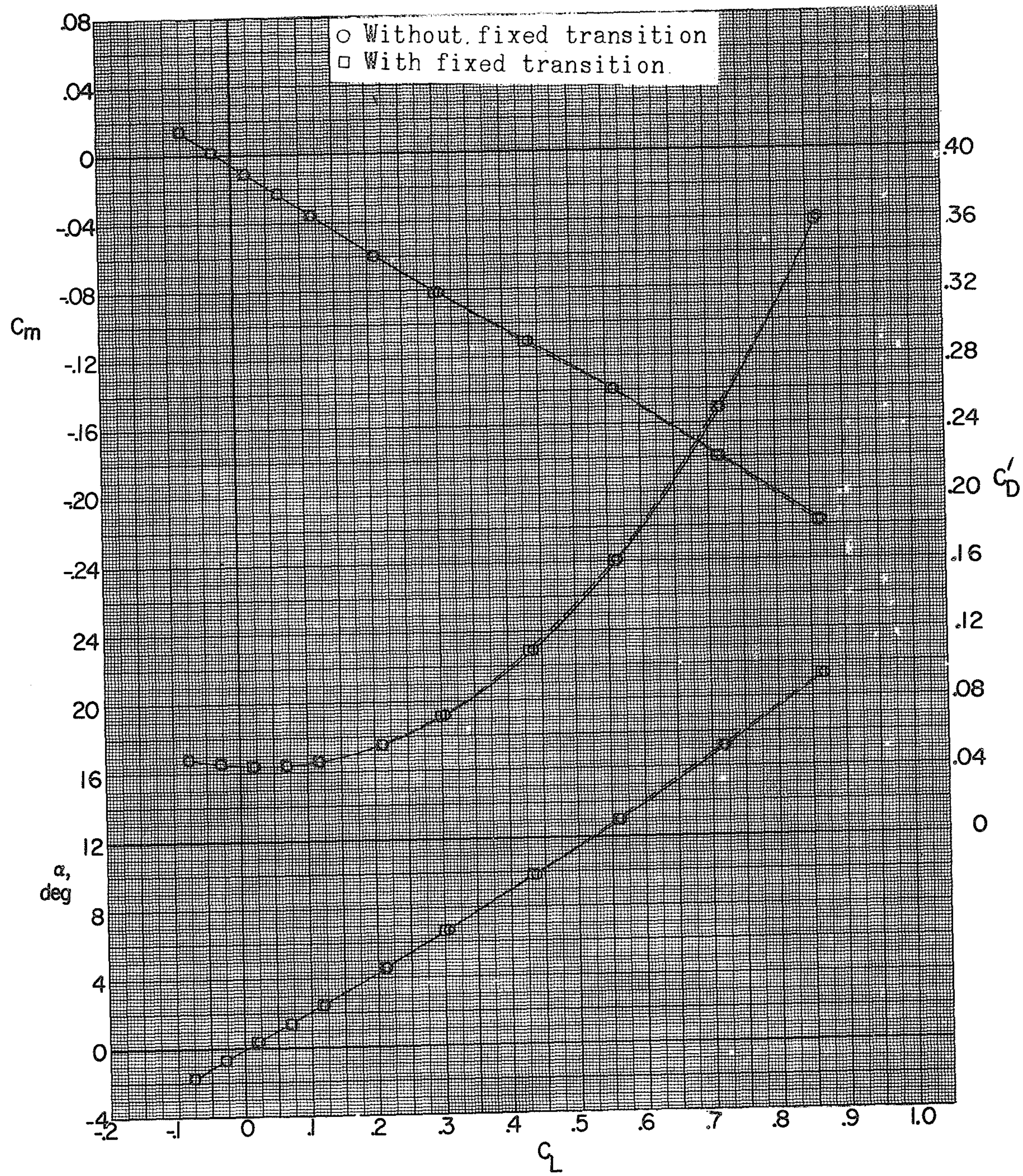

(b) M = 1.87.

Figure 5.- Continued.

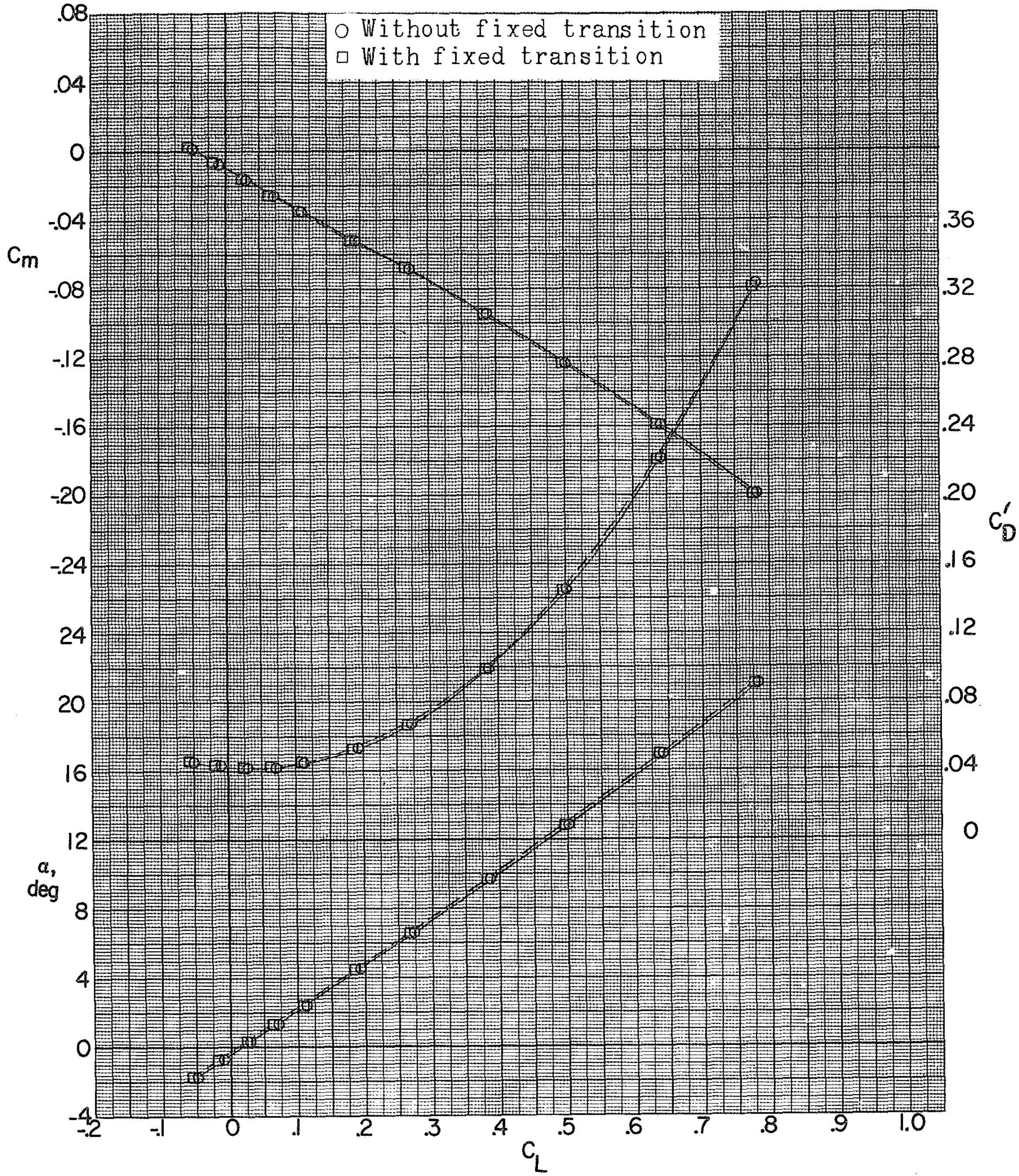

(c) M = 2.16.

Figure 5.- Continued.

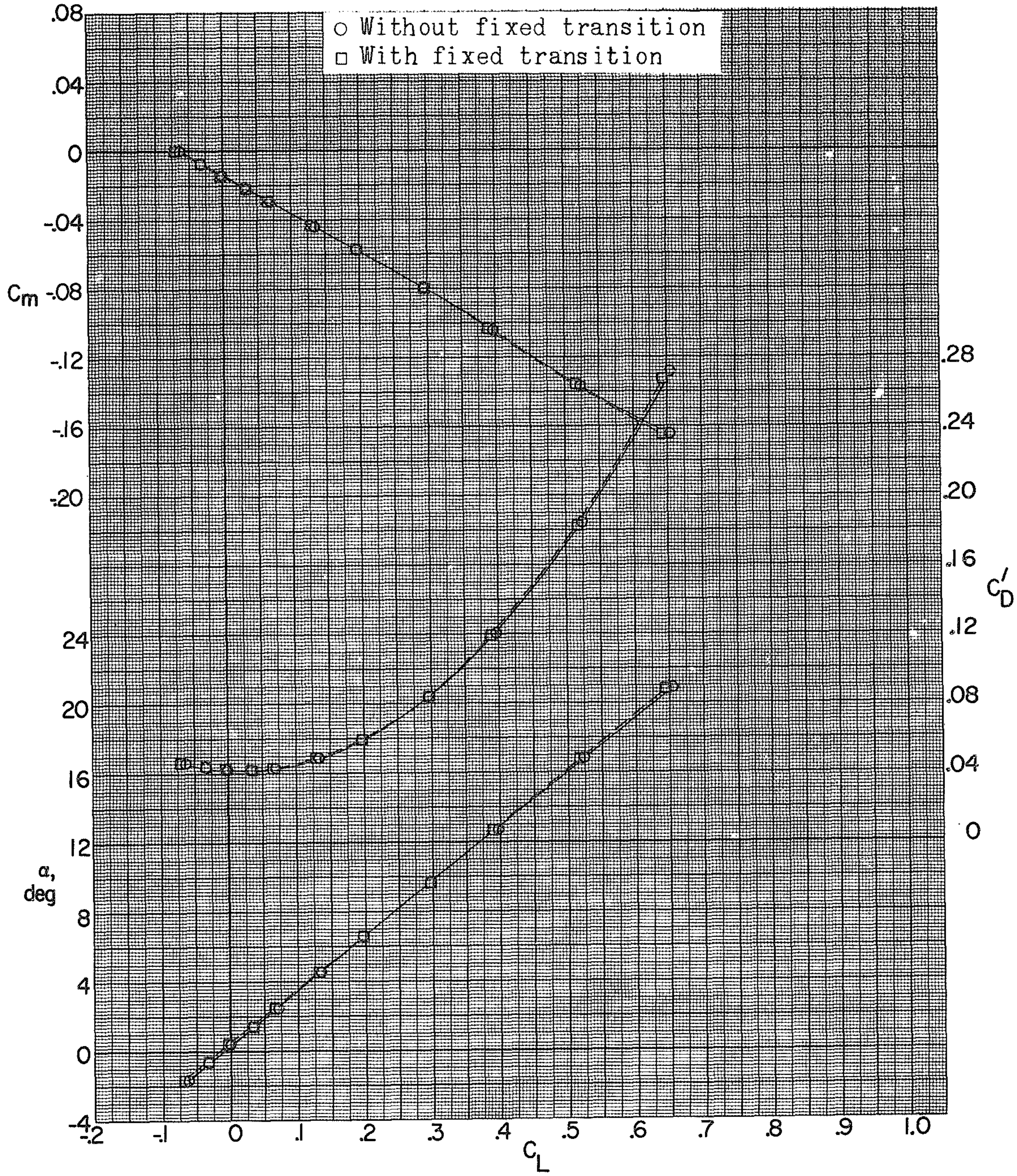

(d) M = 2.53.

Figure 5.- Concluded.

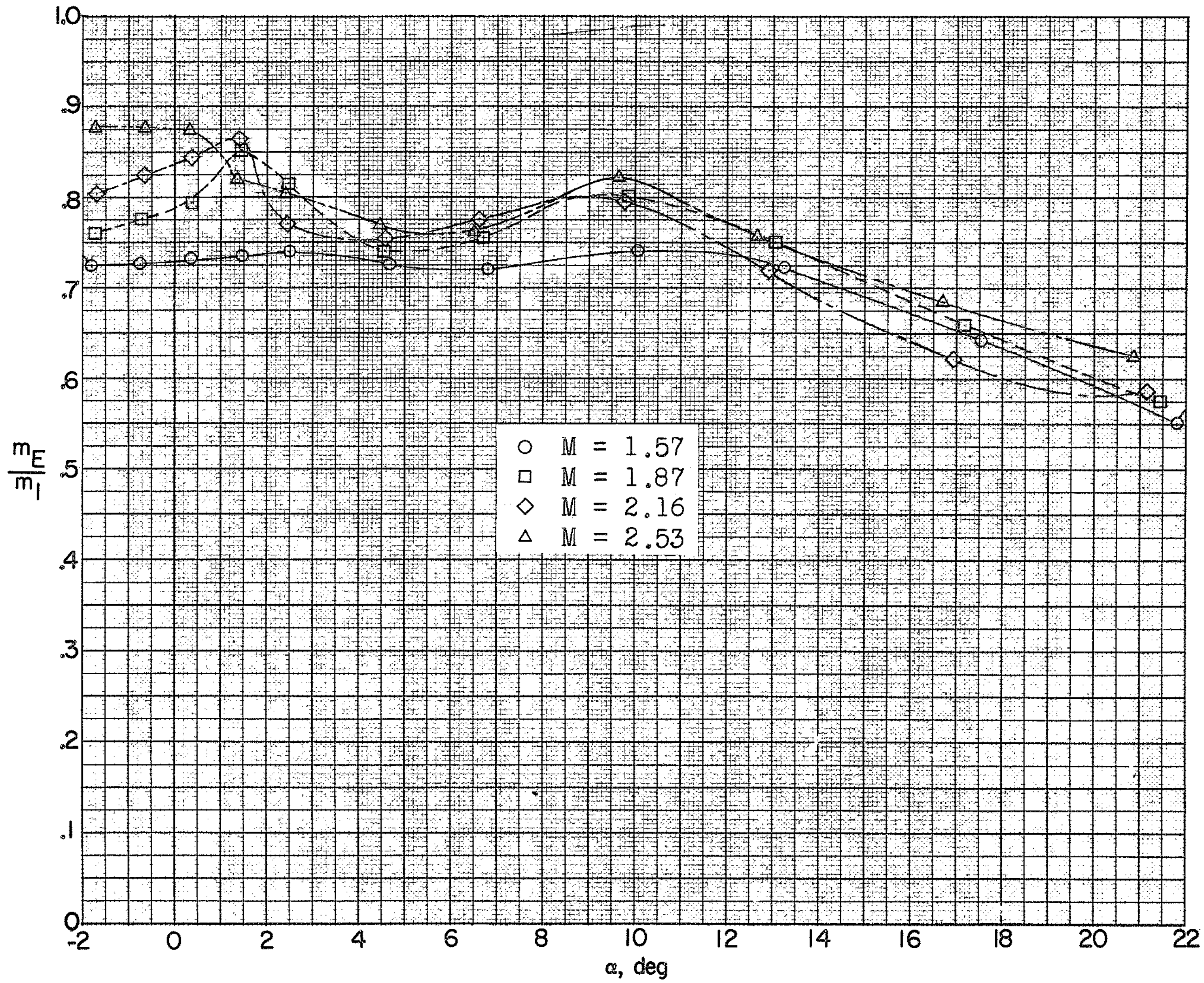

Figure 6.- Variation of mass-flow ratio with angle of attack. (Flagged symbols denote wall-reflected shock waves striking the tail.)

[redacted]

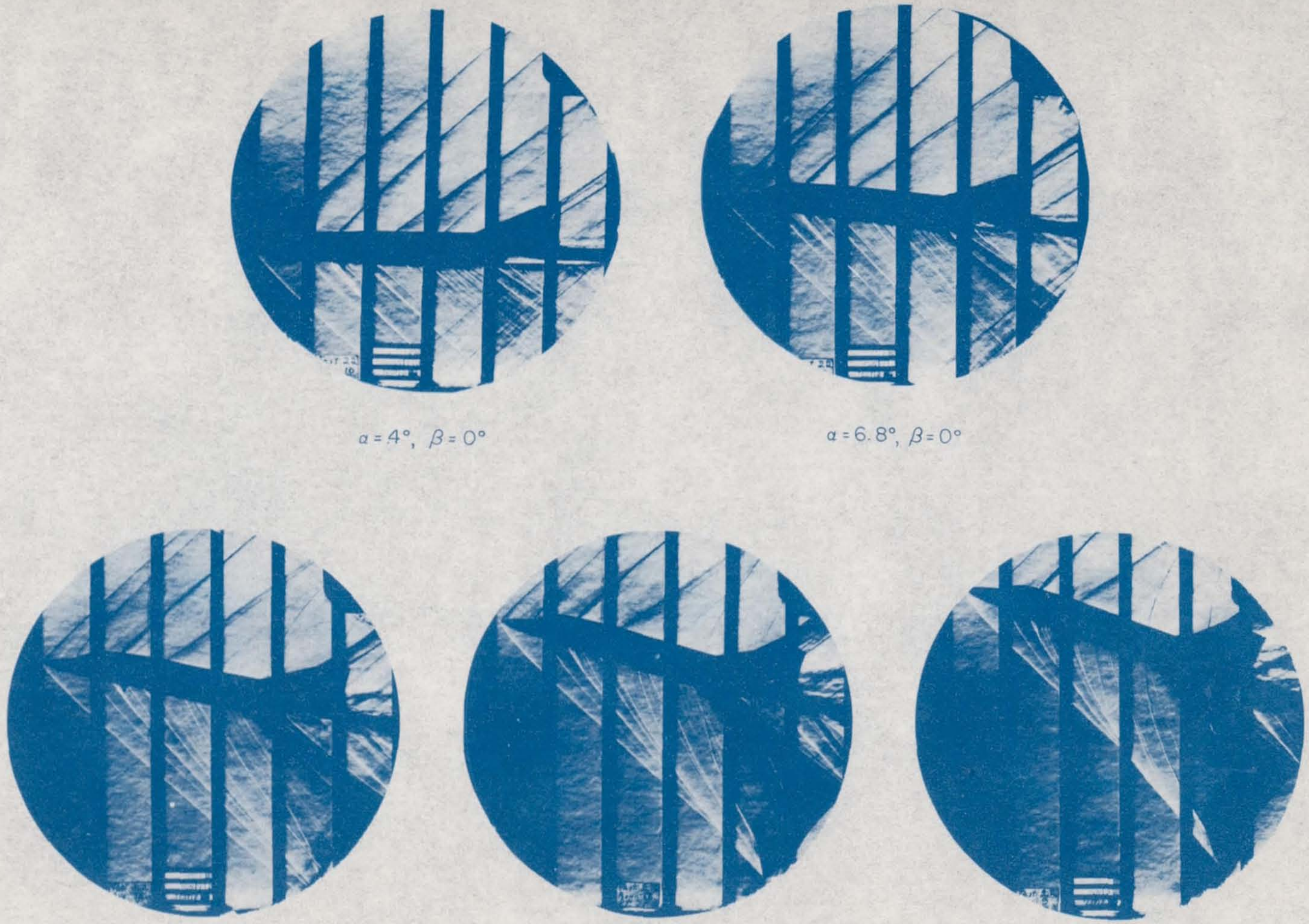

(a) Basic model; M = 1.57.

L-57-108

Figure 7.- Typical schlieren photographs of the 1/20-scale model of McDonnell F4H-1 airplane. Phase II.

[redacted]

~~CONFIDENTIAL~~

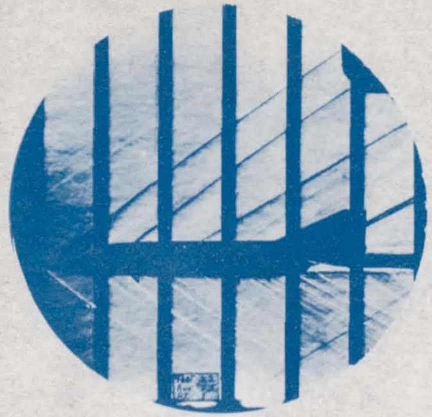

$\alpha = 4°, \beta = 0°$

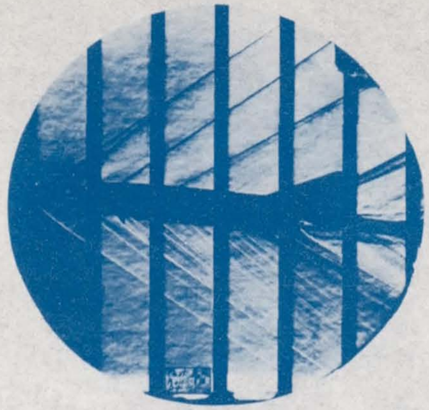

$\alpha = 6.6°, \beta = 0°$

$\alpha = 17.1°, \beta = 0°$

$\alpha = 21.3°, \beta = 0°$

$\alpha = 25.5°, \beta = 0°$

$\alpha = 31.7°, \beta = 0°$

(b) Basic model; M = 1.87. L-57-109

Figure 7.- Continued.

~~CONFIDENTIAL~~

[redacted]

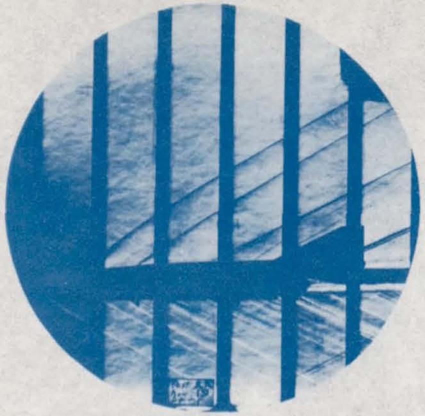

$\alpha = -1.71^\circ$, $\beta = 0^\circ$

$\alpha = .3^\circ$, $\beta = 0^\circ$

$\alpha = 6.5^\circ$, $\beta = 0^\circ$

$\alpha = 12.7^\circ$, $\beta = 0^\circ$

$\alpha = 16.9^\circ$, $\beta = 0^\circ$

$\alpha = 21.14^\circ$, $\beta = 0^\circ$

(c) Basic model; M = 2.16.

L-57-110

Figure 7.- Continued.

$\alpha = -1.7°, \beta = 0°$

$\alpha = .3°, \beta = 0°$

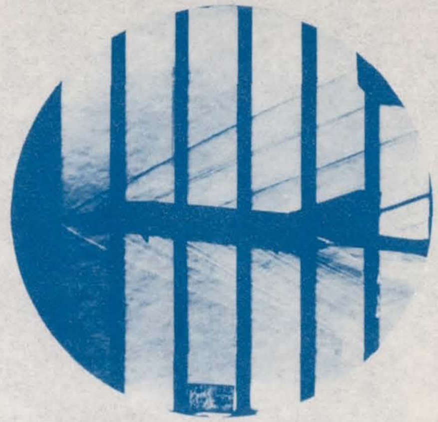

$\alpha = 6.4°, \beta = 0°$

$\alpha = 12.0°, \beta = 0°$

$\alpha = 16.7°, \beta = 0°$

$\alpha = 20.86°, \beta = 0°$

(d) Basic model; M = 2.53. L-57-111

Figure 7.- Continued.

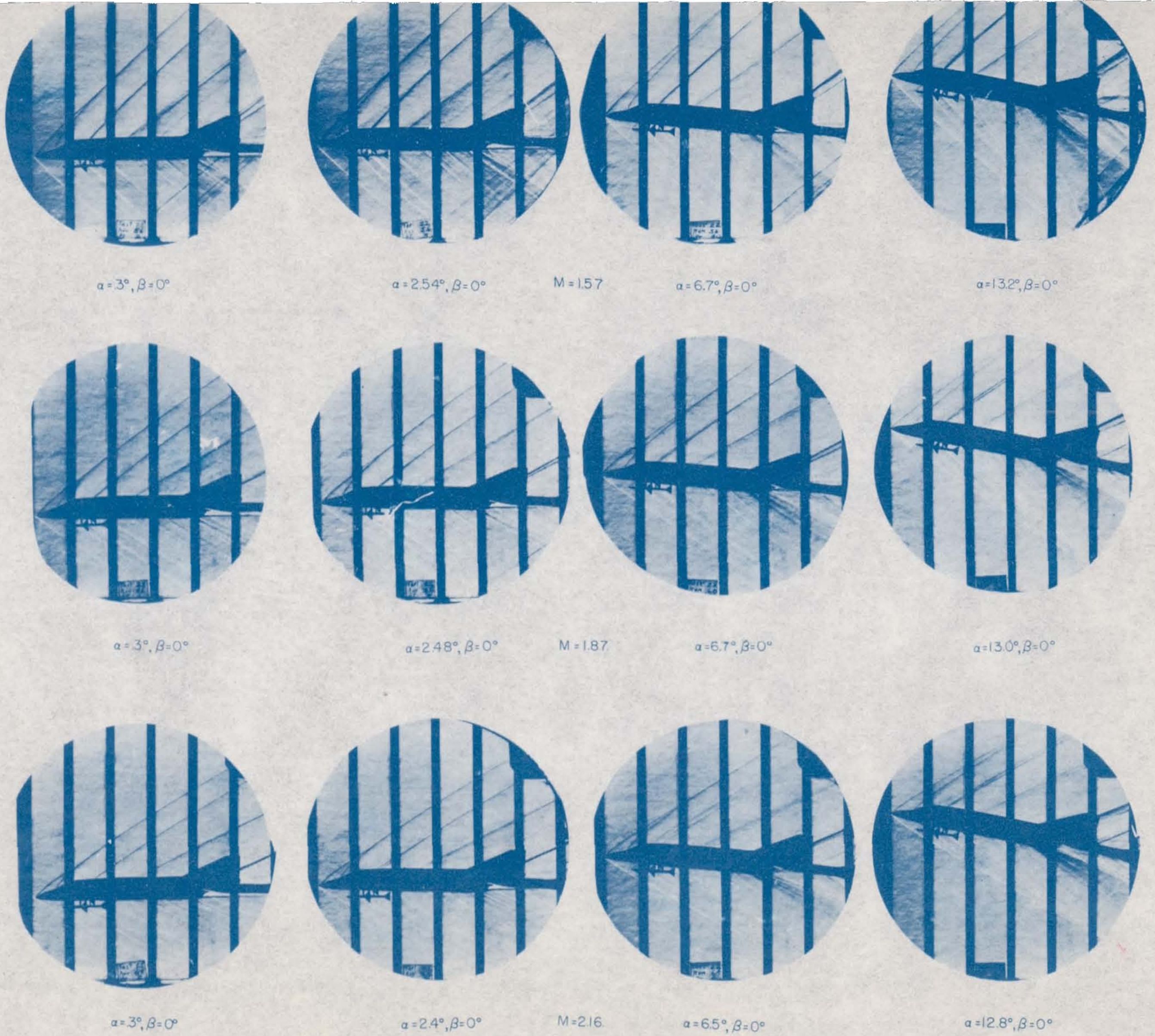

(e) Forward missile extended. L-57-112

Figure 7.- Concluded.

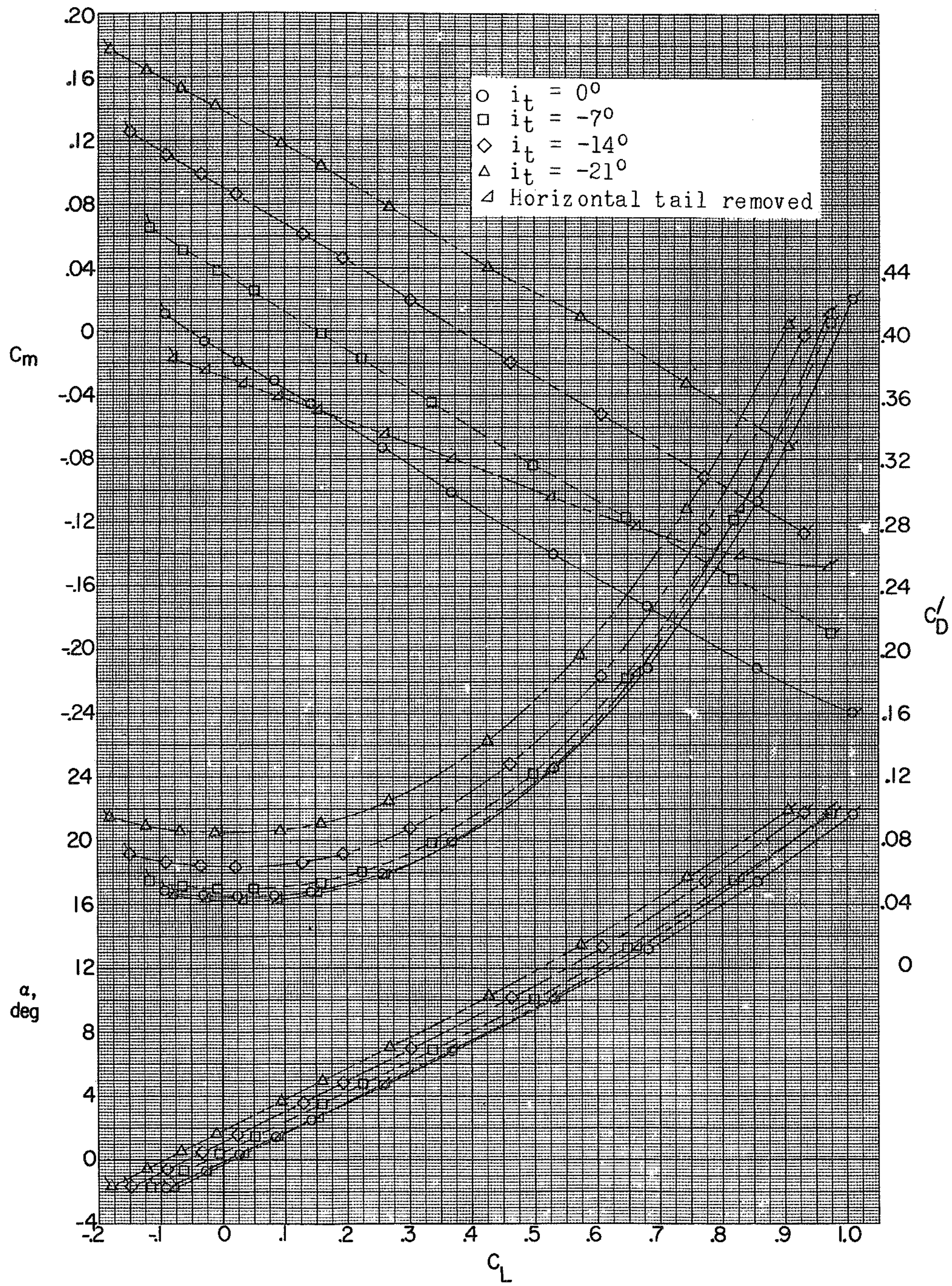

(a) M = 1.57.

Figure 8.- Effect of horizontal tail on aerodynamic characteristics in pitch. (Flagged symbols denote wall-reflected shock waves striking the tail.)

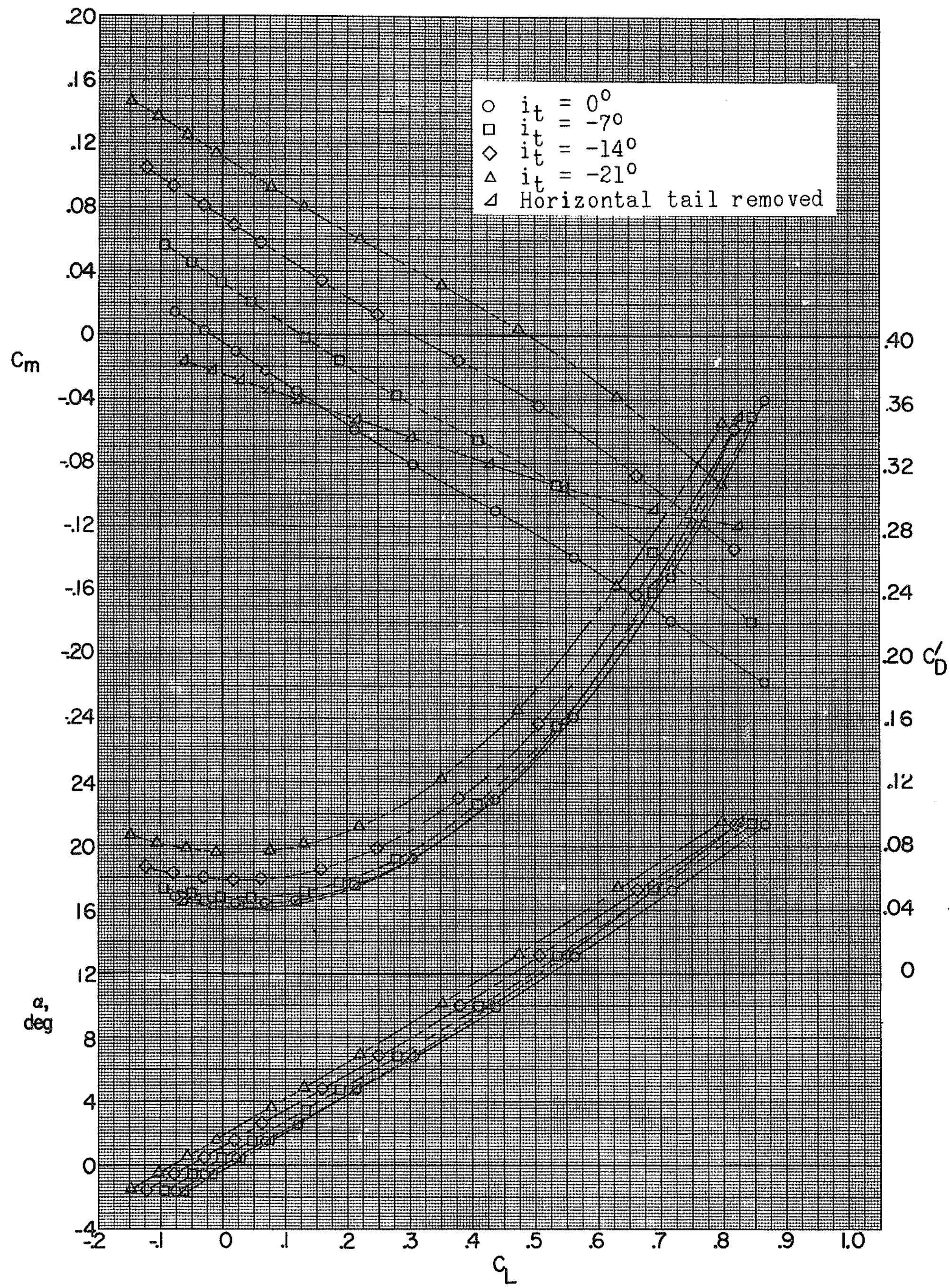

(b) M = 1.87.

Figure 8.- Continued.

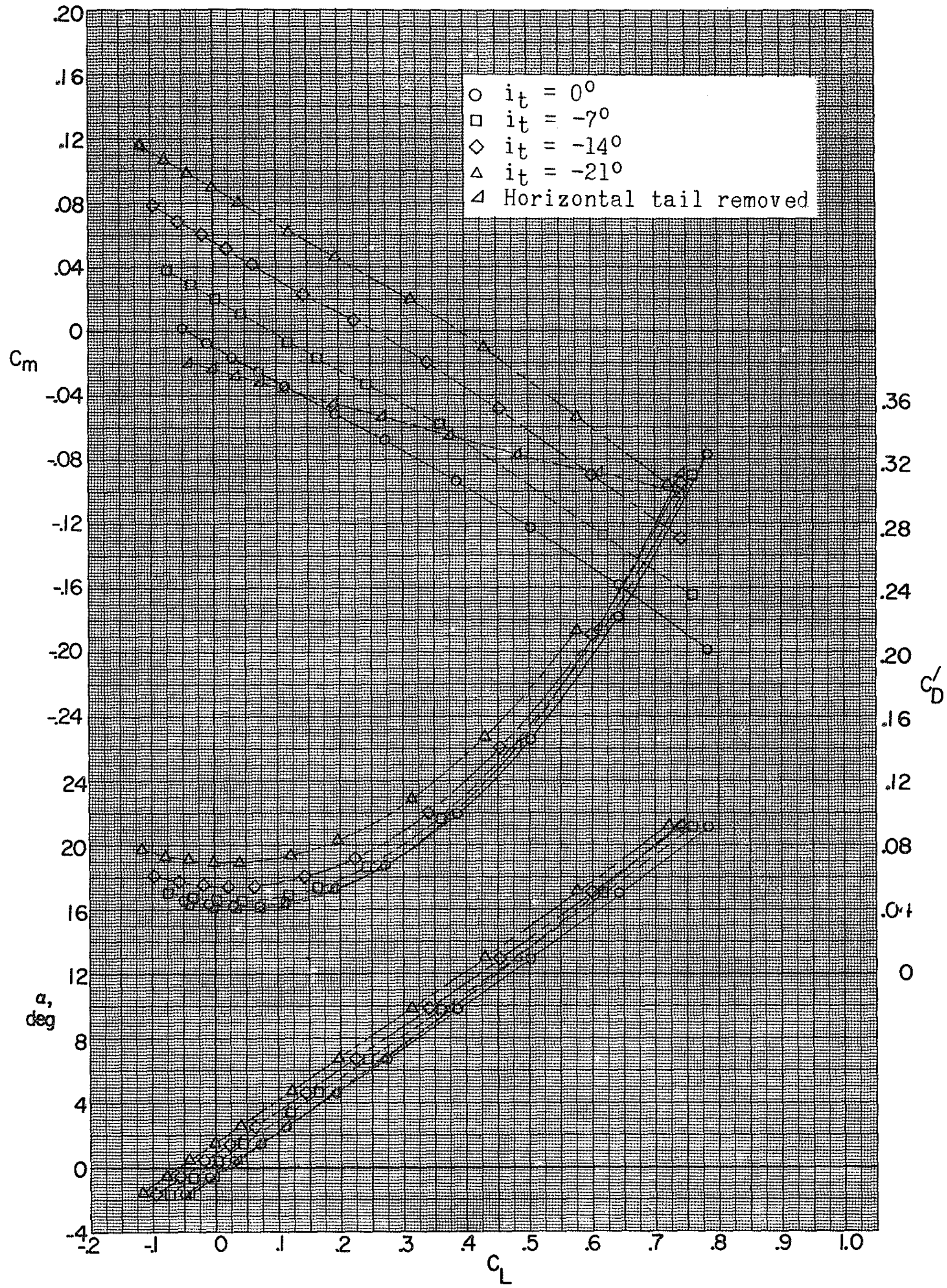

(c) M = 2.16.

Figure 8.- Concluded.

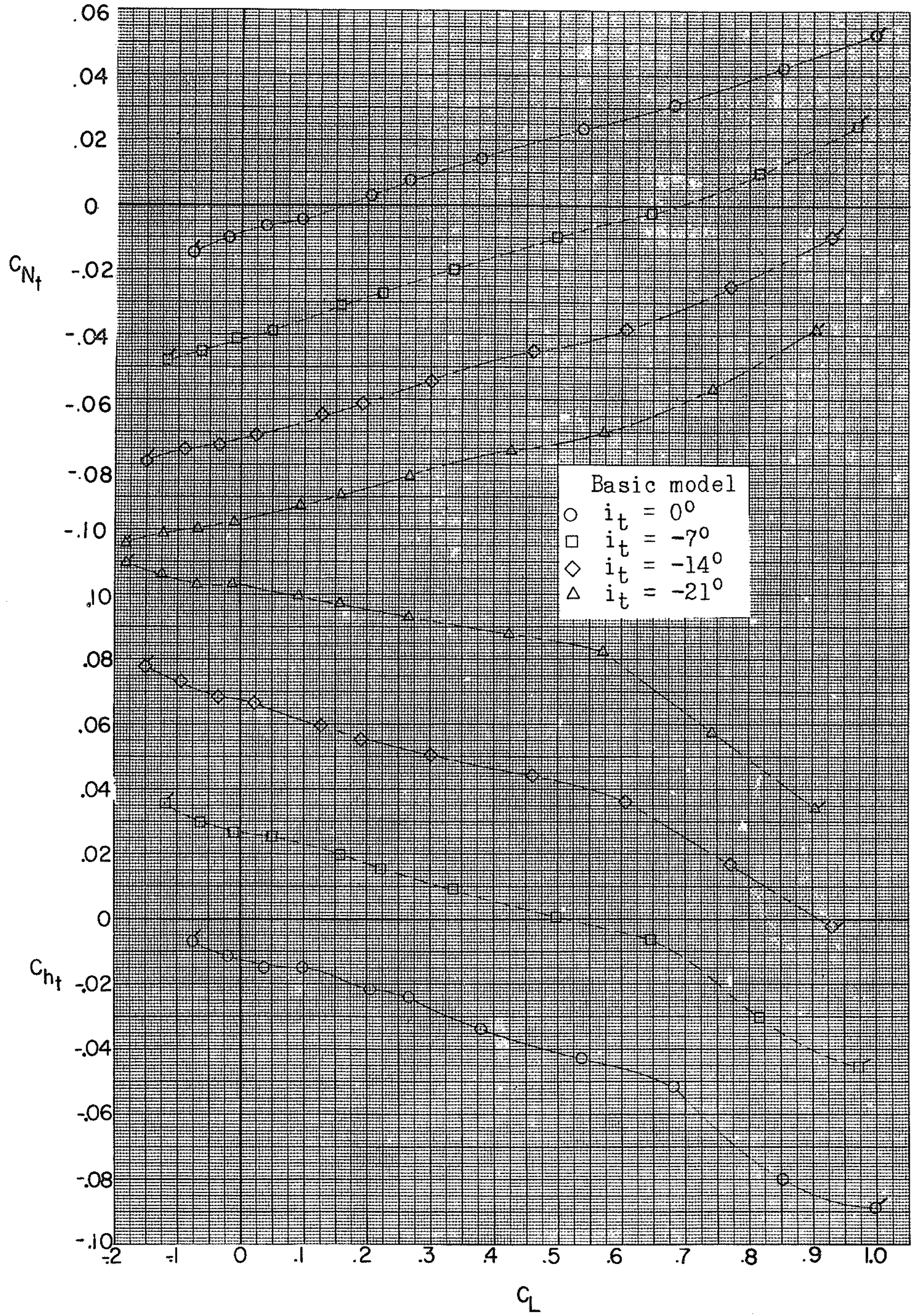

(a) M = 1.57.

Figure 9.- Variation of stabilator hinge-moment and normal-force coefficient with lift coefficient. (Flagged symbols denote wall-reflected shock waves striking the tail.)

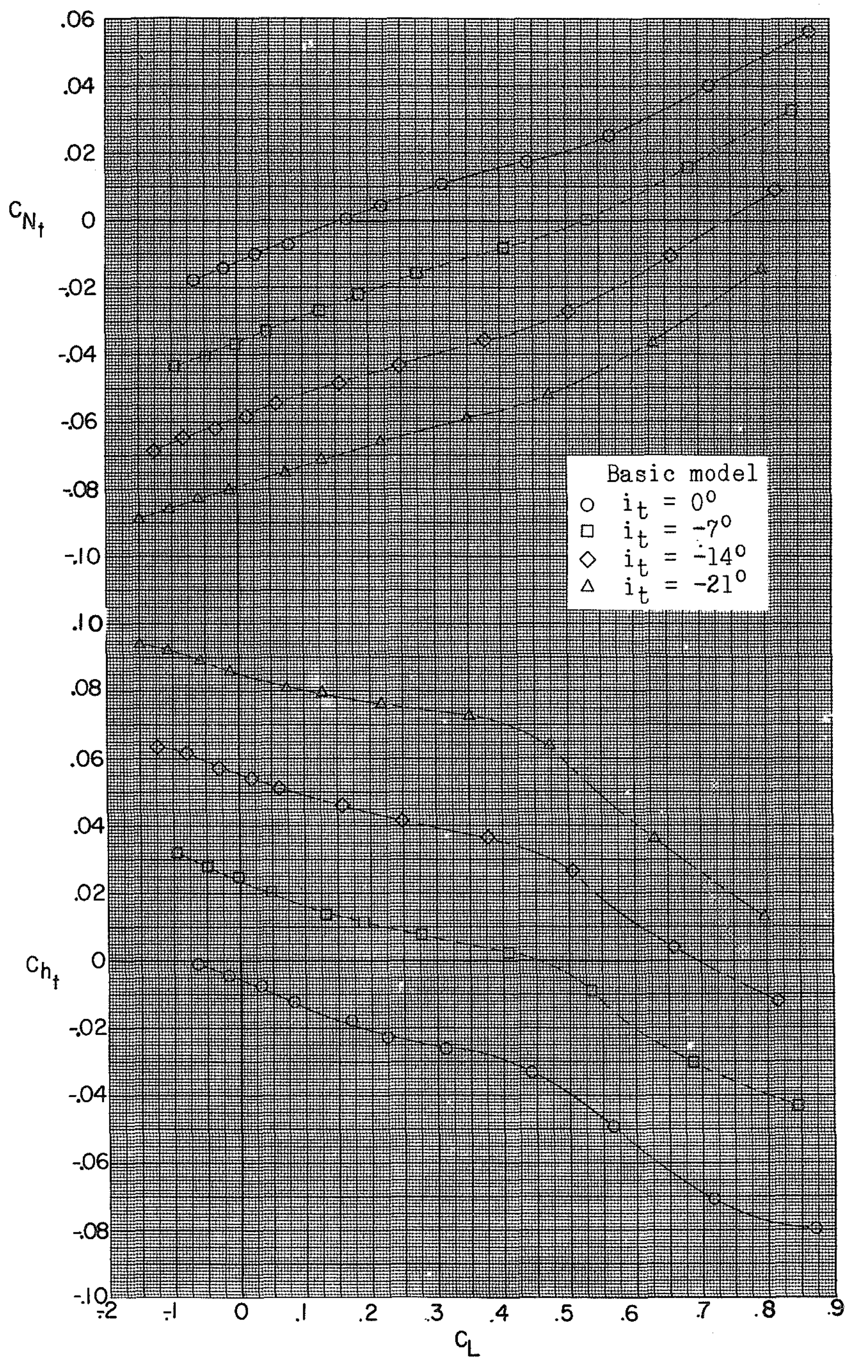

(b) M = 1.87.

Figure 9.- Continued.

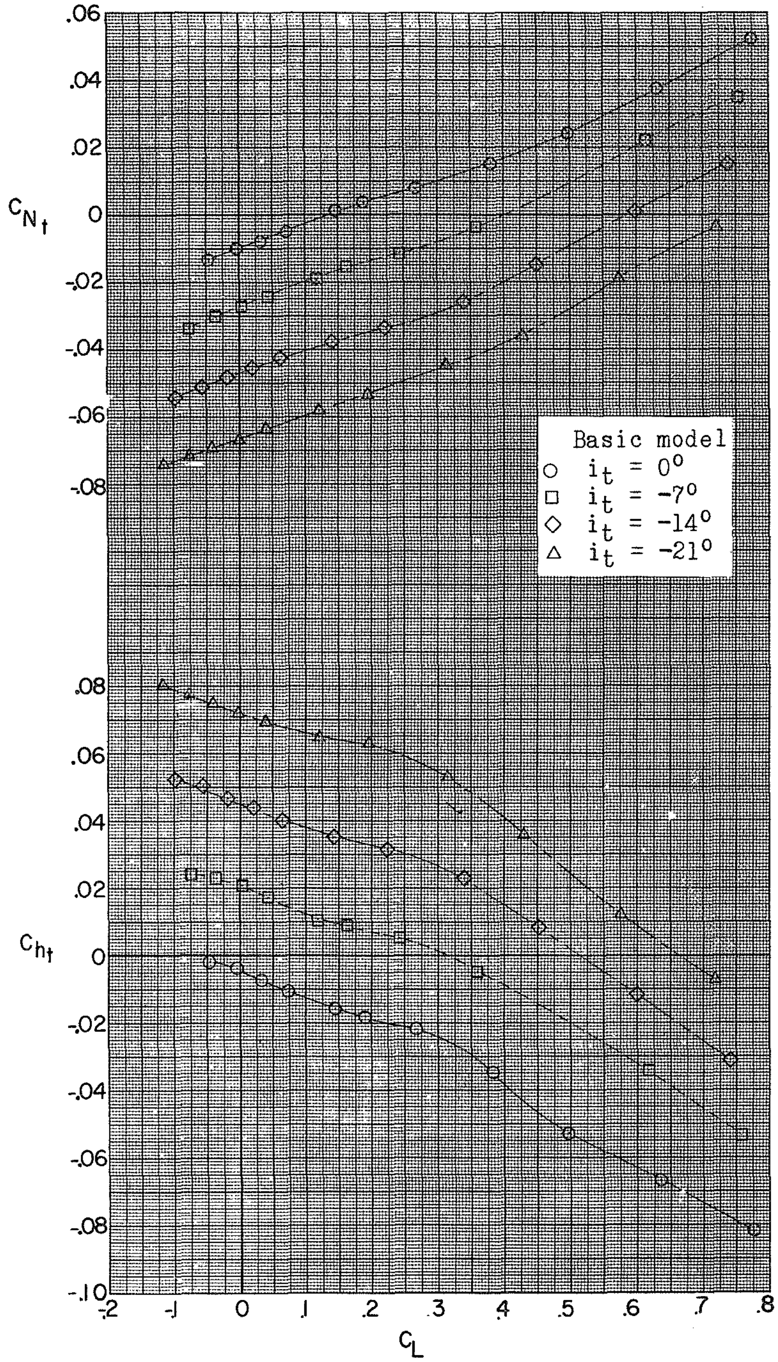

(c) M = 2.16.

Figure 9.- Continued.

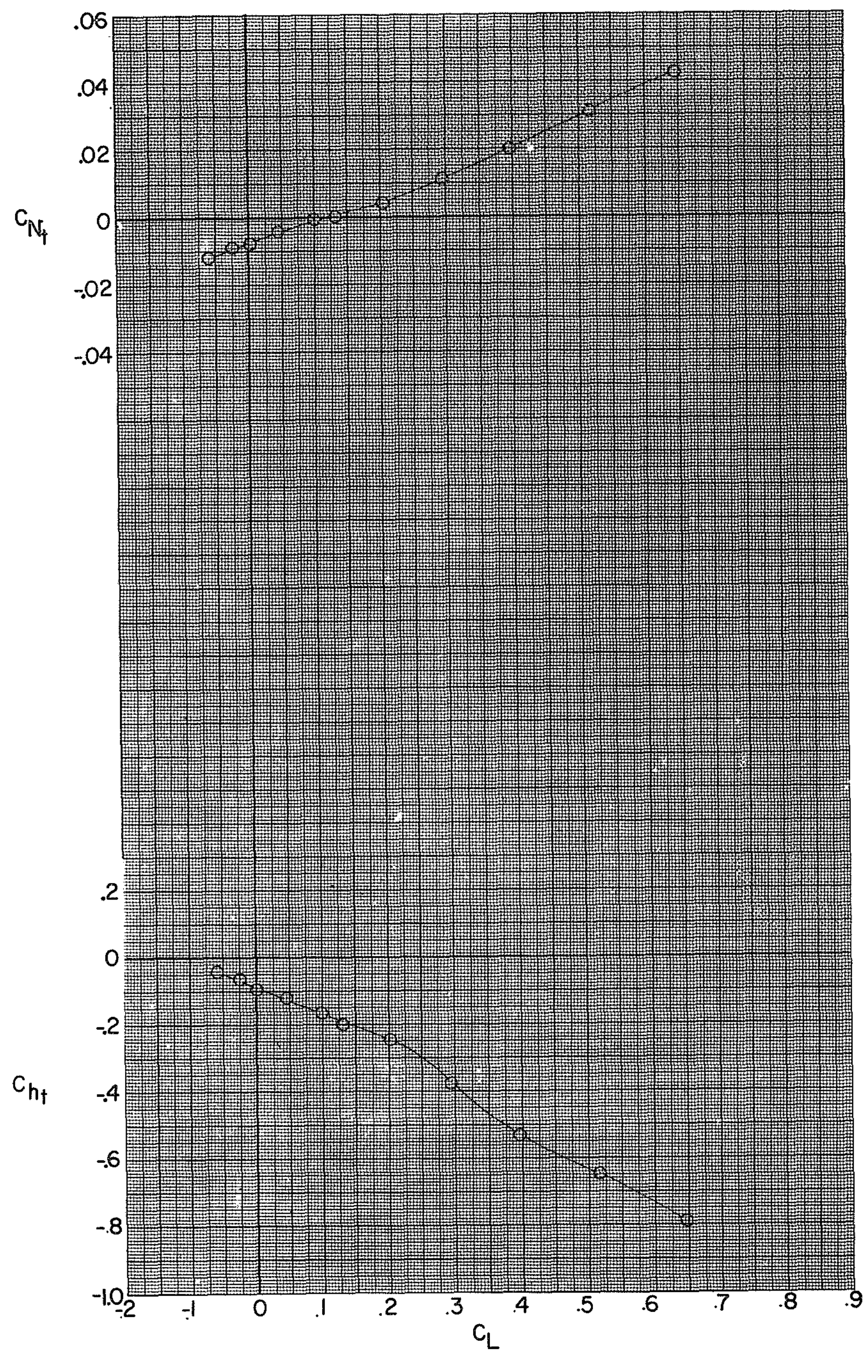

(d) $M = 2.53$; $i_t = 0^{\circ}$.

Figure 9.- Concluded.

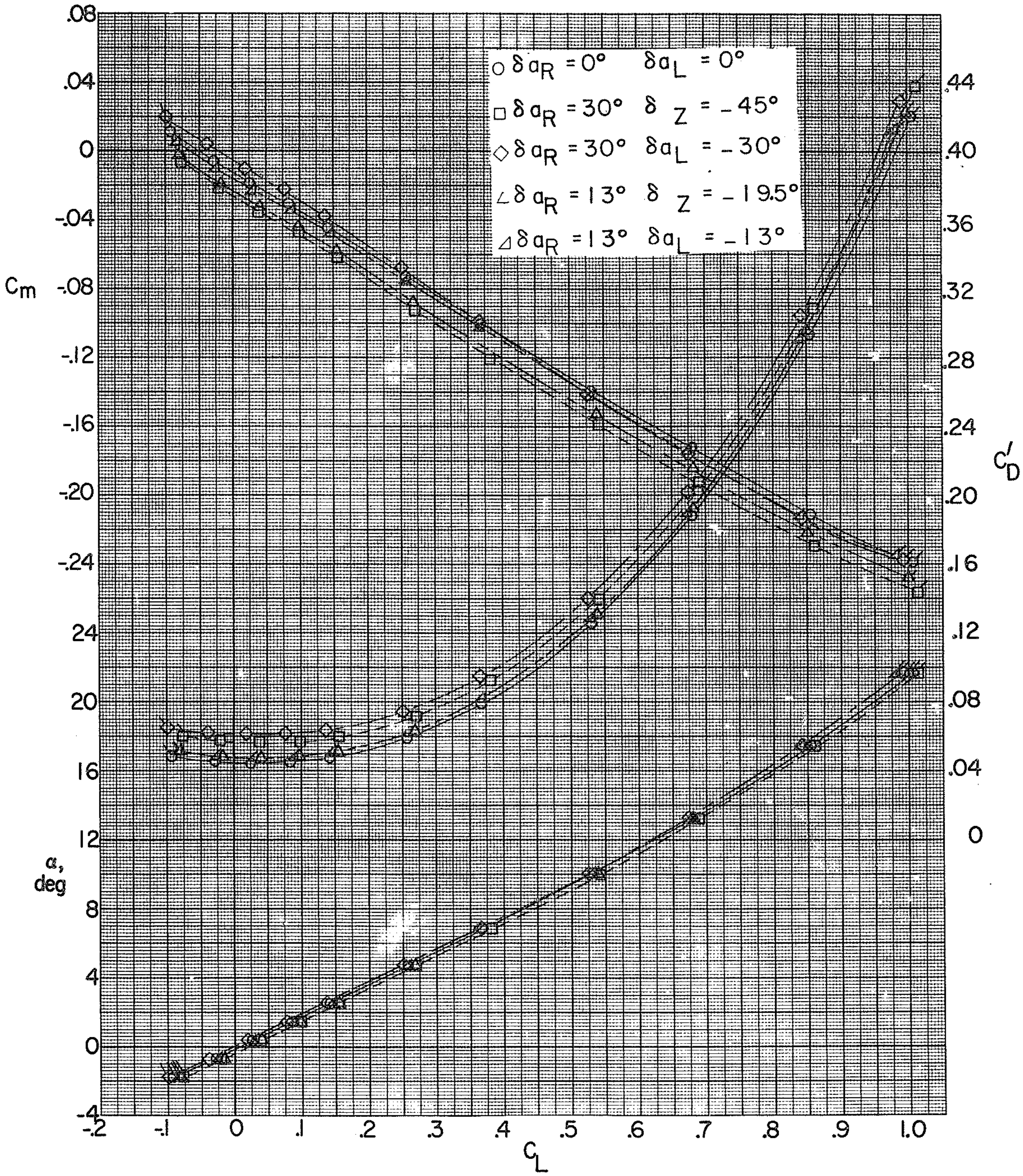

(a) M = 1.57.

Figure 10.- Effect of ailerons and spoilers on aerodynamic characteristics in pitch. (Flagged symbols denote wall-reflected shock waves striking the tail.)

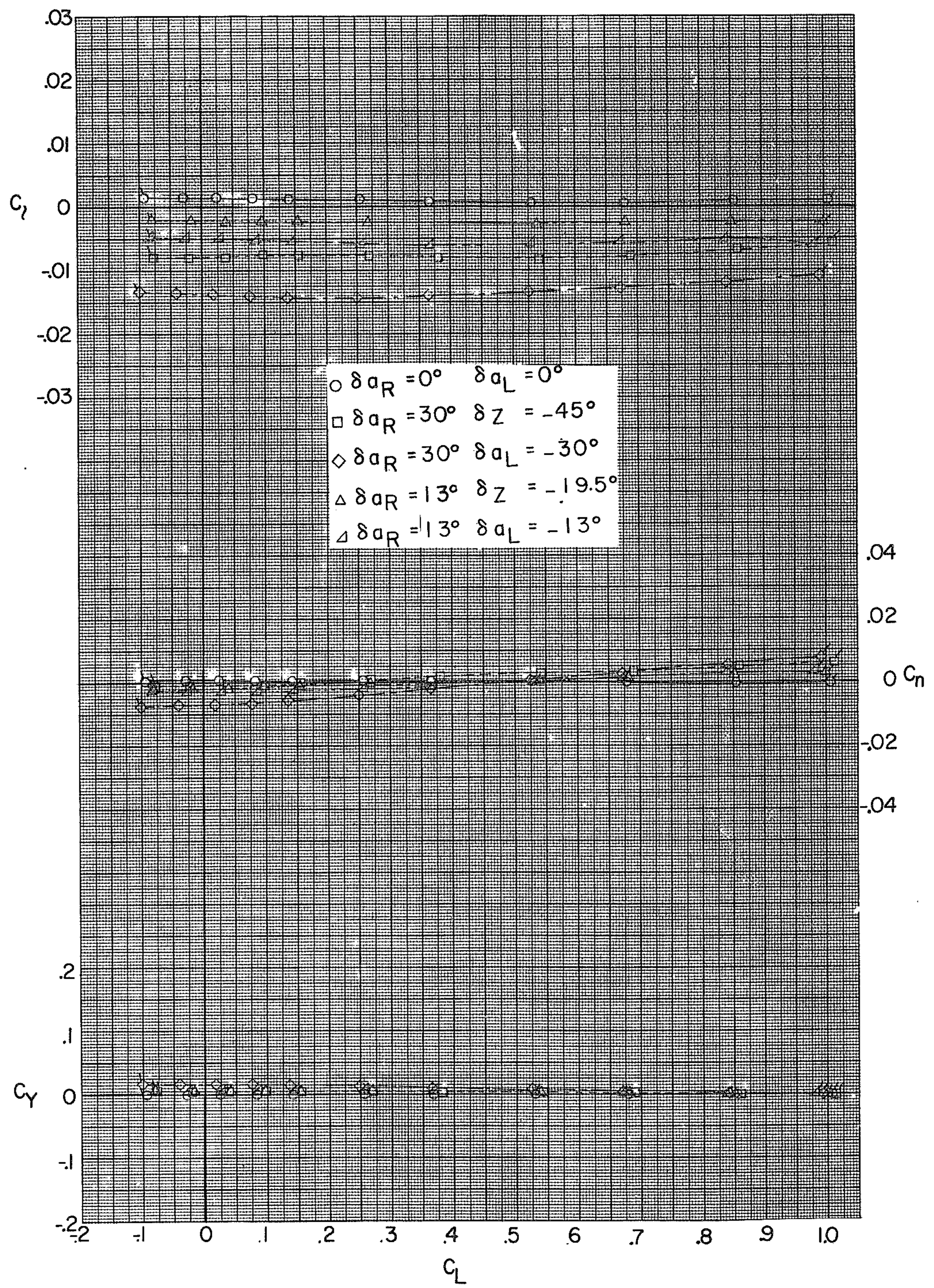

(a) Concluded.

Figure 10.- Continued.

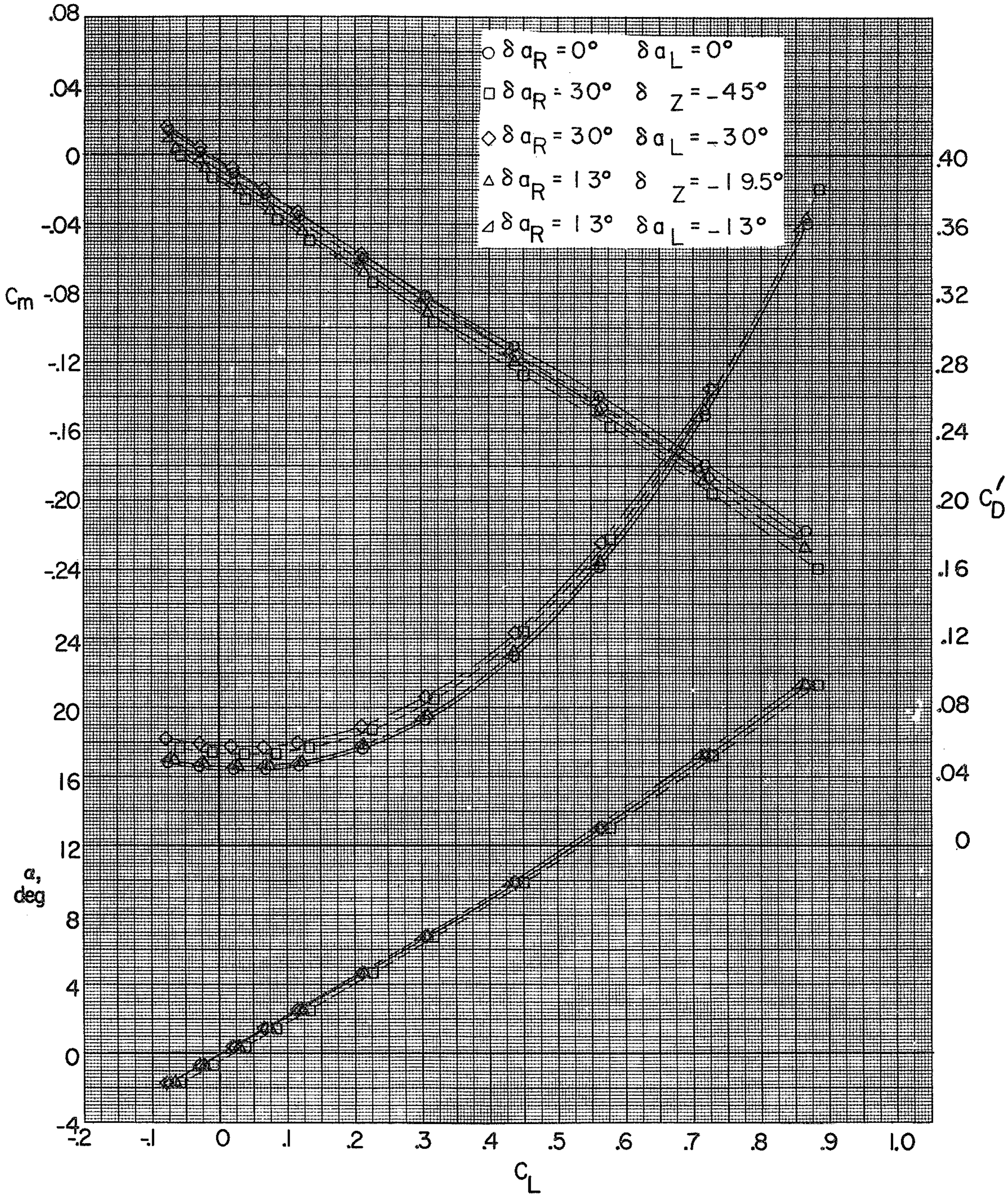

(b) M = 1.87.

Figure 10.- Continued.

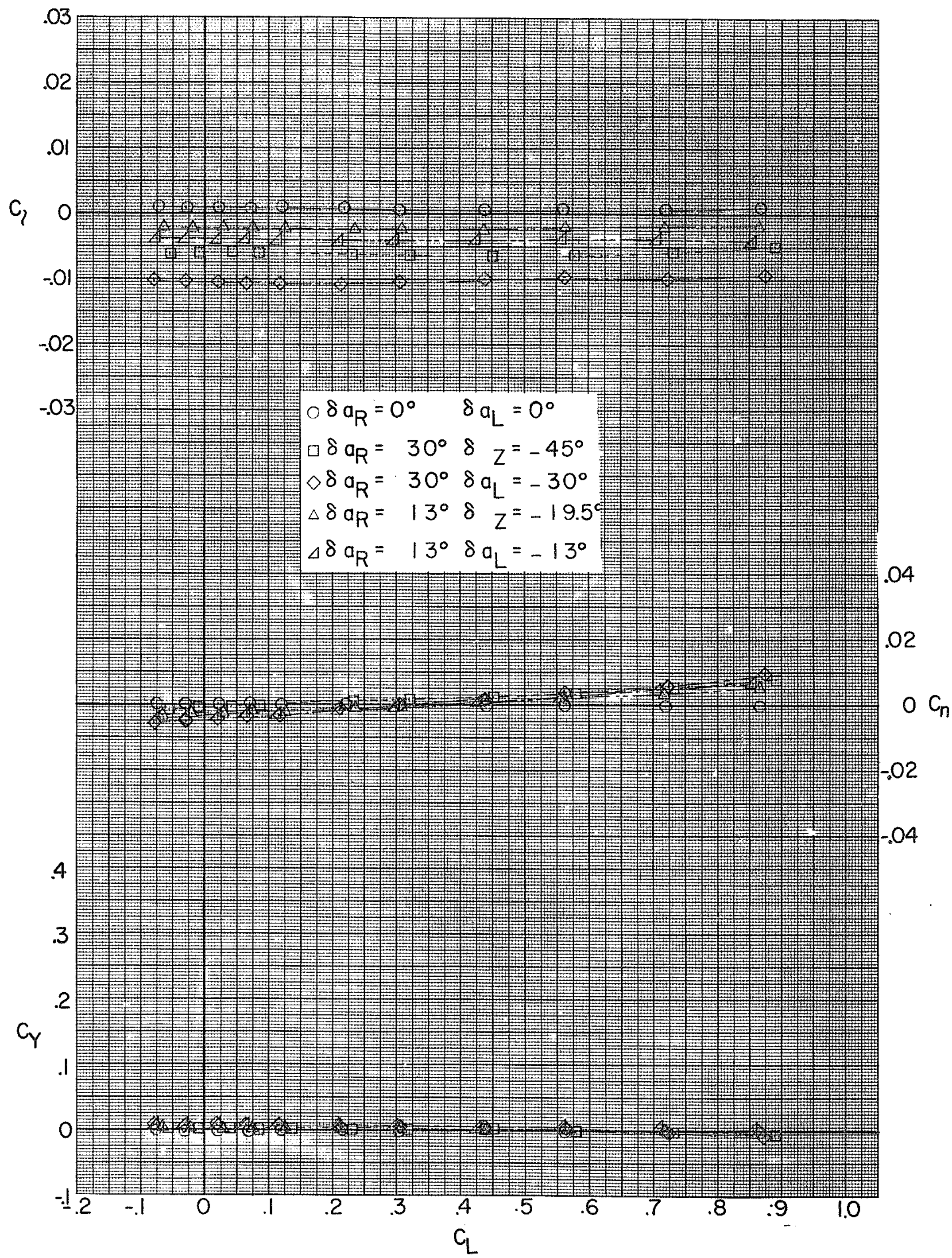

(b) Concluded.

Figure 10.- Continued.

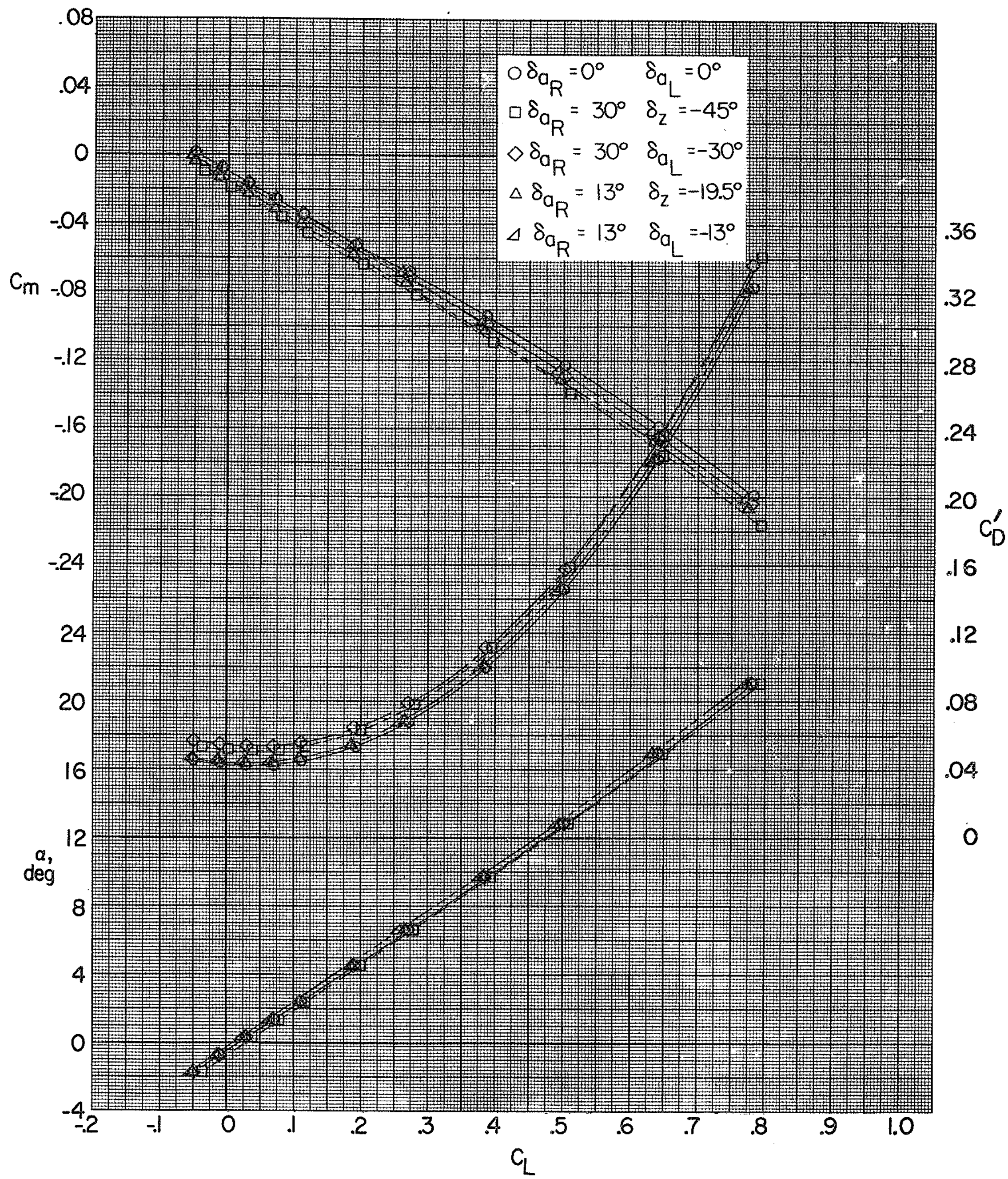

(c) M = 2.16.

Figure 10.- Continued.

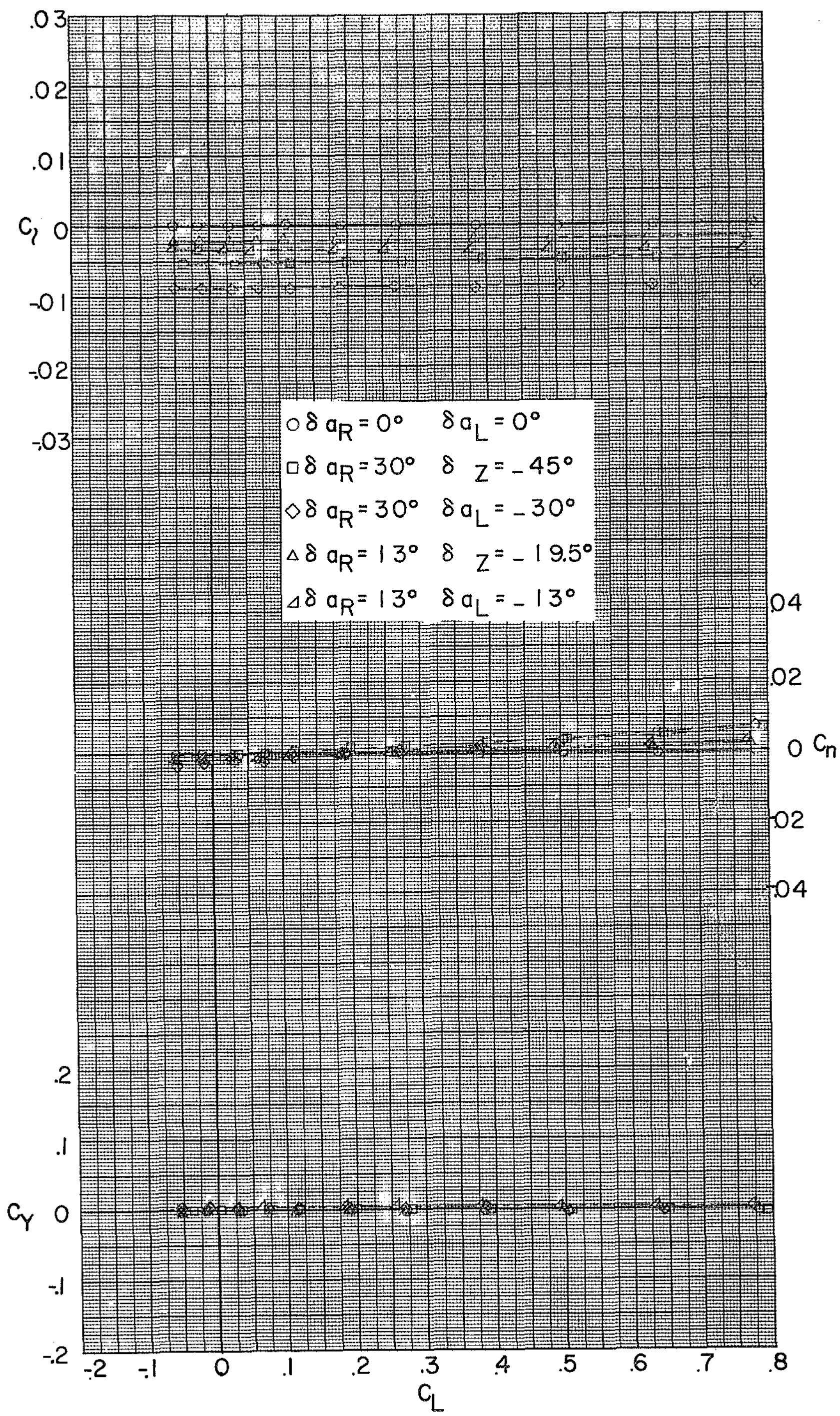

(c) Concluded.

Figure 10.- Concluded.

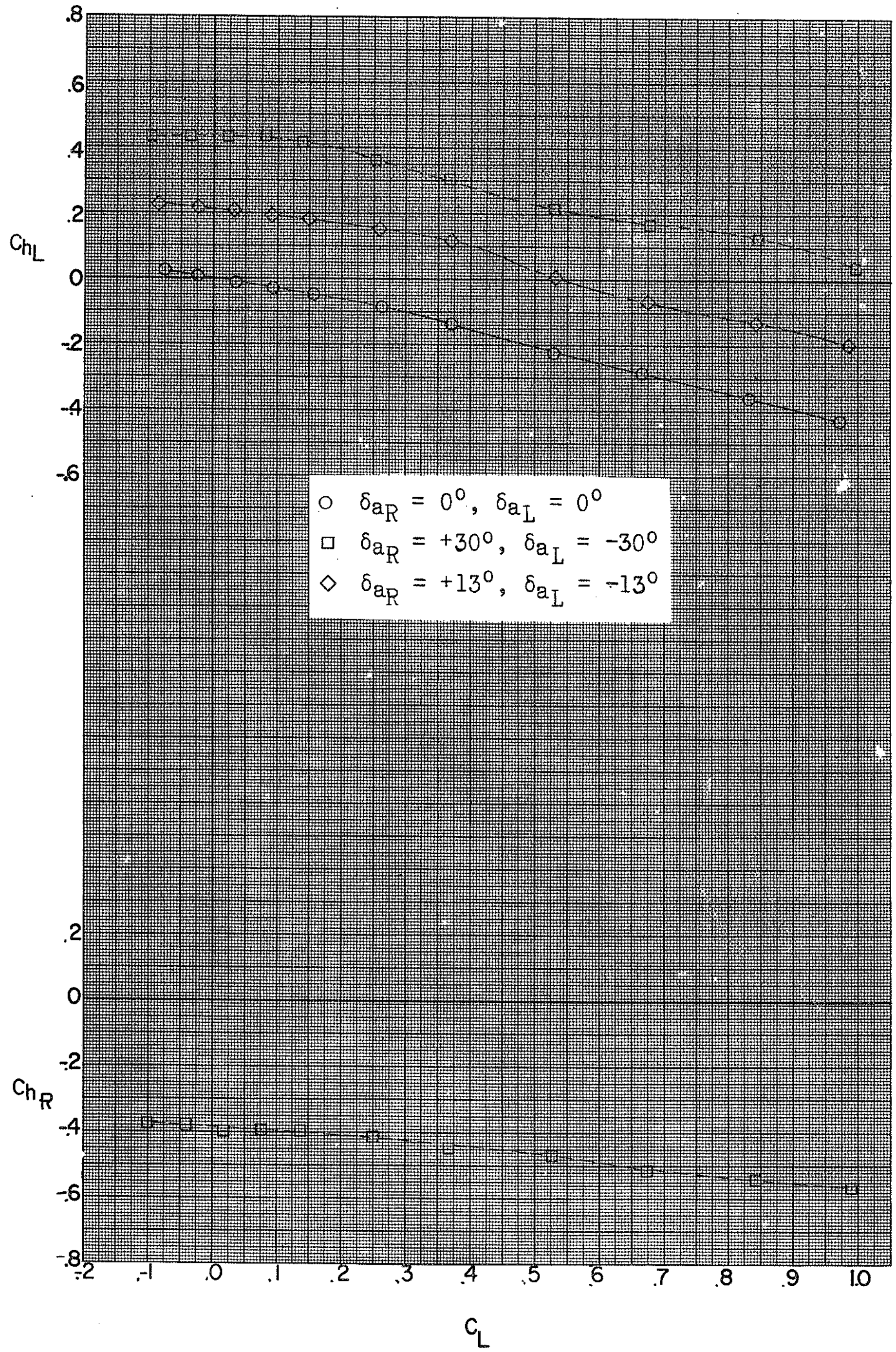

(a) M = 1.57.

Figure 11.- Effect of aileron deflection on aileron hinge-moment coefficient in pitch.

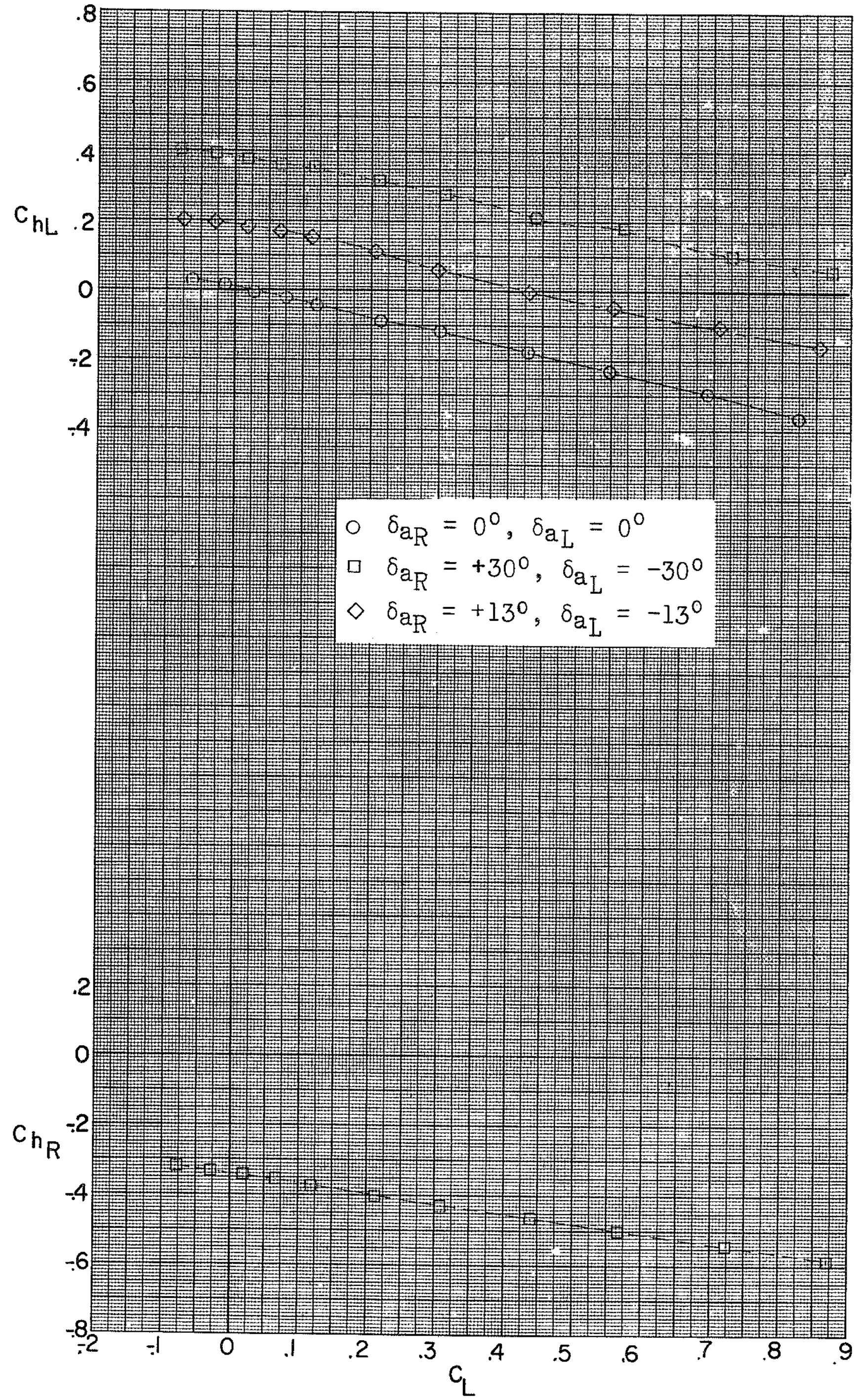

(b) M = 1.87.

Figure 11.- Continued.

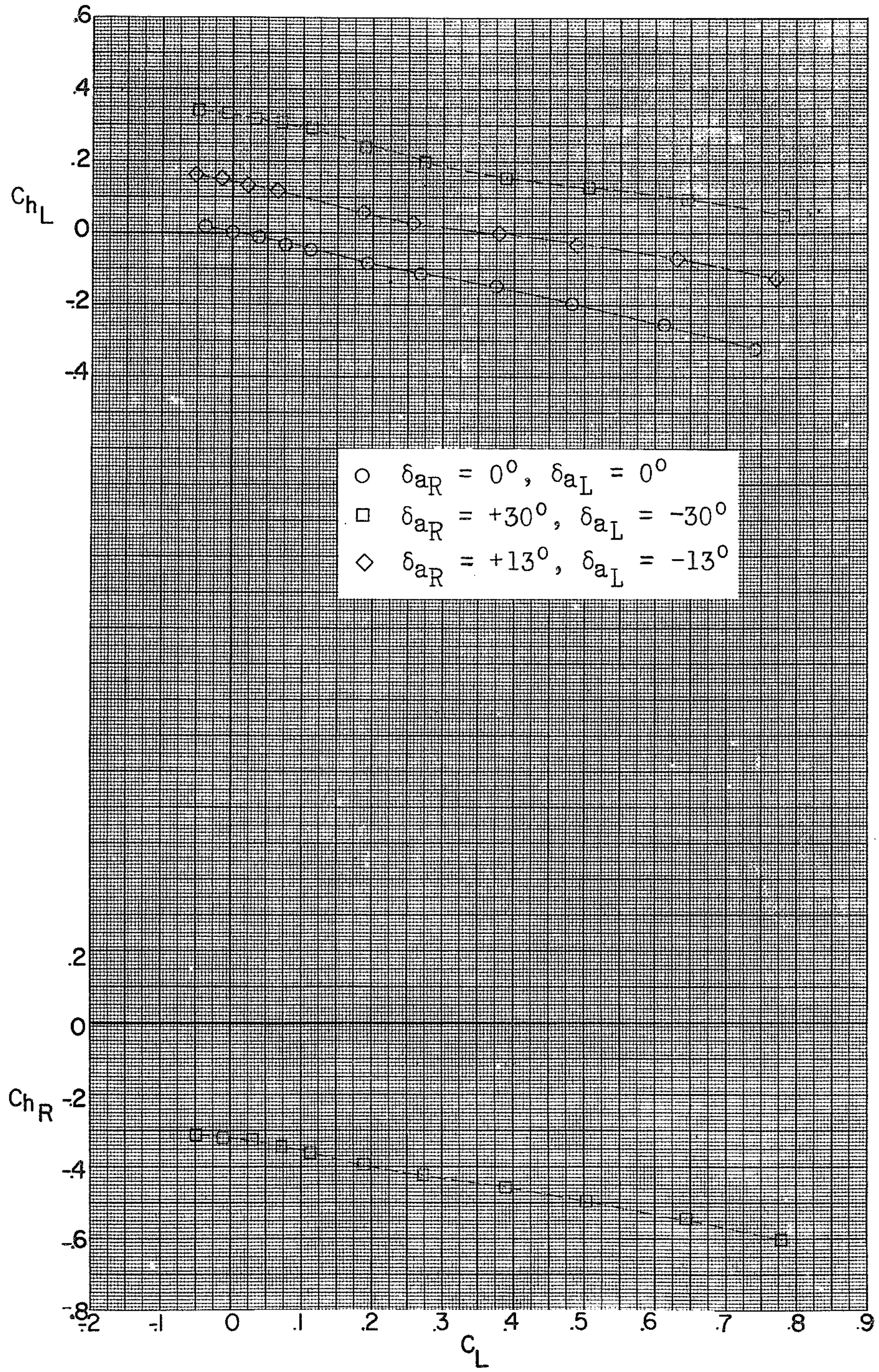

(c) M = 2.16.

Figure 11.- Concluded.

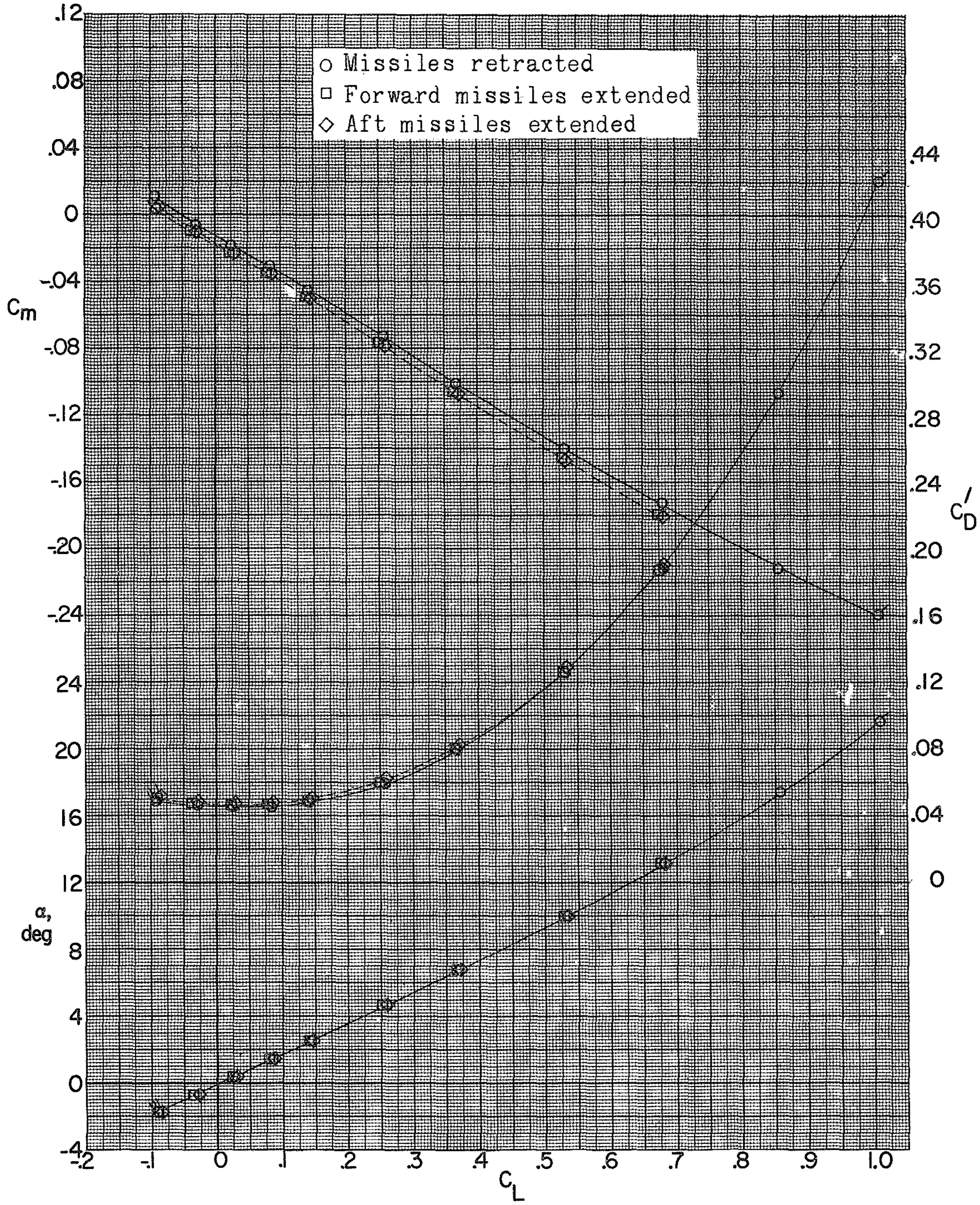

(a) M = 1.57.

Figure 12.- Effect of missiles extended on aerodynamic characteristics in pitch. (Flagged symbols denote wall-reflected shock waves striking the tail.)

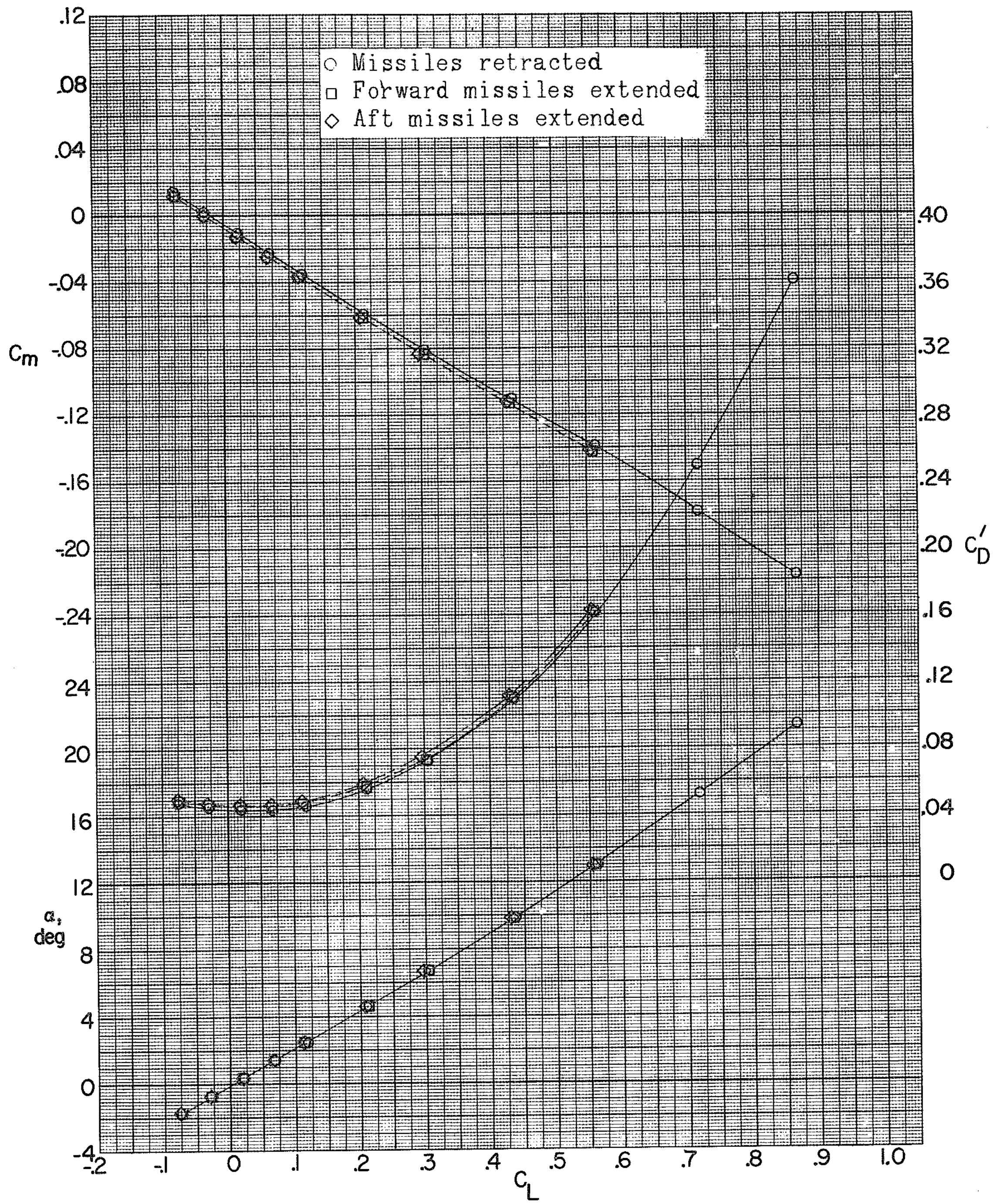

(b) M = 1.87.

Figure 12.- Continued.

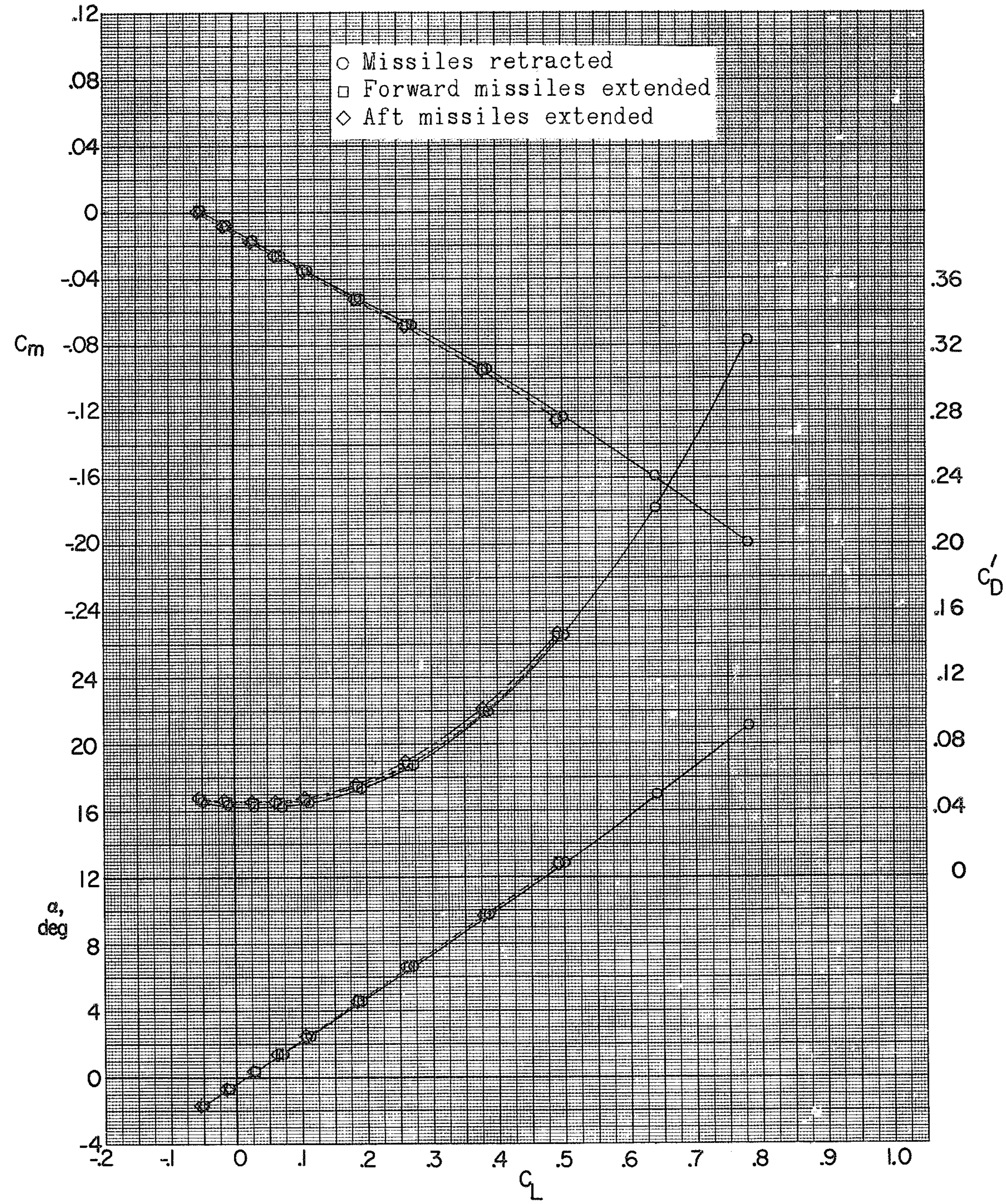

(c) M = 2.16.

Figure 12.- Concluded.

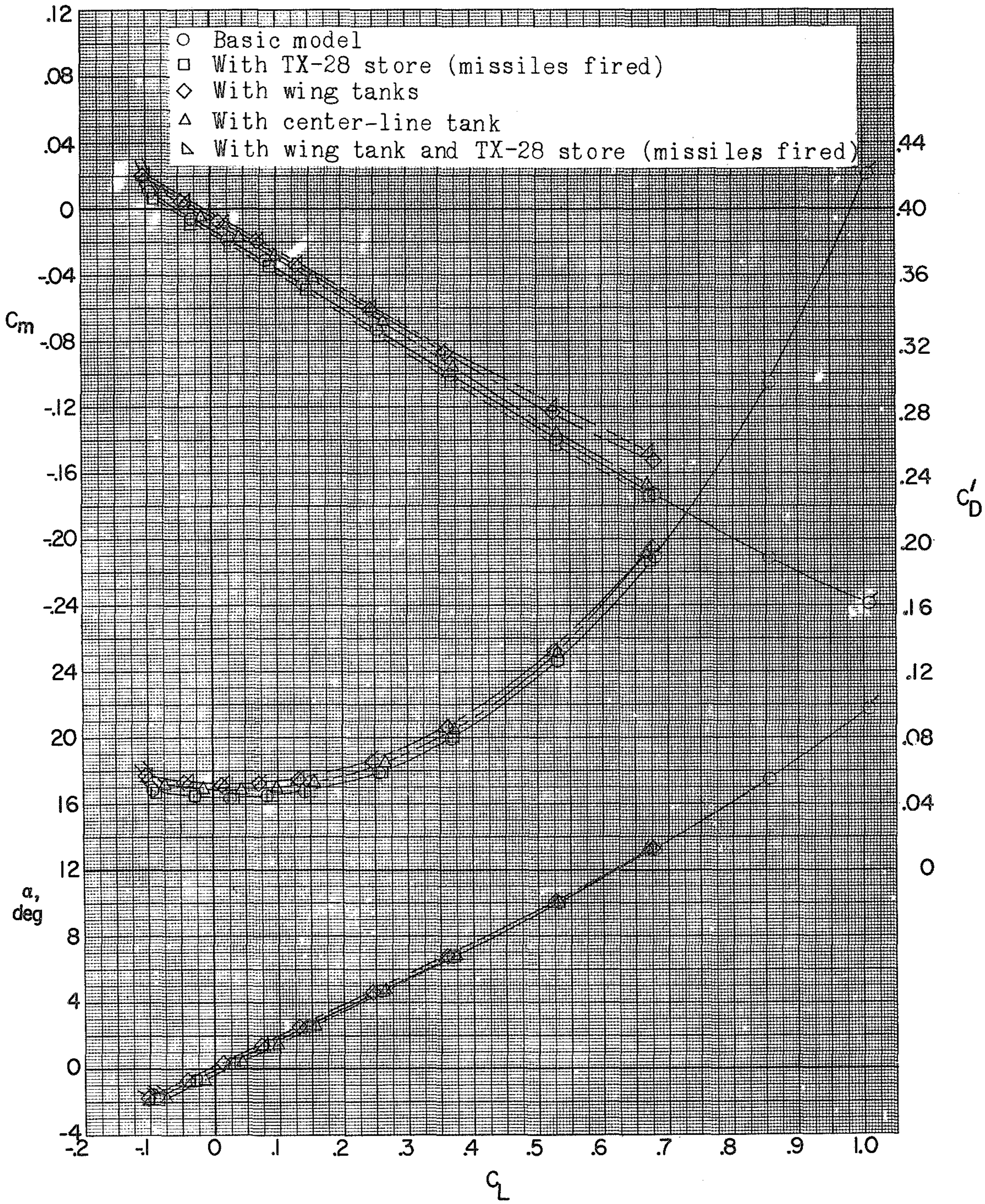

(a) M = 1.57.

Figure 13.- Effect of external stores on aerodynamic characteristics in pitch. (Flagged symbols denote wall-reflected shock waves striking the tail.)

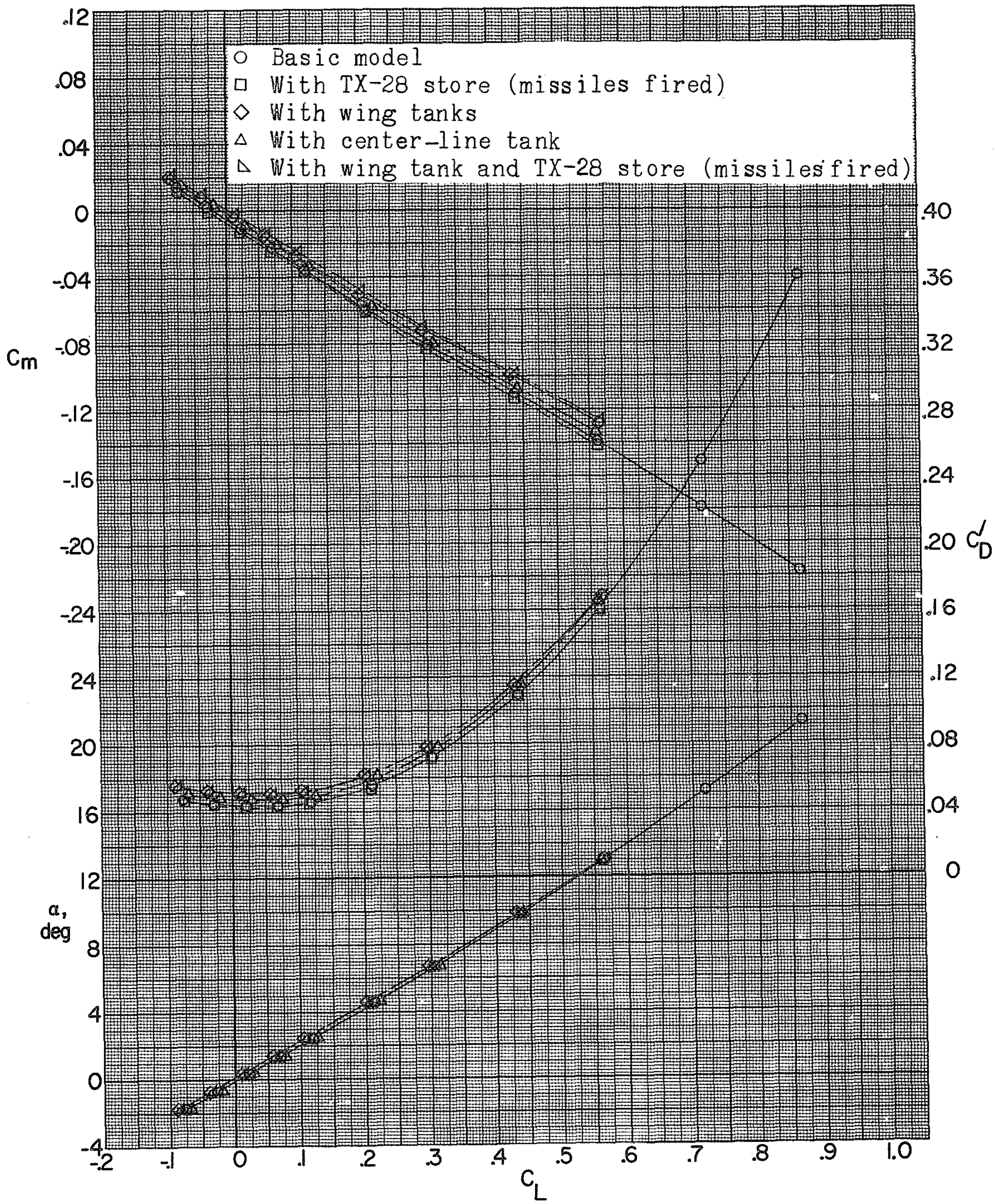

(b) M = 1.87.

Figure 13.- Continued.

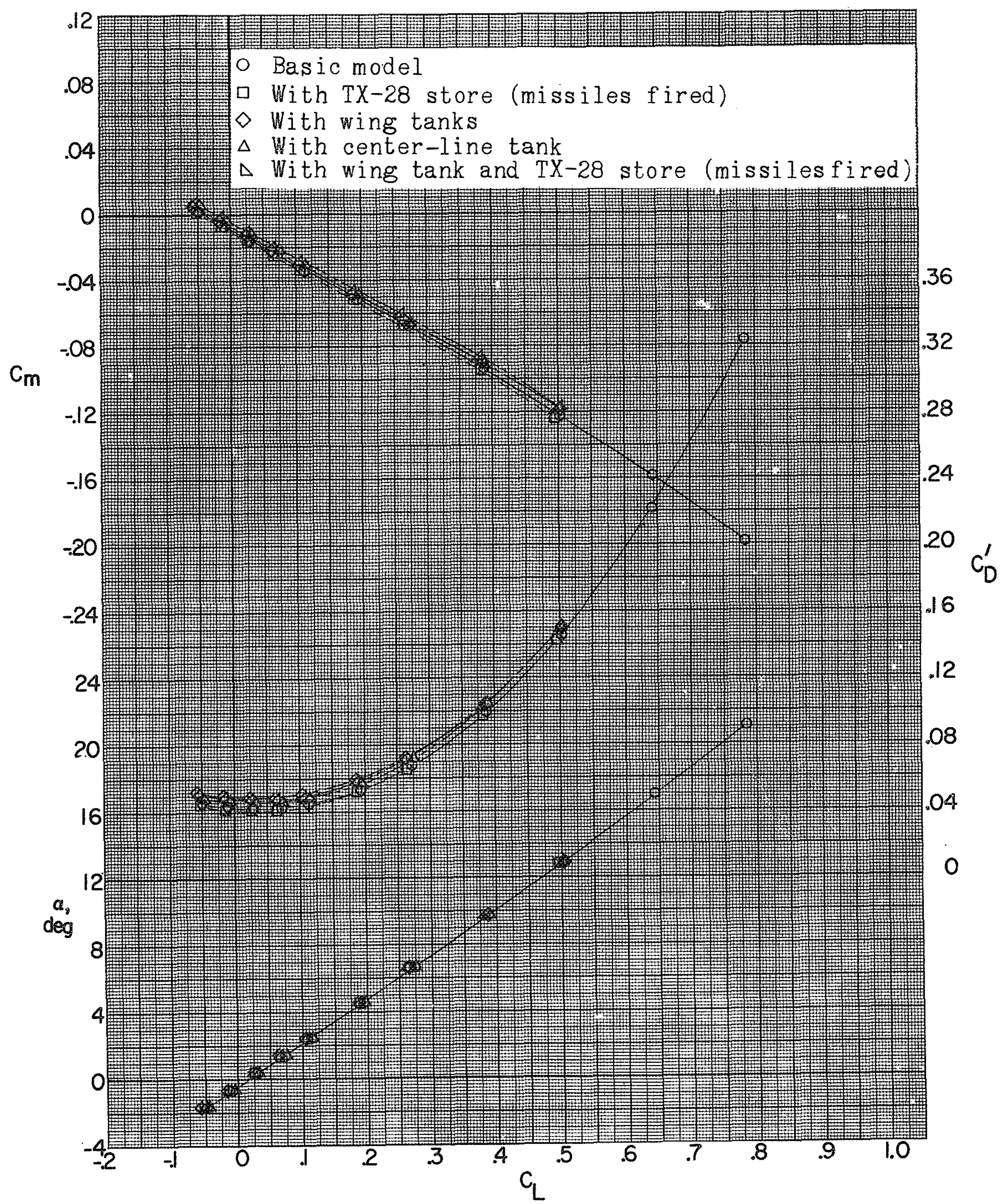

(c) M = 2.16.

Figure 13.- Concluded.

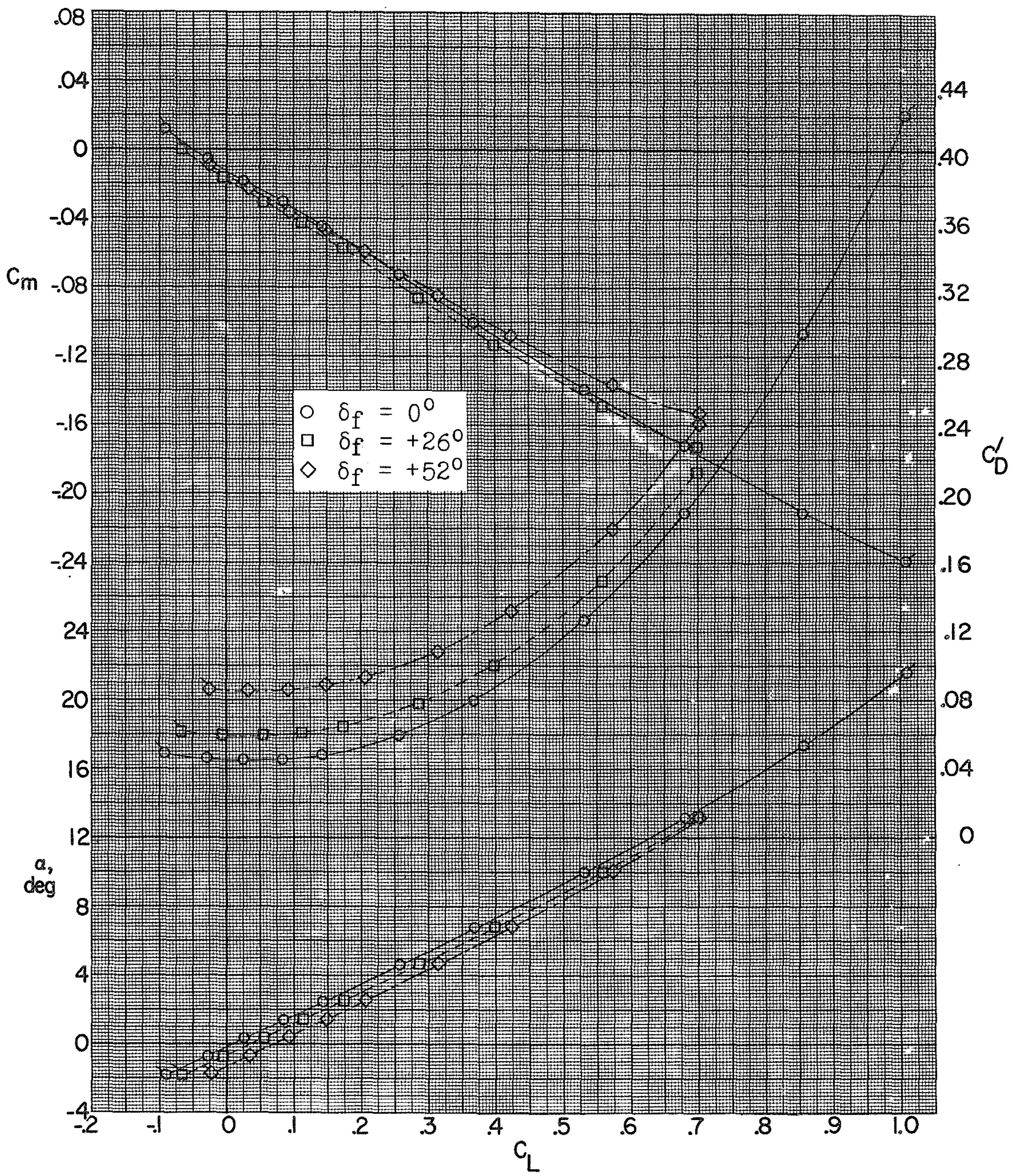

(a) M = 1.57.

Figure 14.- Effect of speed brakes on aerodynamic characteristics in pitch. (Flagged symbols denote wall-reflected shock waves striking the tail.)

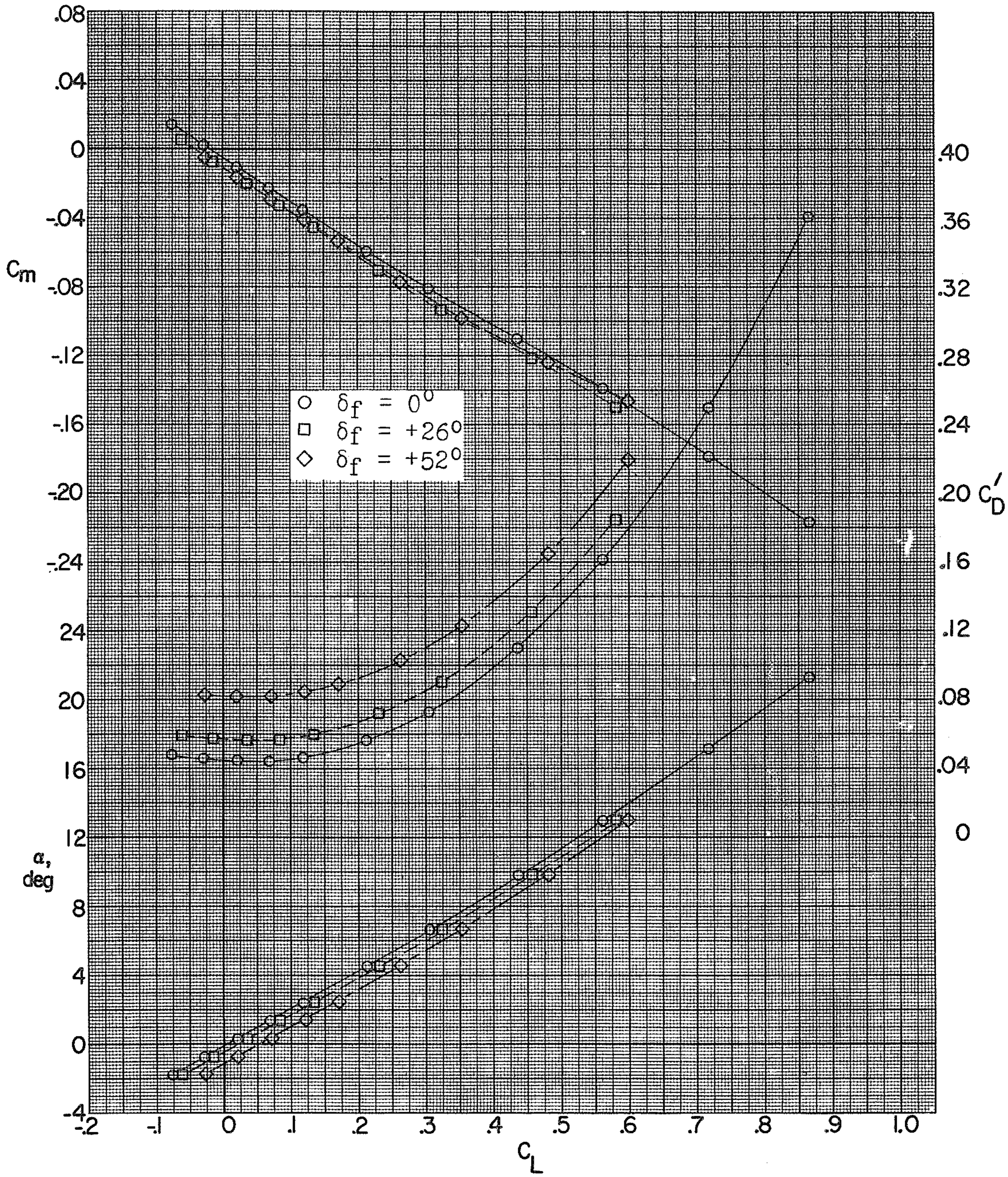

(b) M = 1.87.

Figure 14.- Continued.

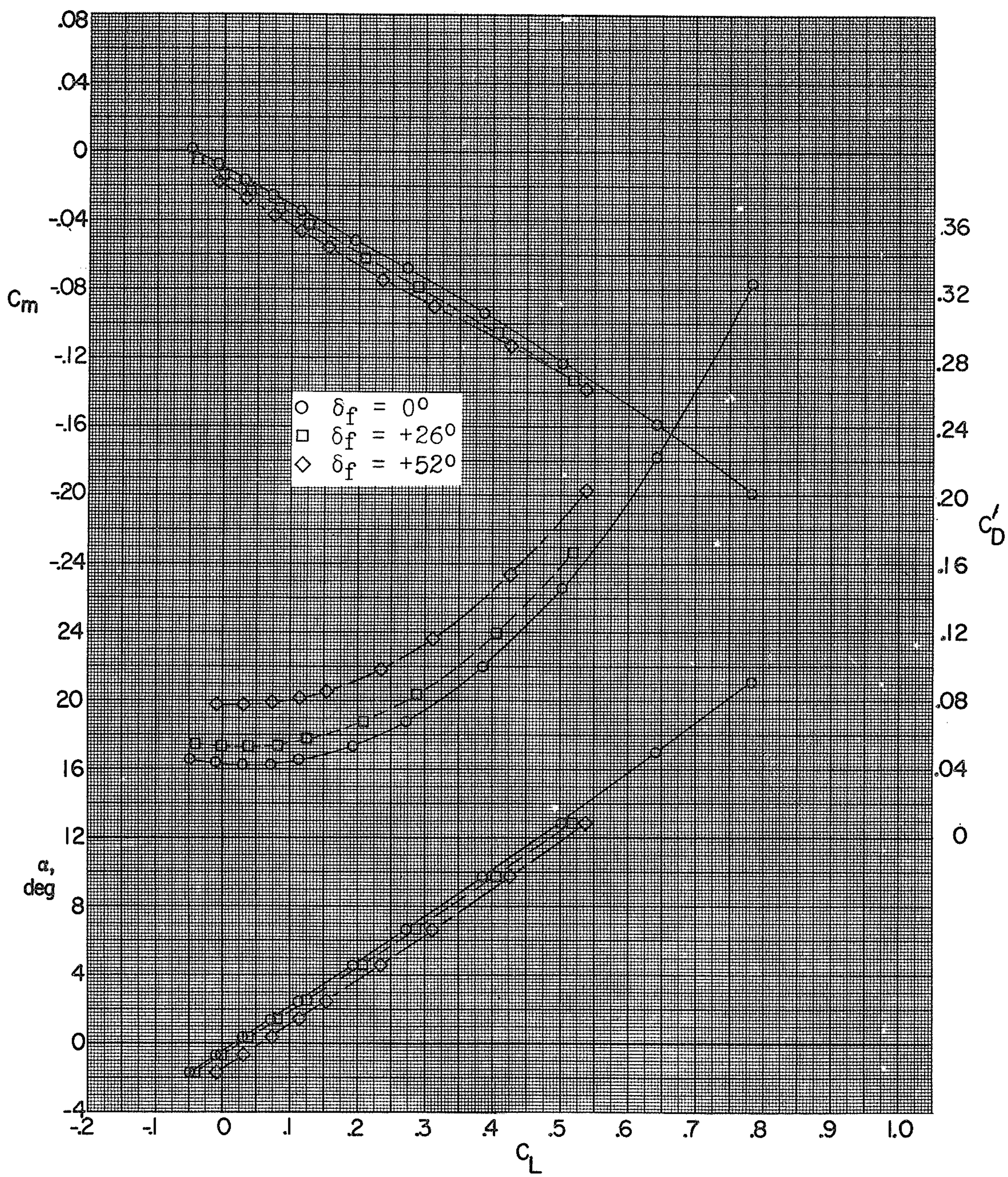

(c) M = 2.16.

Figure 14.- Concluded.

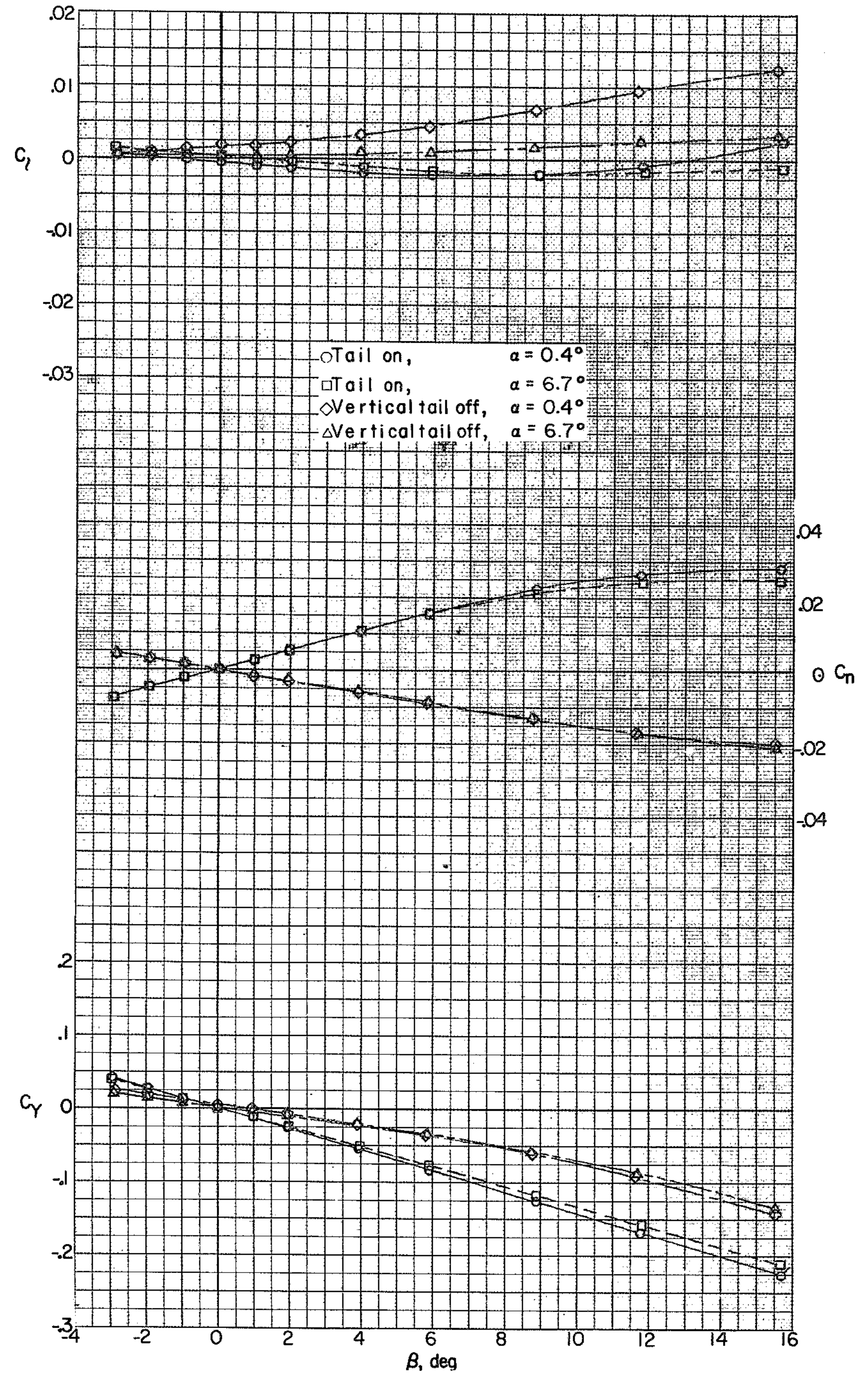

(a) M = 1.57.

Figure 15.- Effect of vertical tail on aerodynamic characteristics in sideslip. (Flagged symbols denote wall-reflected shock waves striking the tail.)

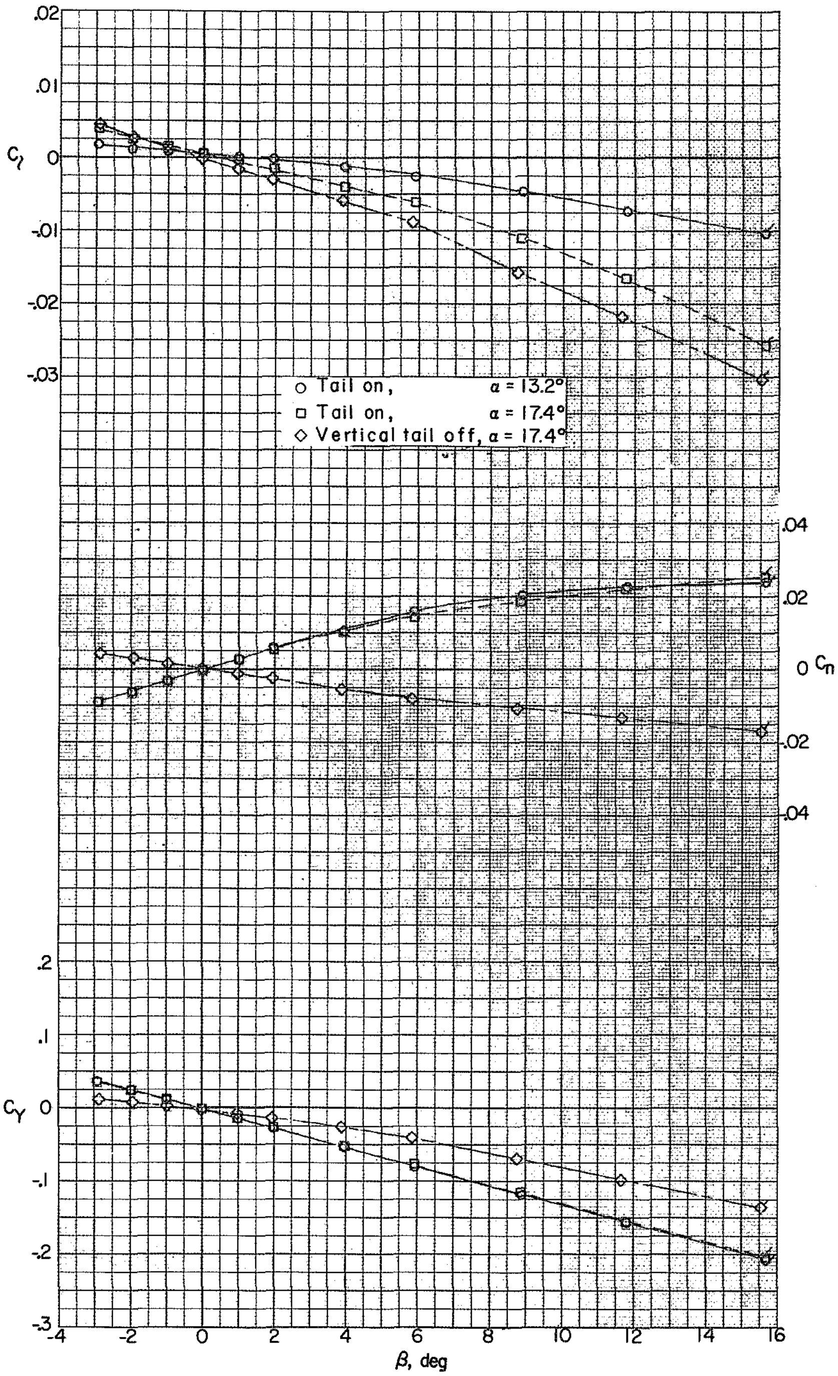

(a) Concluded.

Figure 15.- Continued.

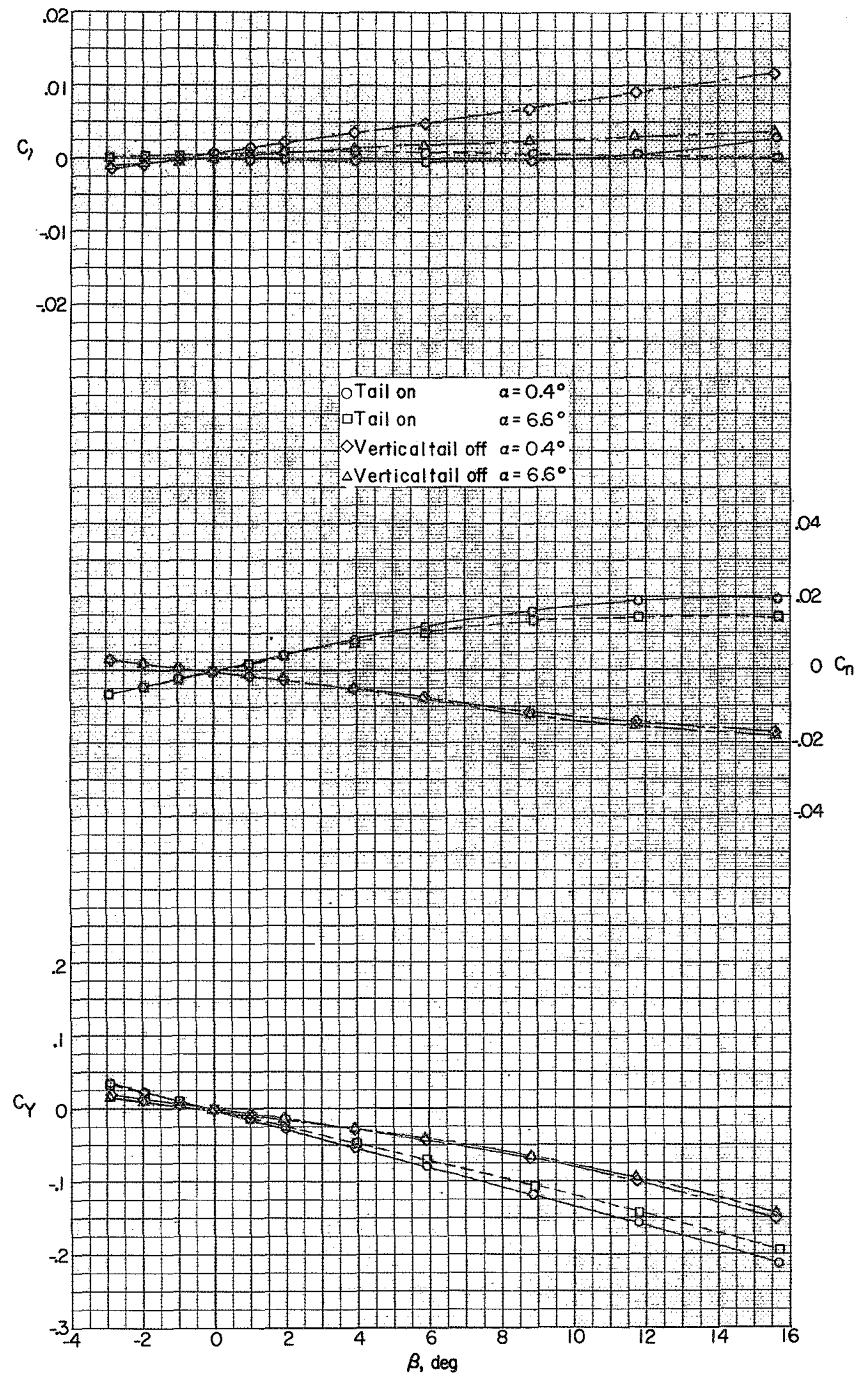

(b) M = 1.87.

Figure 15.- Continued.

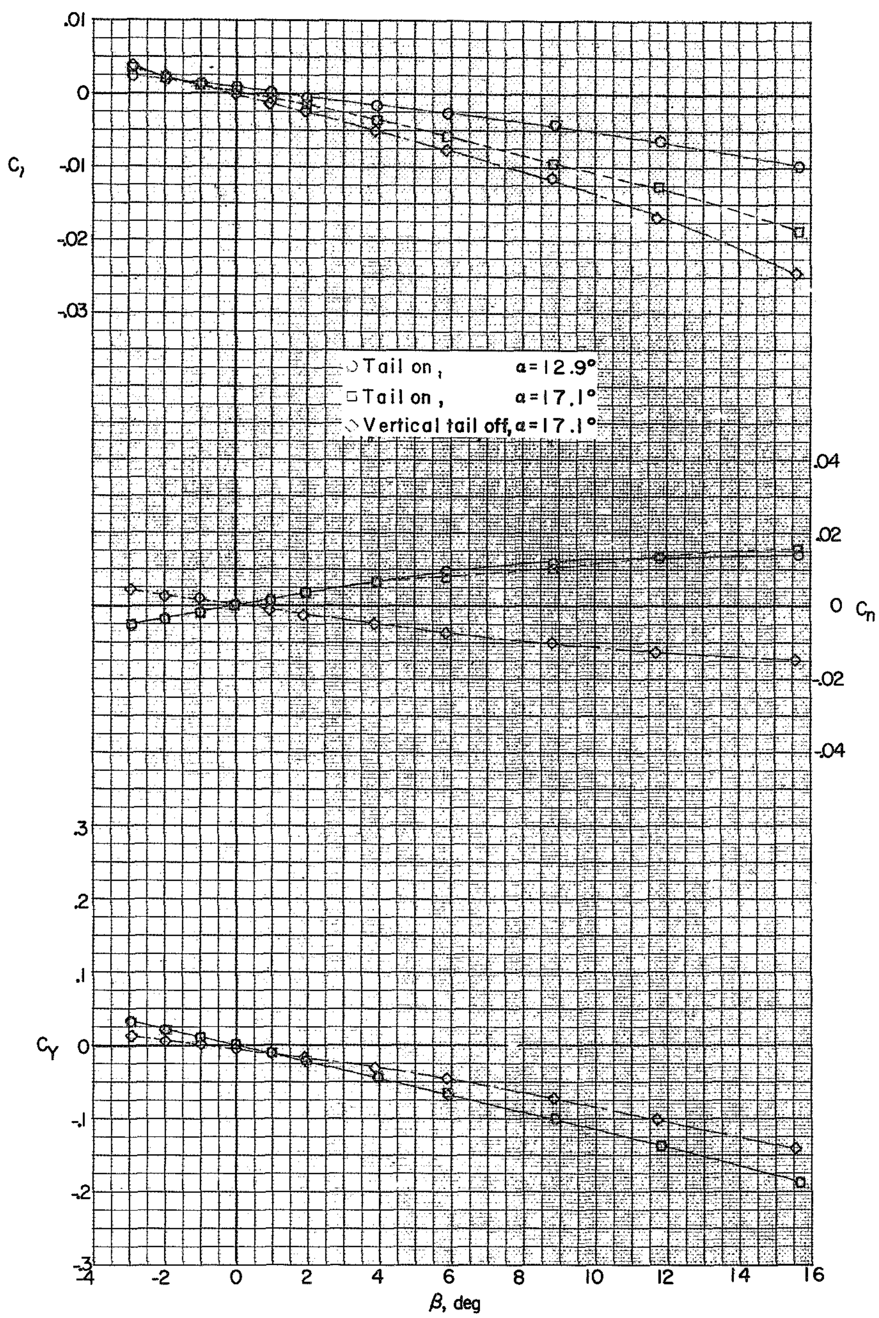

(b) Continued.

Figure 15.- Continued.

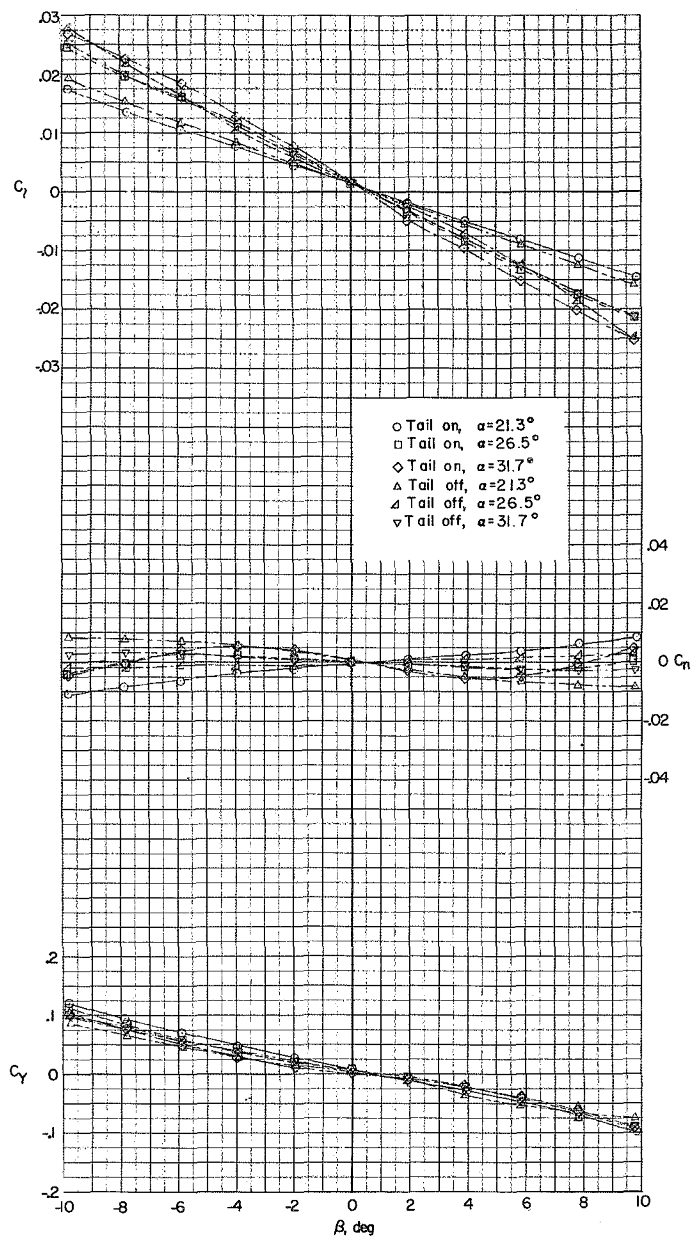

(b) Continued.

Figure 15.- Continued.

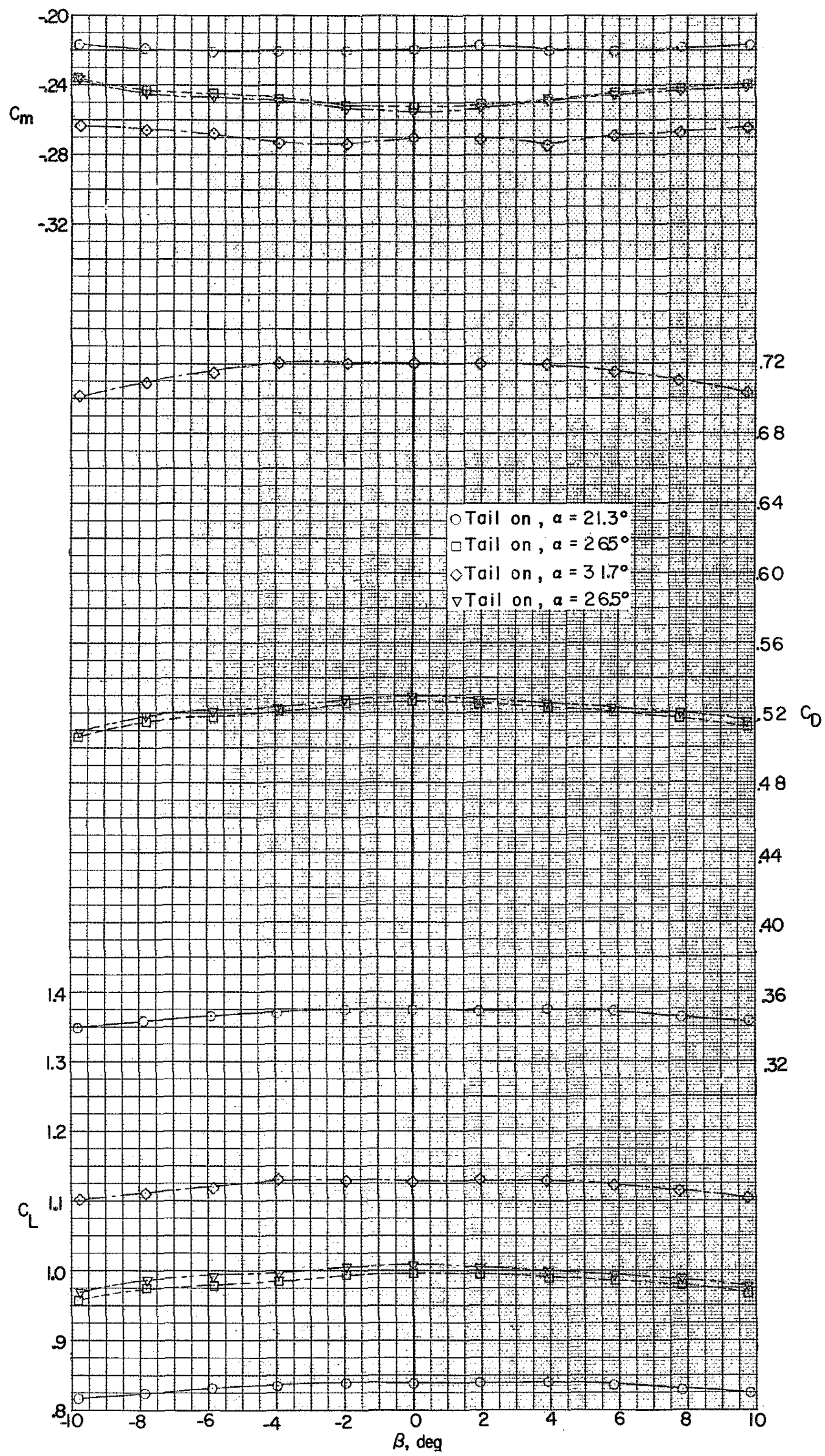

(b) Concluded.

Figure 15.- Continued.

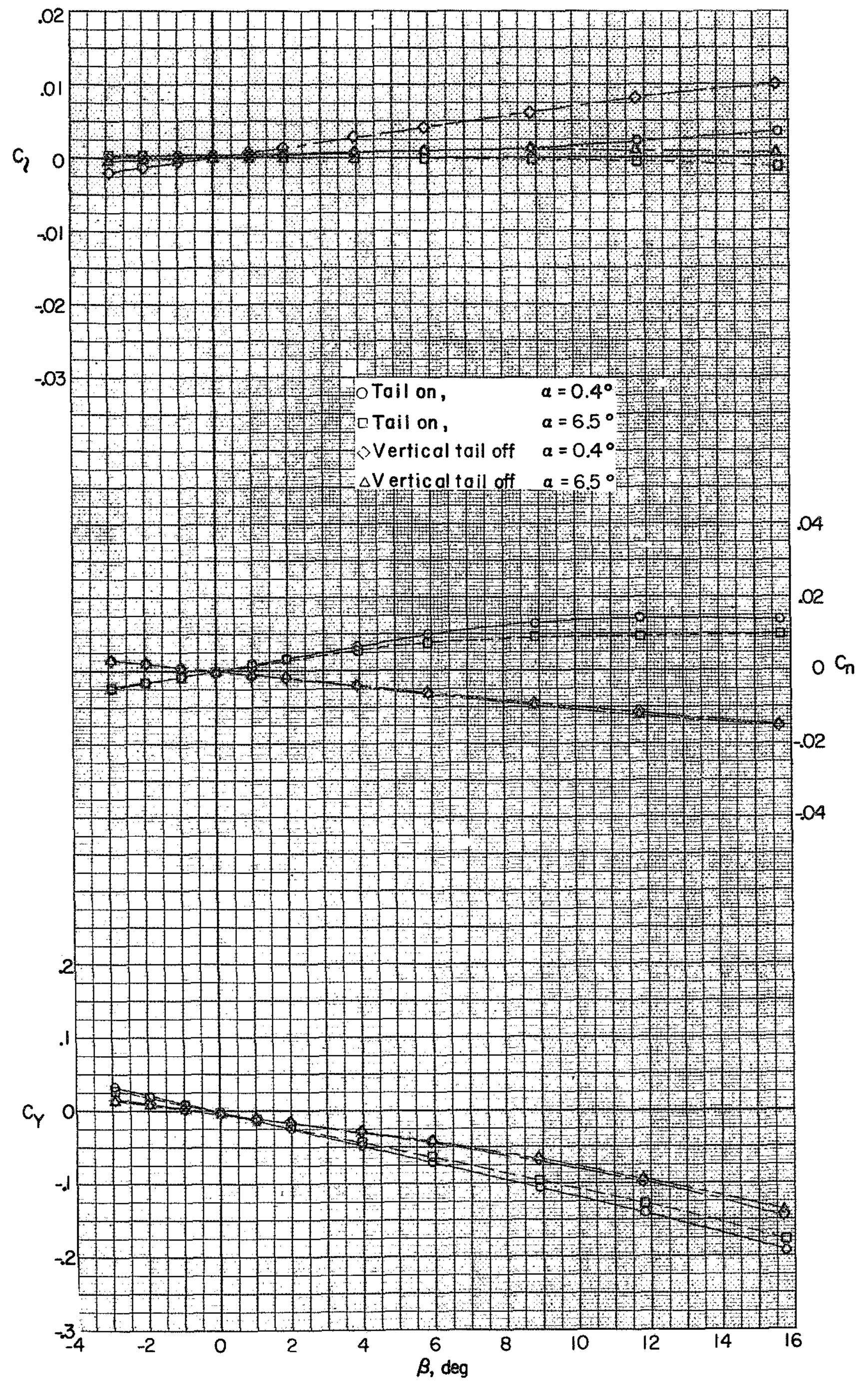

(c) M = 2.16.

Figure 15.- Continued.

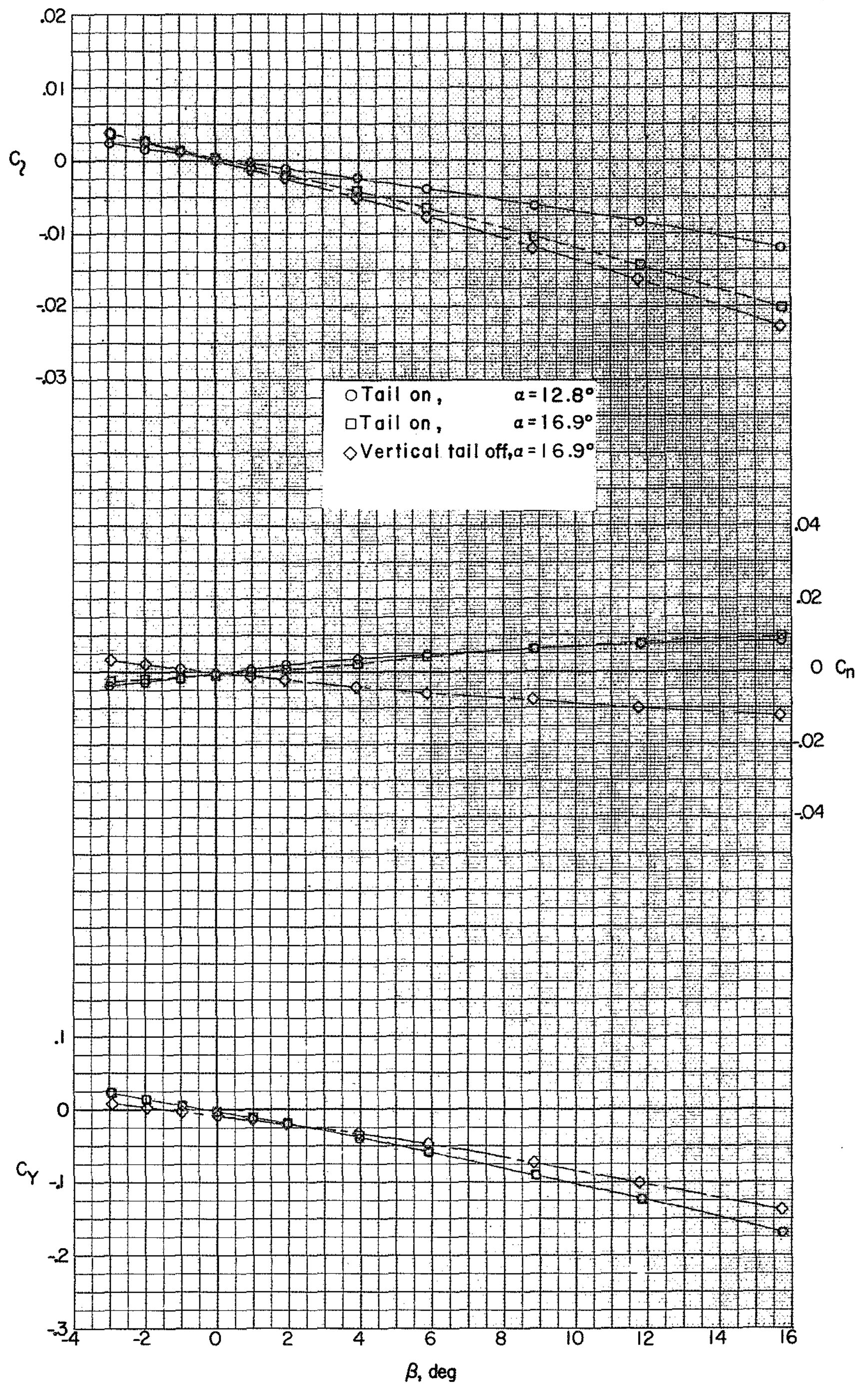

(c) Concluded.

Figure 15.- Continued.

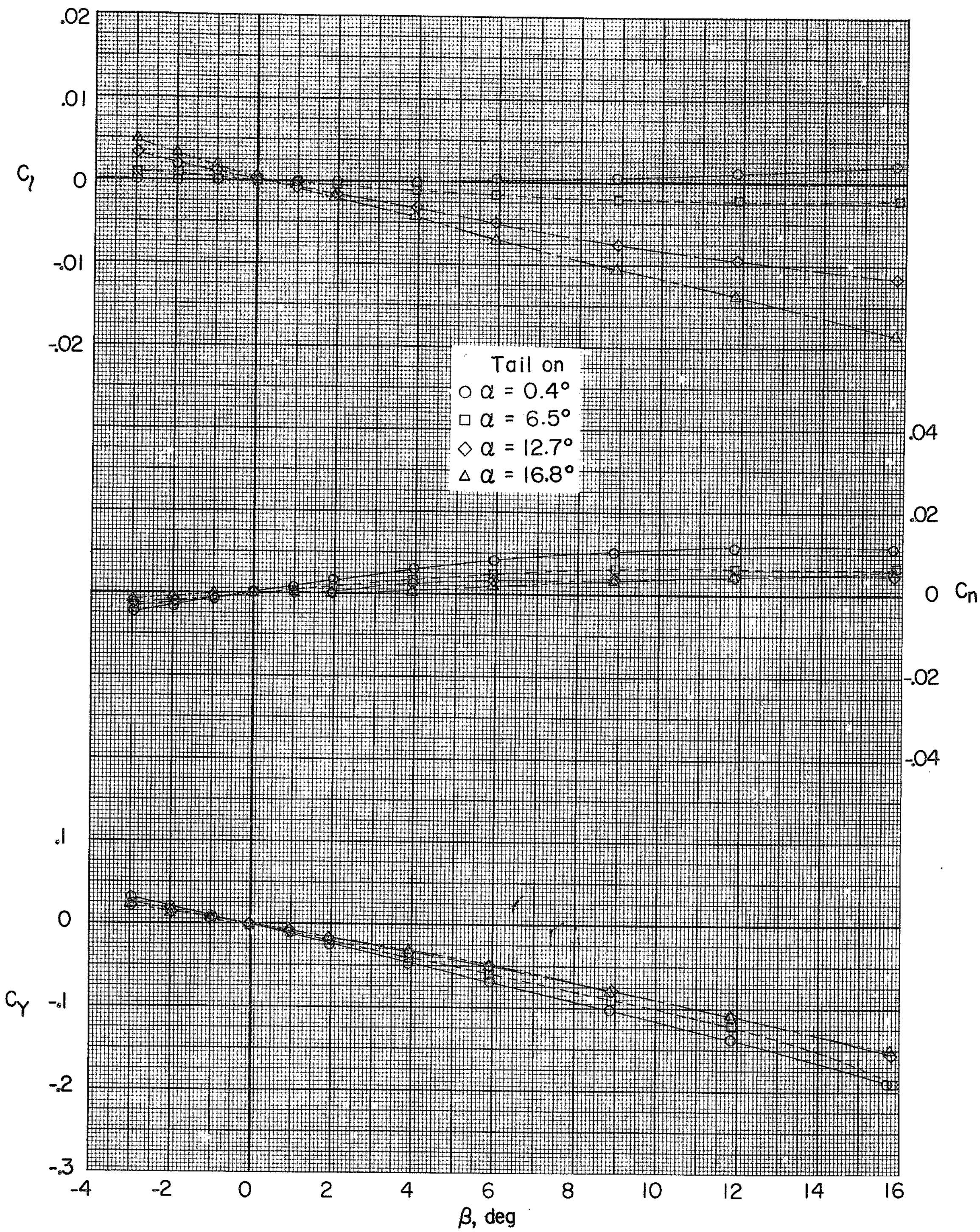

(d) M = 2.53.

Figure 15.- Concluded.

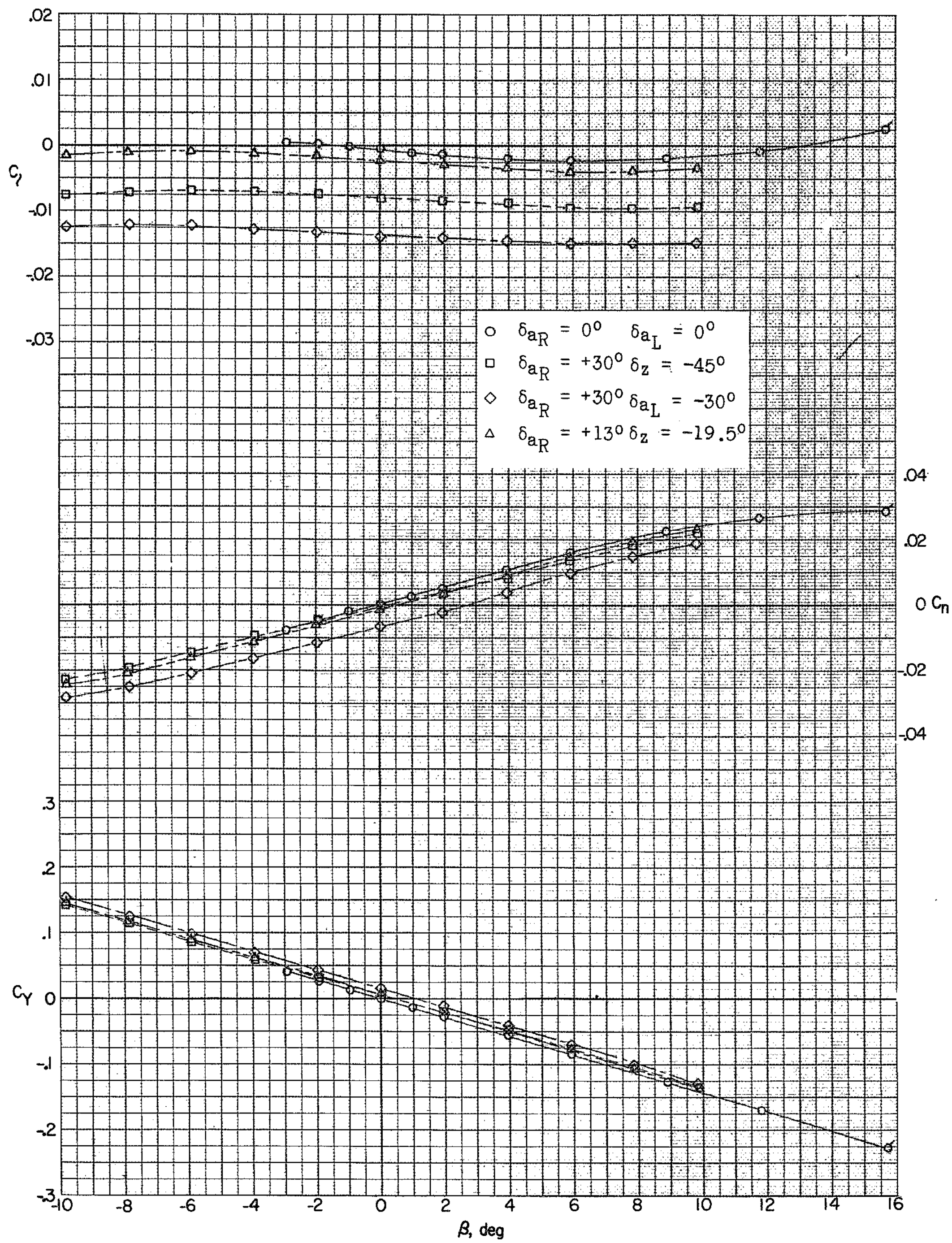

(a) $M = 1.57$; $\alpha = 0.4^\circ$.

Figure 16.- Effect of aileron and spoiler deflection on aerodynamic characteristics in sideslip. (Flagged symbols denote wall-reflected shock waves striking the tail.)

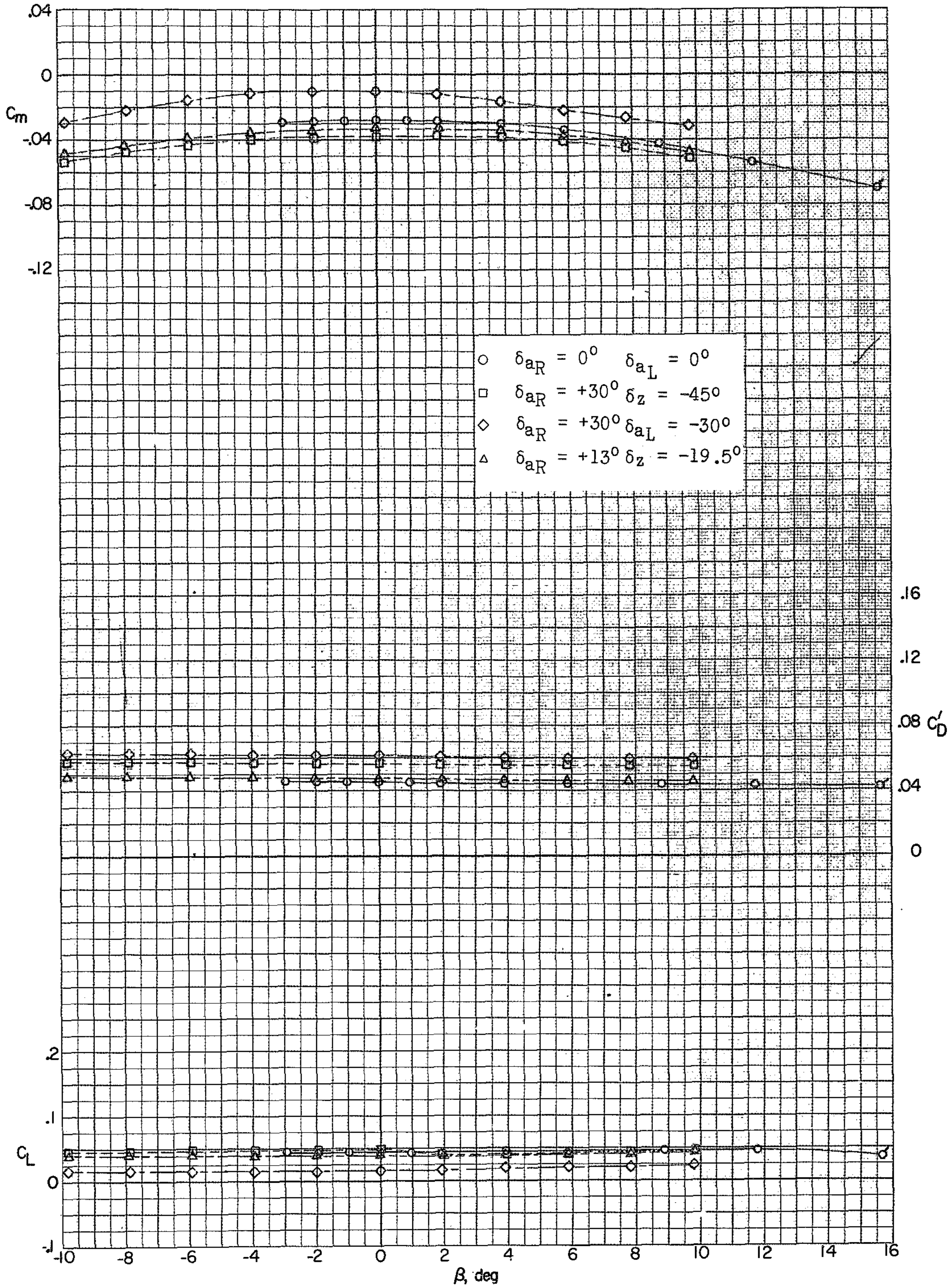

(a) Concluded.

Figure 16.- Continued.

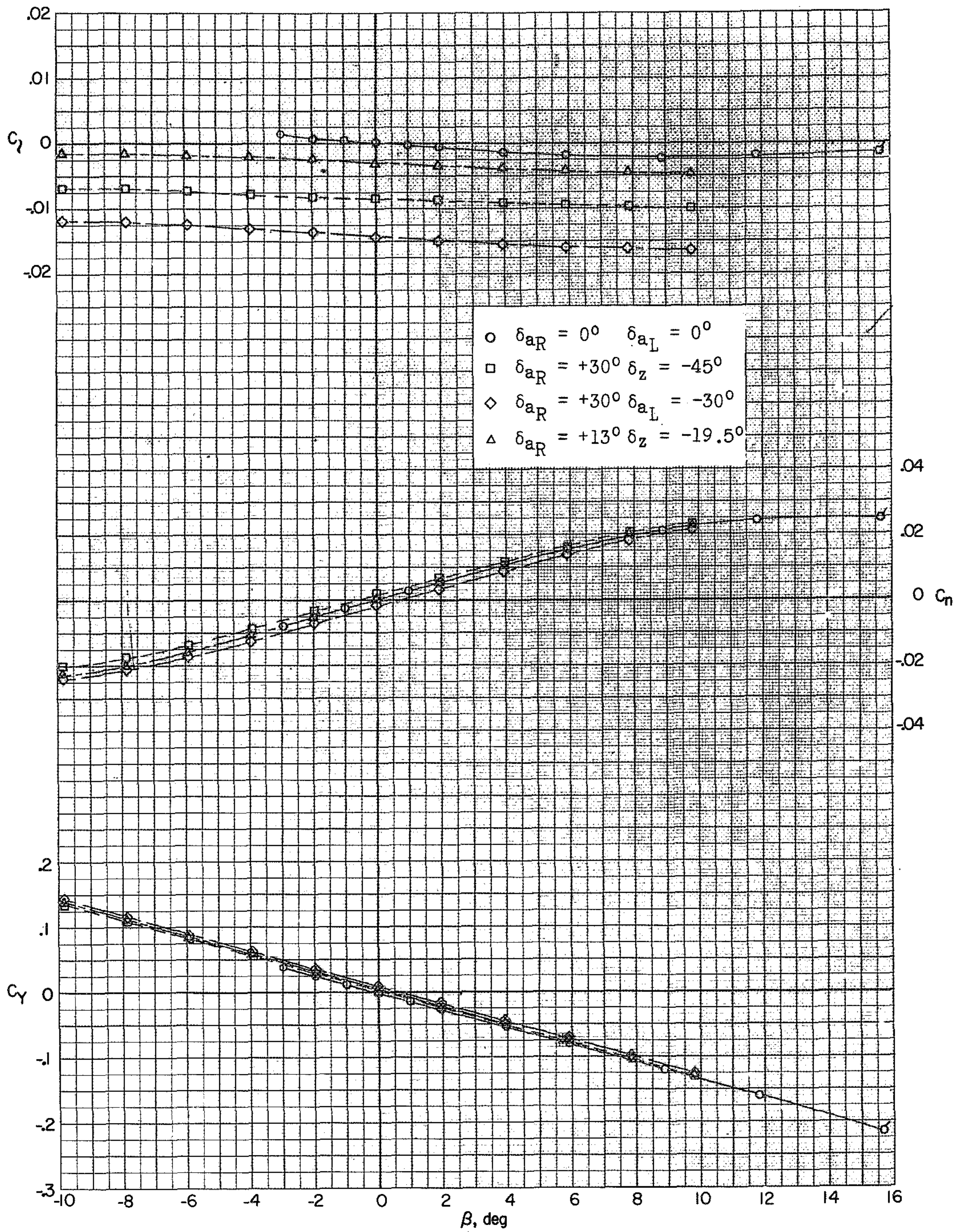

(b) $M = 1.57$; $\alpha = 6.7^\circ$.

Figure 16.- Continued.

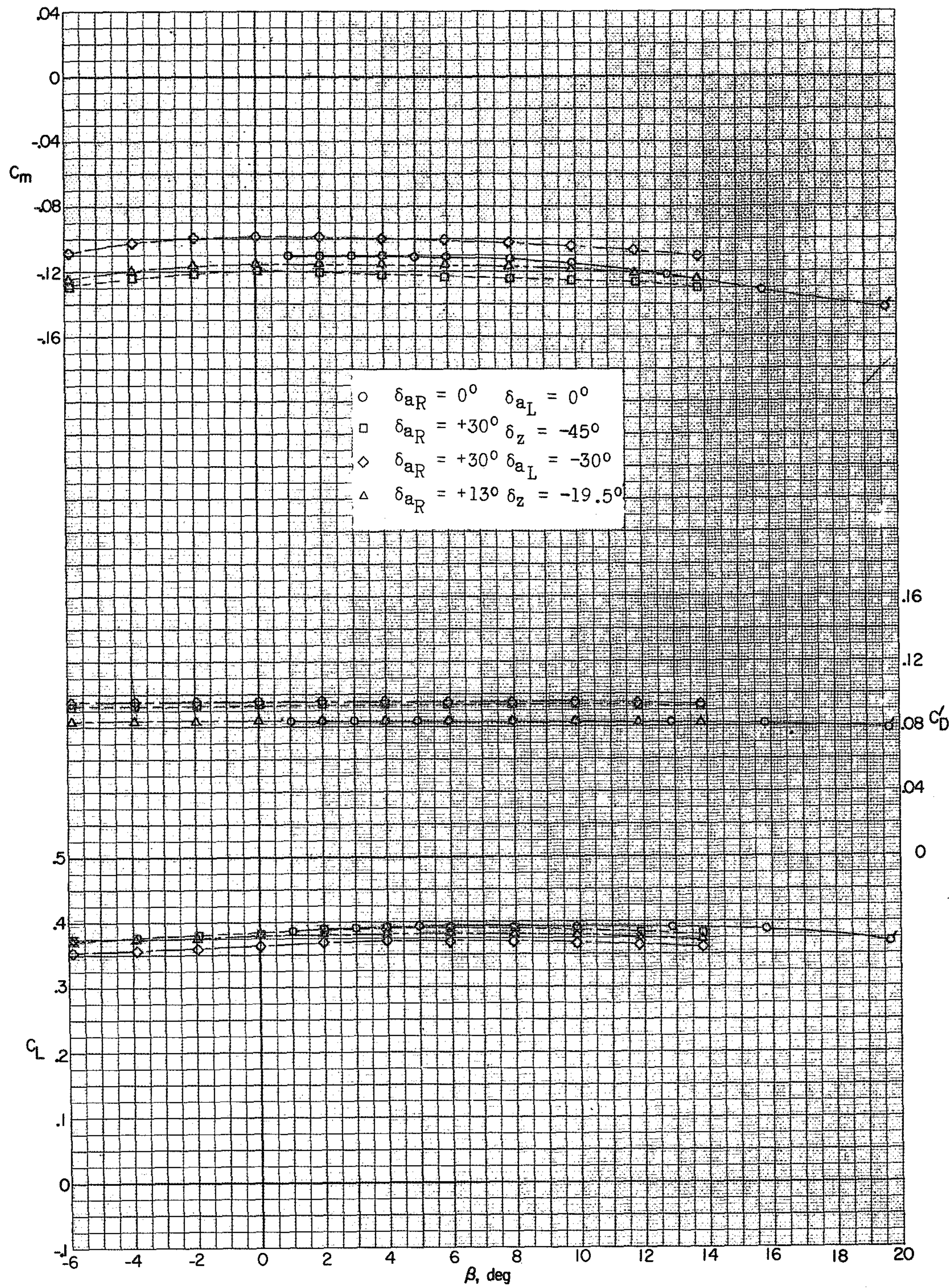

(b) Concluded.

Figure 16.- Continued.

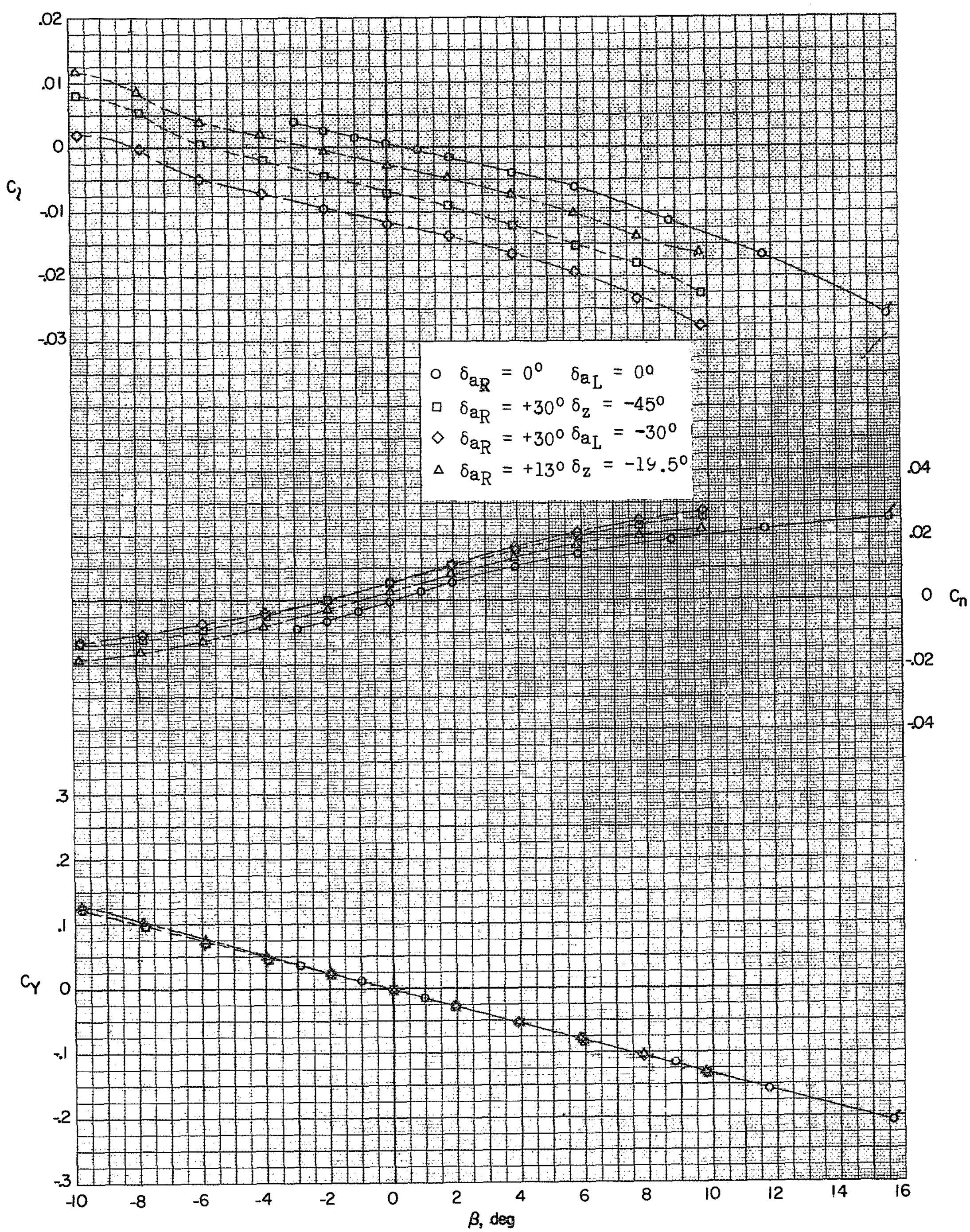

(c) M = 1.57; α = 17.4°.

Figure 16.- Continued.

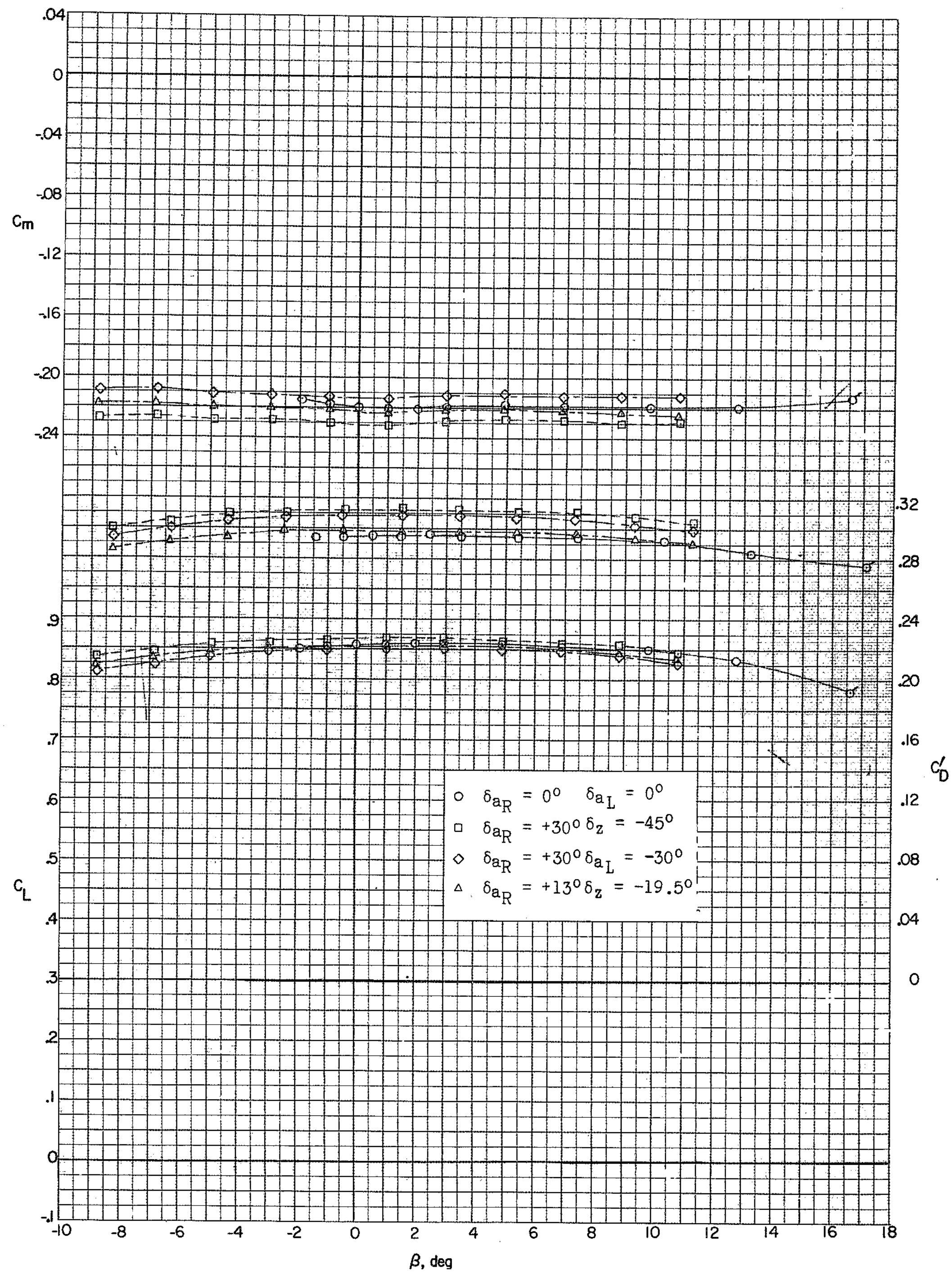

(c) Concluded.

Figure 16.- Continued.

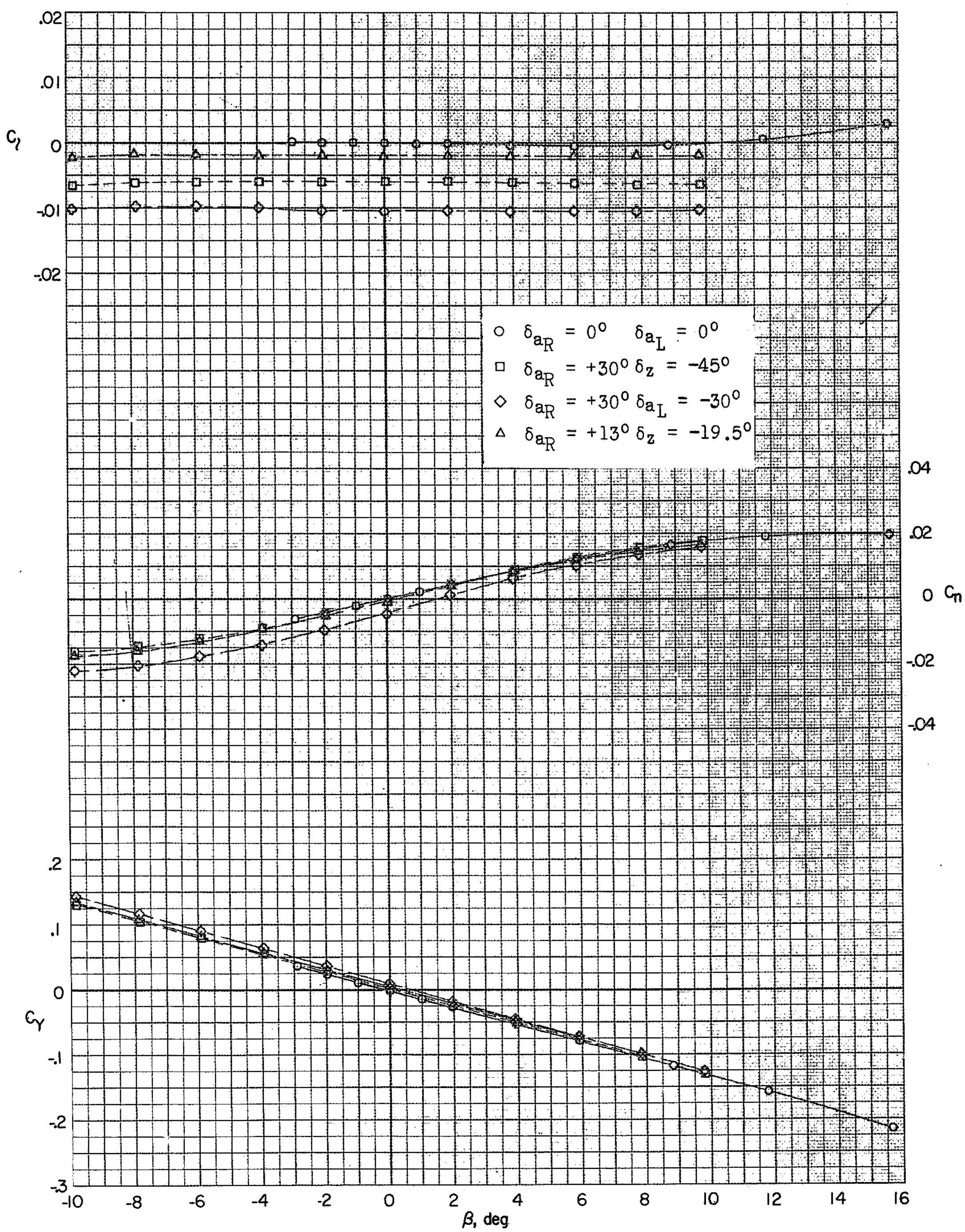

(d) $M = 1.87$; $\alpha = 0.4^\circ$.

Figure 16.- Continued.

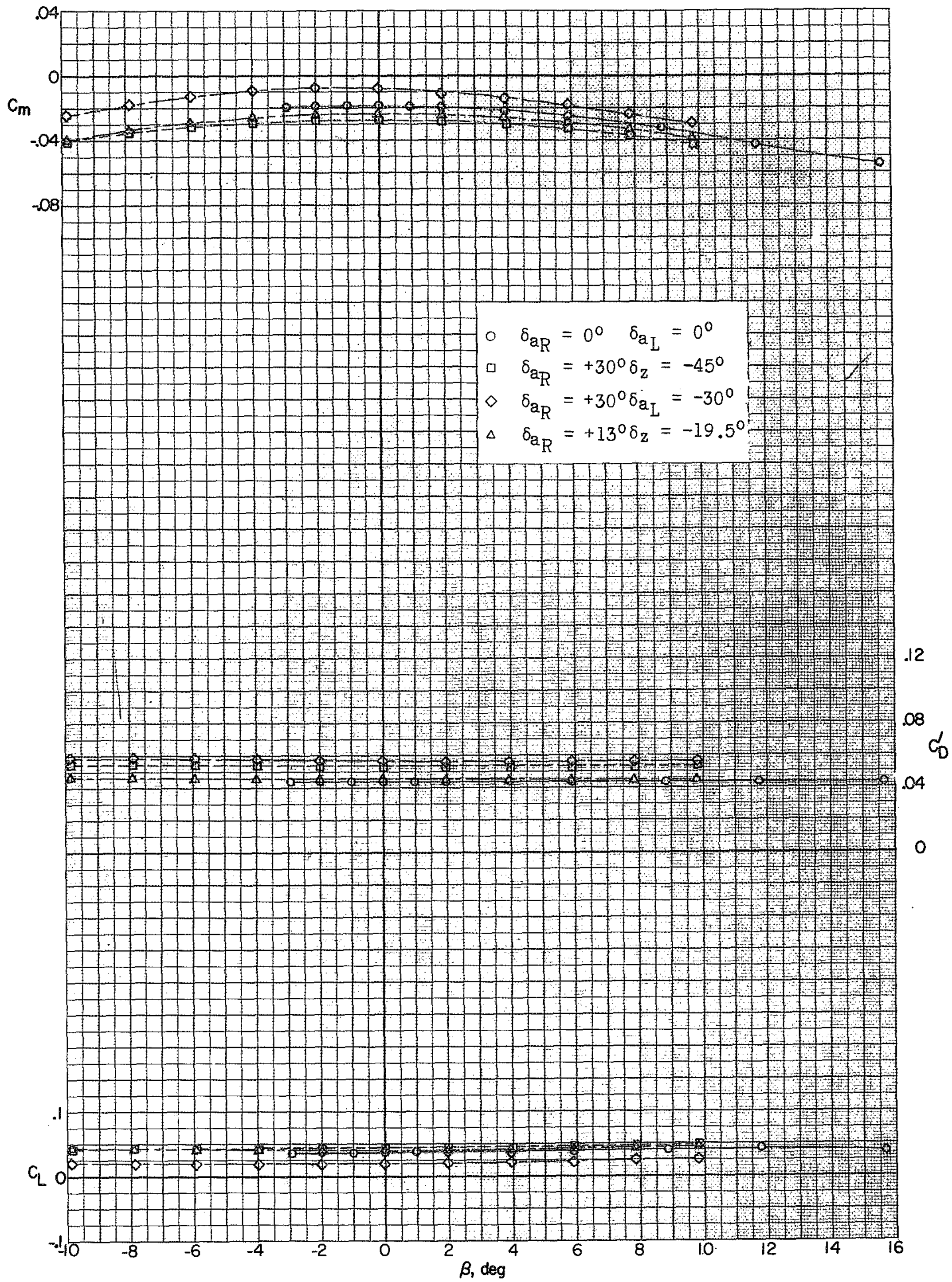

(d) Concluded.

Figure 16.- Continued.

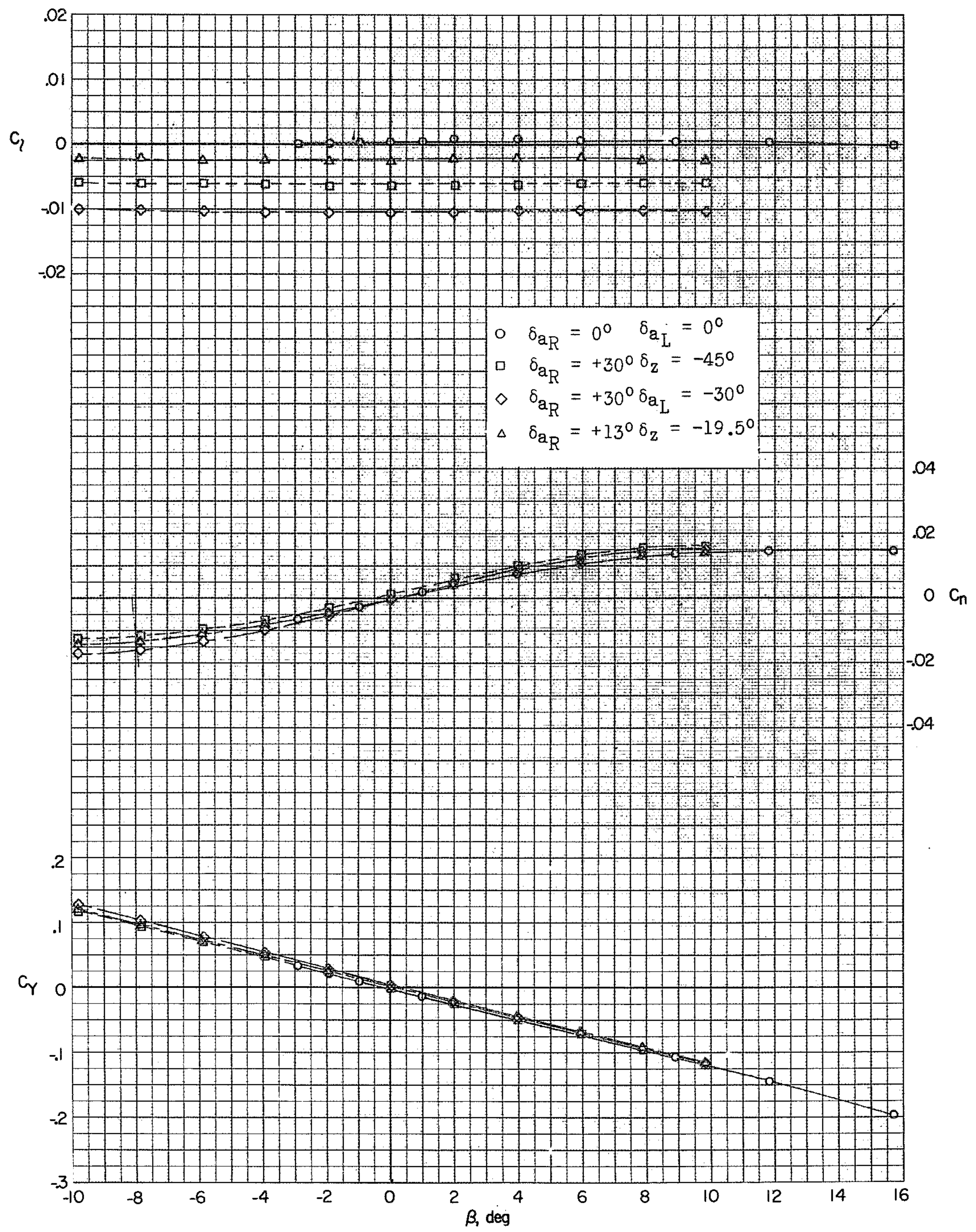

(e) $M = 1.87$; $\alpha = 6.6^{\circ}$.

Figure 16.- Continued.

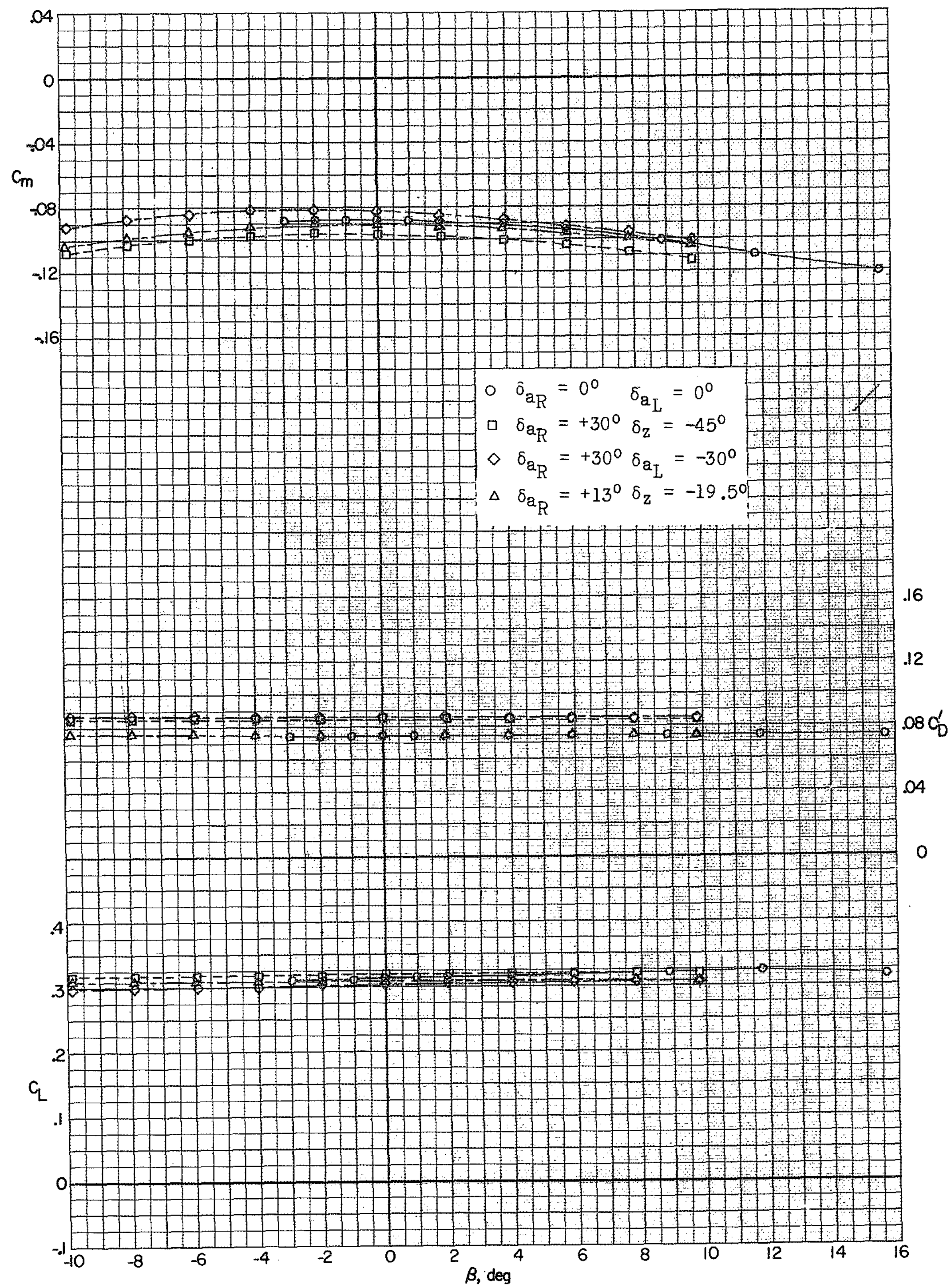

(e) Concluded.

Figure 16.- Continued.

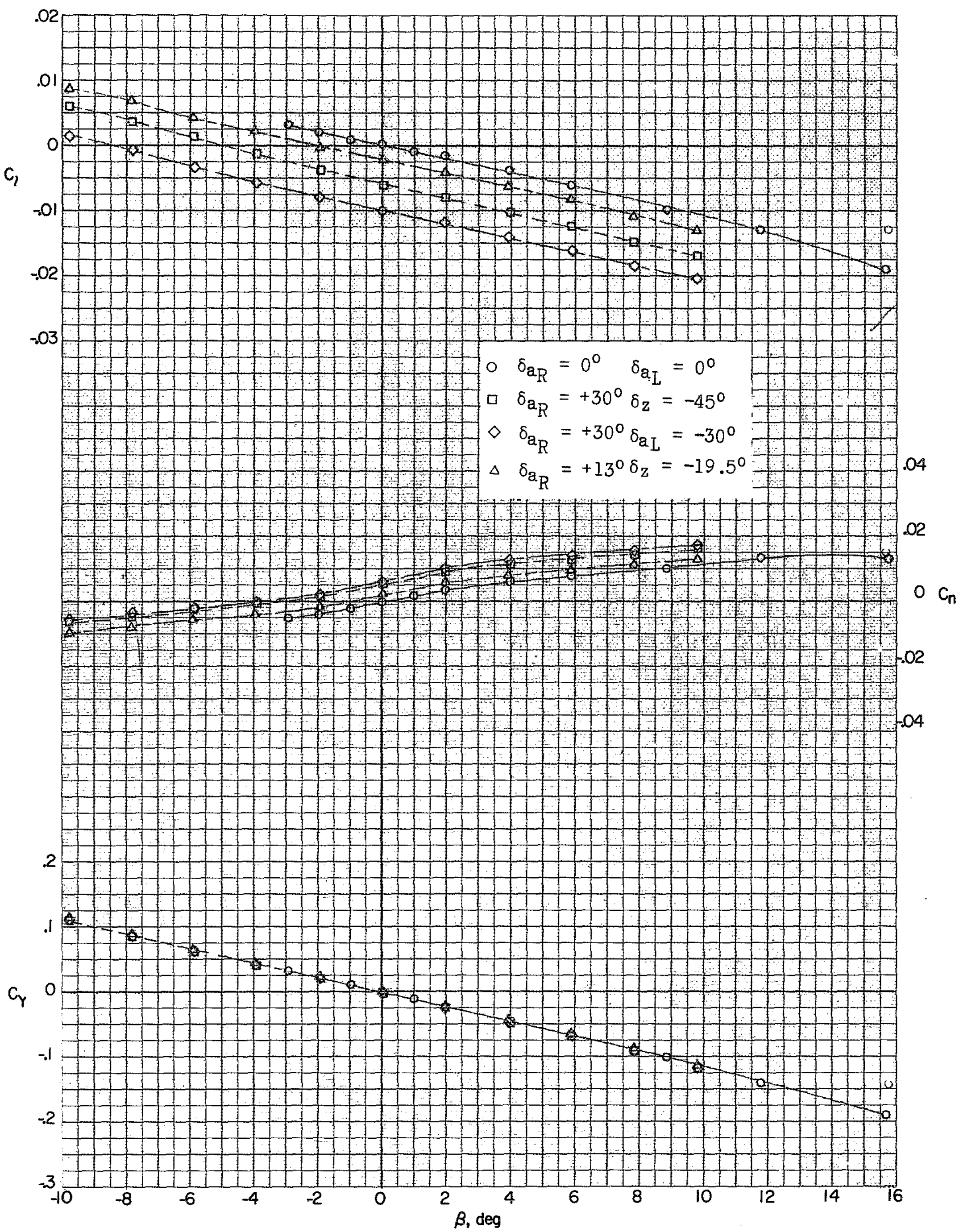

(f) $M = 1.87$; $\alpha = 17.1^{\circ}$.

Figure 16.- Continued.

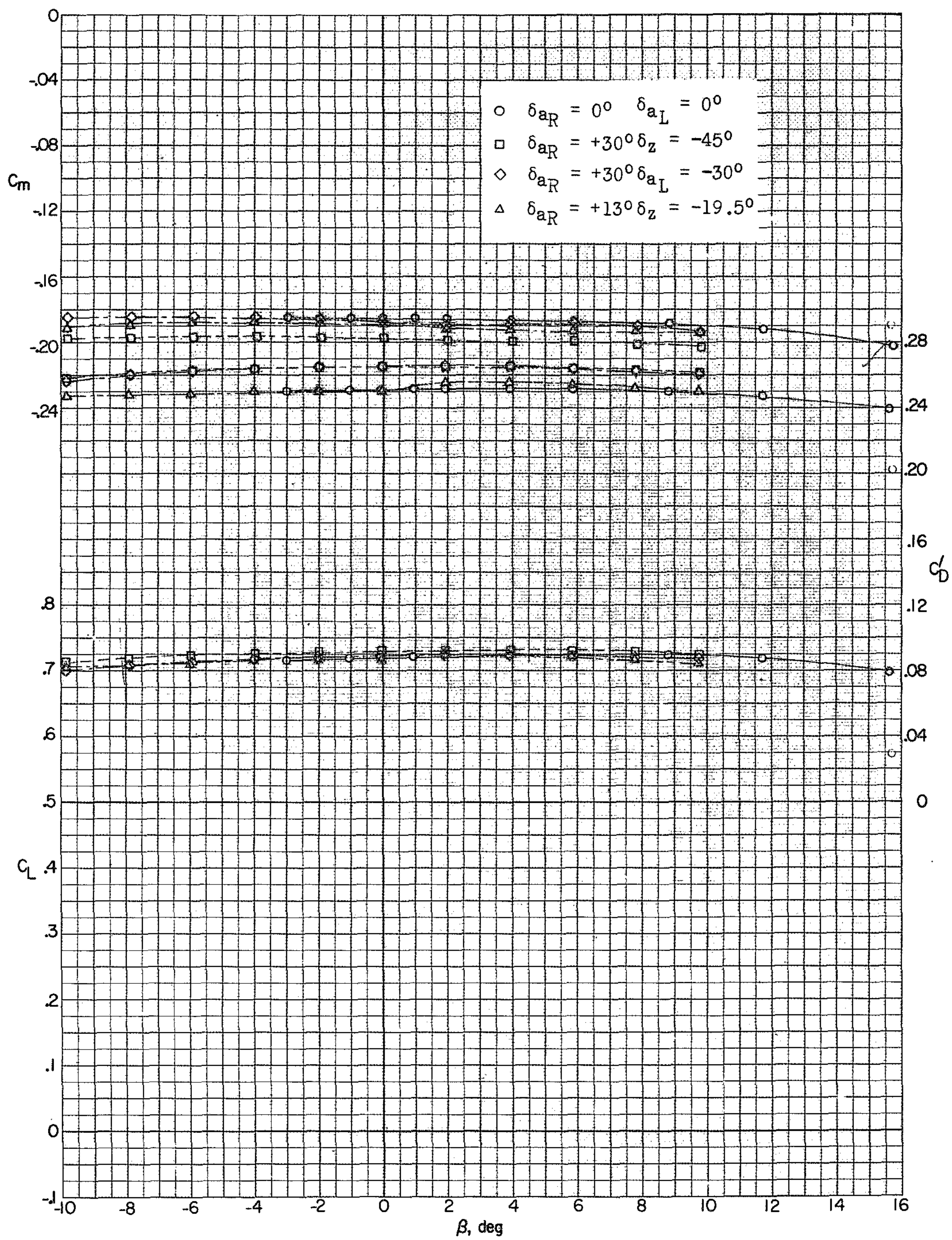

(f) Concluded.

Figure 16.- Continued.

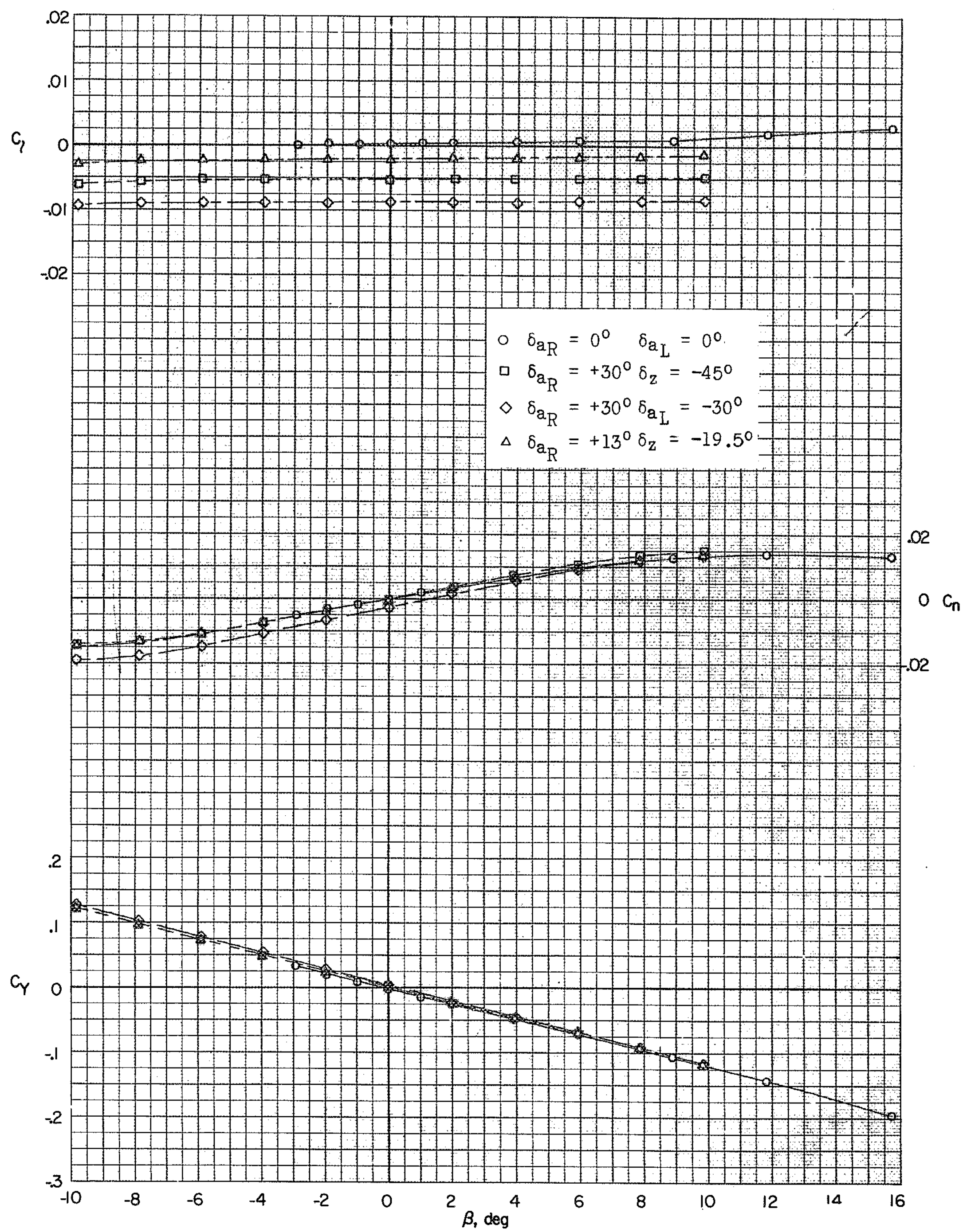

(g) M = 2.16. $\alpha = 0.4°$.

Figure 16.- Continued.

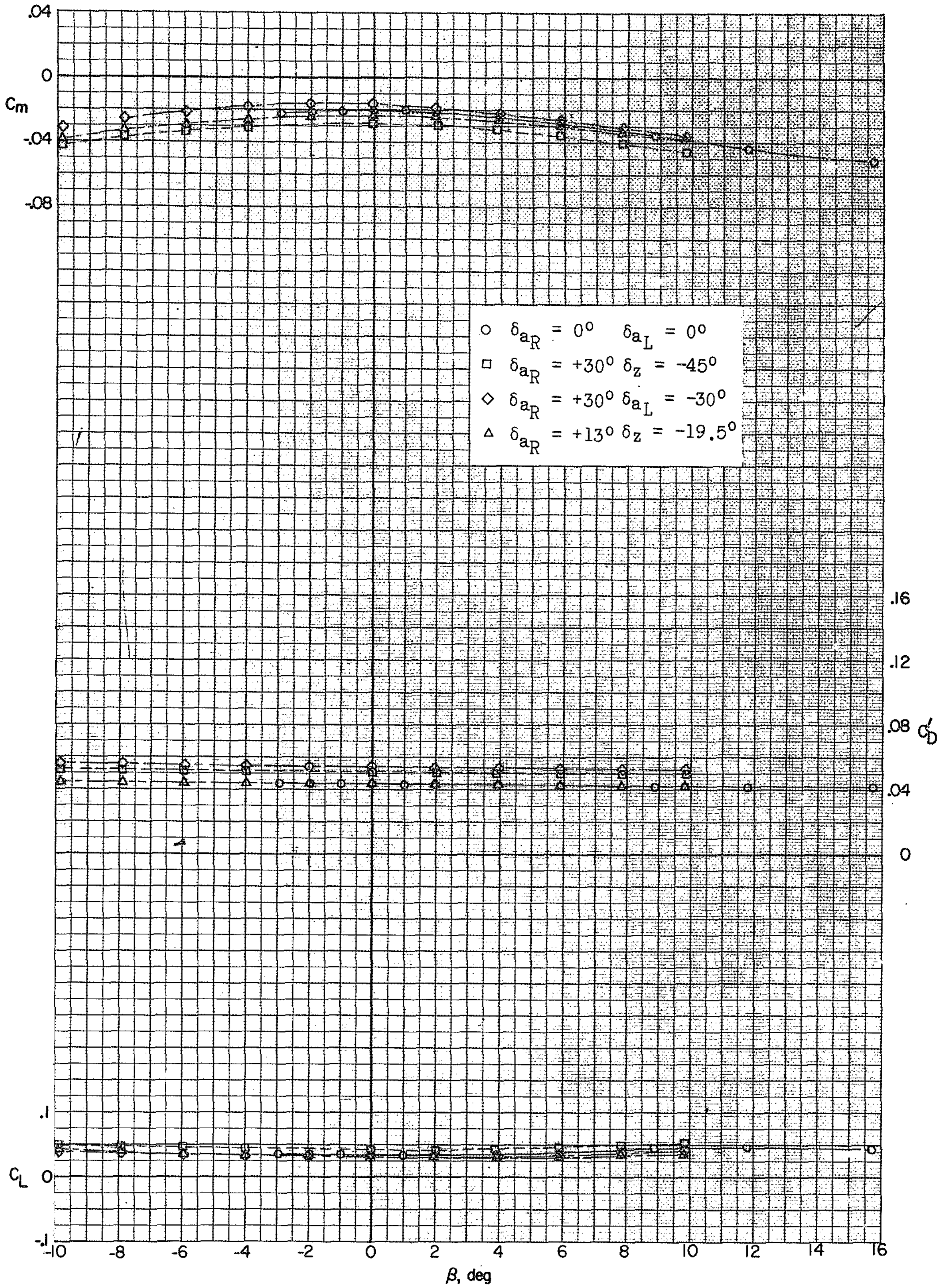

(g) Concluded.

Figure 16.- Continued.

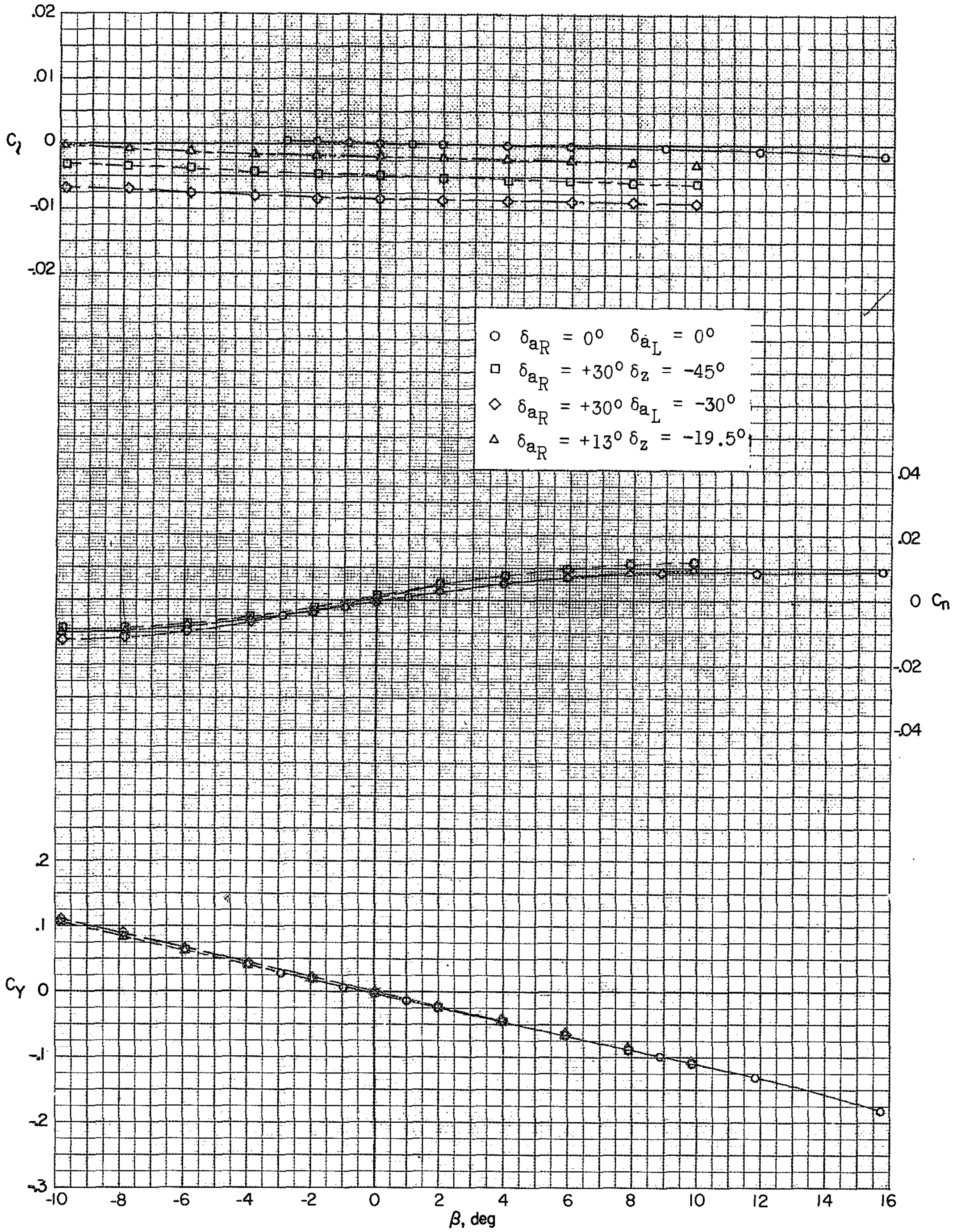

(h) $M = 2.16$; $\alpha = 6.5^\circ$.

Figure 16.- Continued.

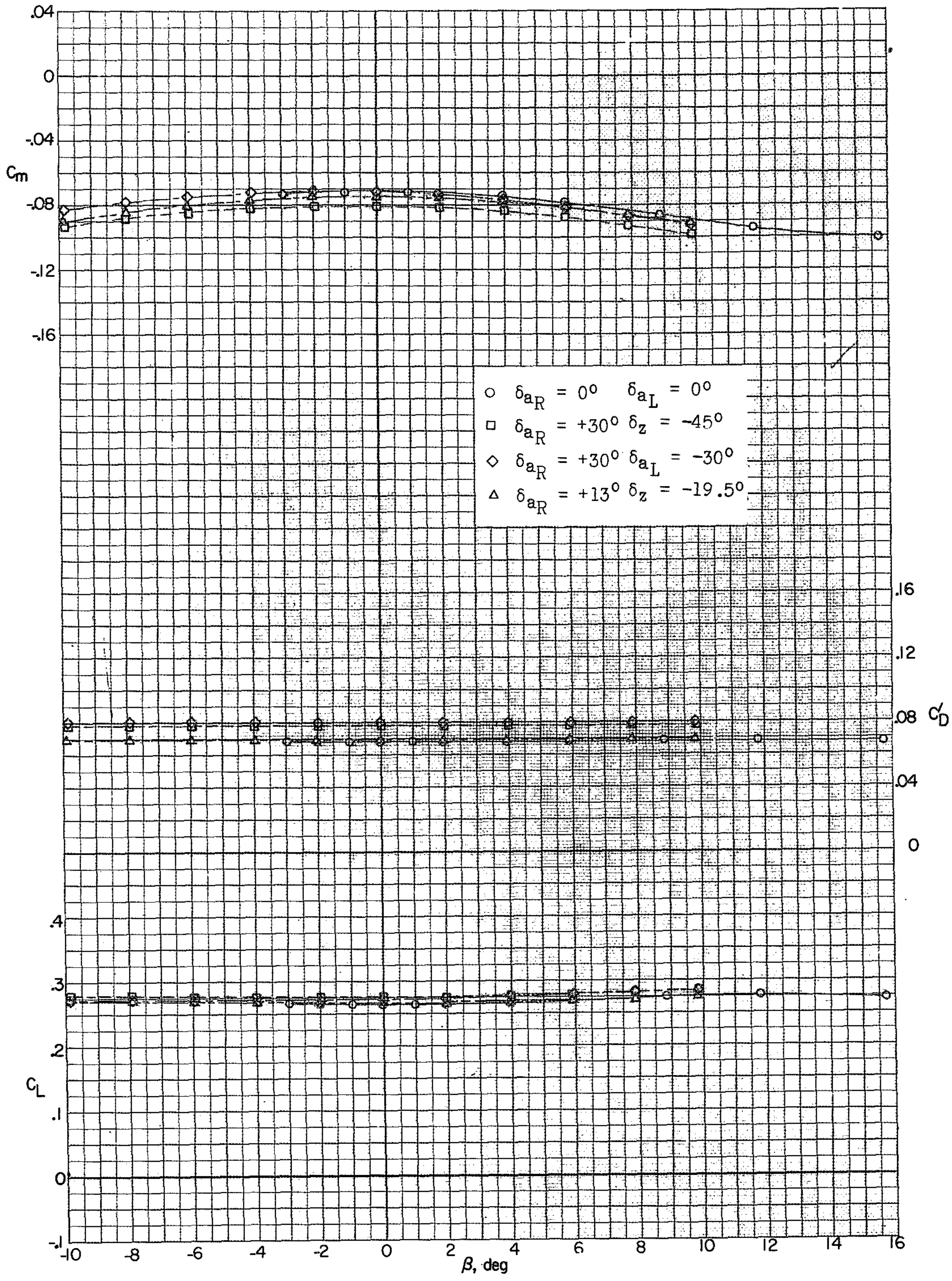

(h) Concluded.

Figure 16.- Continued.

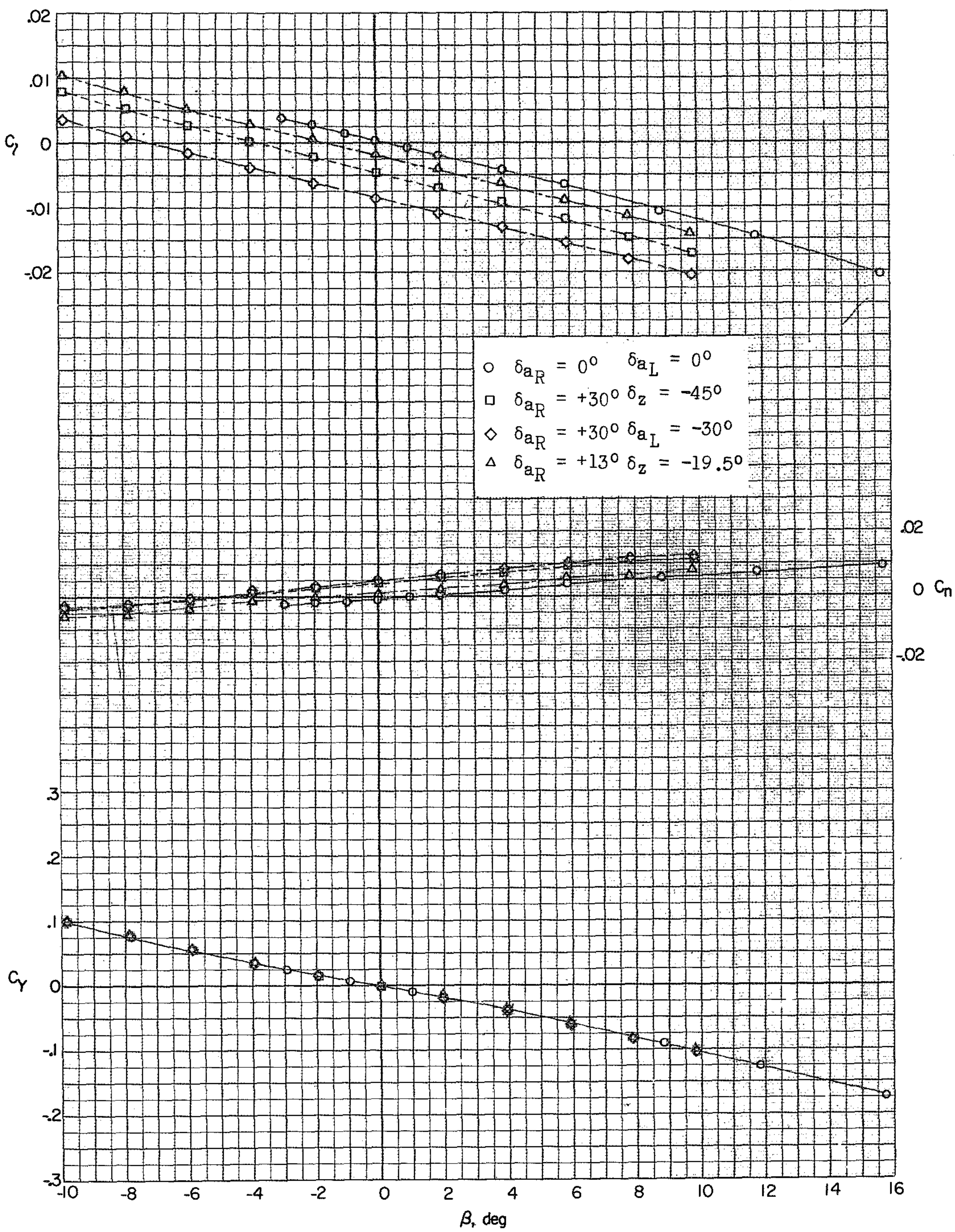

(i) $M = 2.16$; $\alpha = 16.9^\circ$.

Figure 16.- Continued.

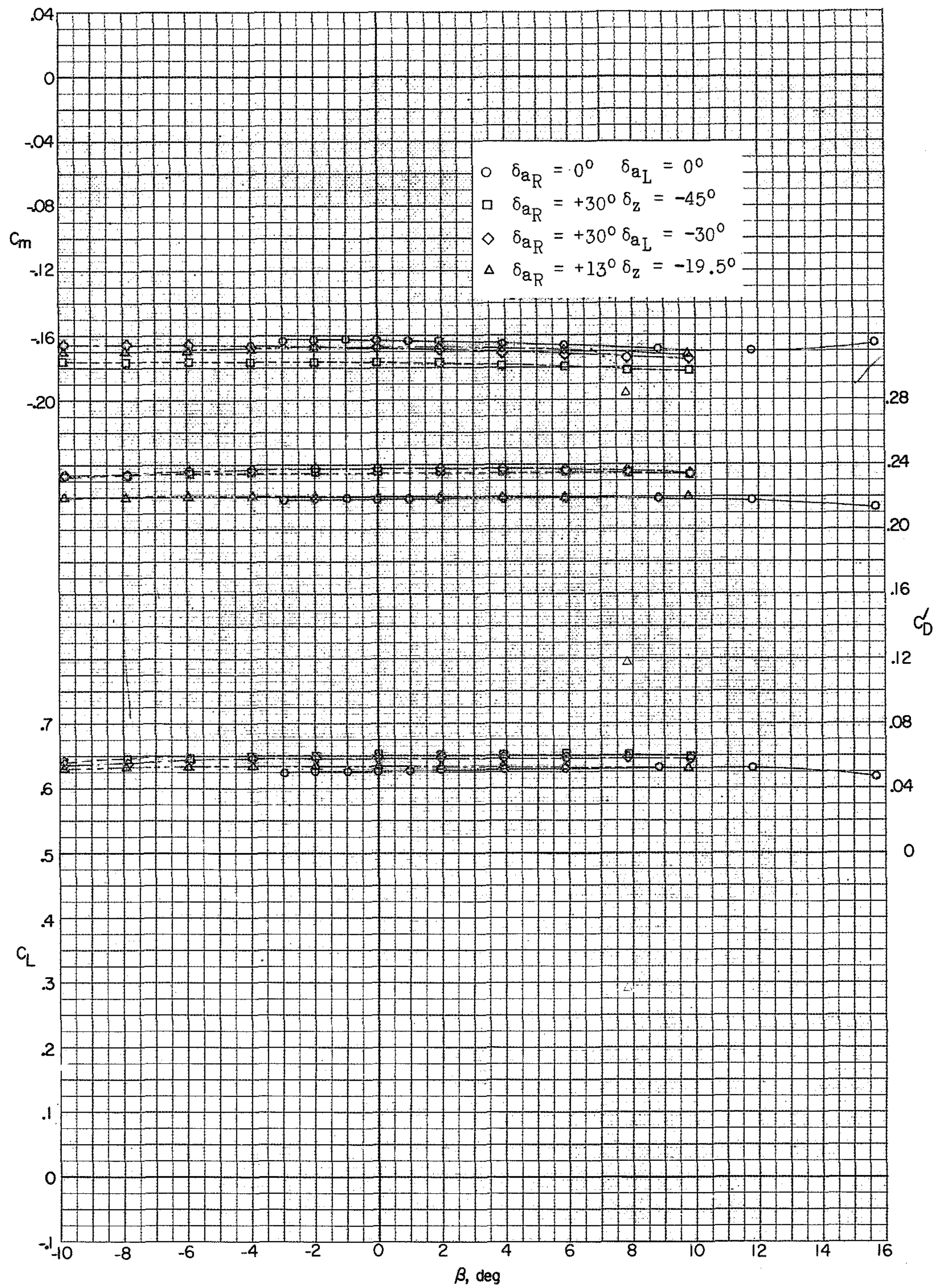

(i) Concluded.

Figure 16.- Concluded.

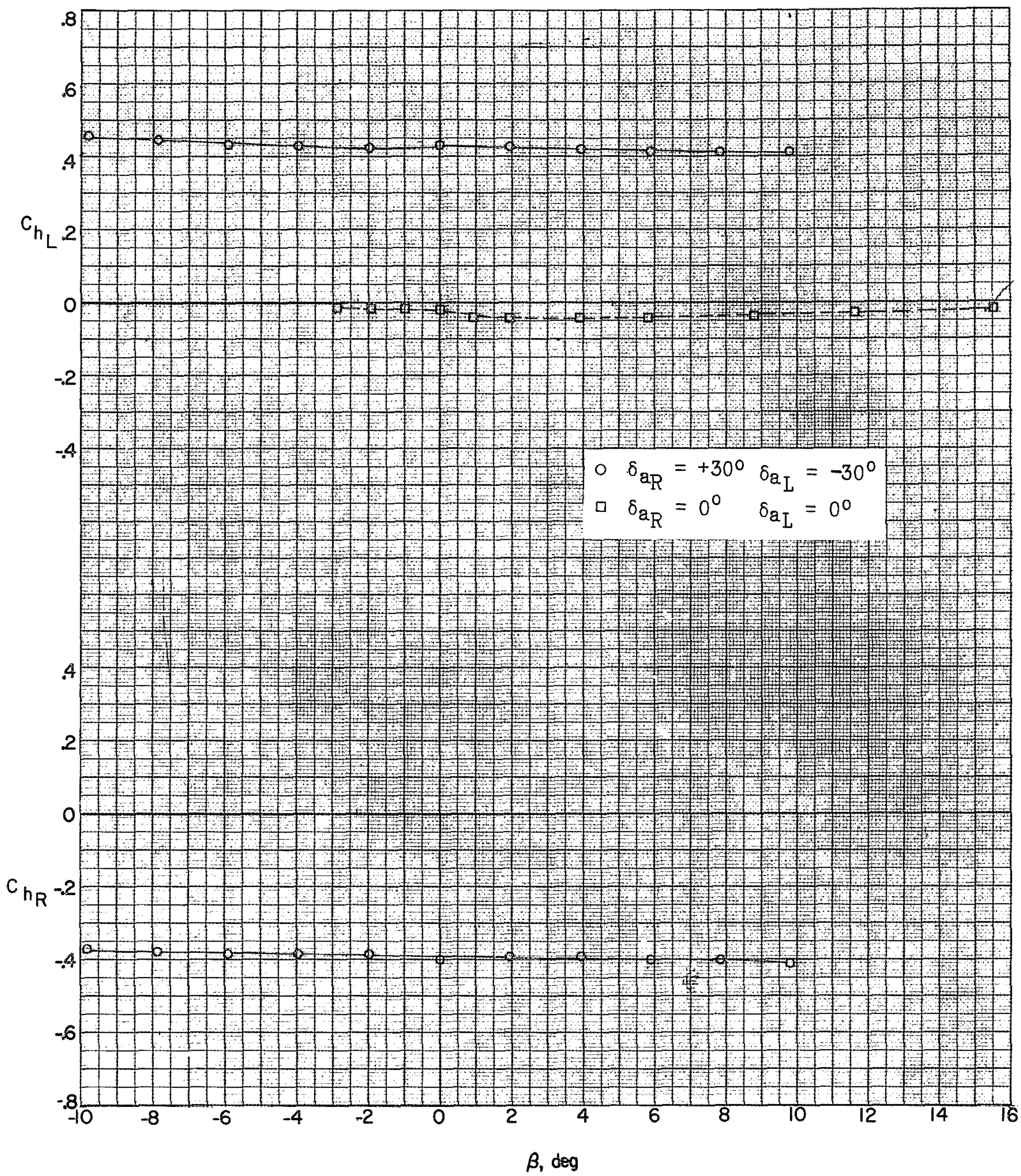

(a) $M = 1.57$; $\alpha = 0.4^{\circ}$.

Figure 17.- Effect of aileron deflection on aileron hinge-moment coefficient in sideslip.

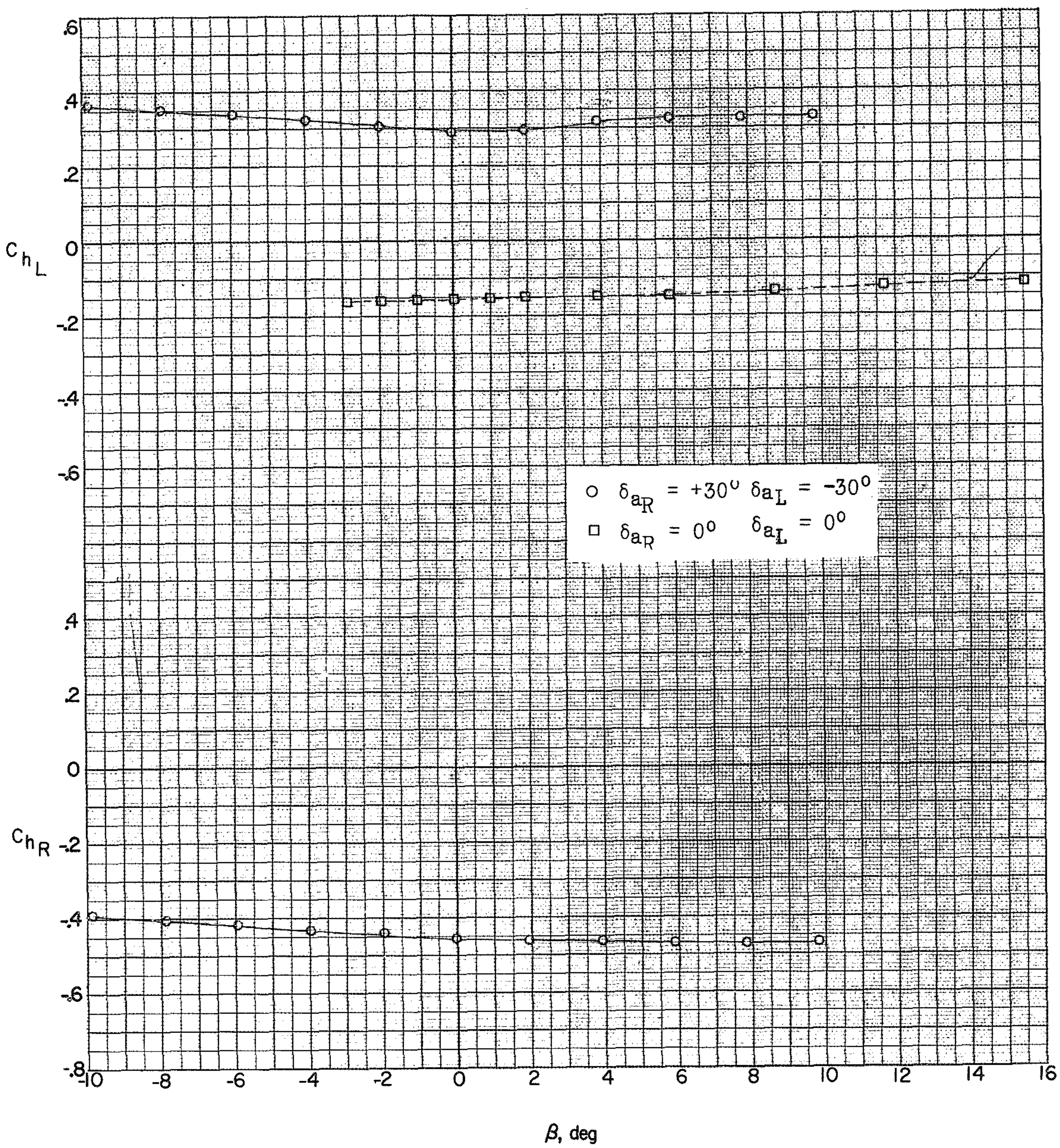

(b) $M = 1.57$; $\alpha = 6.7^\circ$.

Figure 17.- Continued.

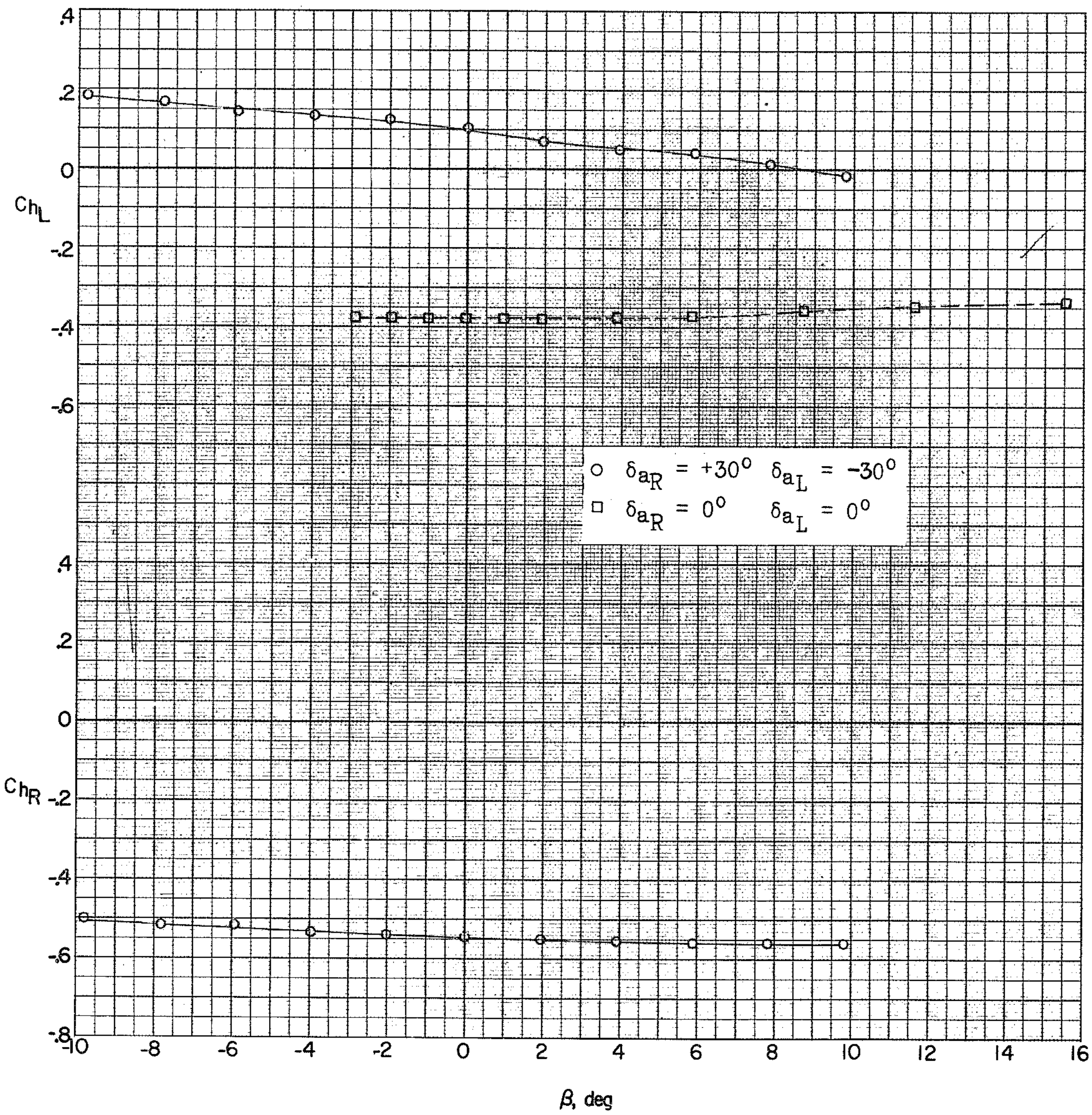

(c) M = 1.57; α = 17.4°.

Figure 17.- Continued.

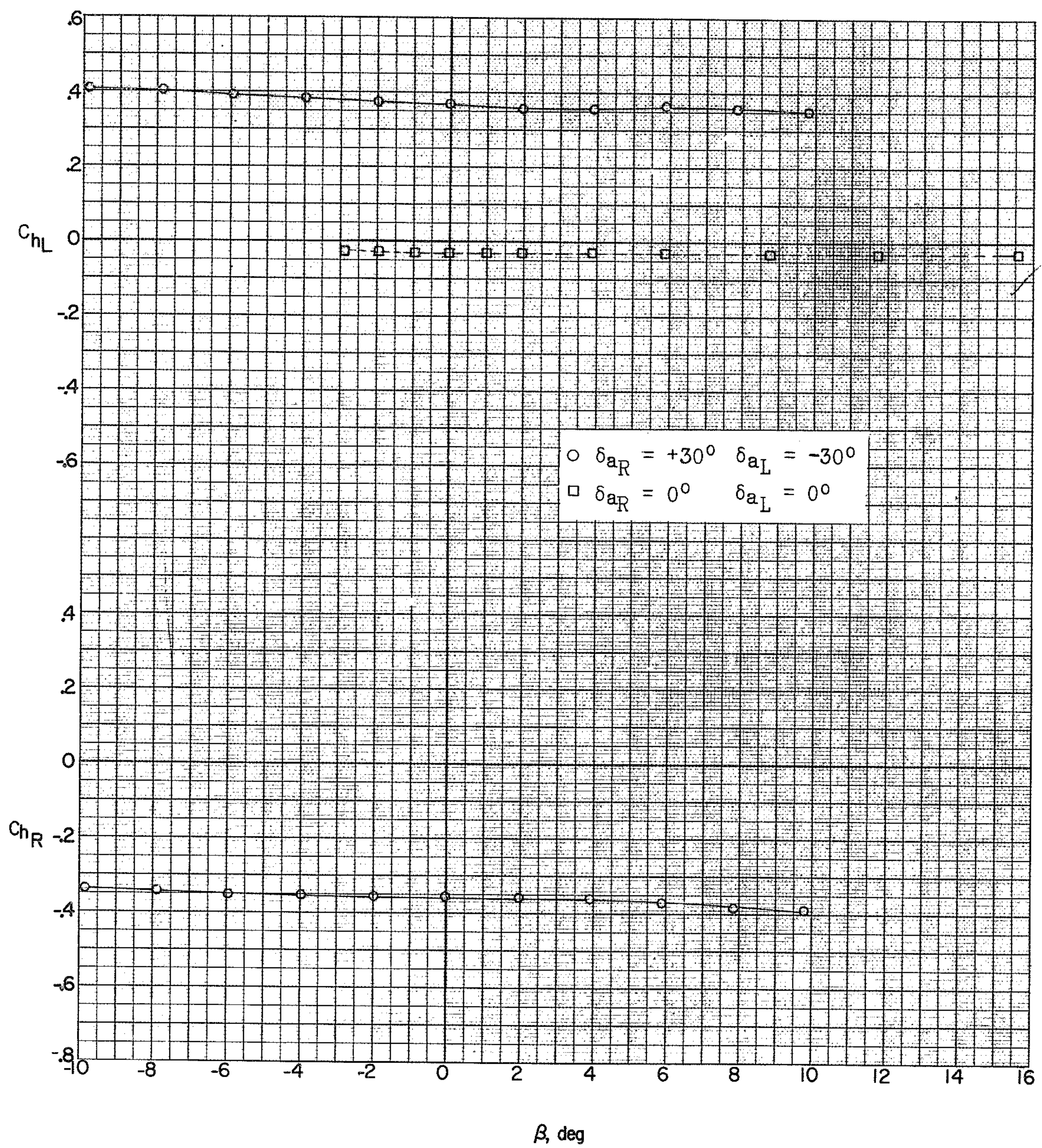

(d) $M = 1.87$; $\alpha = 0.4^\circ$.

Figure 17.- Continued.

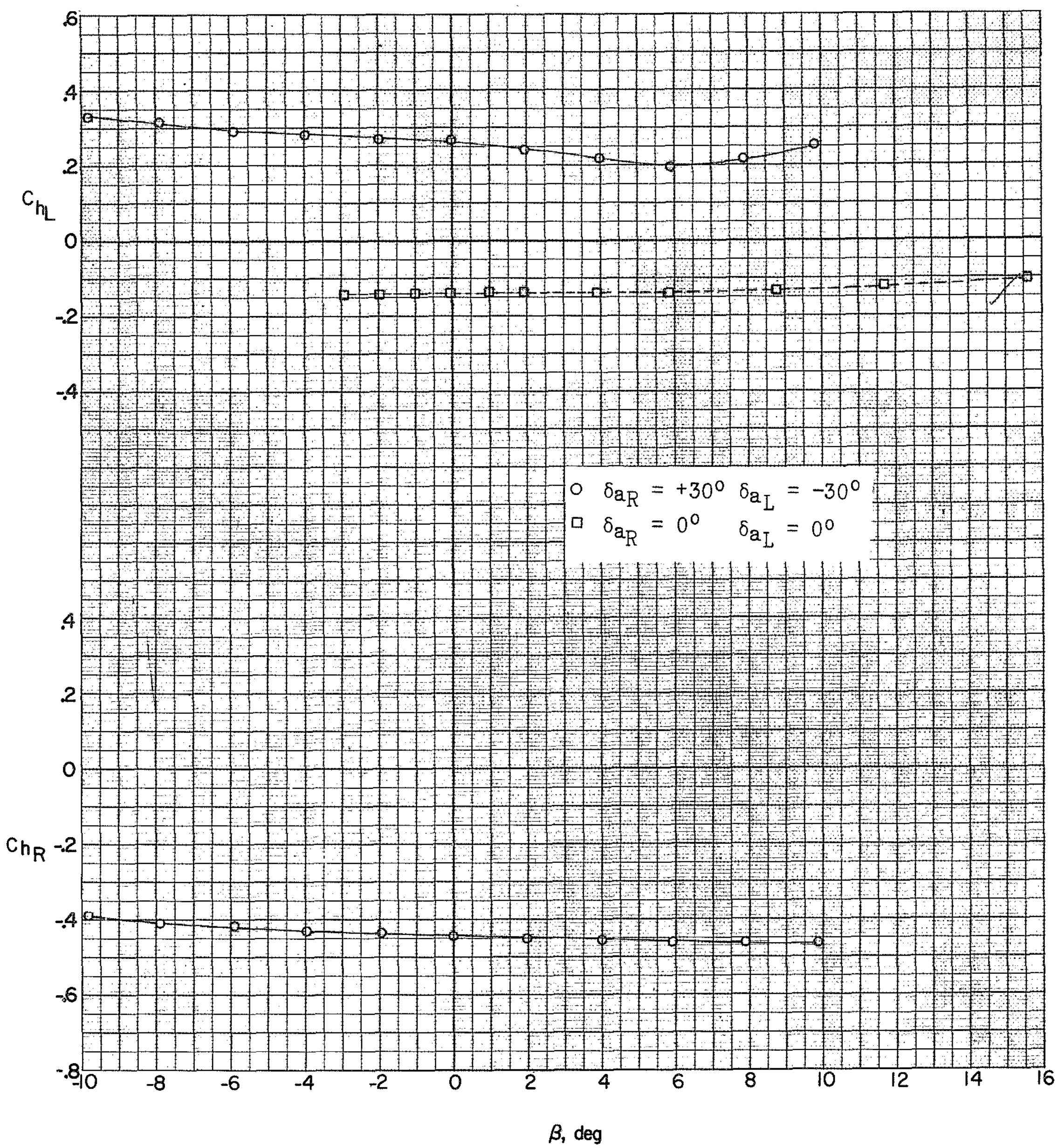

(e) $M = 1.87$; $\alpha = 6.6^\circ$.

Figure 17.- Continued.

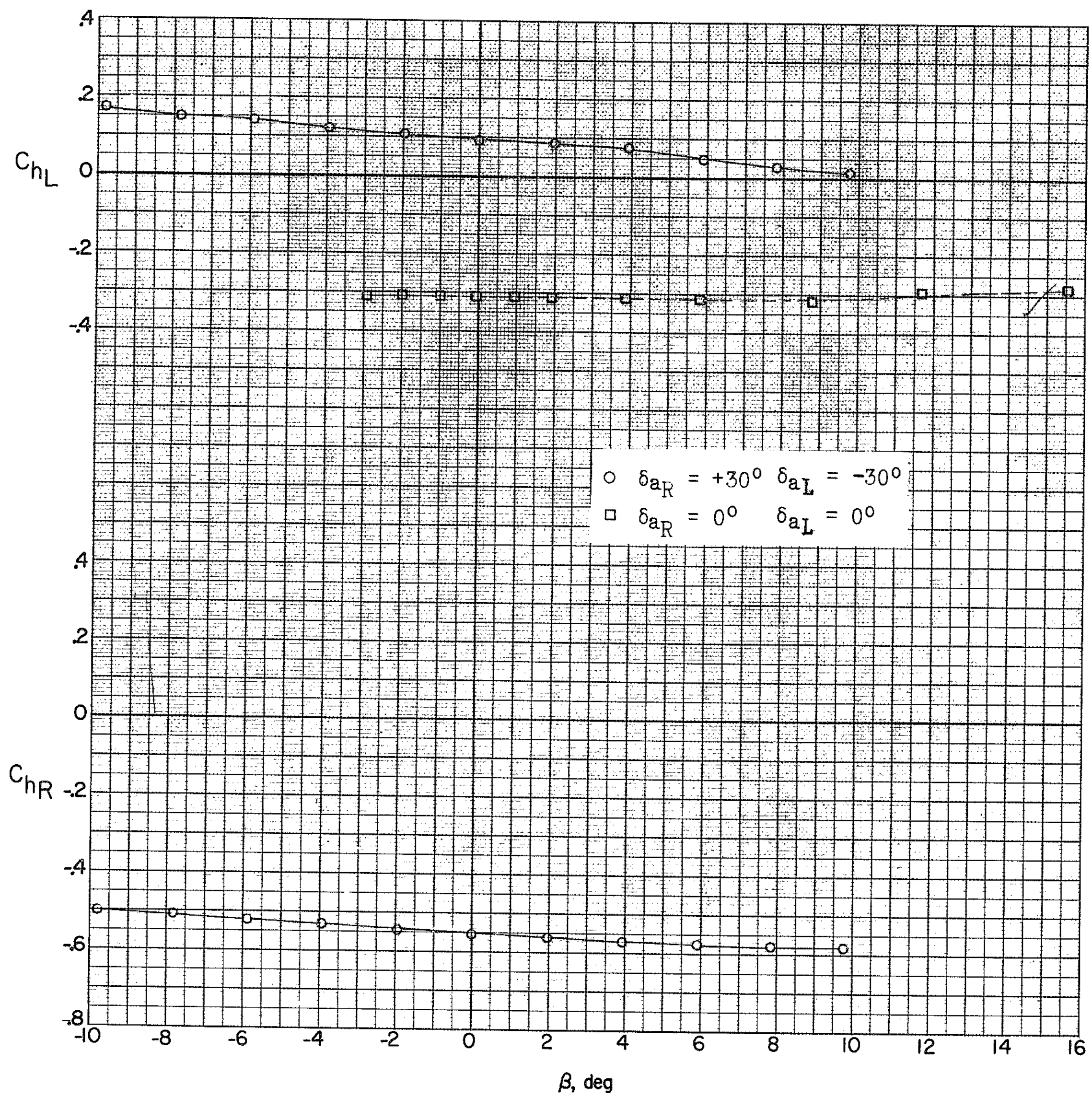

(f) M = 1.87; α = 17.1°.

Figure 17.- Continued.

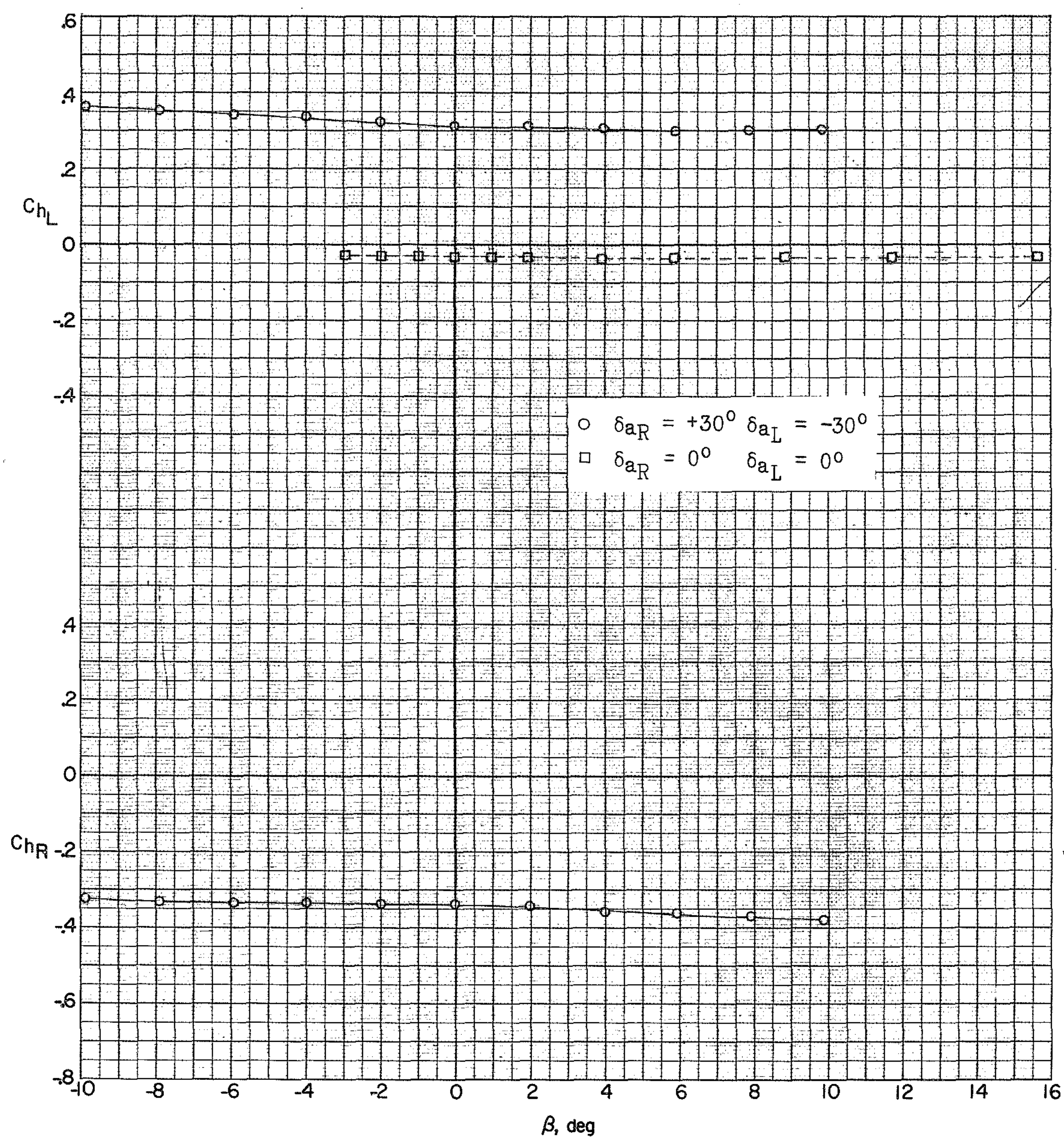

(g) $M = 2.16$; $\alpha = 0.4^{\circ}$.

Figure 17.- Continued.

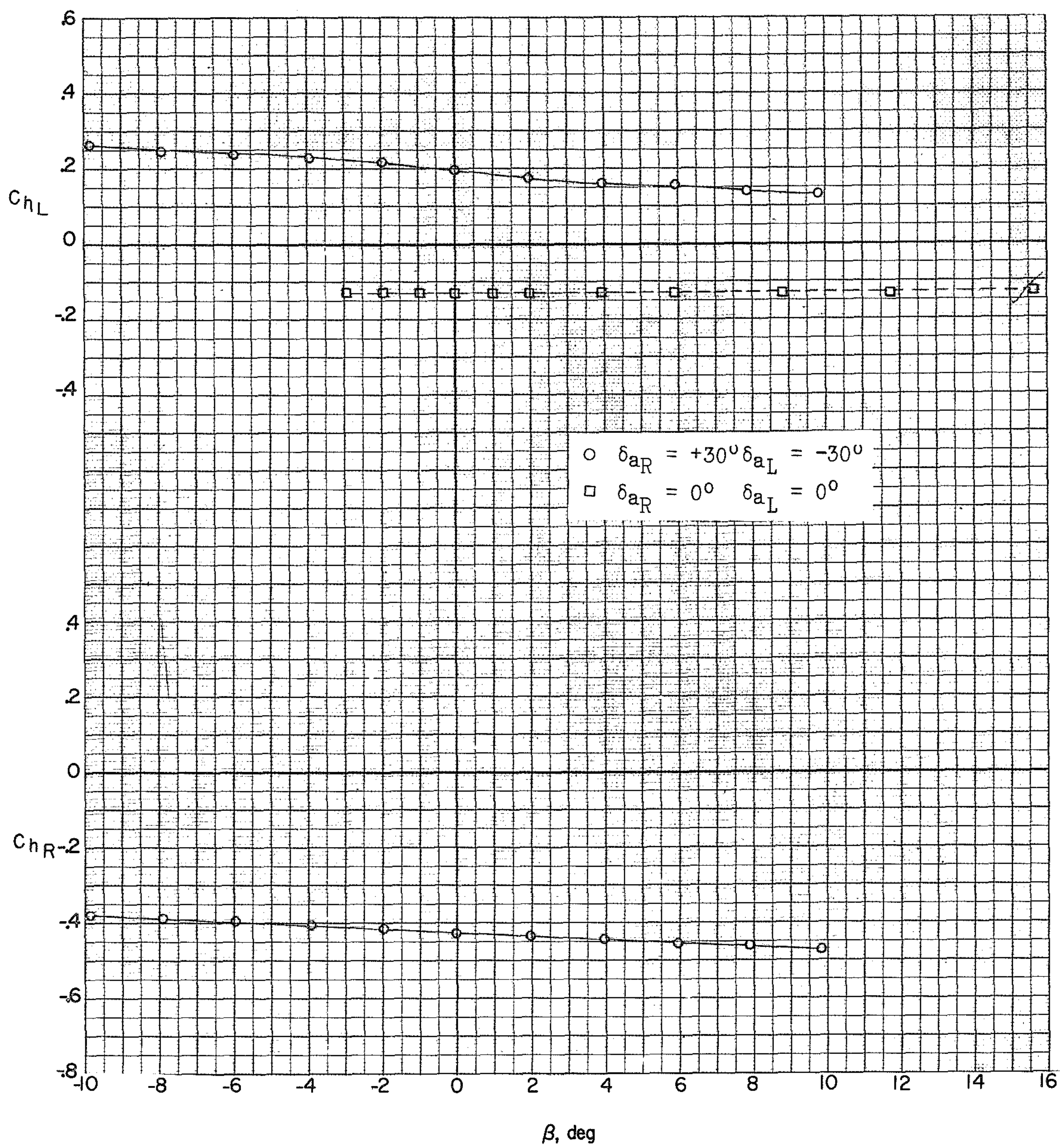

(h) $M = 2.16$; $\alpha = 6.5^{\circ}$.

Figure 17.- Continued.

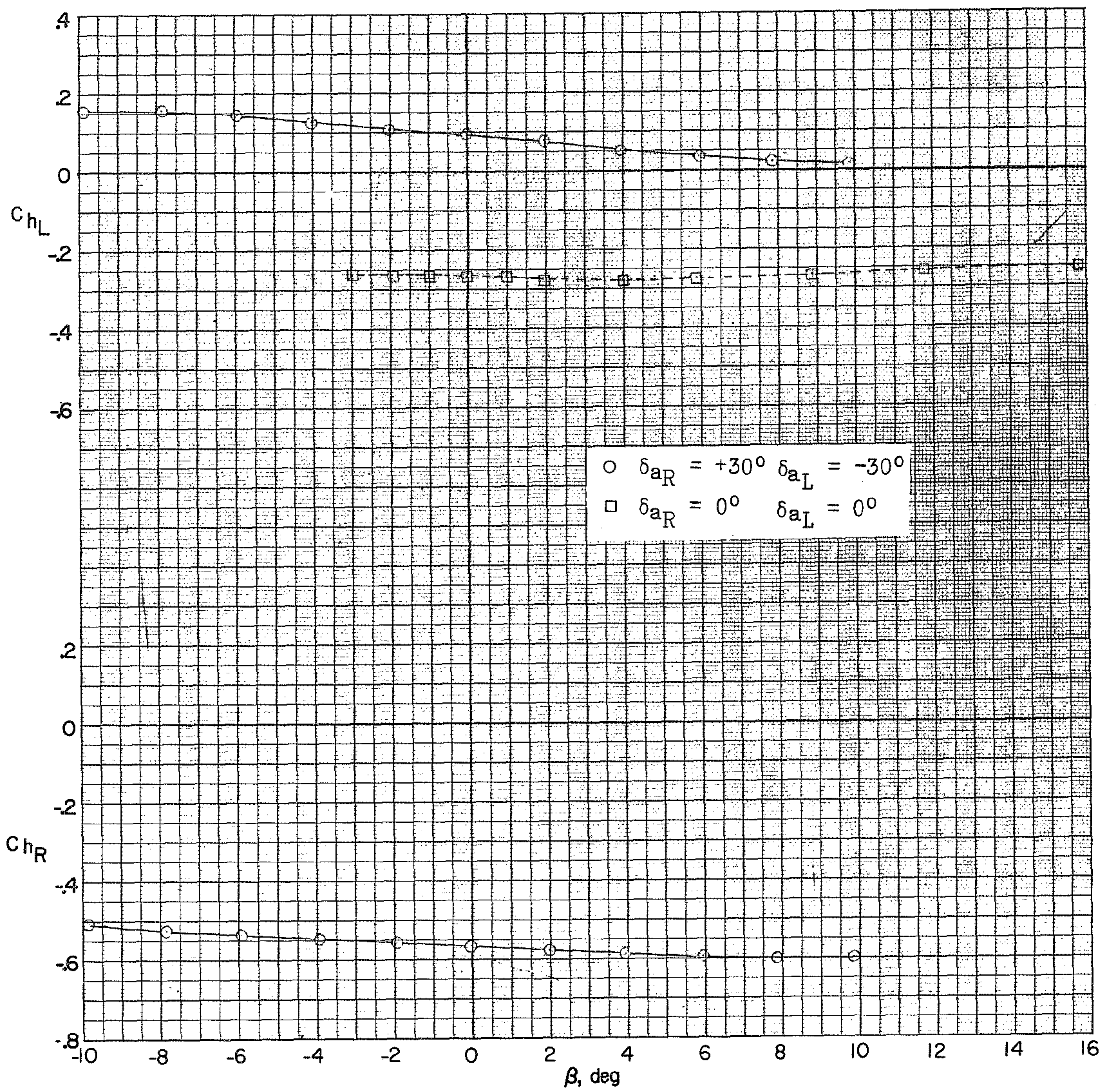

(i) $M = 2.16$; $\alpha = 16.9^{\circ}$.

Figure 17.- Concluded.

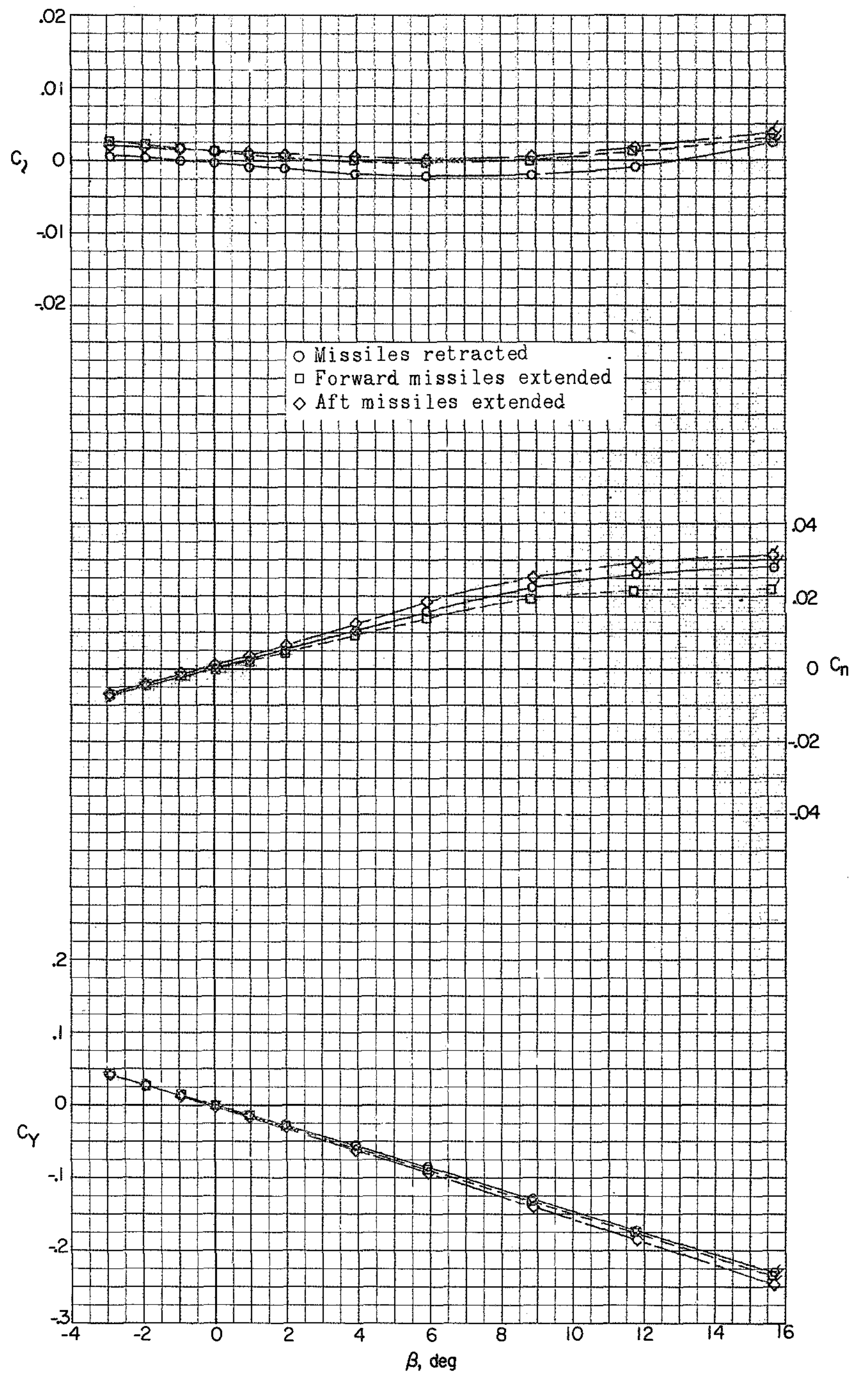

(a) M = 1.57; α = 0.4°.

Figure 18.- Effect of extended missiles on aerodynamic characteristics in sideslip. (Flagged symbols denote wall-reflected shock waves striking the tail.)

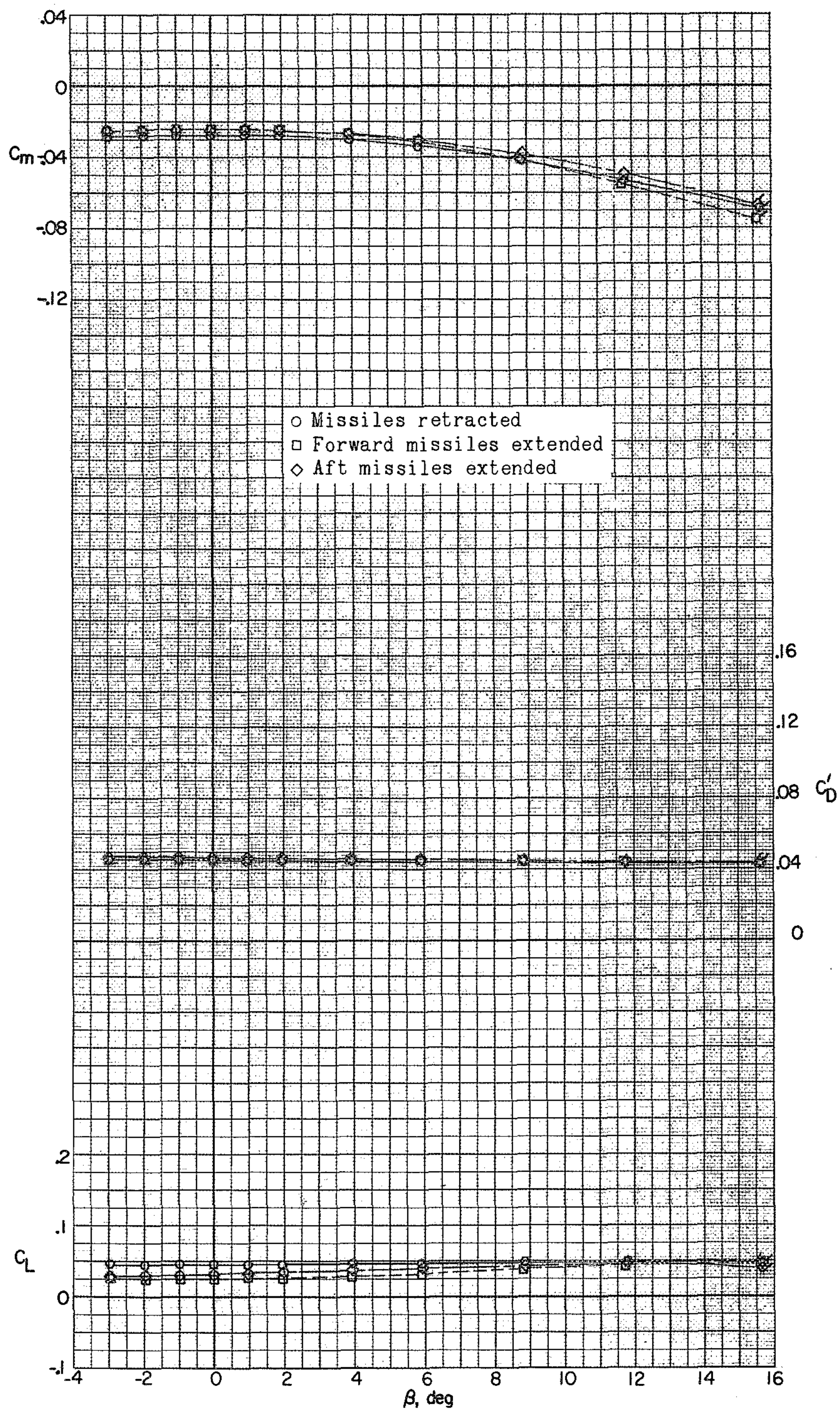

(a) Concluded.

Figure 18.- Continued.

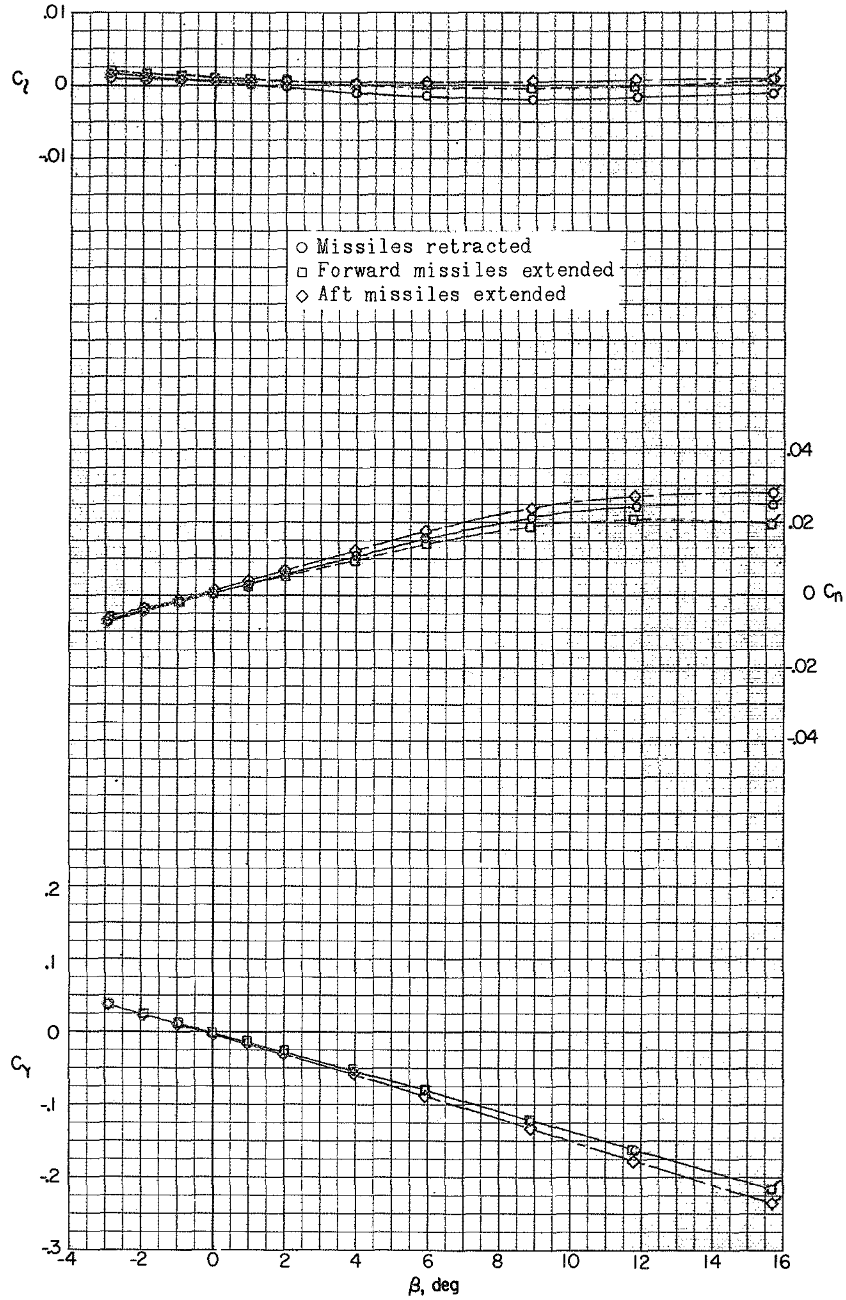

(b) M = 1.57; α = 6.7°.

Figure 18.- Continued.

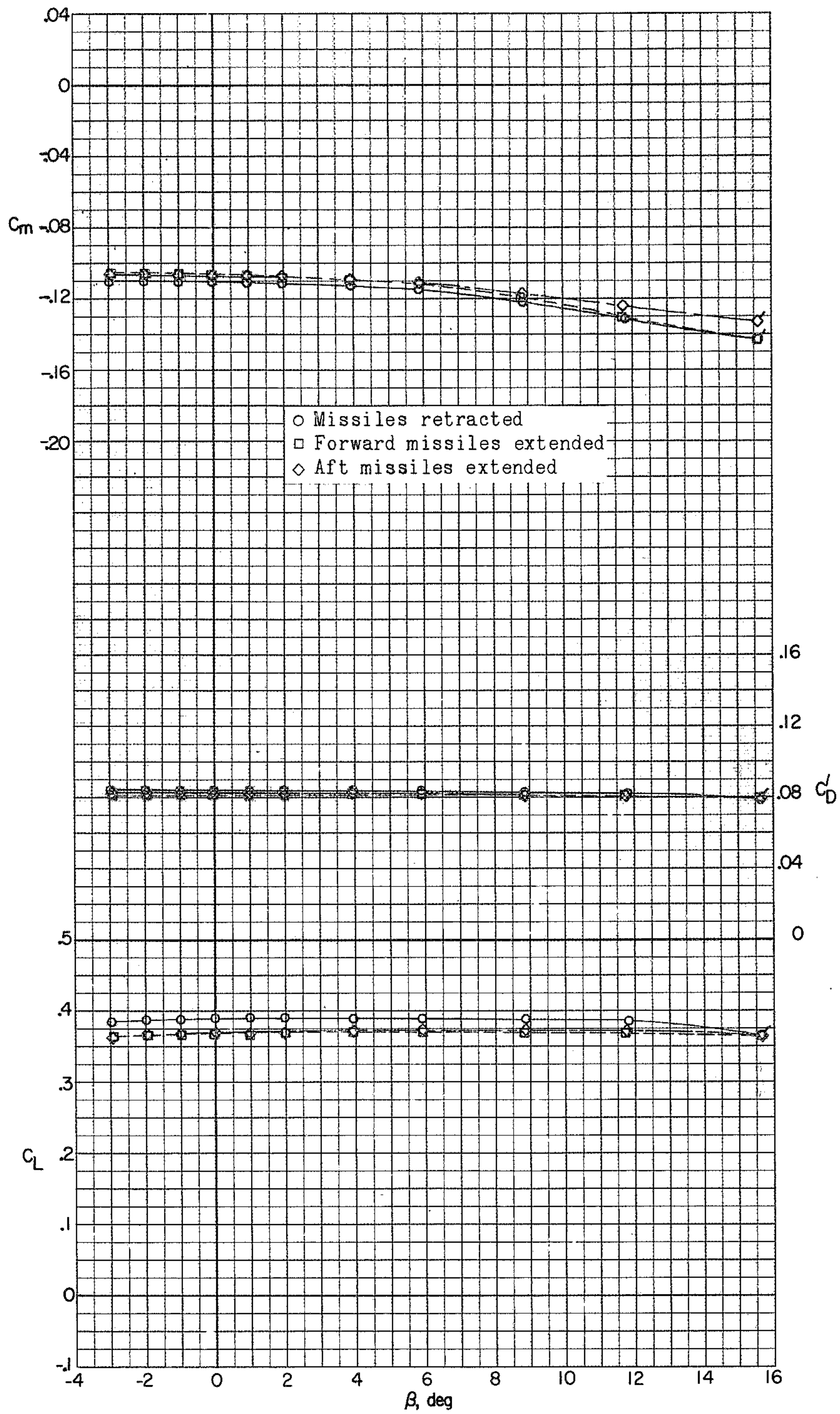

(b) Concluded.

Figure 18.- Continued.

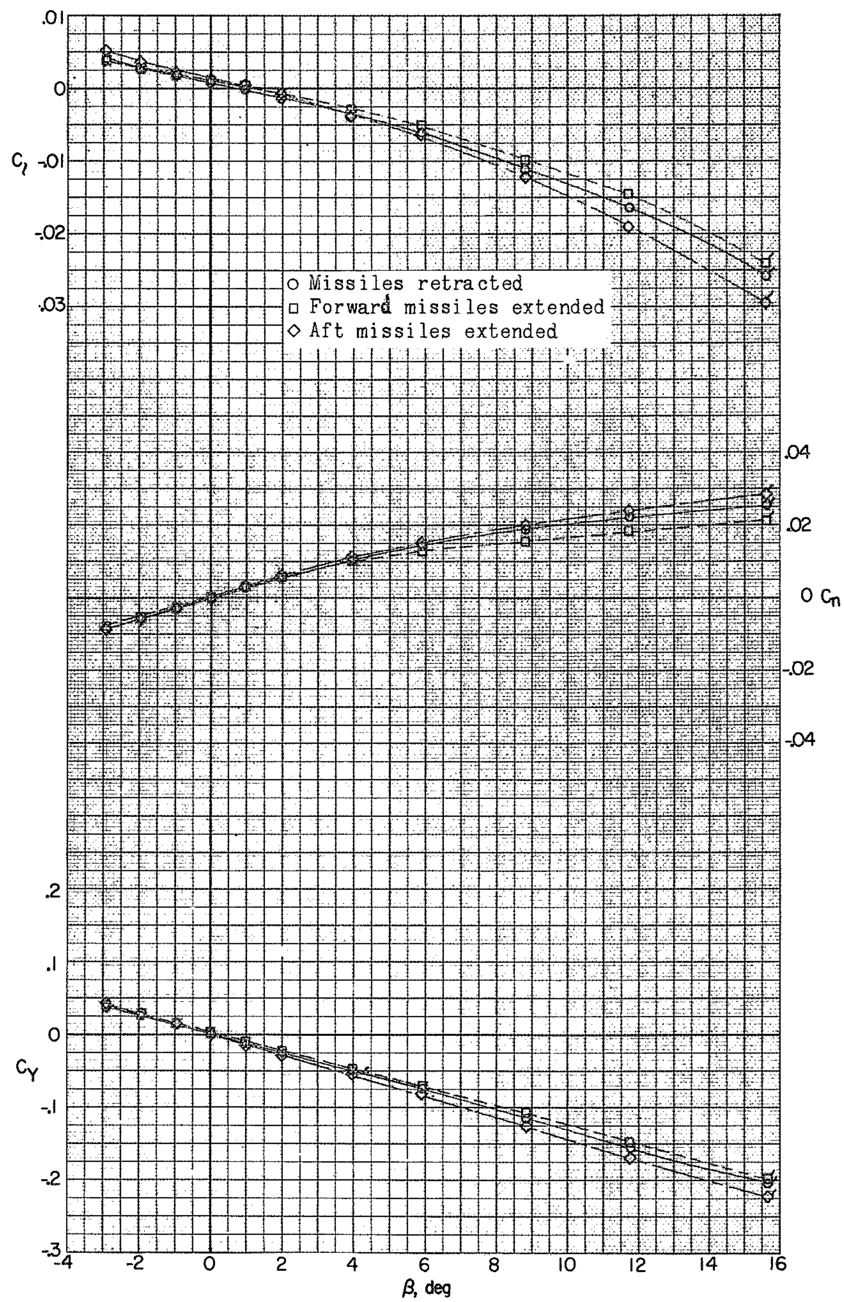

(c) $M = 1.57$; $\alpha = 17.4^{\circ}$.

Figure 18.- Continued.

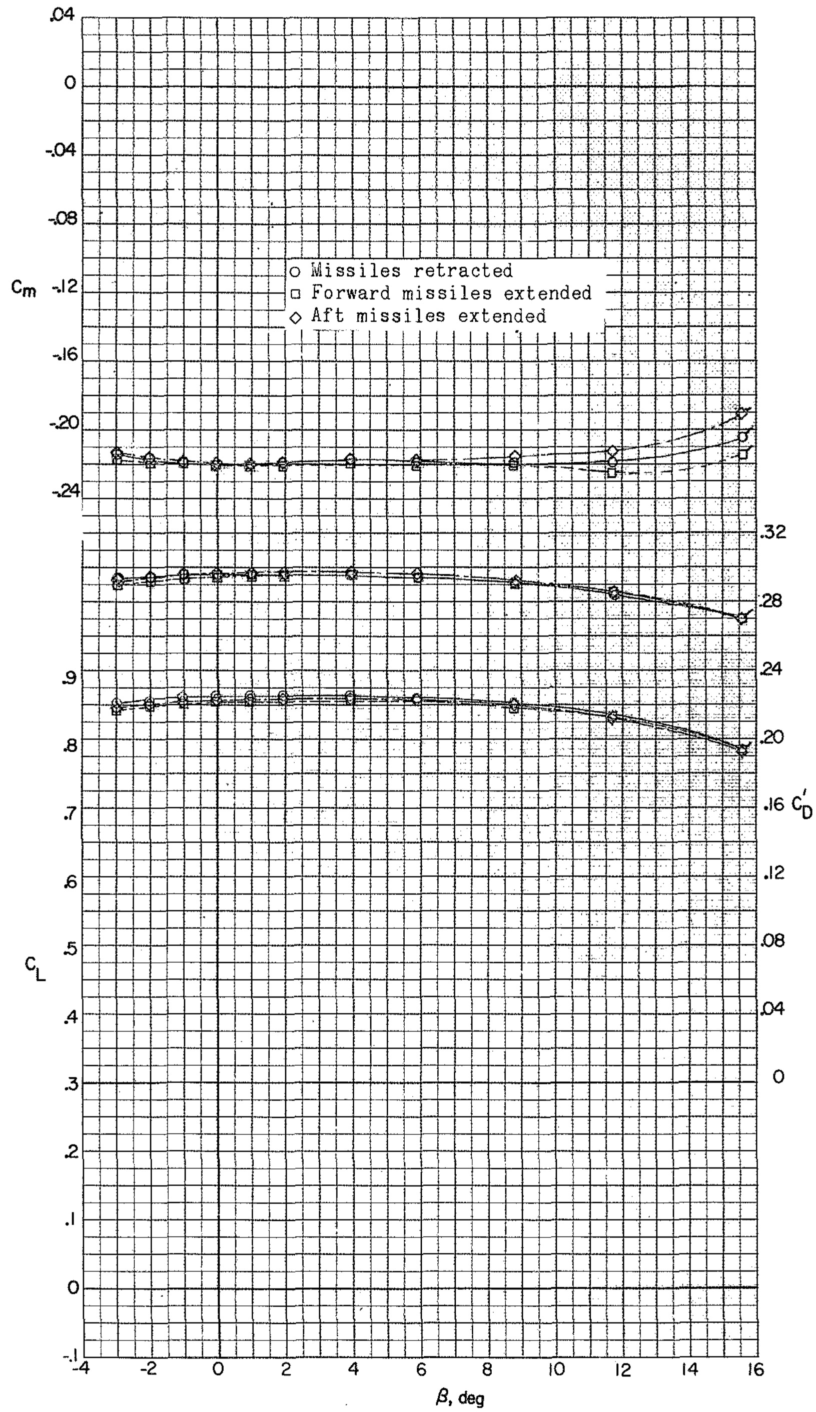

(c) Concluded.

Figure 18.- Continued.

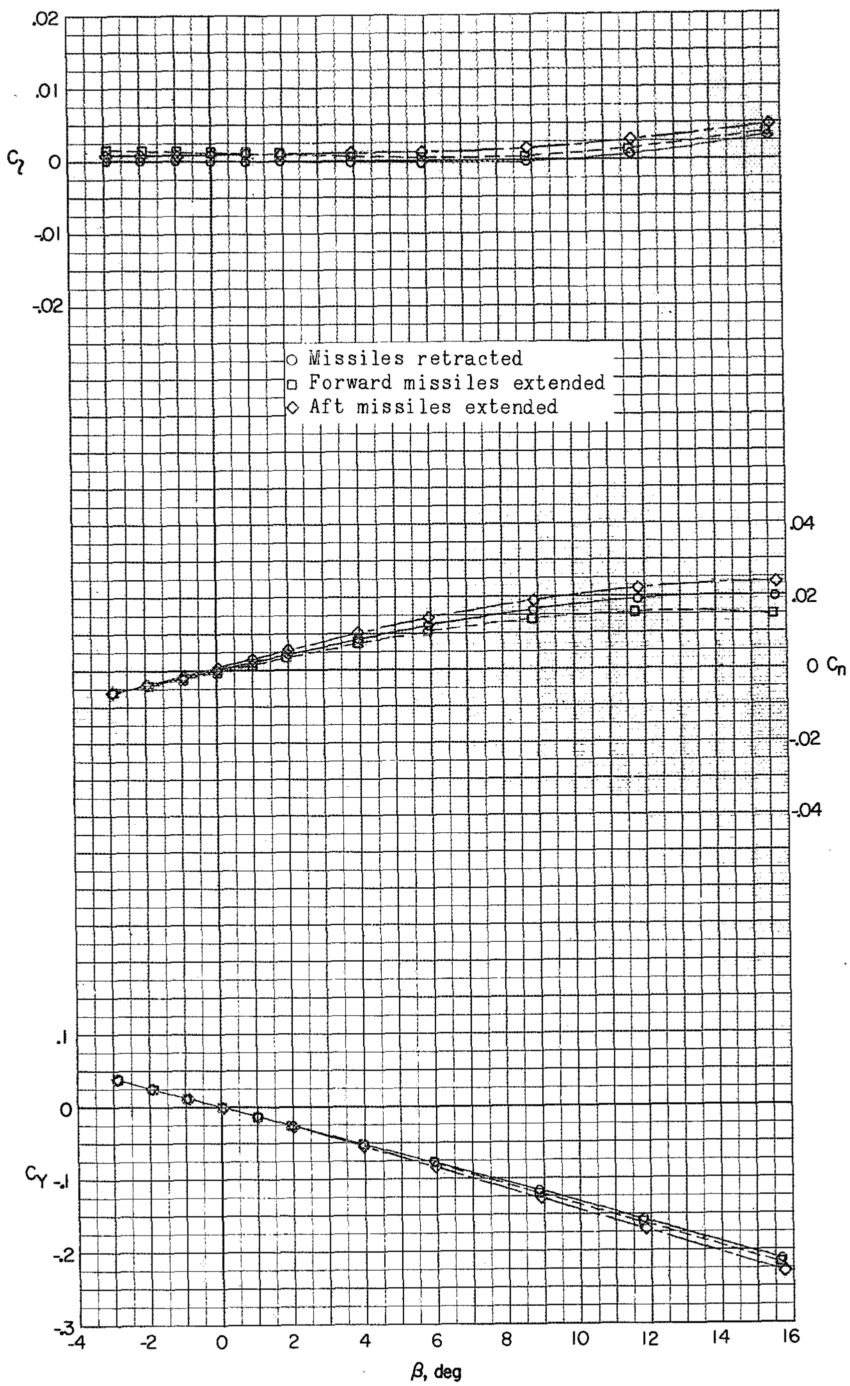

(d) M = 1.87; α = 0.4°.

Figure 18.- Continued.

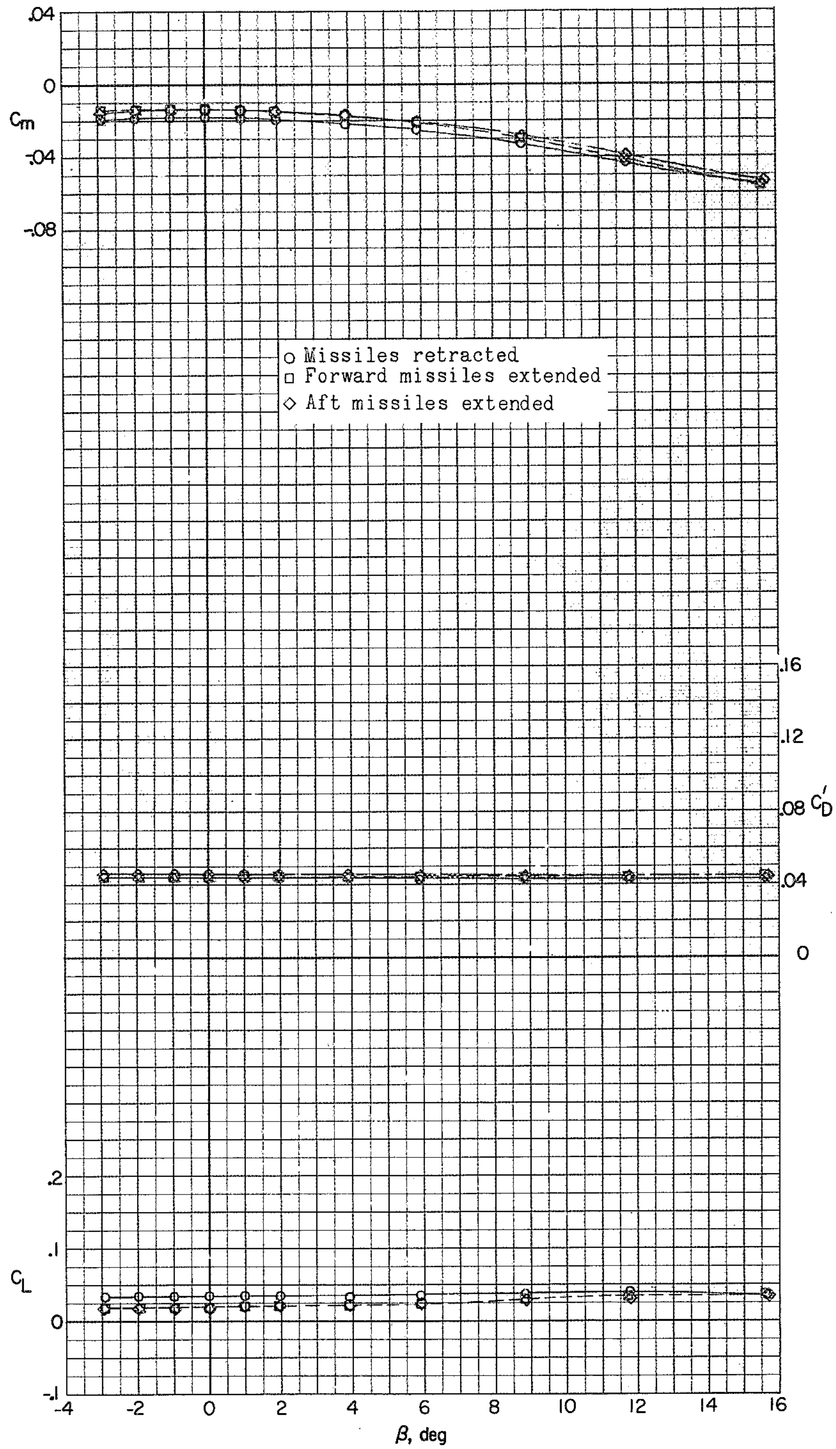

(d) Concluded.

Figure 18.- Continued.

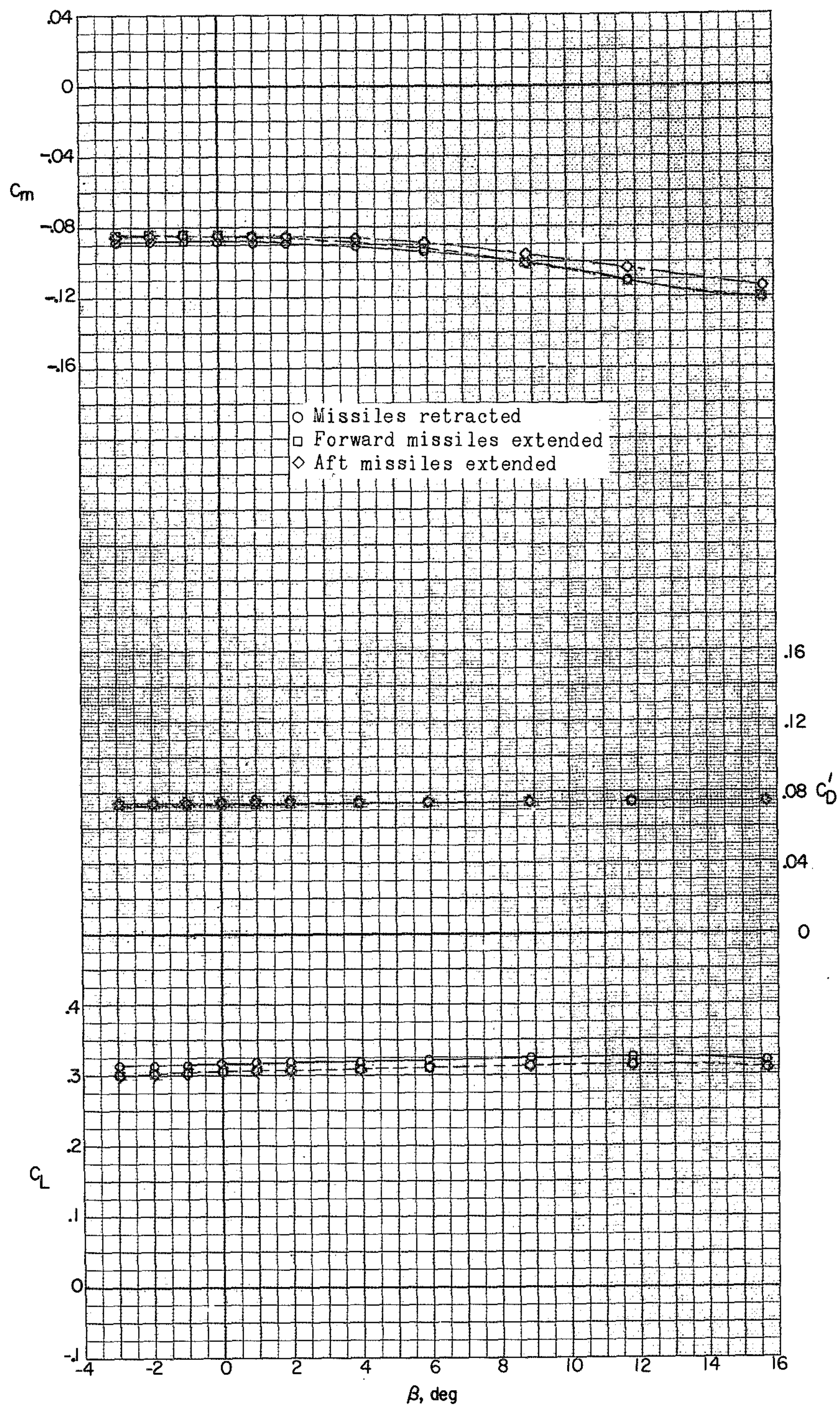

(e) M = 1.87; α = 6.6°.

Figure 18.- Continued.

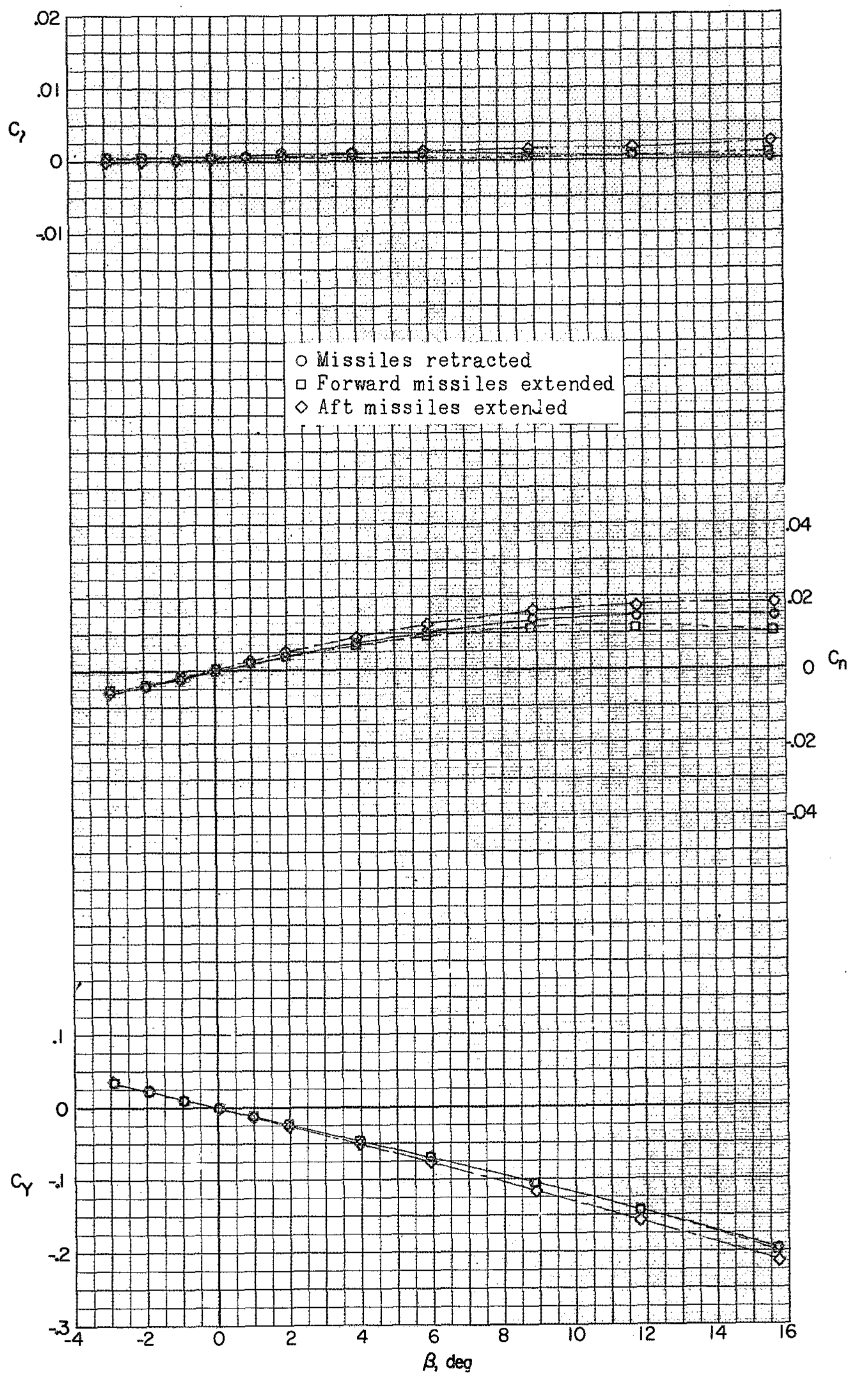

(e) Concluded.

Figure 18.- Continued.

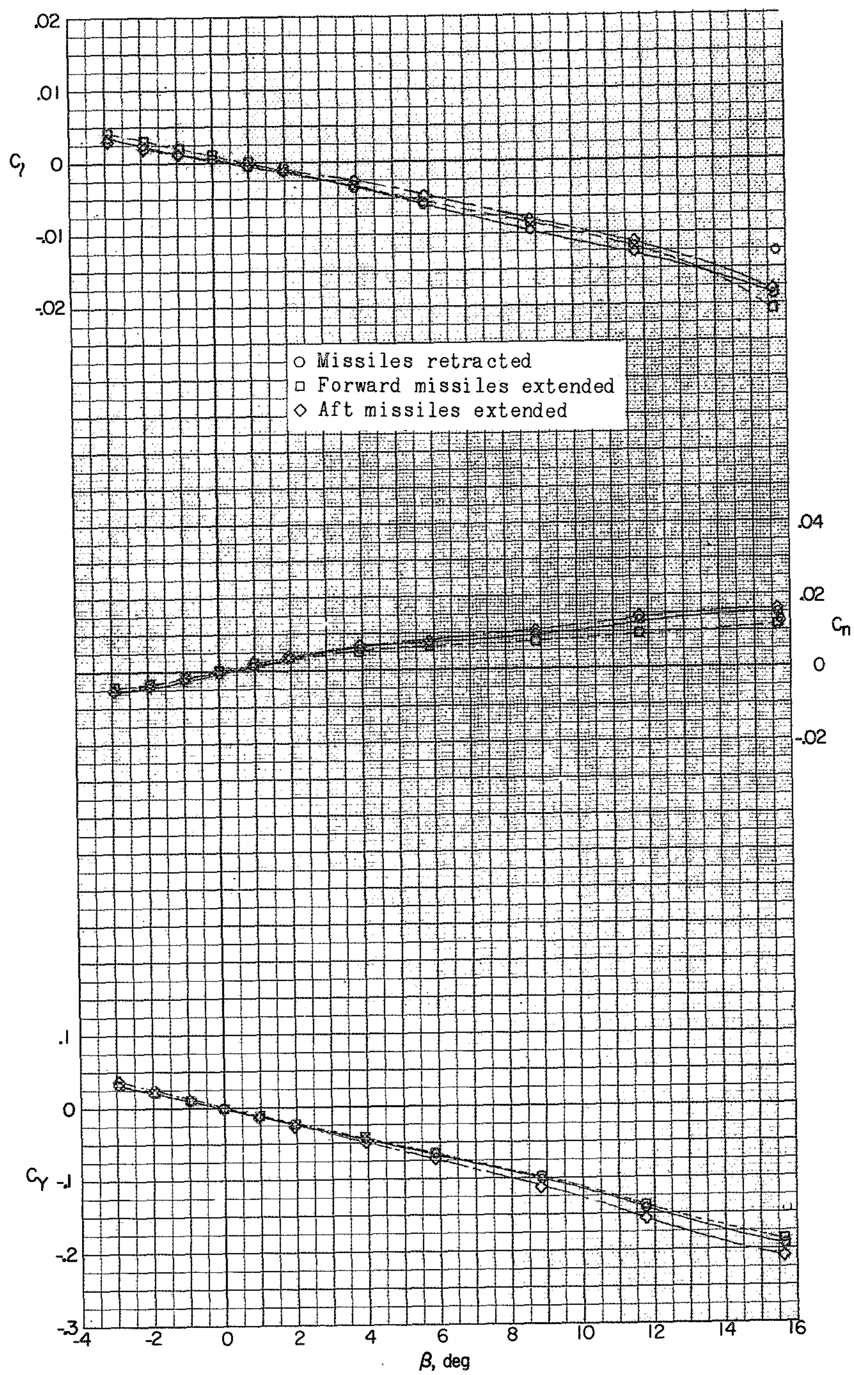

(f) $M = 1.87$; $\alpha = 17.1^{\circ}$.

Figure 18.- Continued.

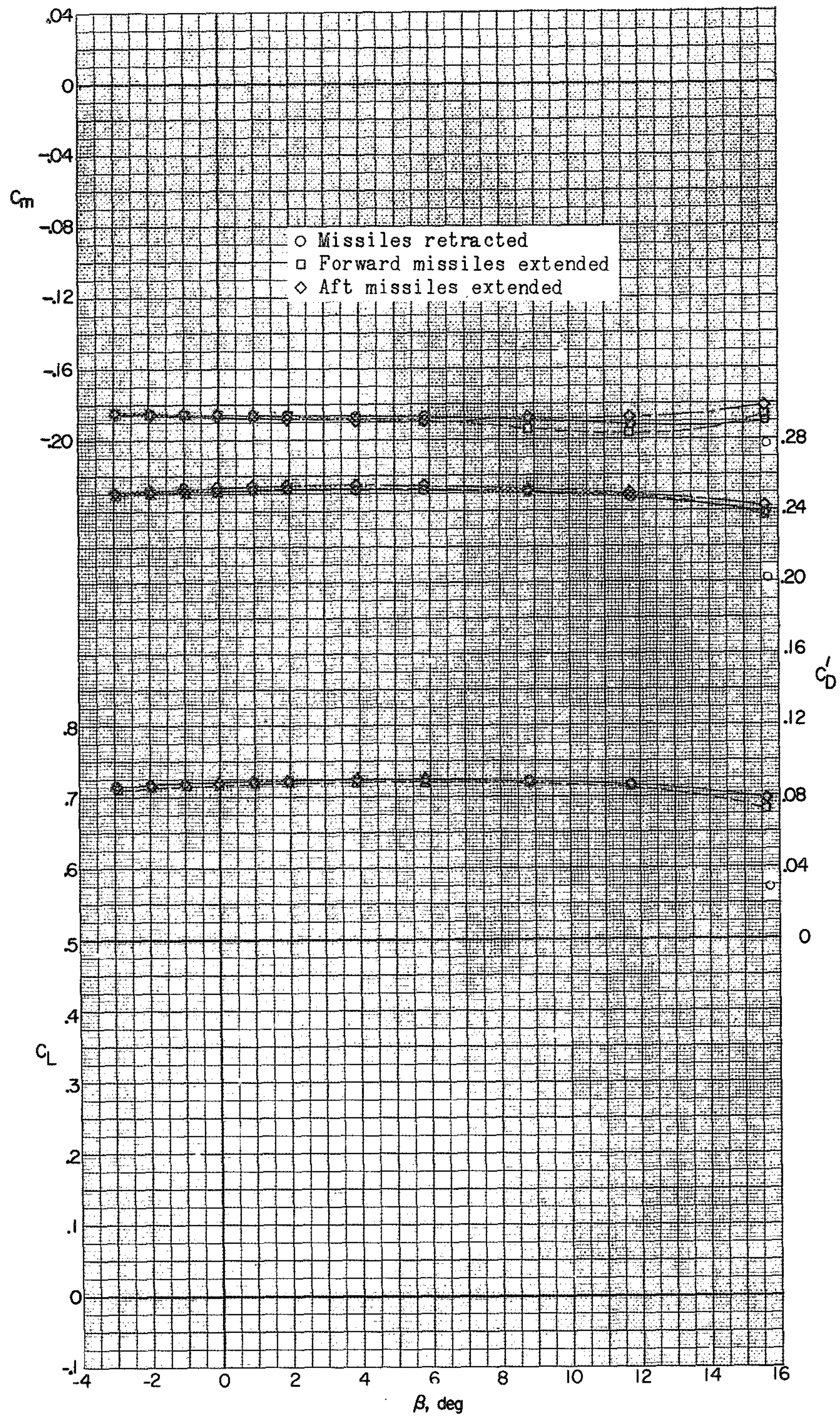

(f) Concluded.

Figure 18.- Continued.

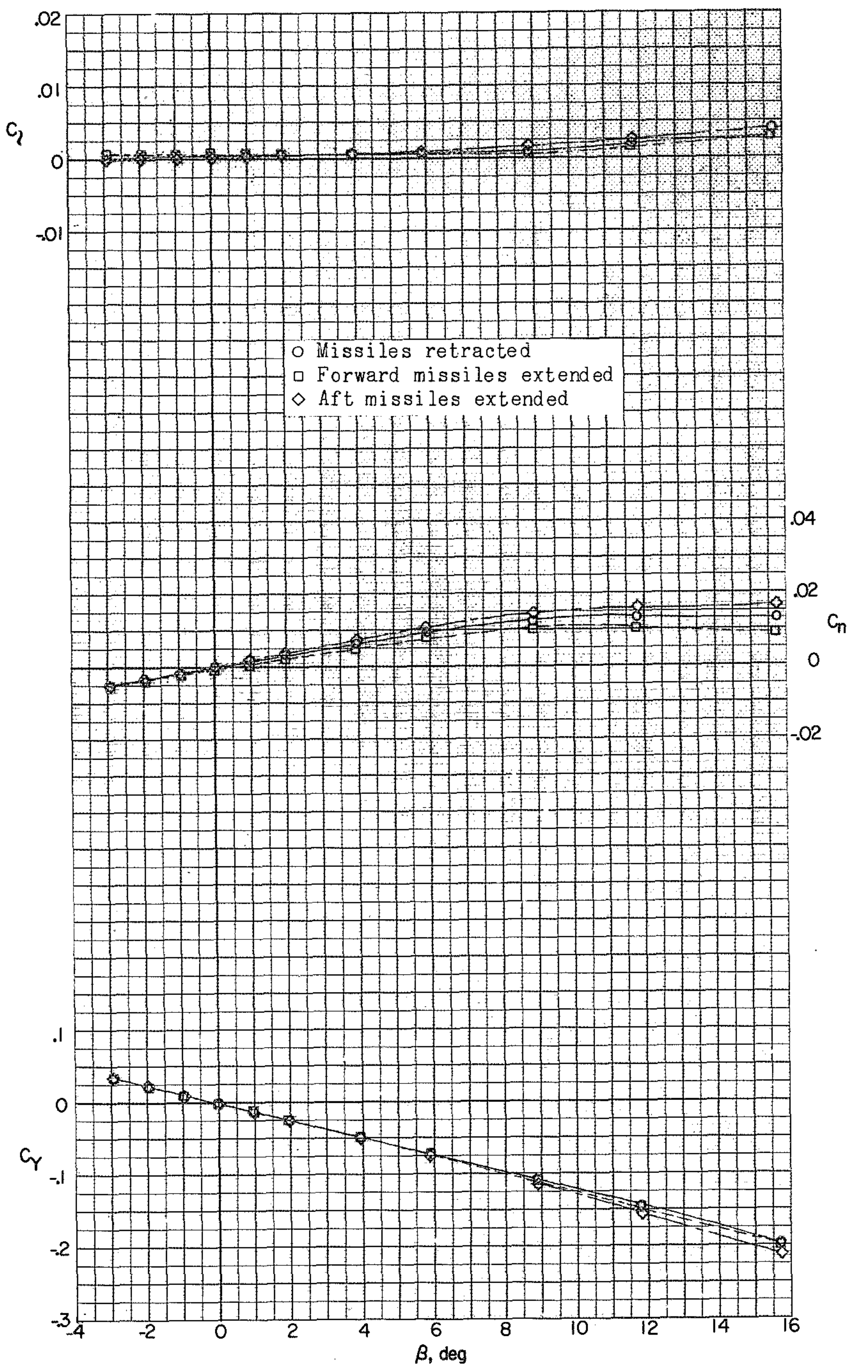

(g) $M = 2.16$; $\alpha = 0.4^{\circ}$.

Figure 18.- Continued.

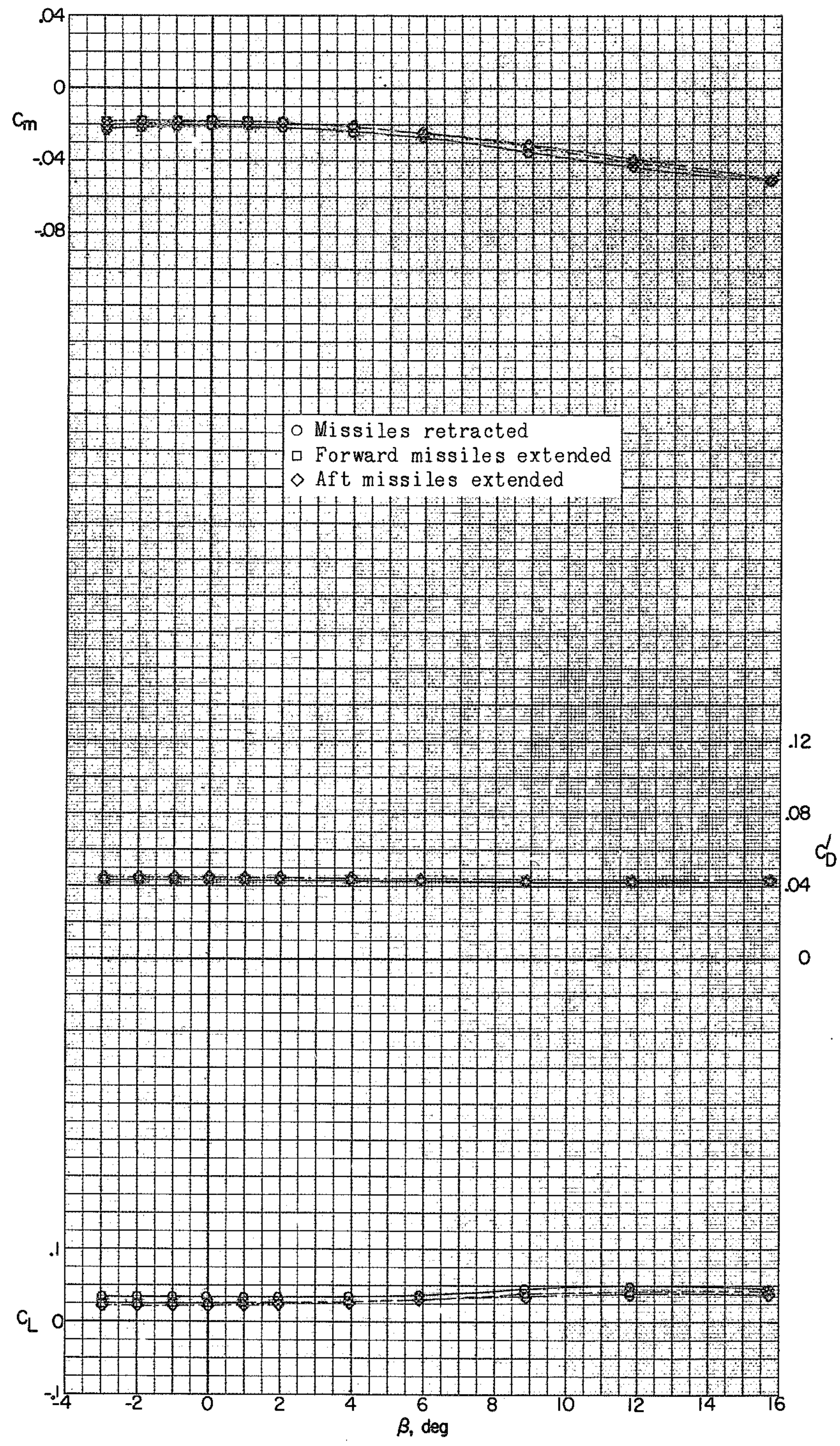

(g) Concluded.

Figure 18.- Continued.

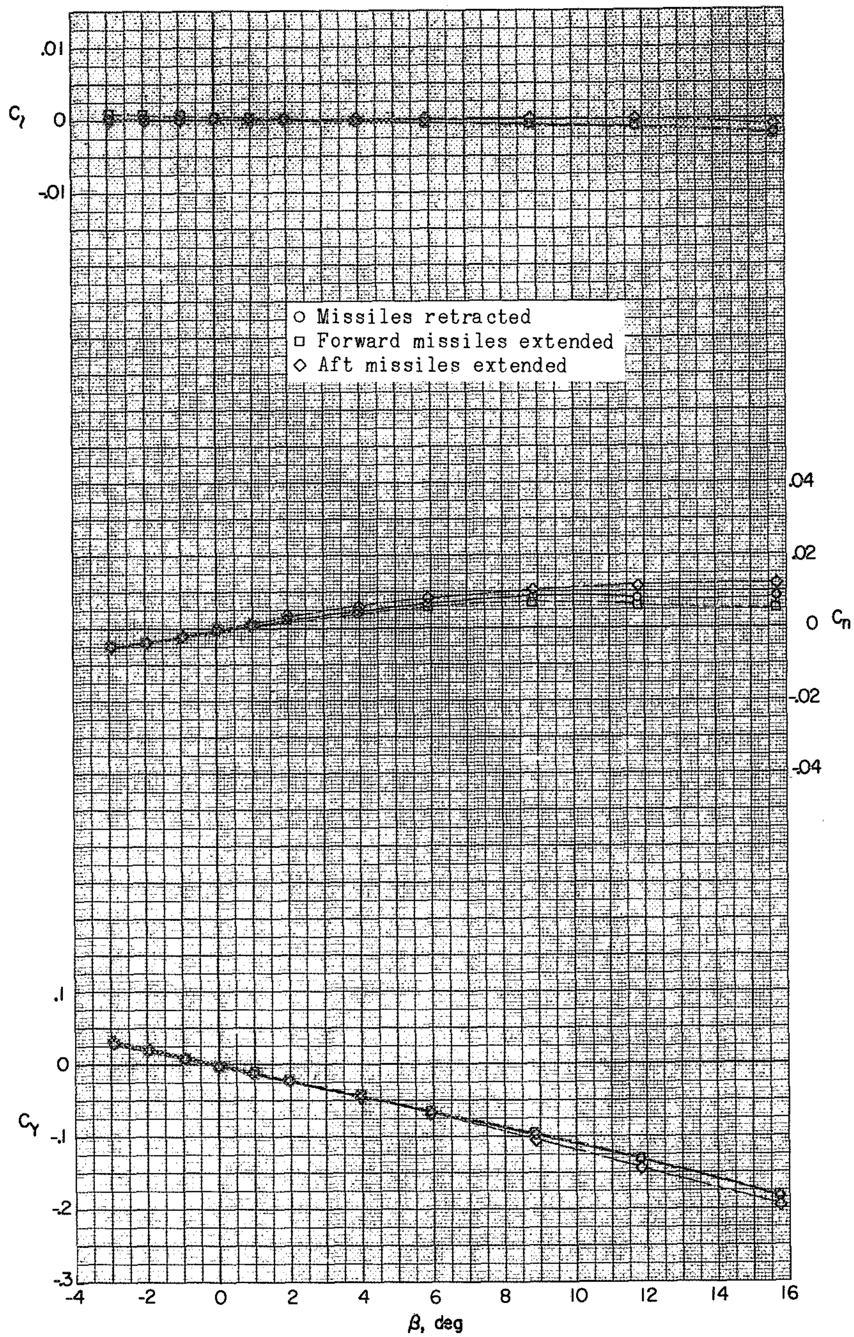

(h) $M = 2.16$; $\alpha = 6.5^{\circ}$.

Figure 18.- Continued.

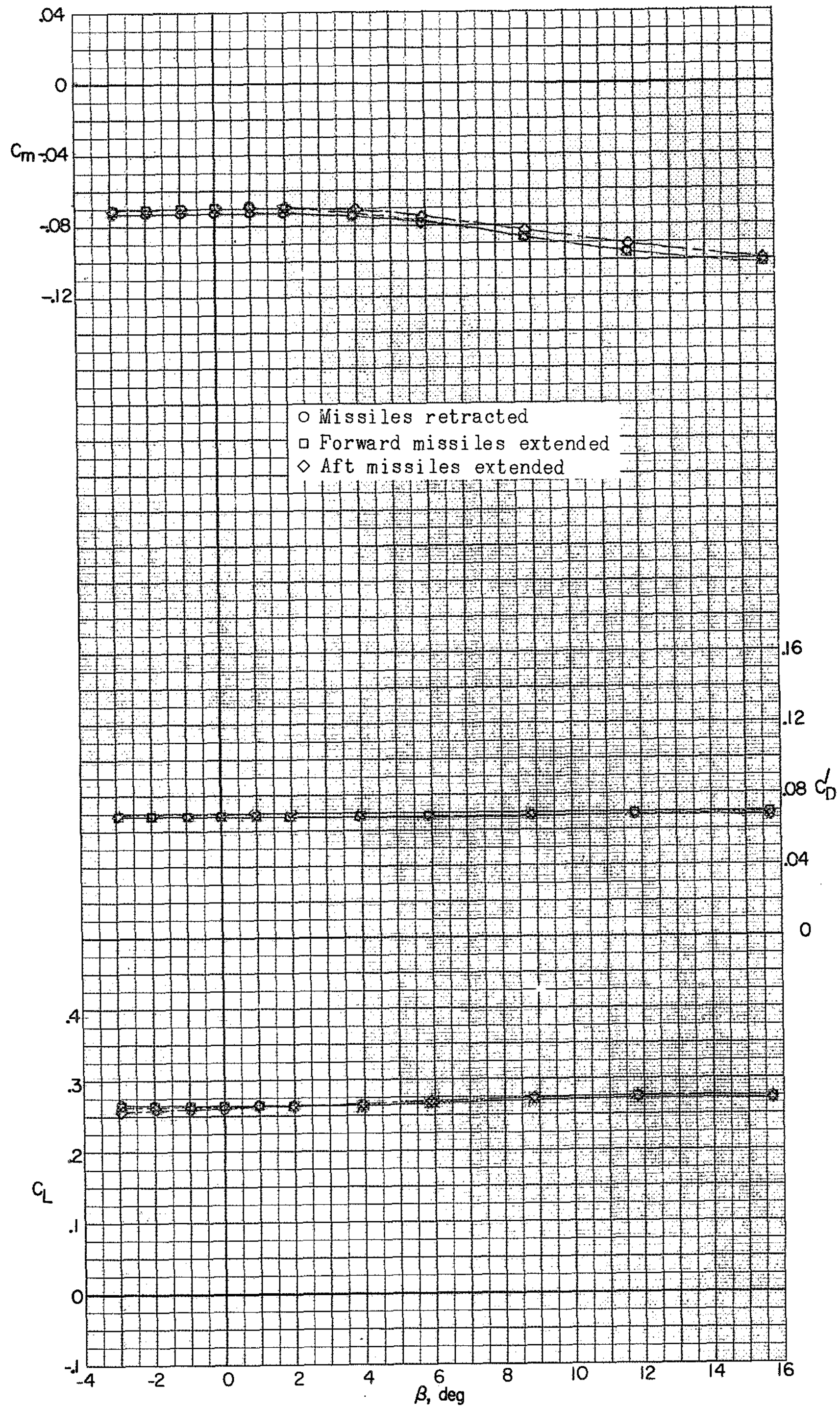

(h) Concluded.

Figure 18.- Continued.

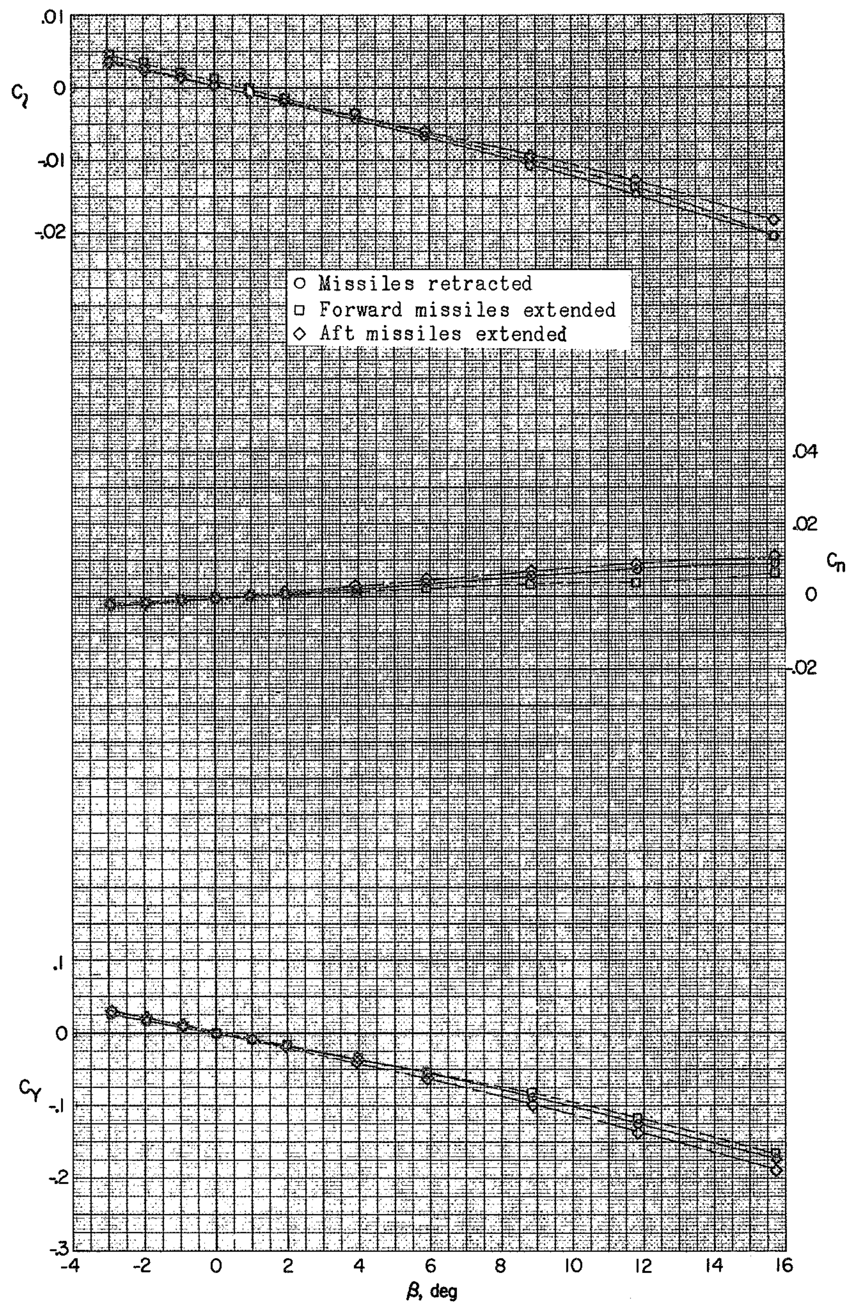

(i) $M = 2.16$; $\alpha = 16.9^{\circ}$.

Figure 18.- Continued.

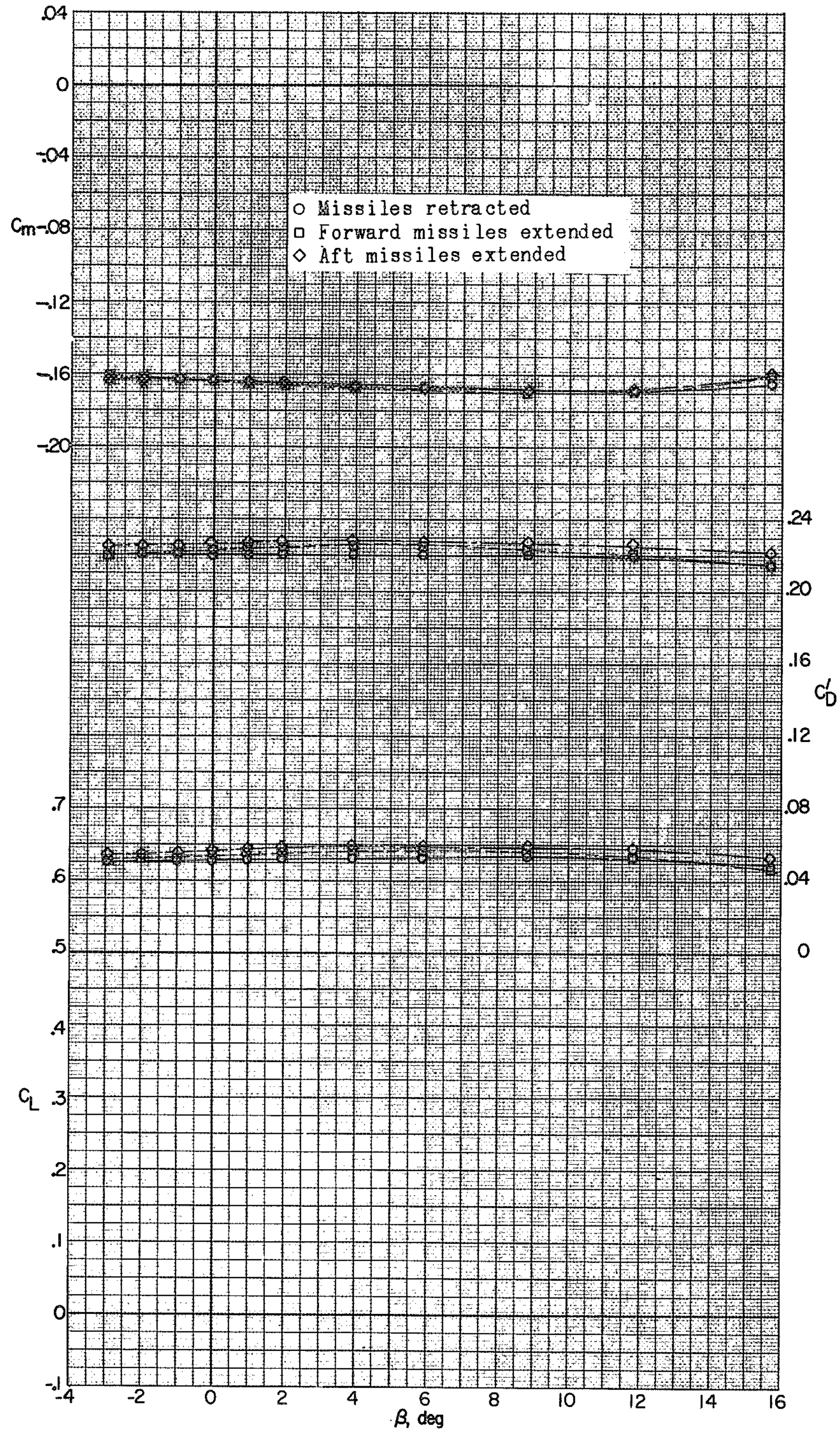

(i) Concluded.

Figure 18.- Concluded.

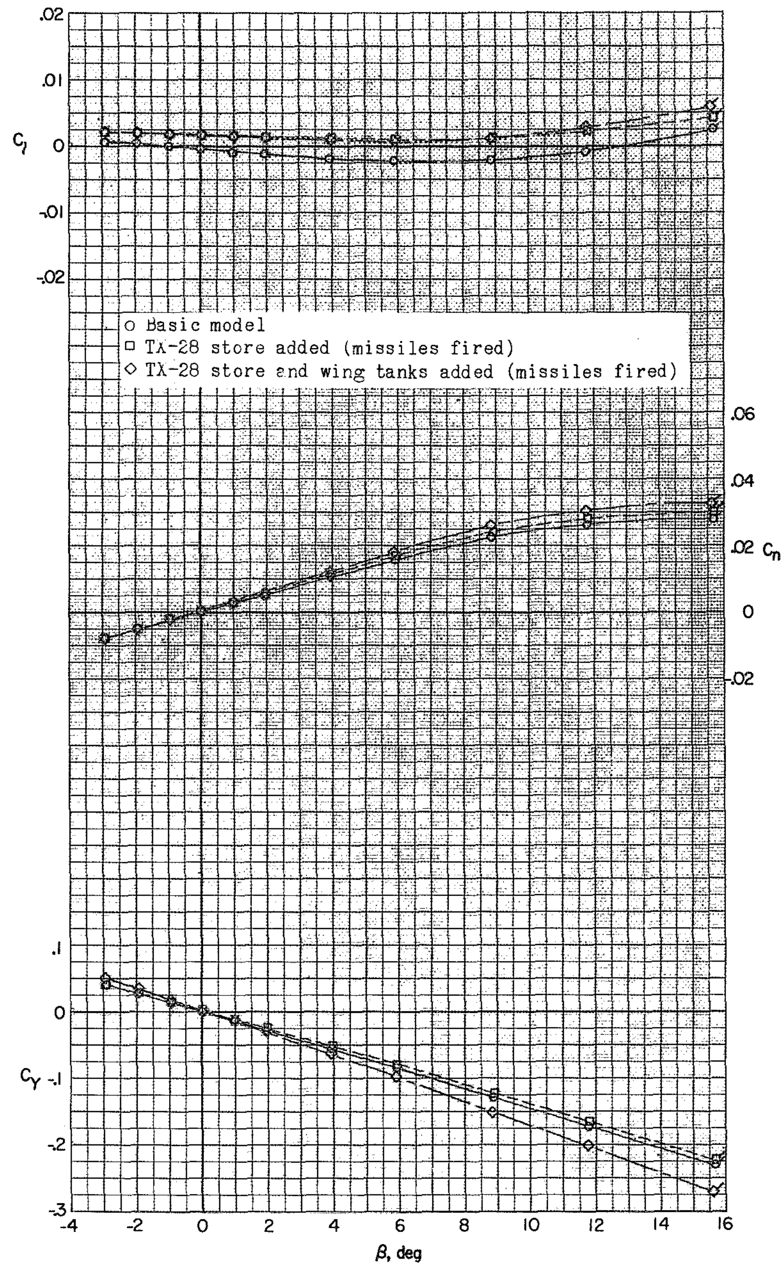

(a) M = 1.57; α = 0.4°.

Figure 19.- Effect of external stores on aerodynamic characteristics in sideslip. (Flagged symbols denote wall-reflected shock waves striking the tail.)

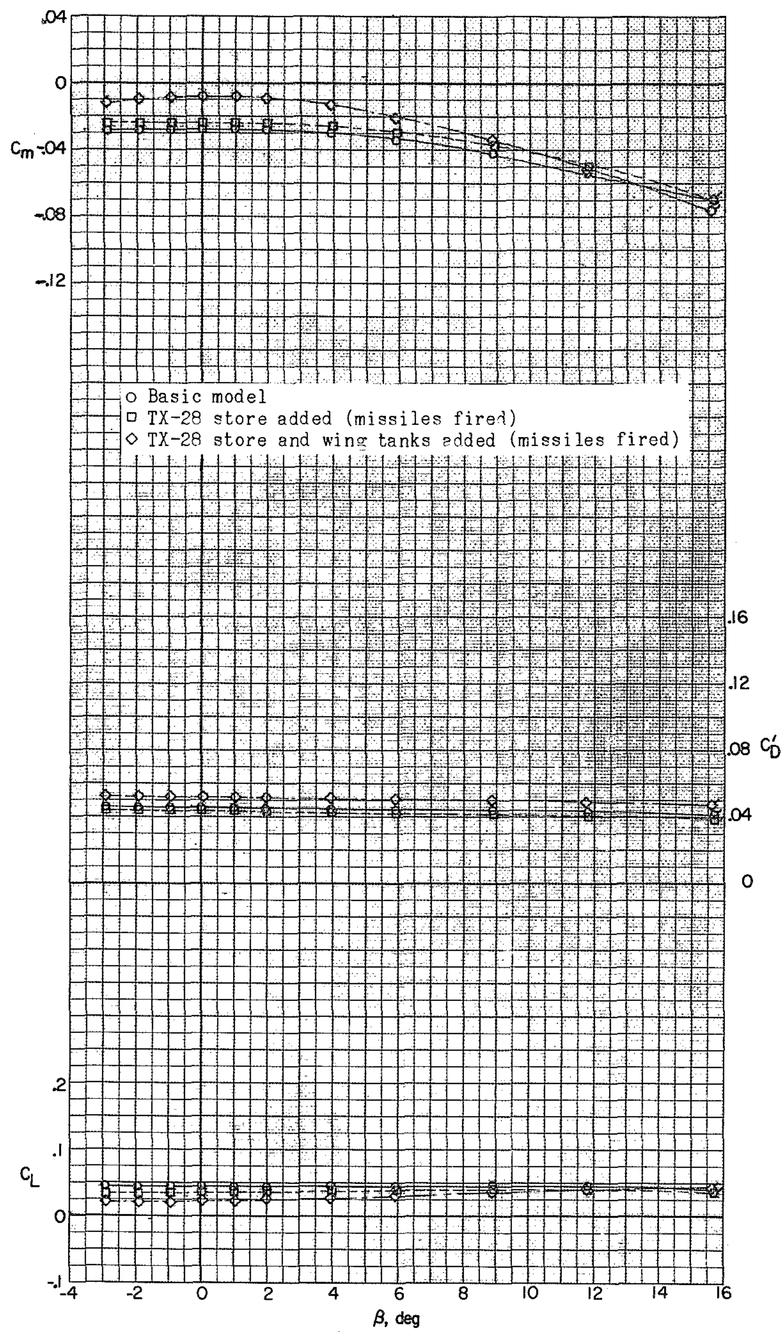

(a) Concluded.

Figure 19.- Continued.

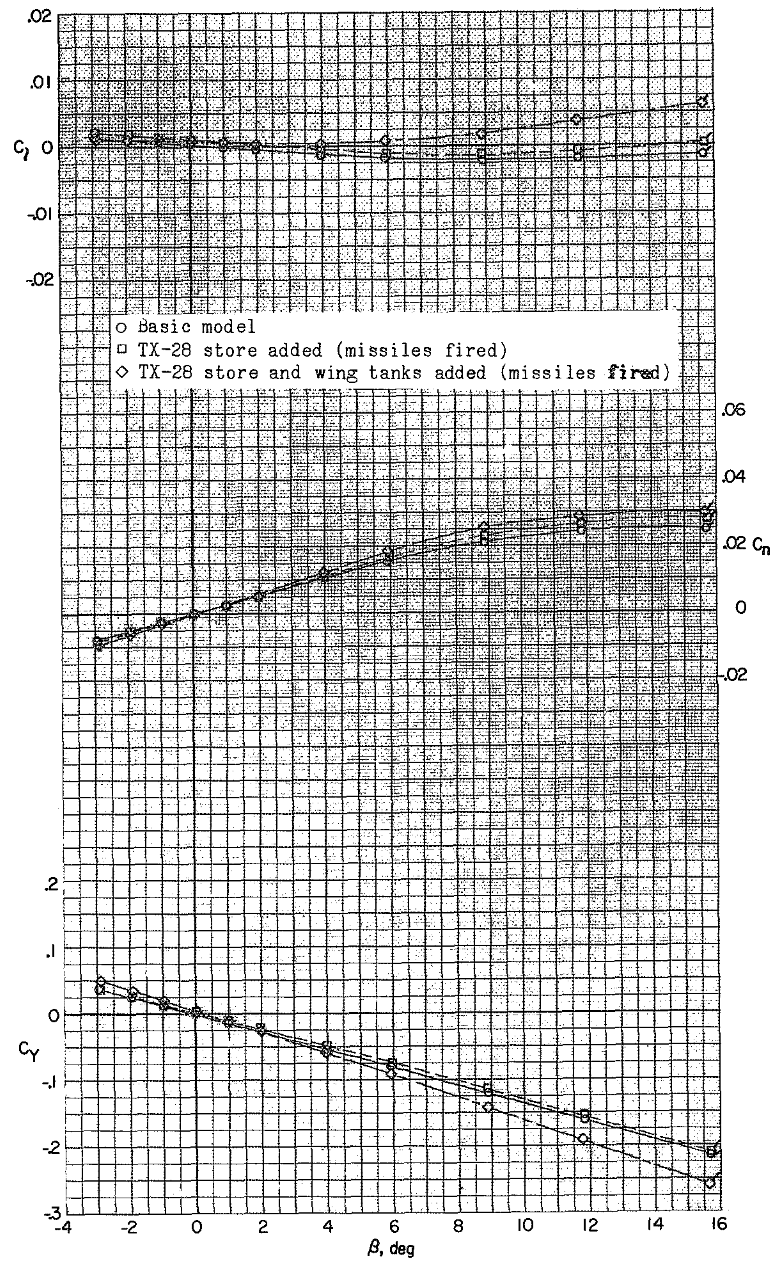

(b) M = 1.57; $\alpha = 6.7^{\circ}$.

Figure 19.- Continued.

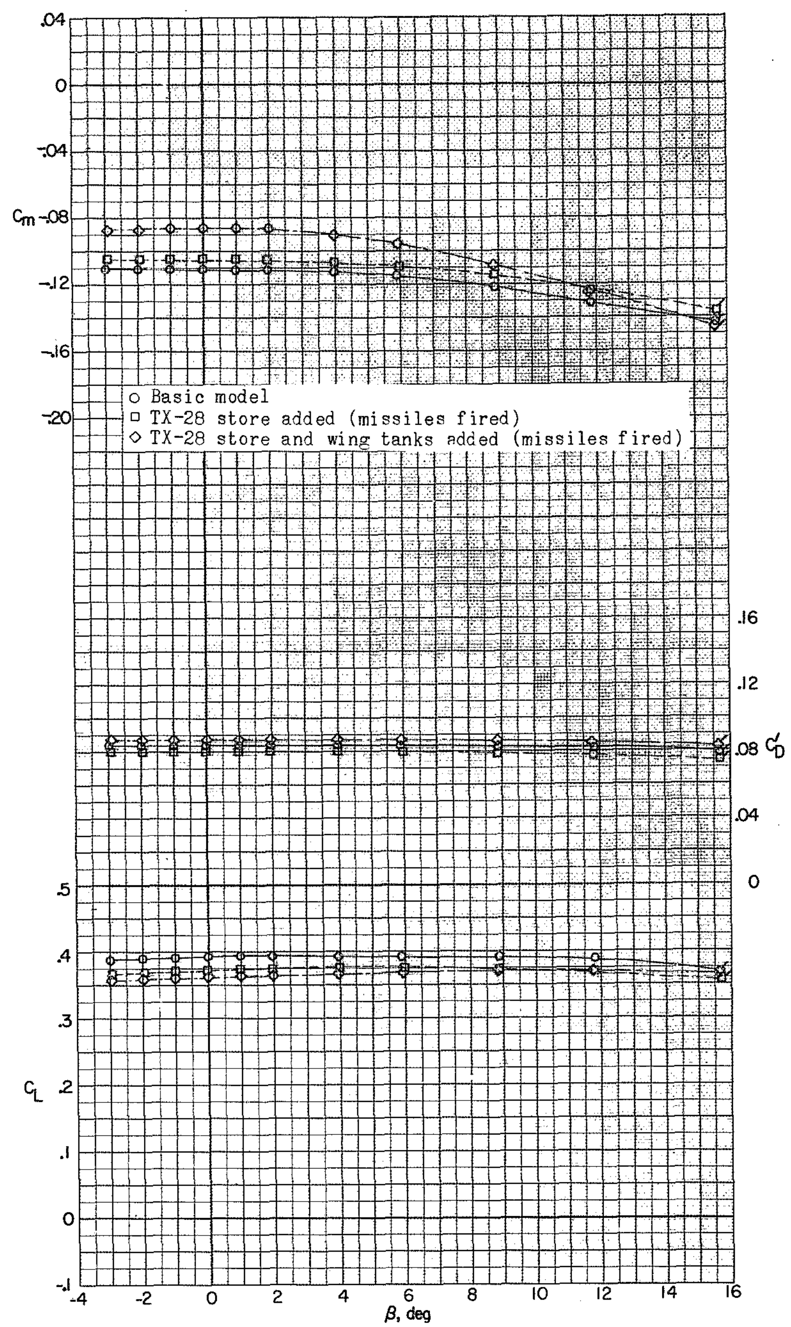

(b) Concluded.

Figure 19.- Continued.

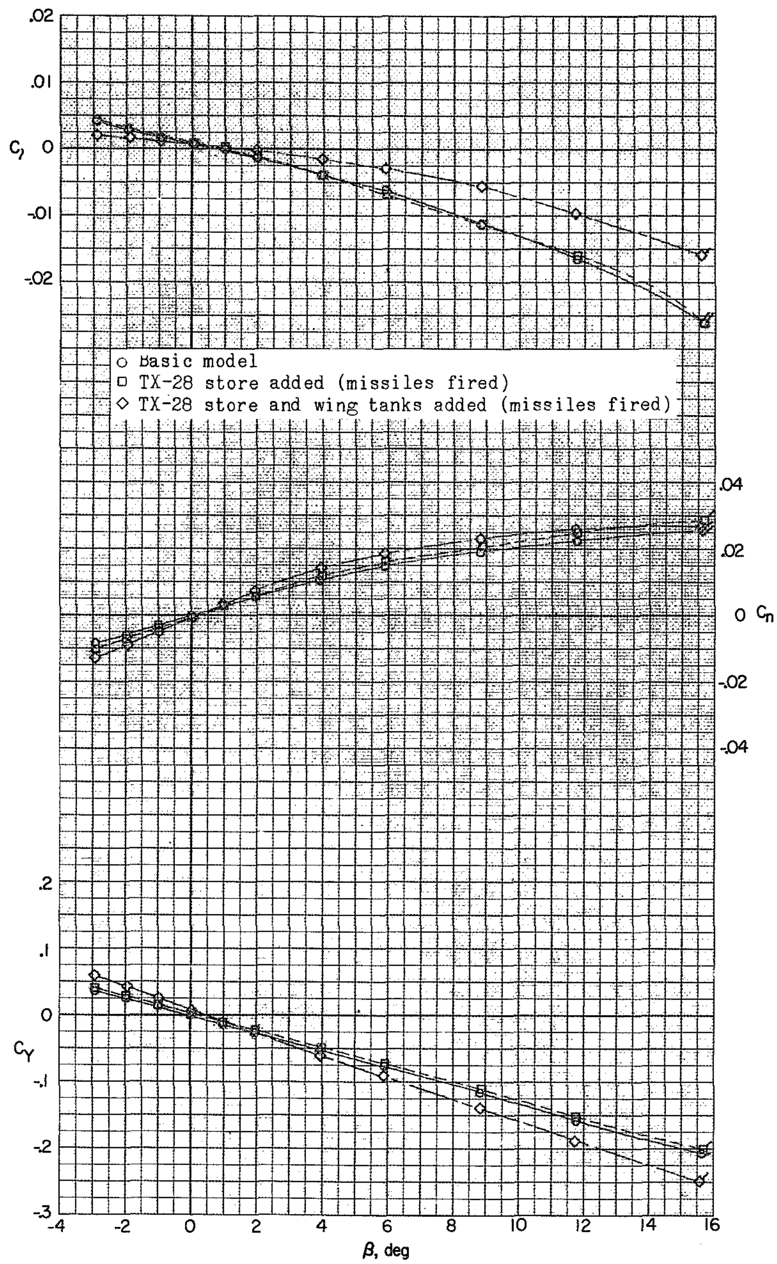

(c) M = 1.57; α = 17.4°.

Figure 19.- Continued.

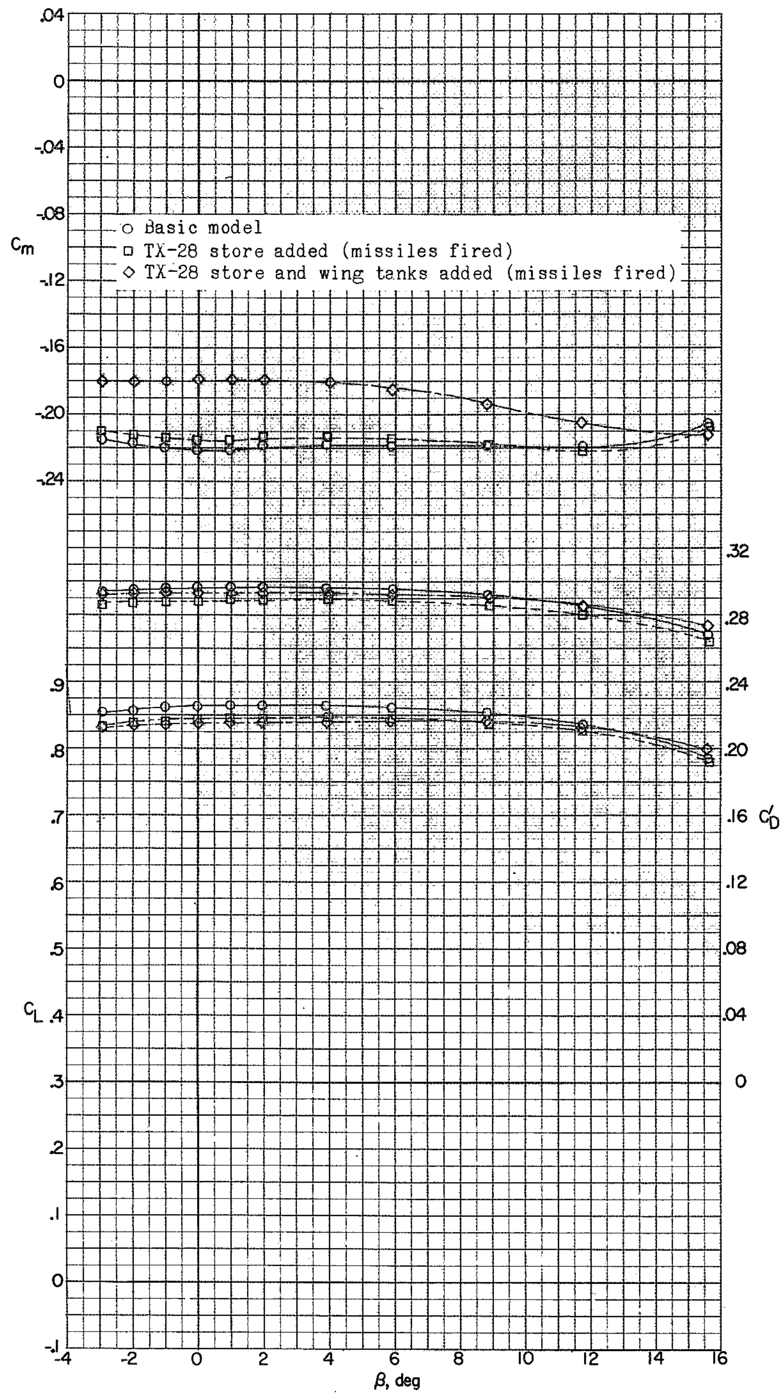

(c) Concluded.

Figure 19.- Continued.

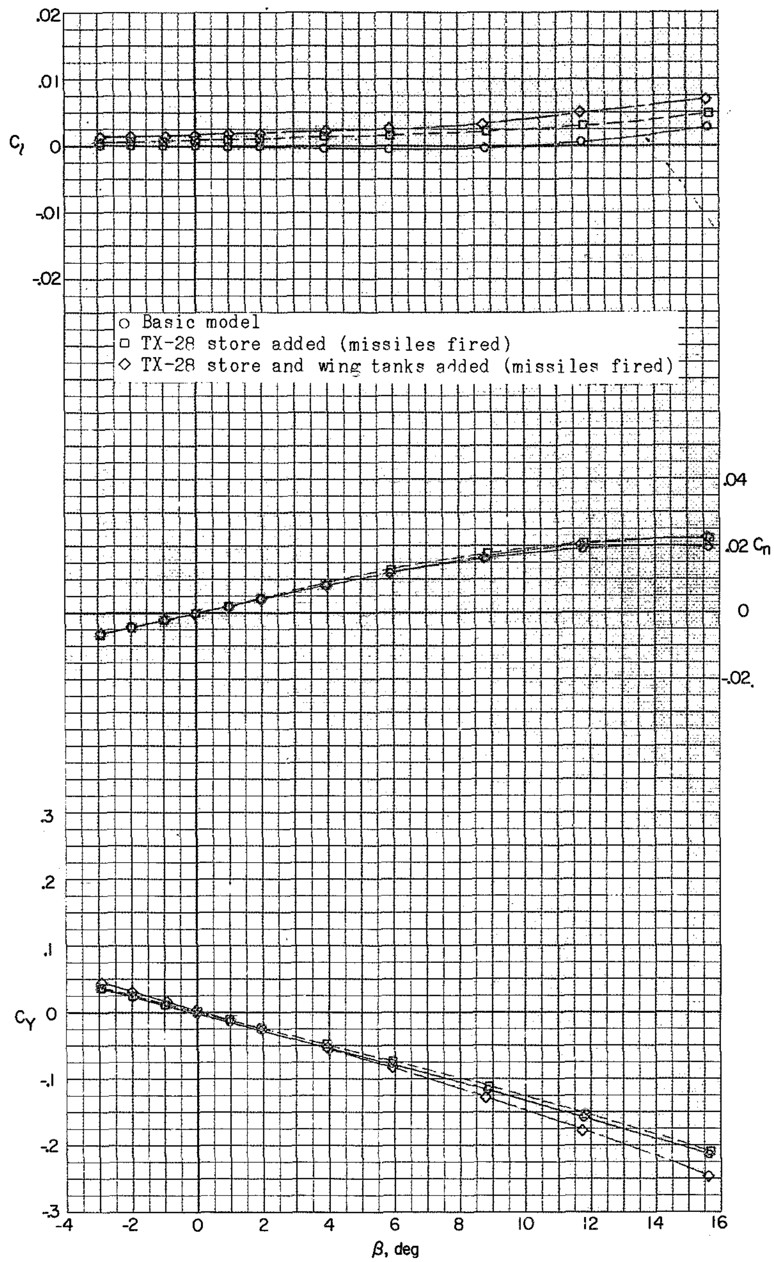

(d) $M = 1.87$; $\alpha = 0.4^{\circ}$.

Figure 19.- Continued.

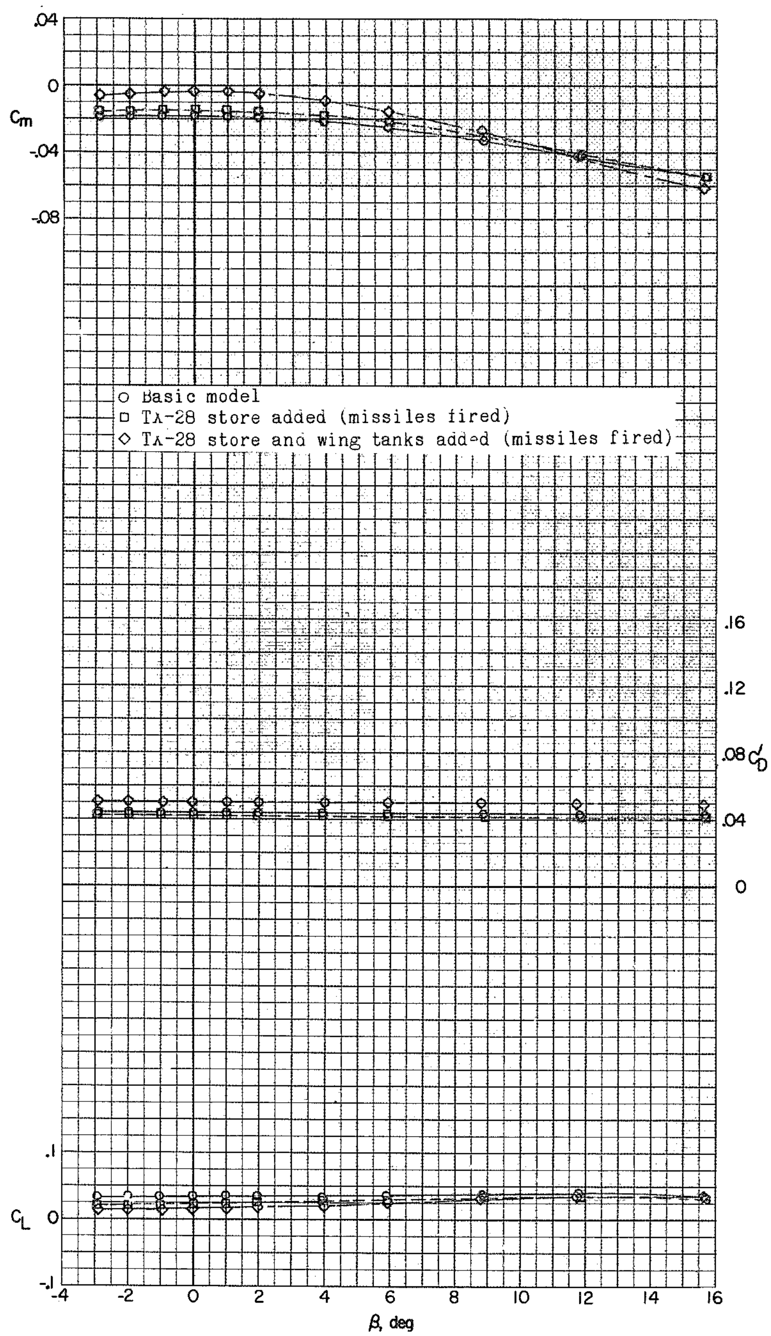

(d) Concluded.

Figure 19.- Continued.

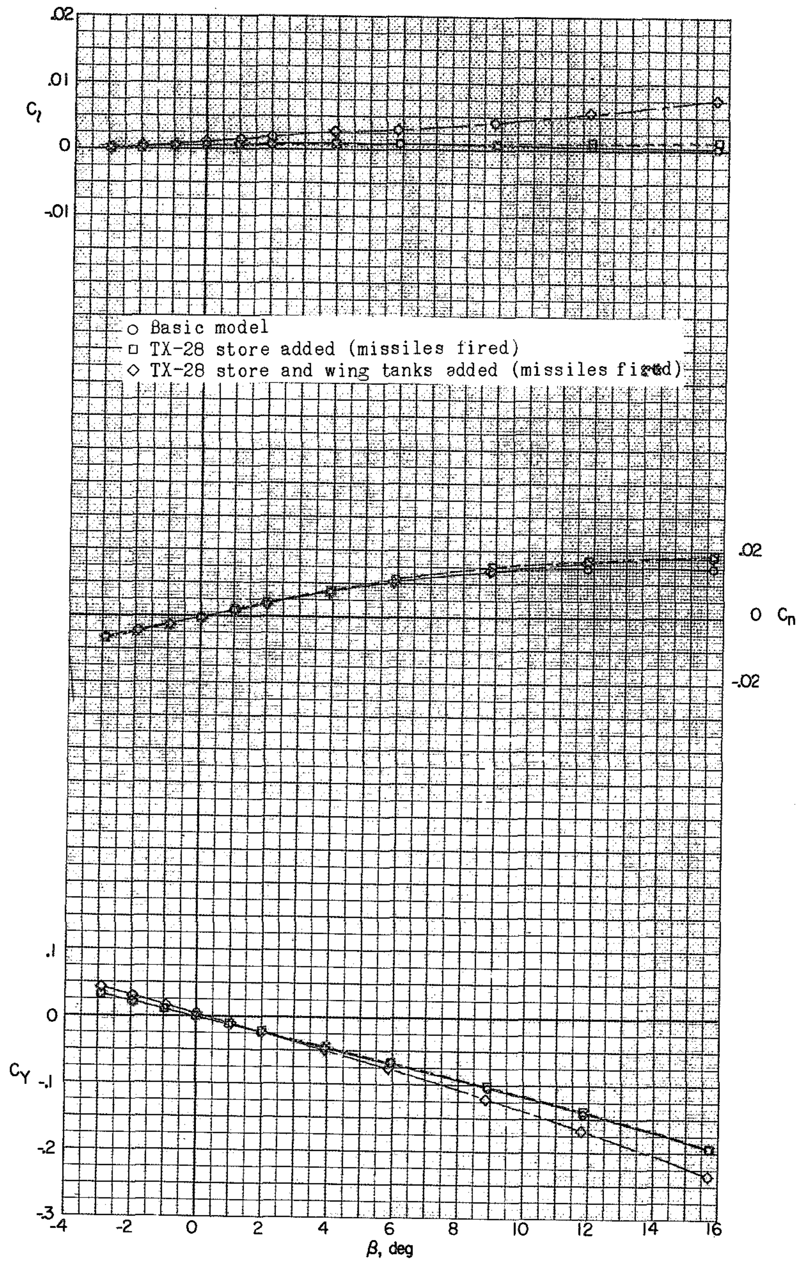

(e) $M = 1.87$; $\alpha = 6.6^{\circ}$.

Figure 19.- Continued.

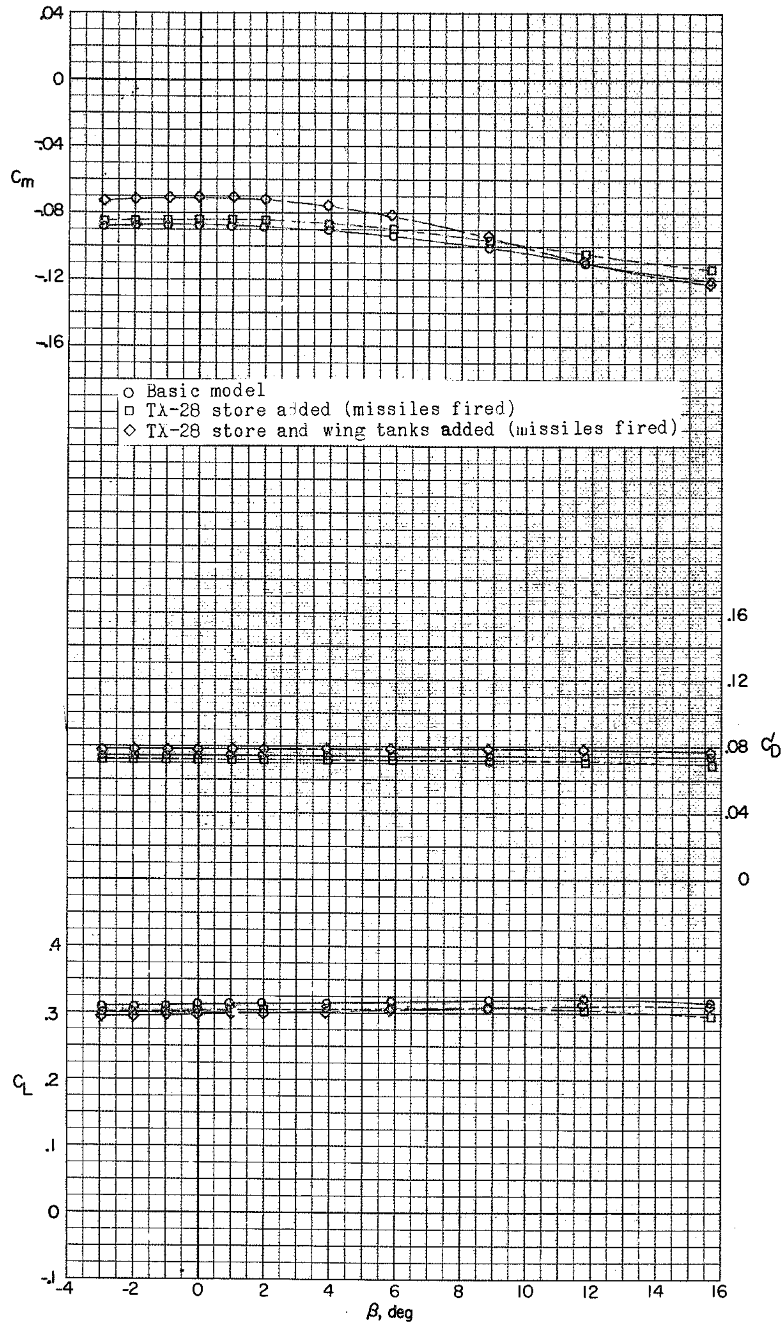

(e) Concluded.

Figure 19.- Continued.

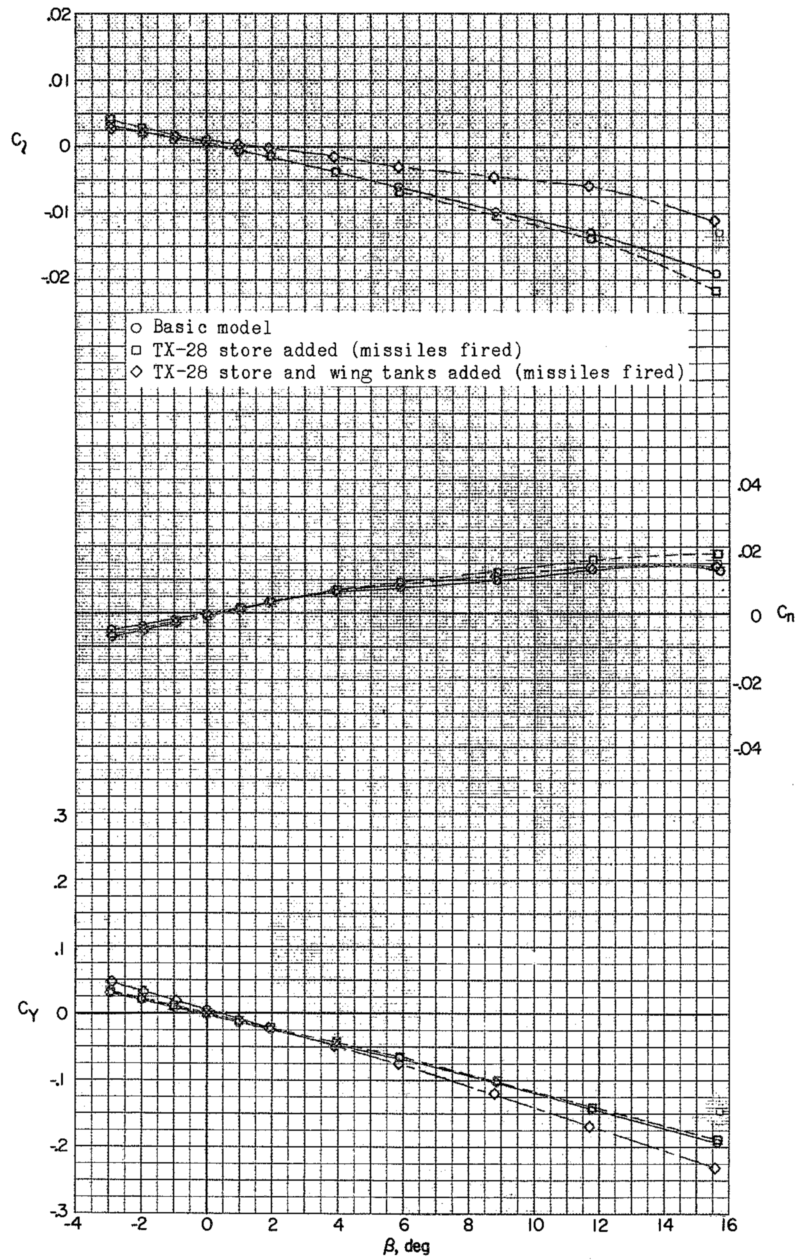

(f) $M = 1.87$; $\alpha = 17.1^{\circ}$.

Figure 19.- Continued.

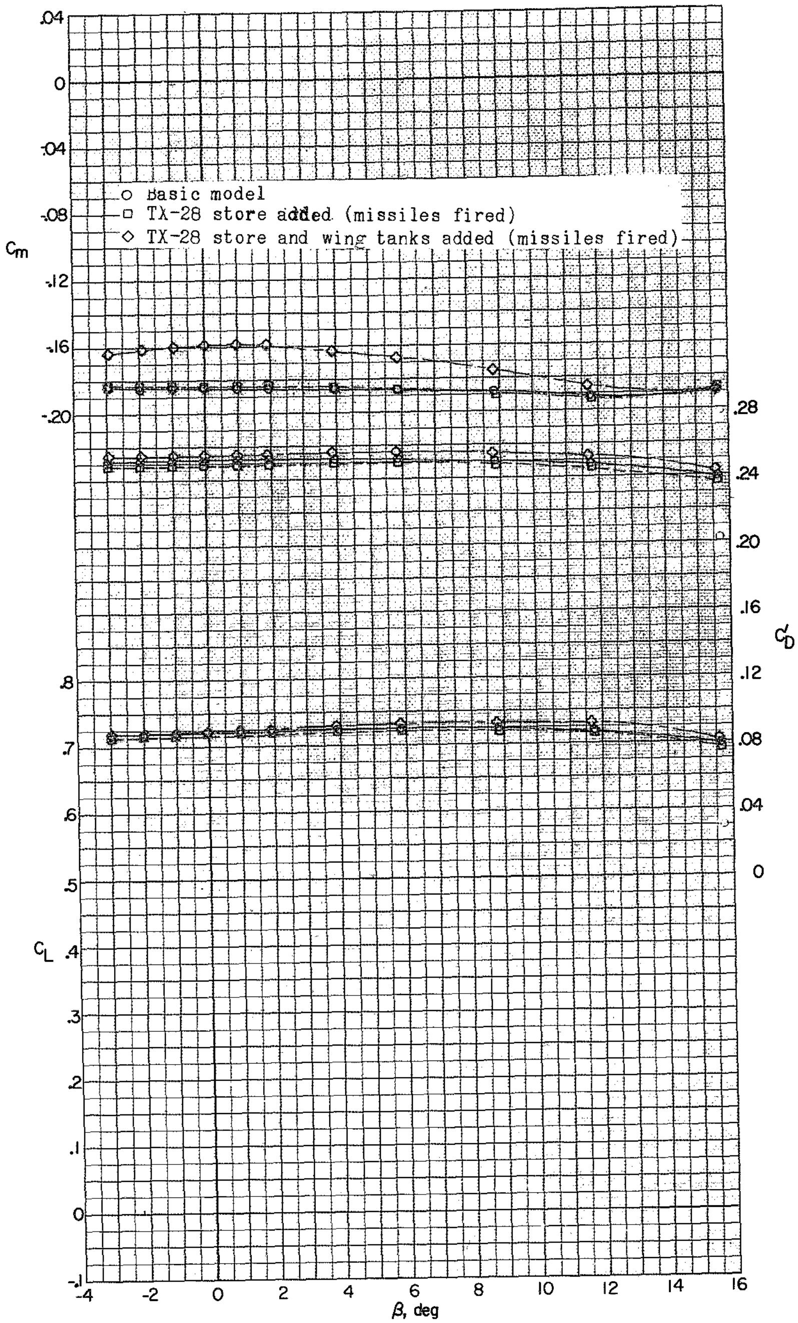

(f) Concluded.

Figure 19.- Continued.

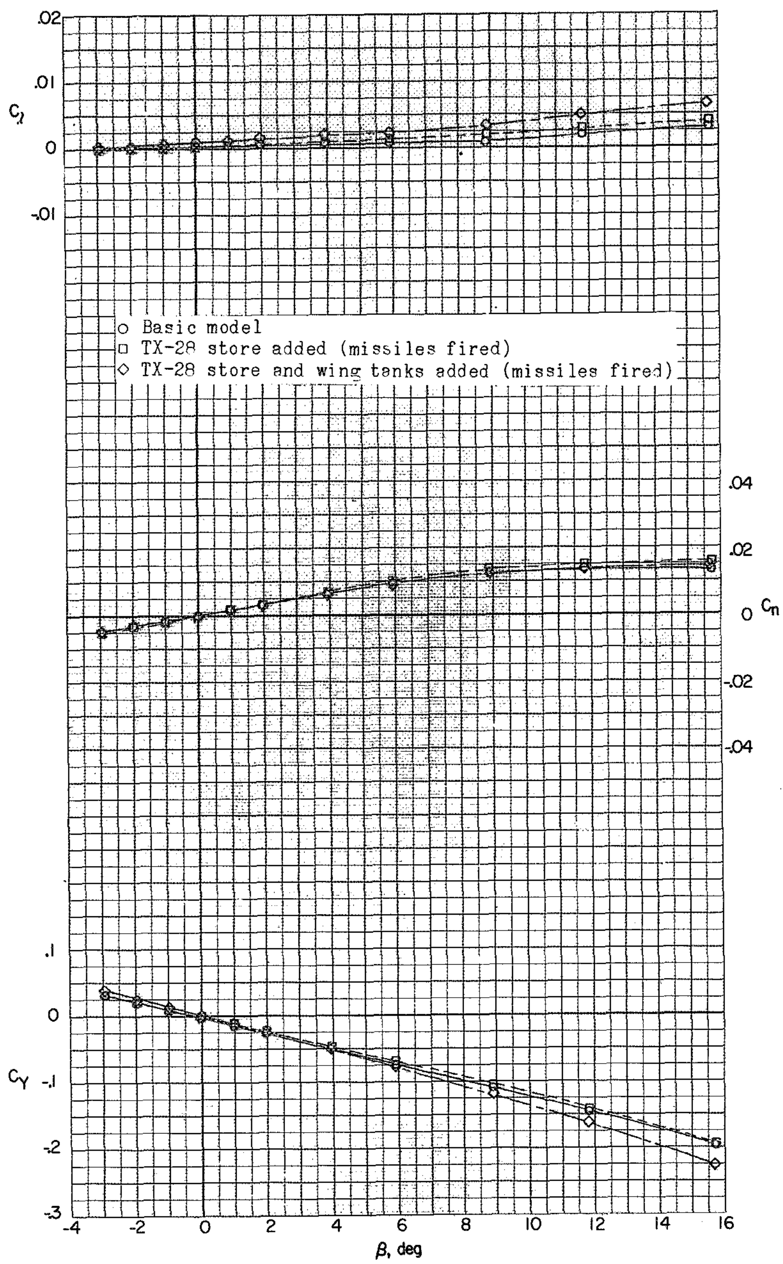

(g) $M = 2.16$; $\alpha = 0.4^{\circ}$.

Figure 19.- Continued.

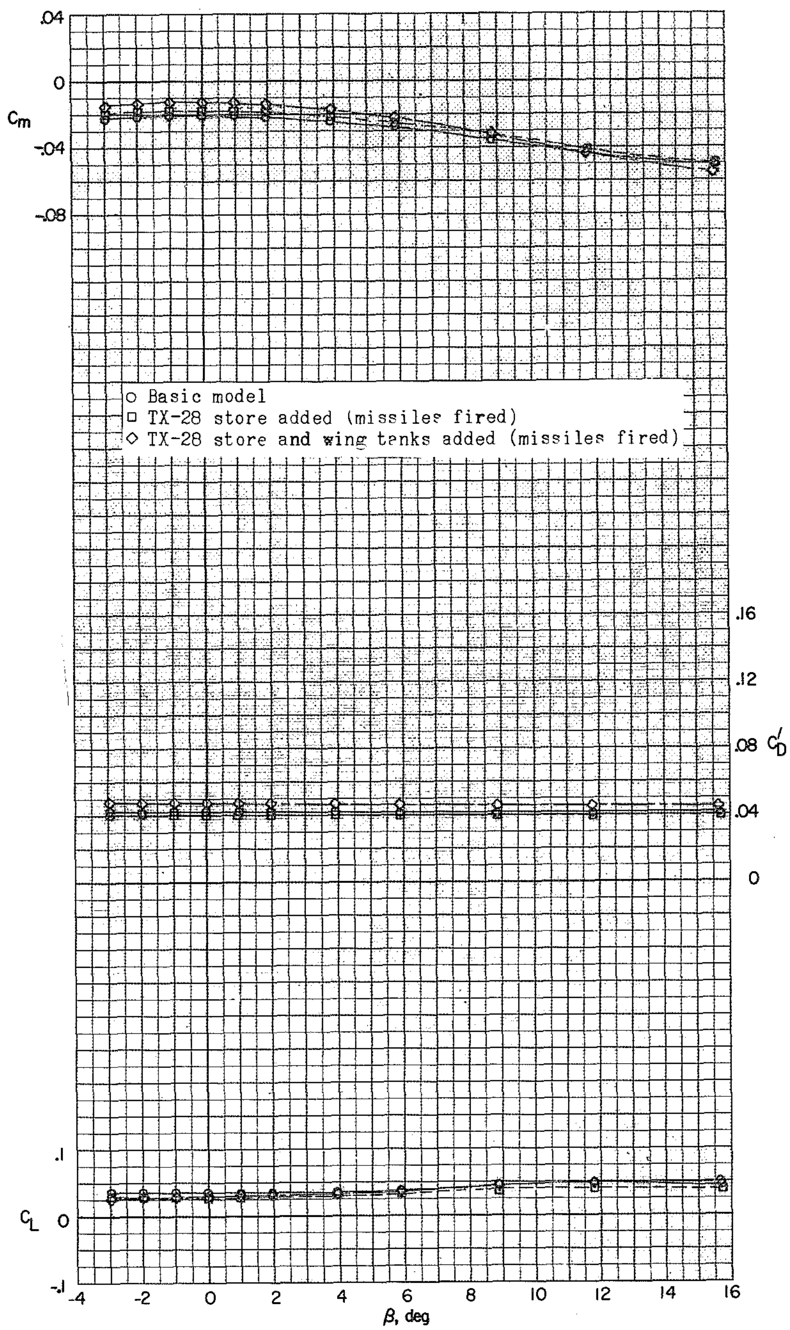

(g) Concluded.

Figure 19.- Continued.

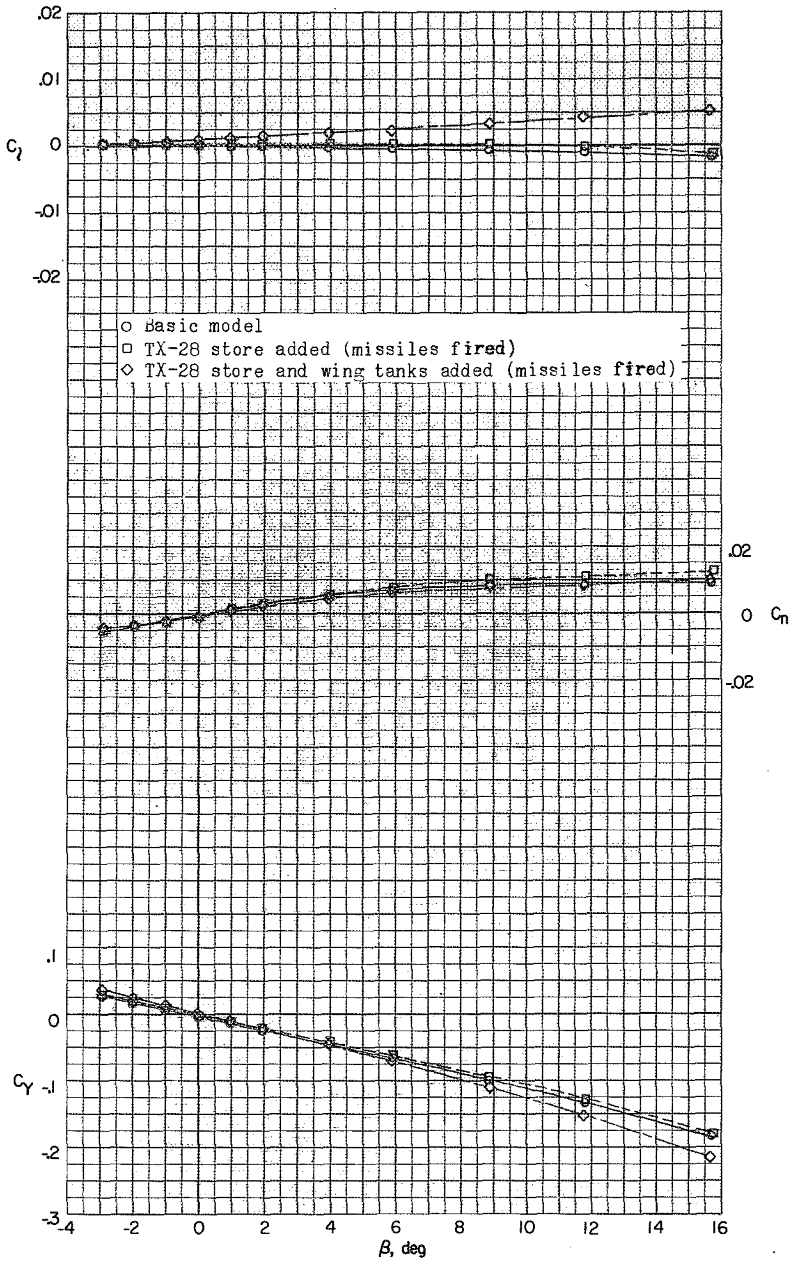

(h) M = 2.16; $\alpha = 6.5^{\circ}$.

Figure 19.- Continued.

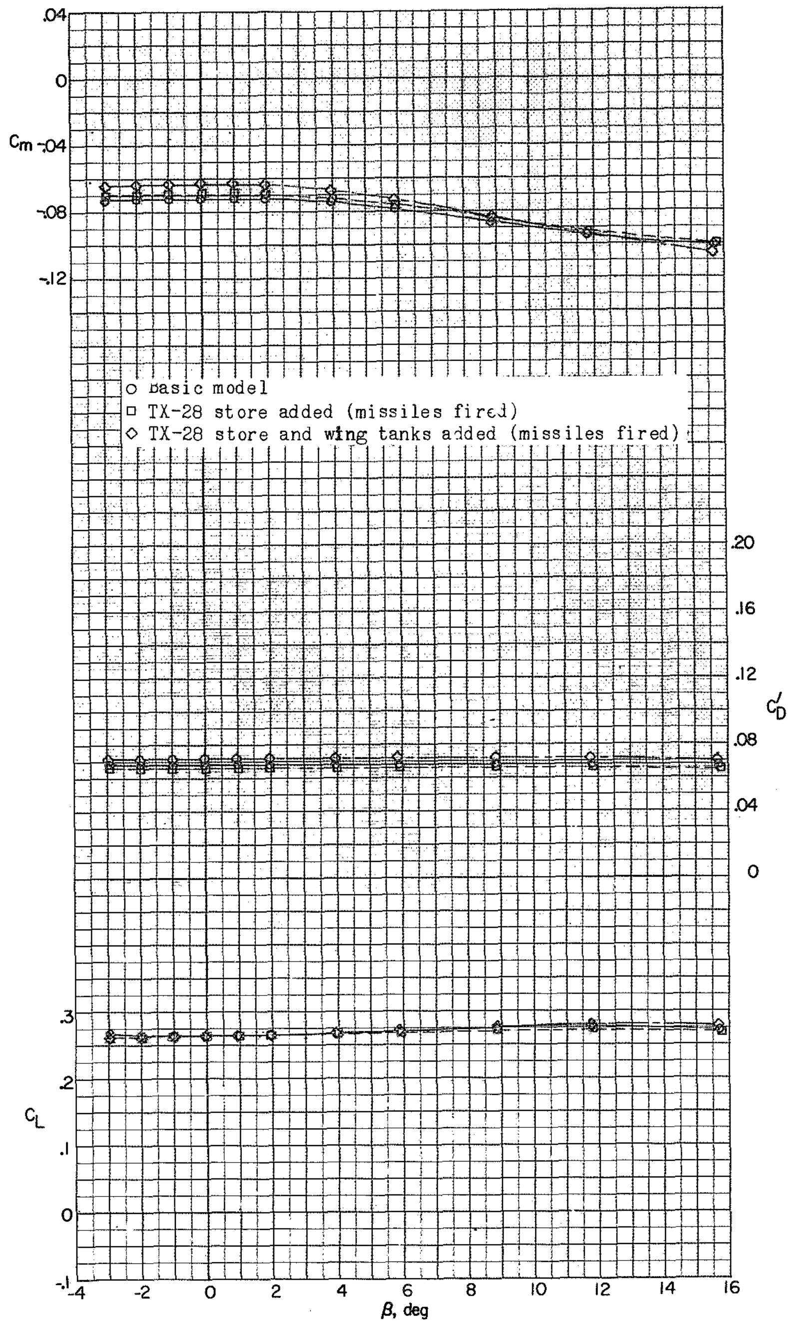

(h) Concluded.

Figure 19.- Continued.

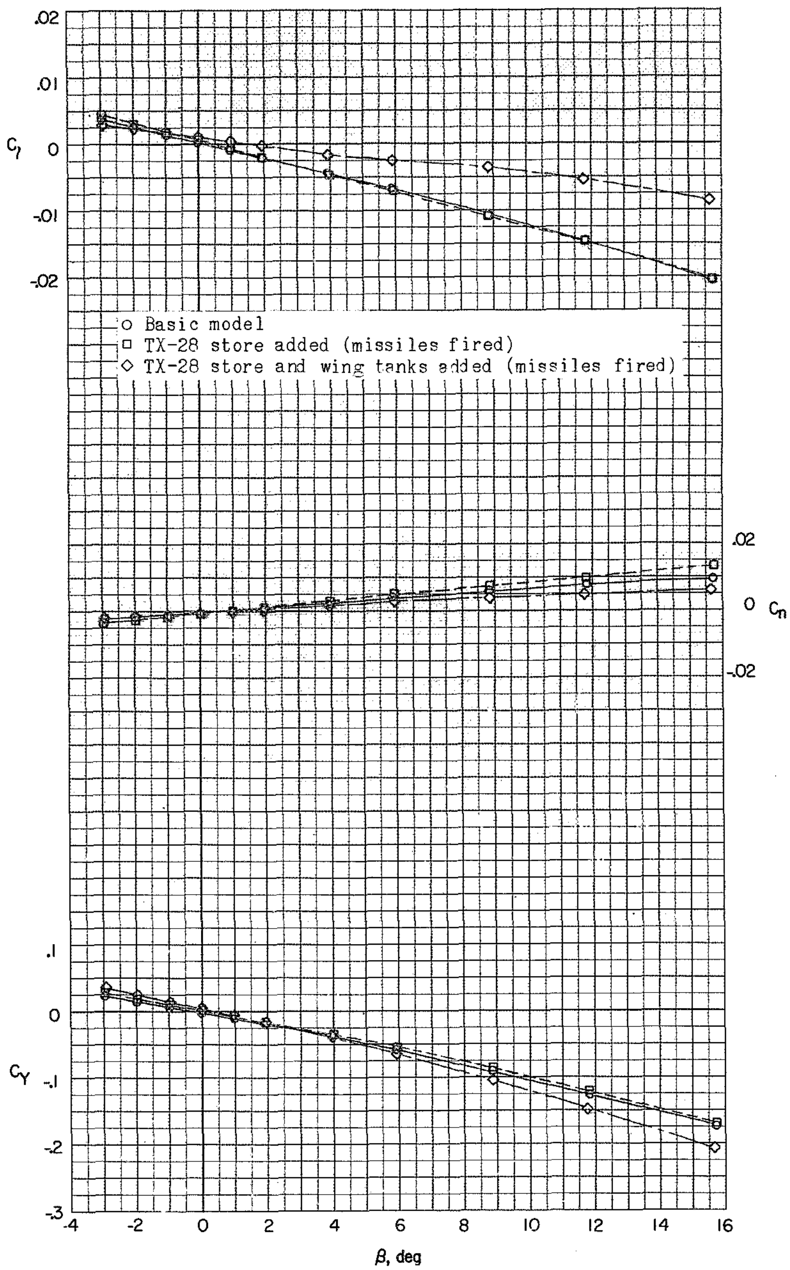

(i) $M = 2.16$; $\alpha = 16.9^{\circ}$.

Figure 19.- Continued.

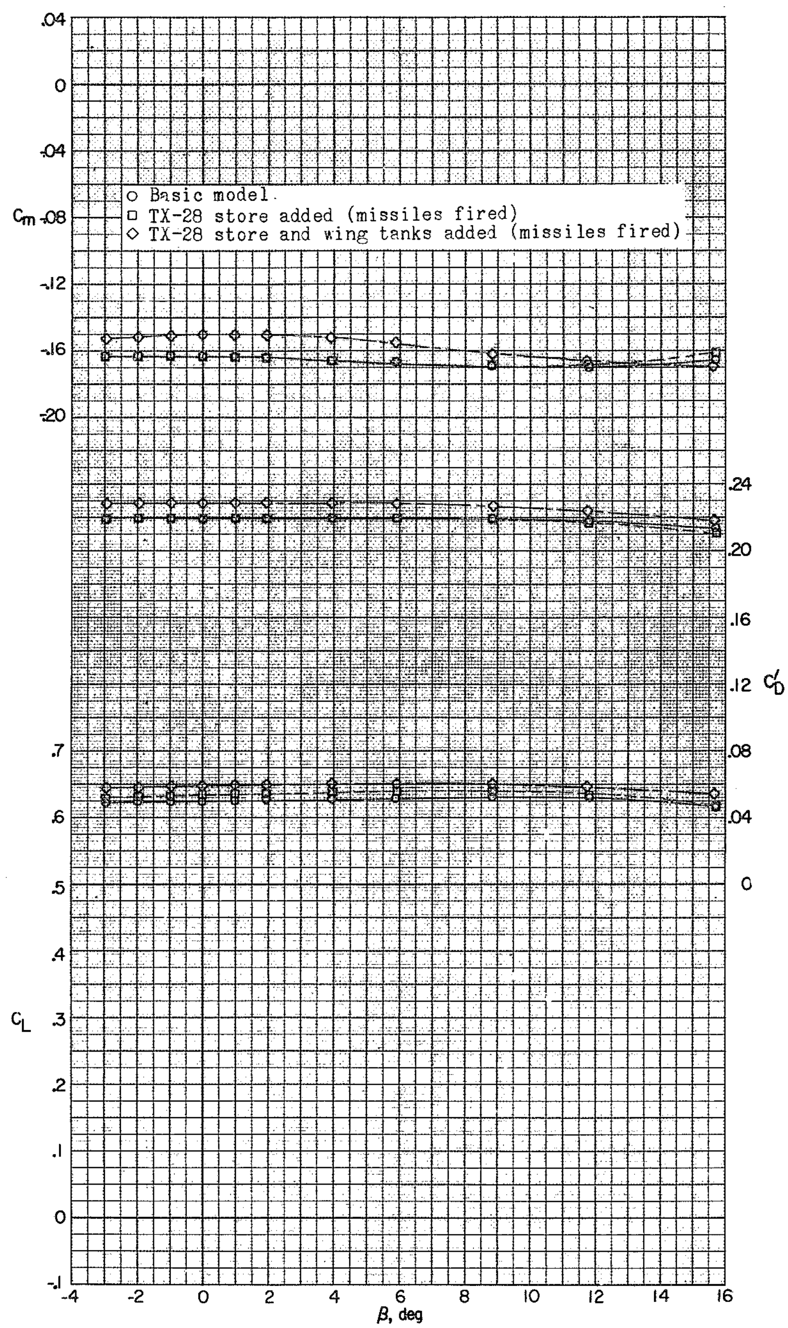

(i) Concluded.

Figure 19.- Concluded.

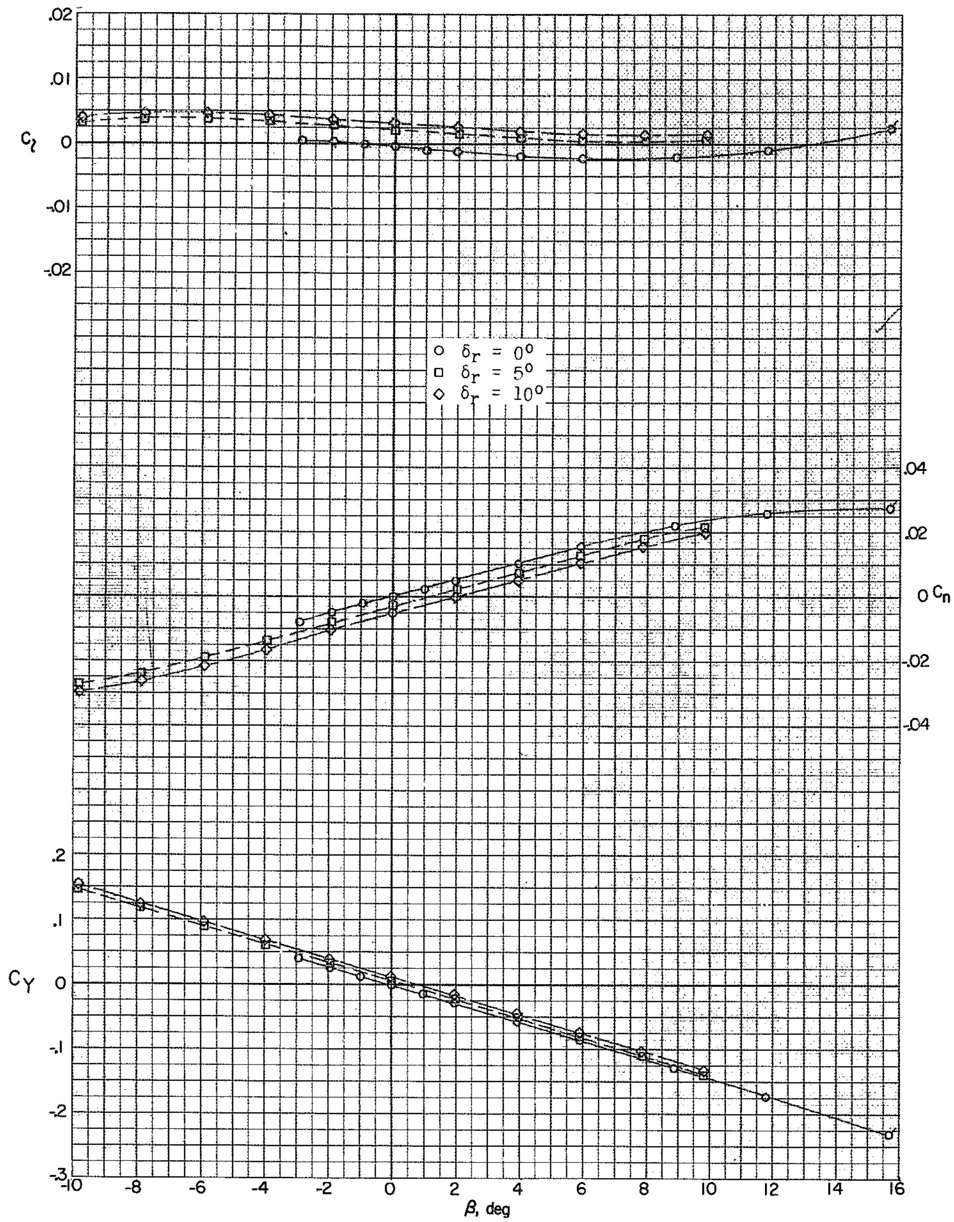

(a) $M = 1.57$; $\alpha = 0.4^\circ$.

Figure 20.- Effect of rudder deflection on aerodynamic characteristics in sideslip. (Flagged symbols denote wall-reflected shock waves striking the tail.)

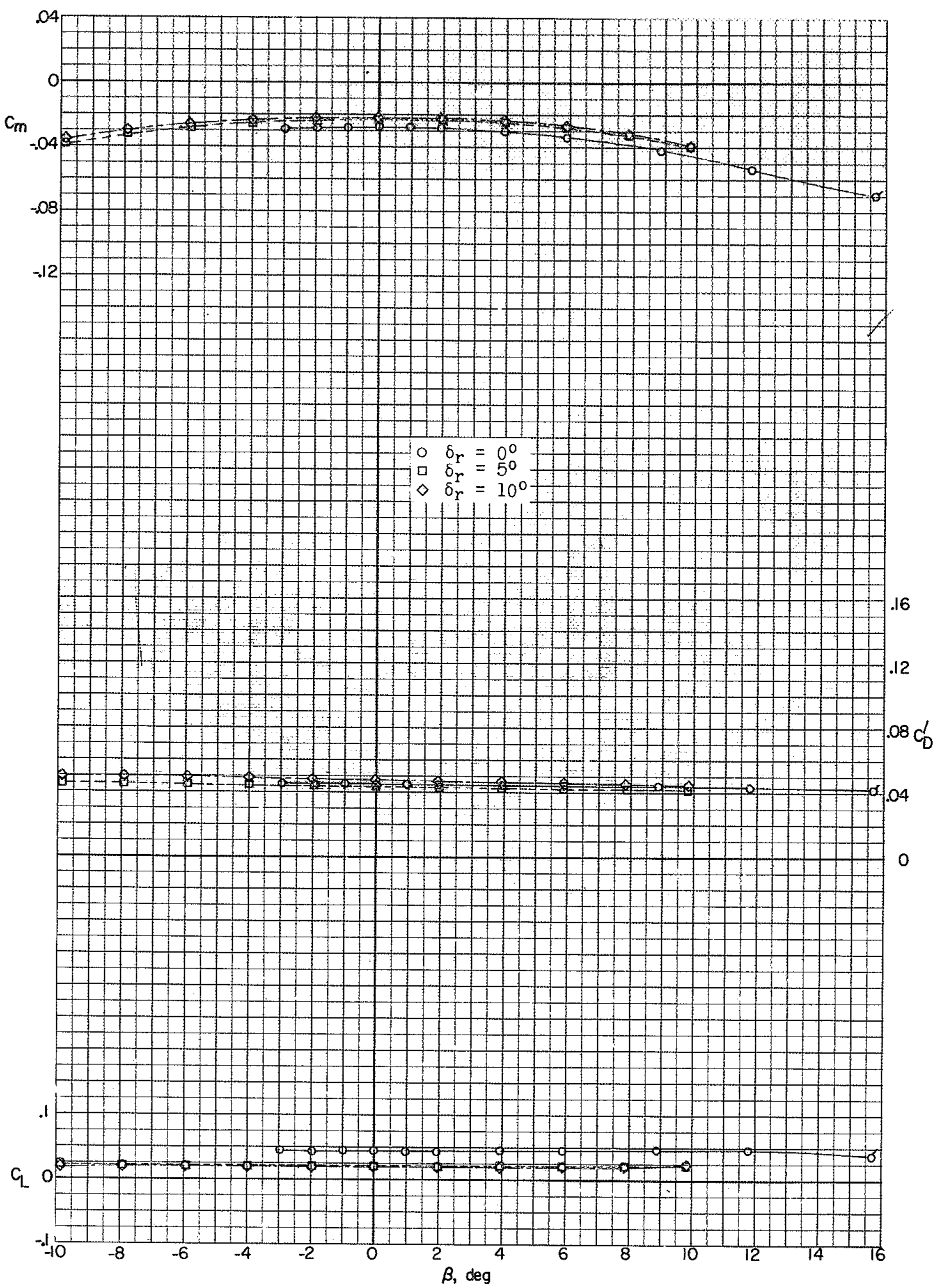

(a) Concluded.

Figure 20.- Continued.

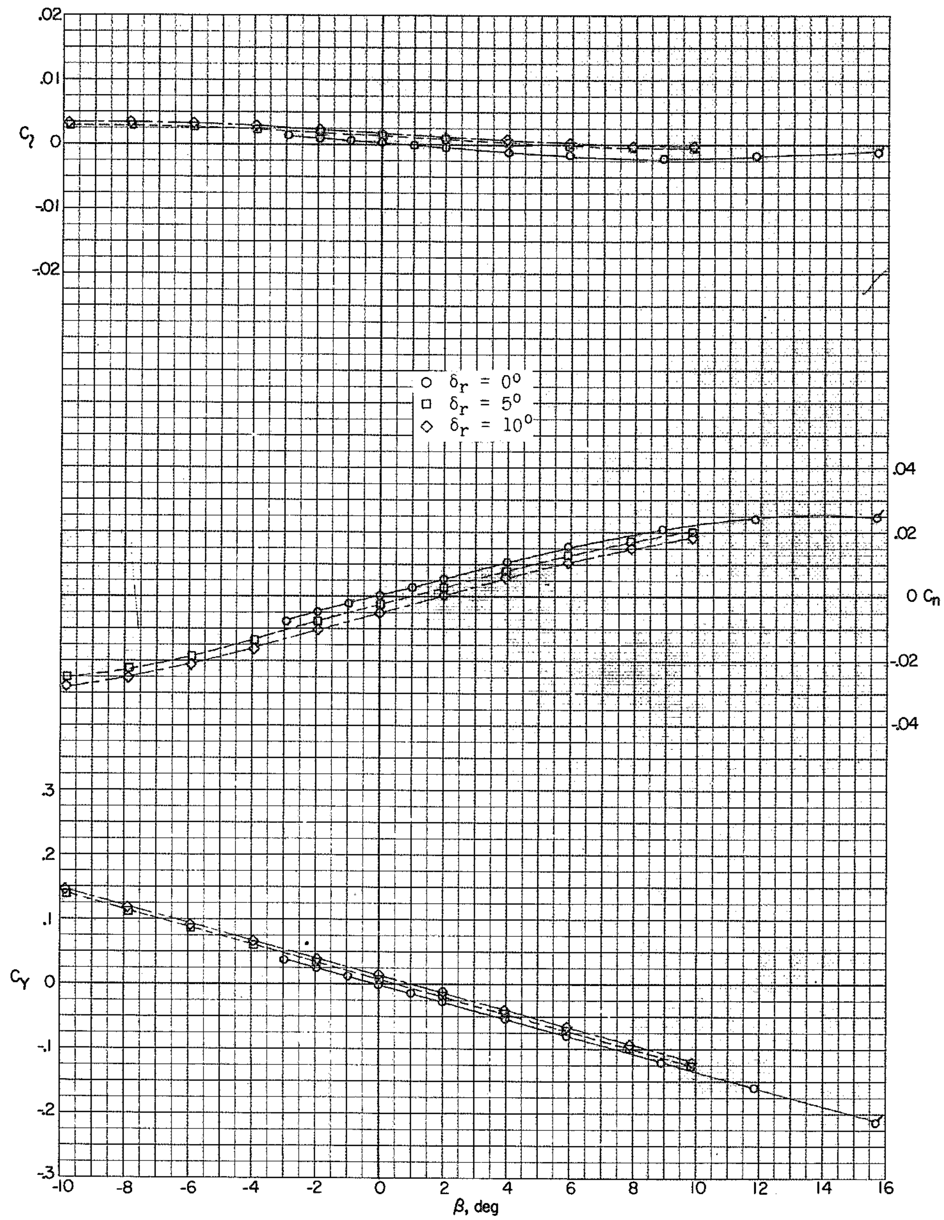

(b) M = 1.57; α = 6.7°.

Figure 20.- Continued.

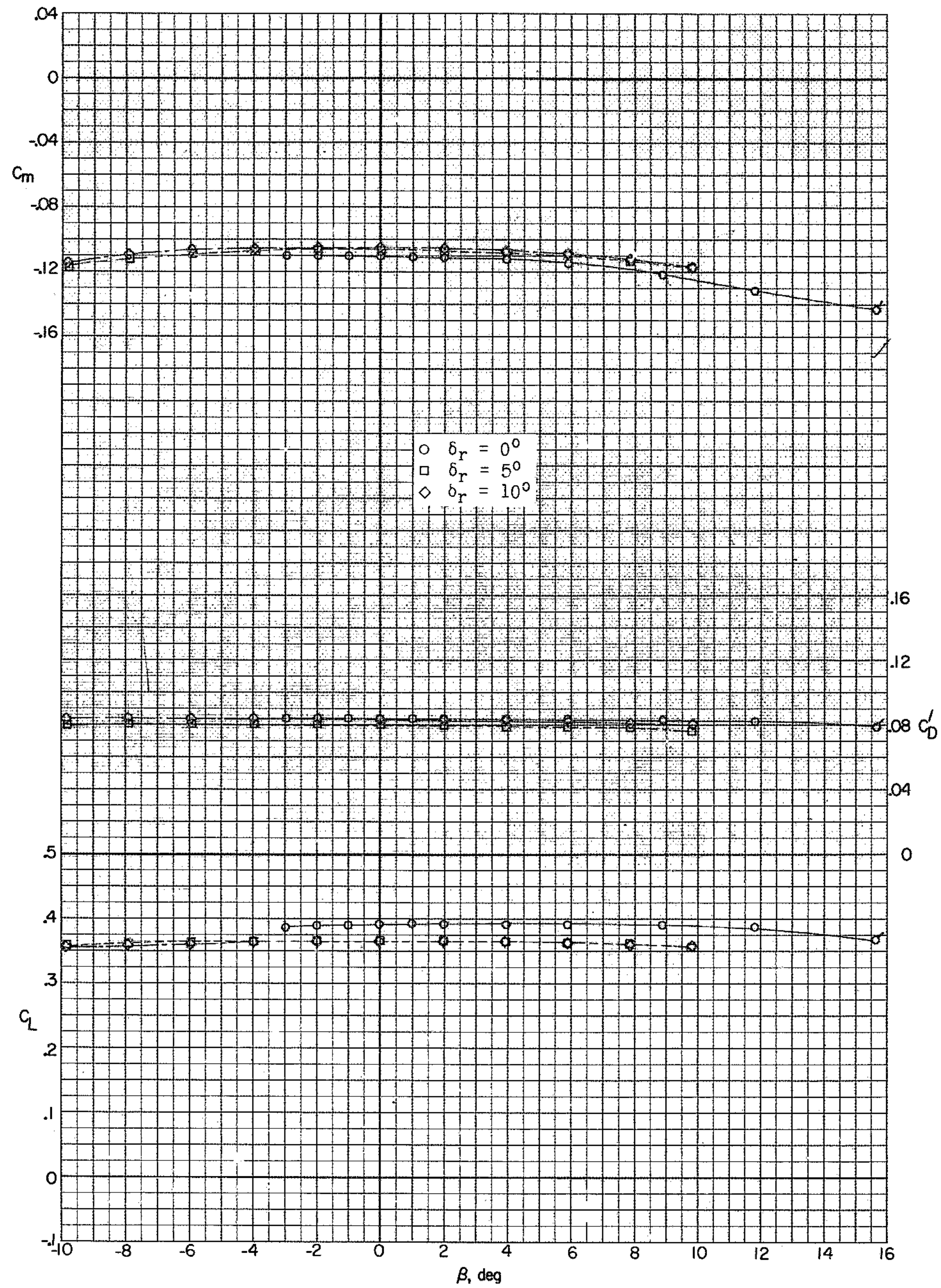

(b) Concluded.

Figure 20.- Continued.

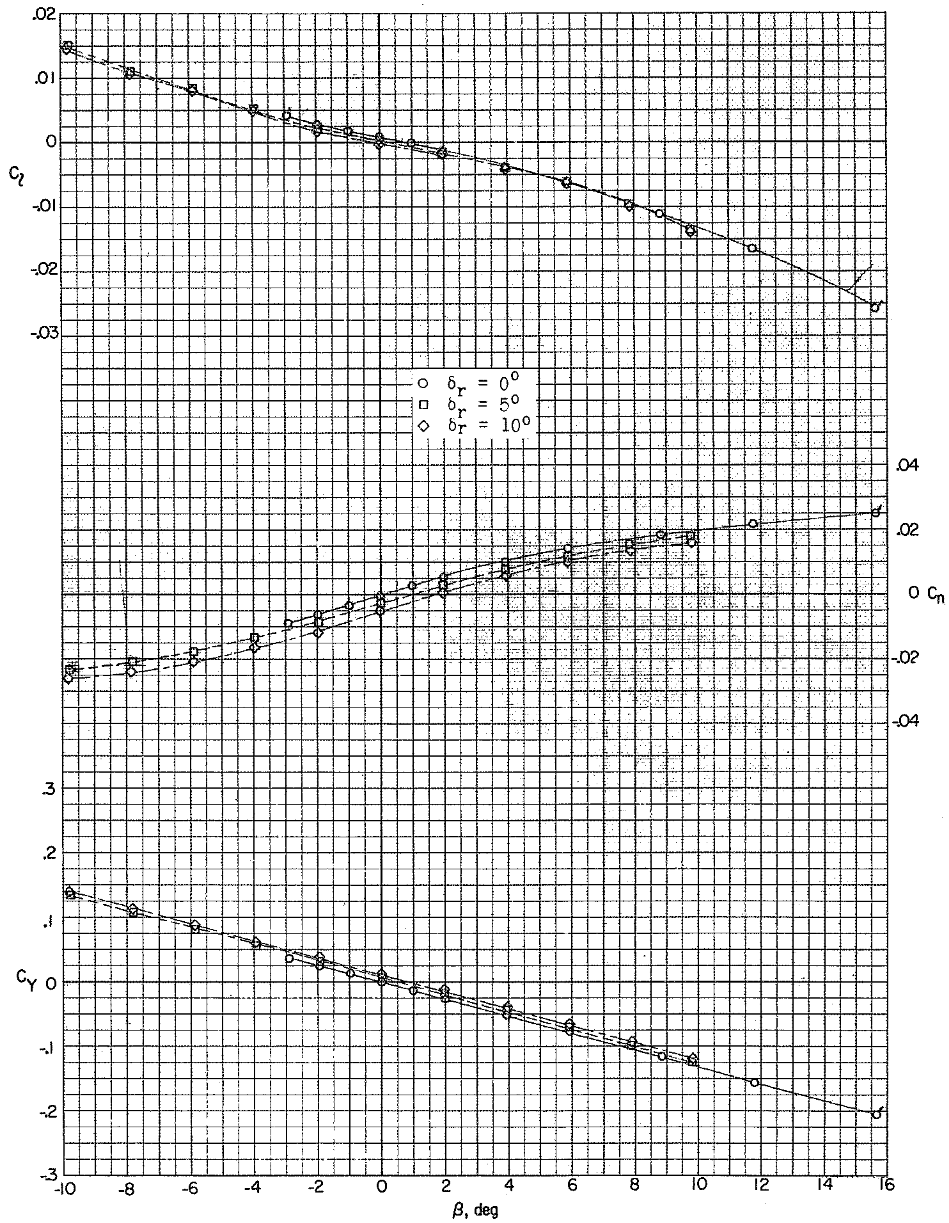

(c) $M = 1.57$; $\alpha = 17.4^o$.

Figure 20.- Continued.

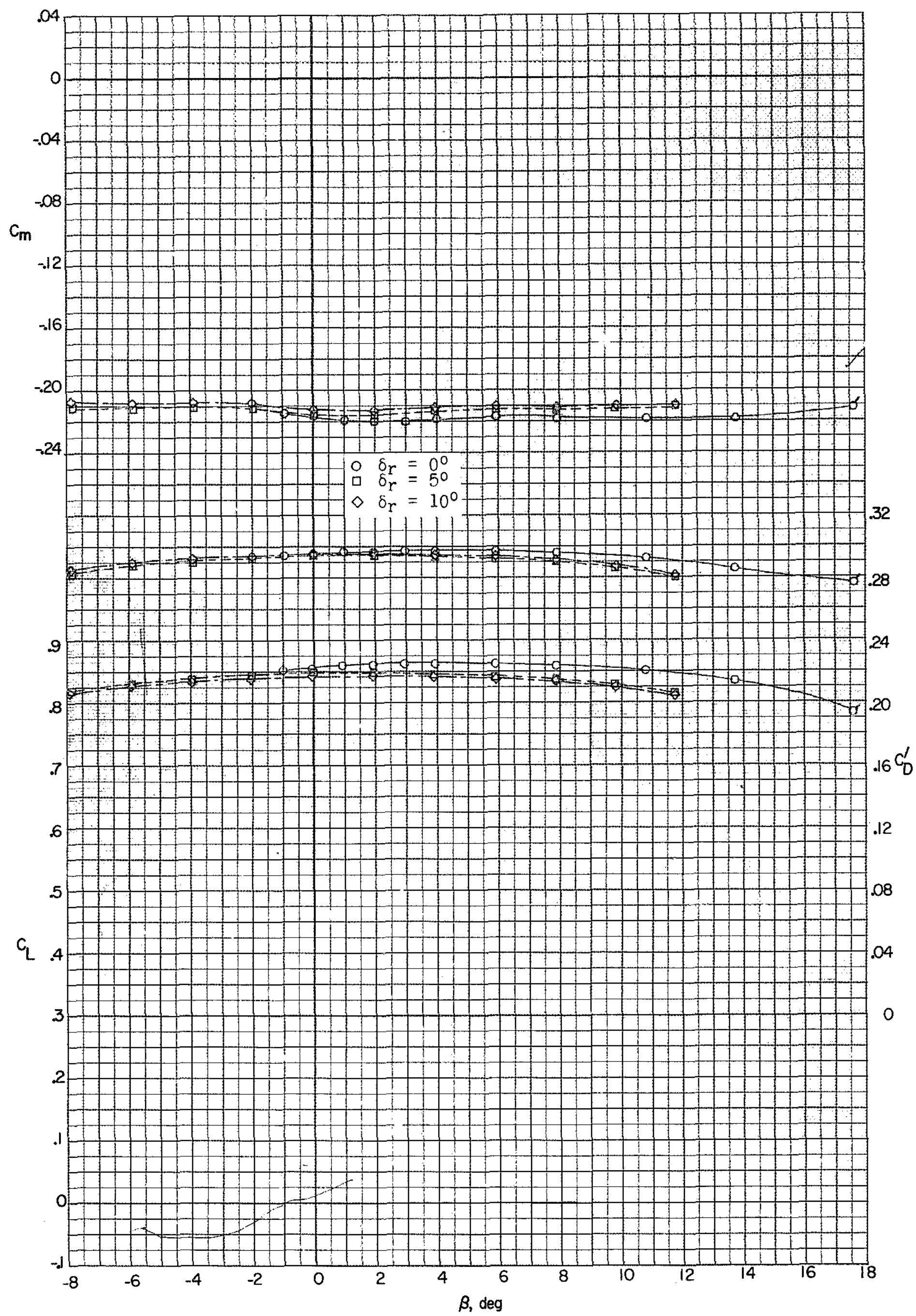

(c) Concluded.

Figure 20.- Continued.

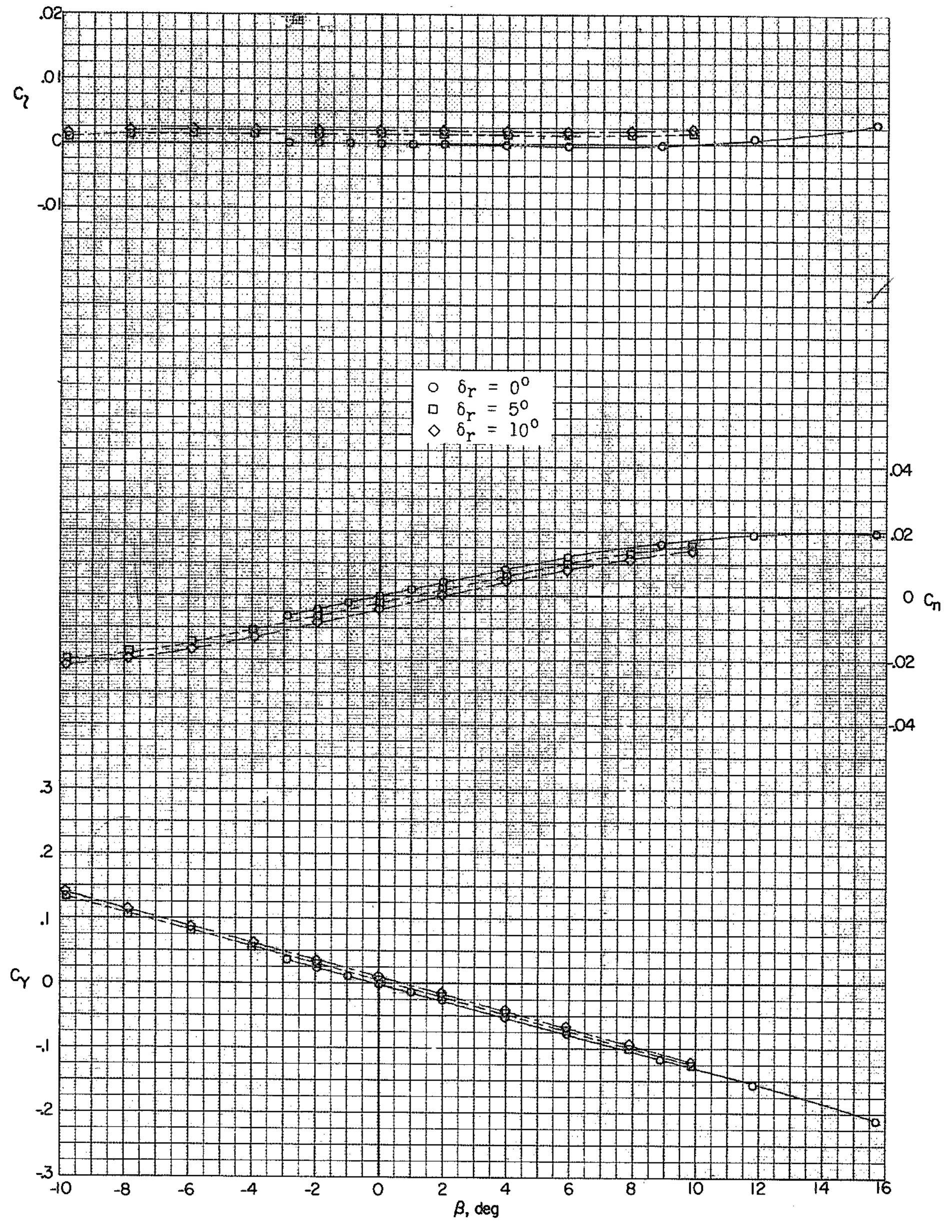

(d) $M = 1.87$; $\alpha = 0.4^{\circ}$.

Figure 20.- Continued.

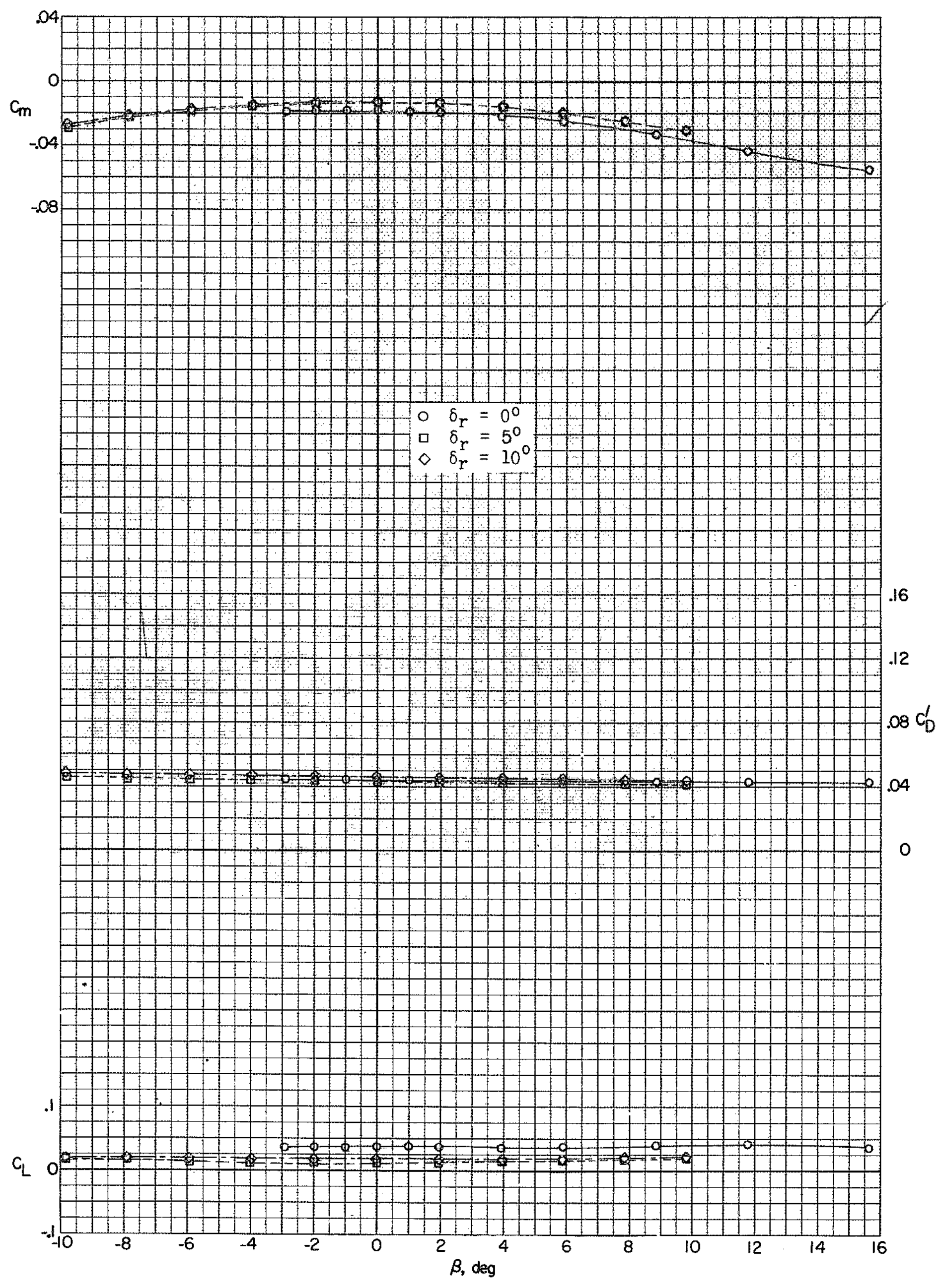

(d) Concluded.

Figure 20.- Continued.

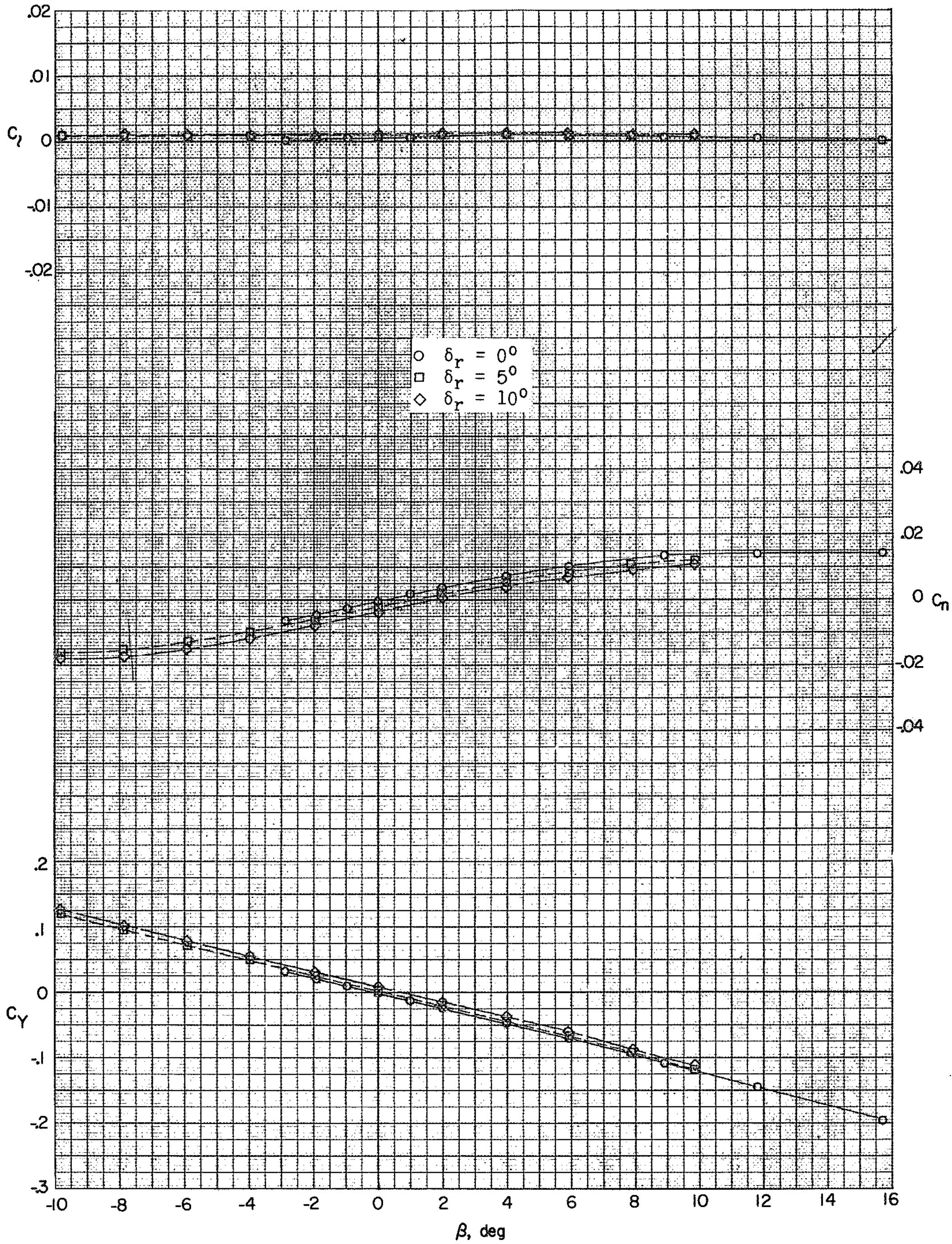

(e) $M = 1.87$; $\alpha = 6.6^o$.

Figure 20.- Continued.

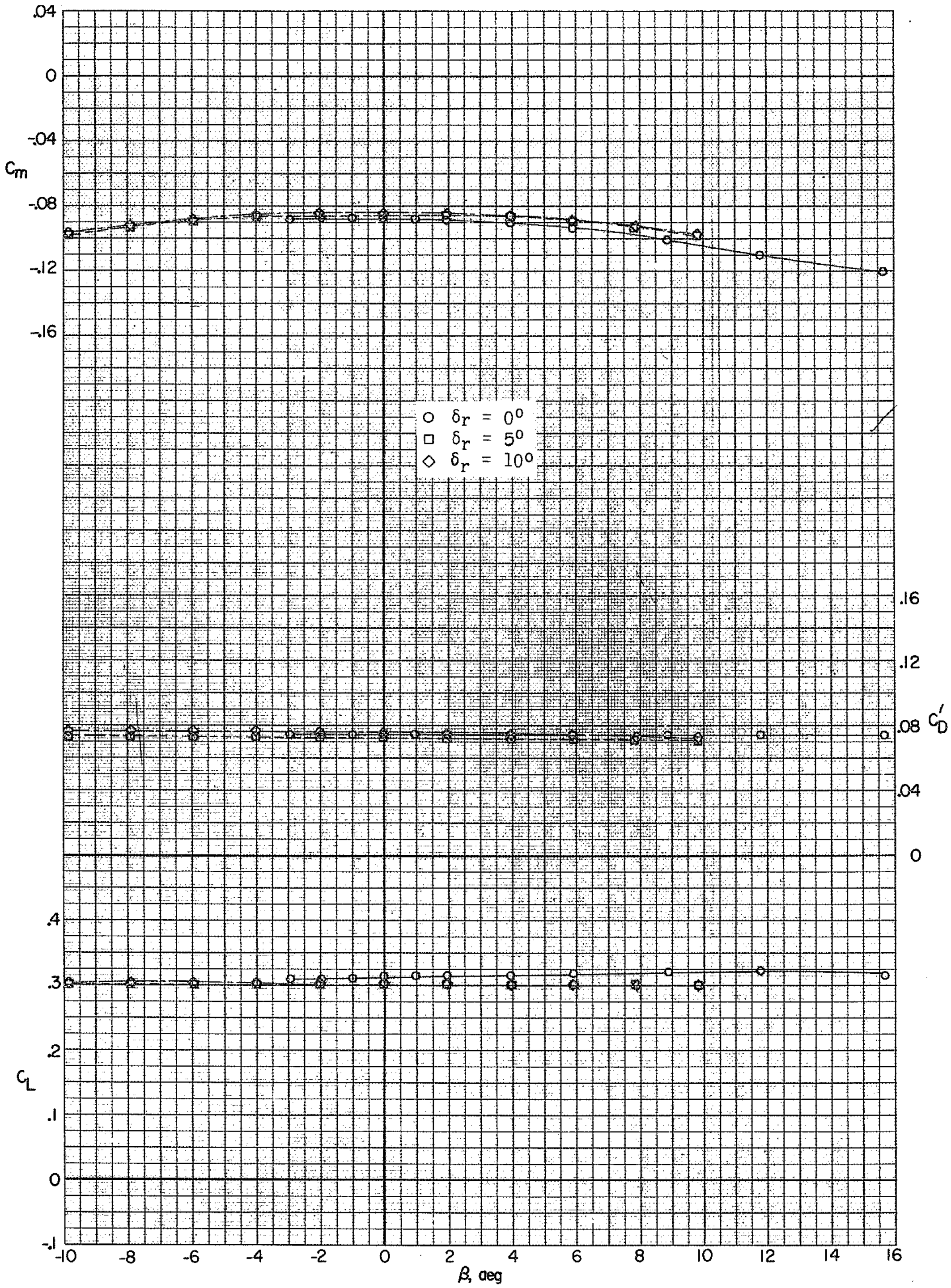

(e) Concluded.

Figure 20.- Continued.

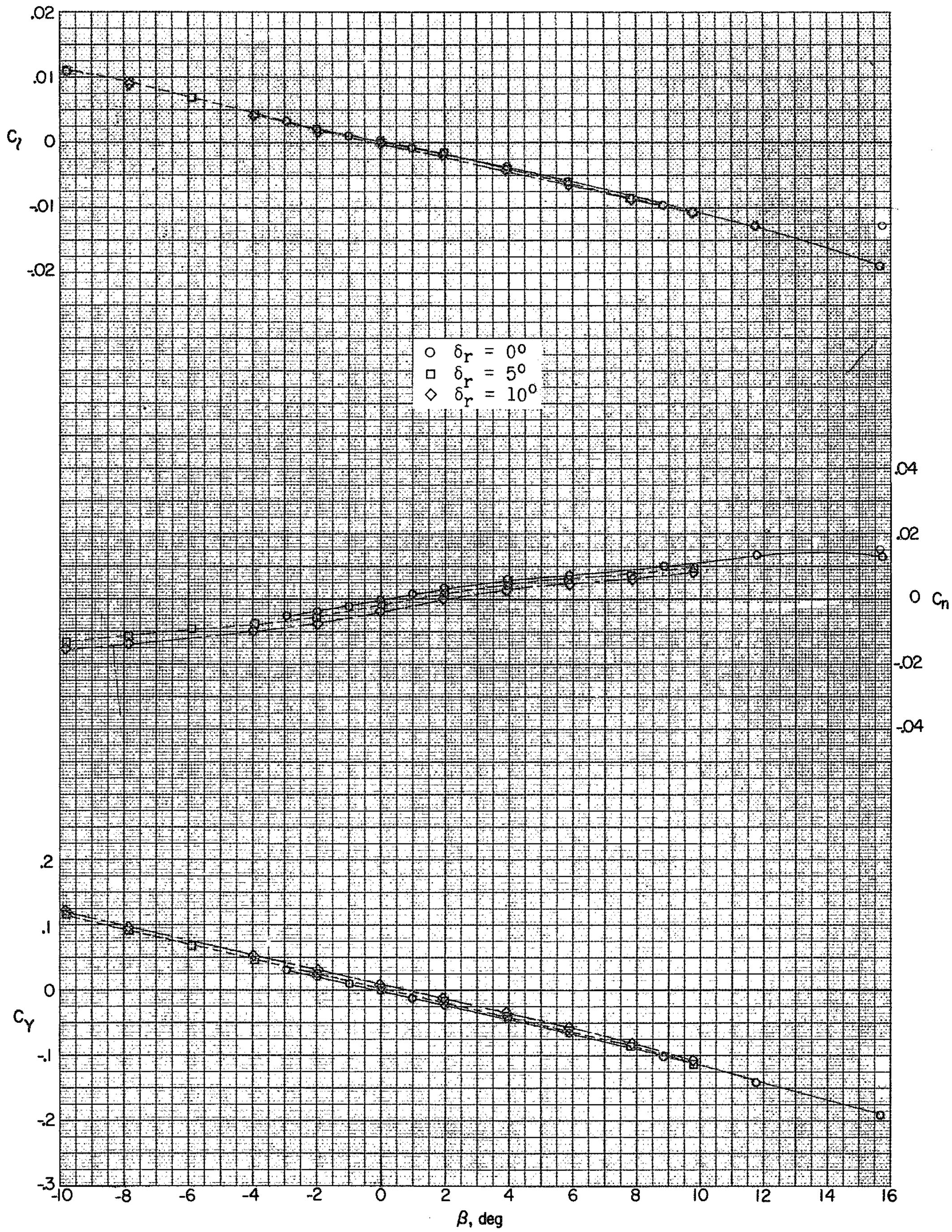

(f) M = 1.87; α = 17.1°.

Figure 20.- Continued.

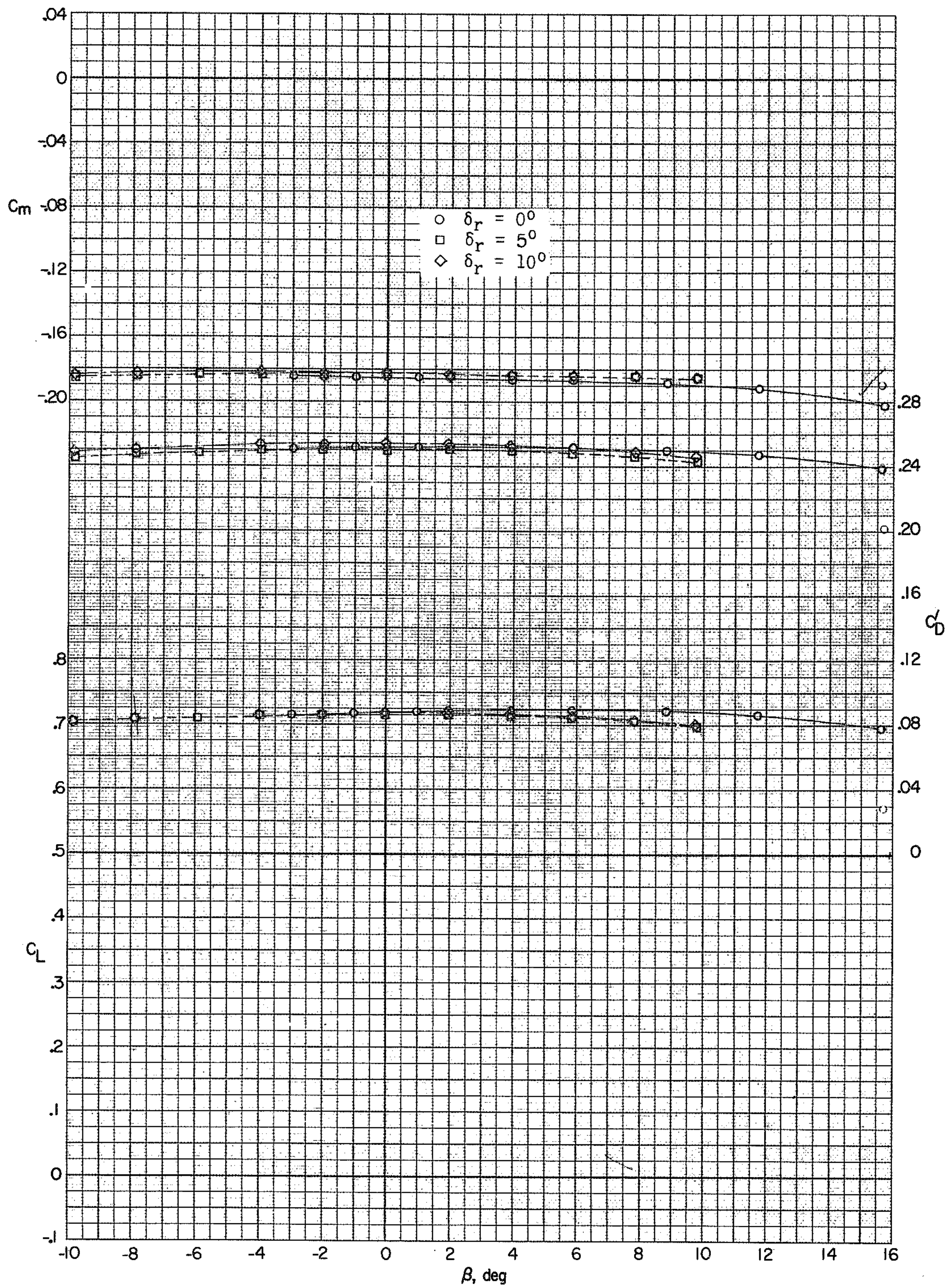

(f) Concluded.

Figure 20.- Continued.

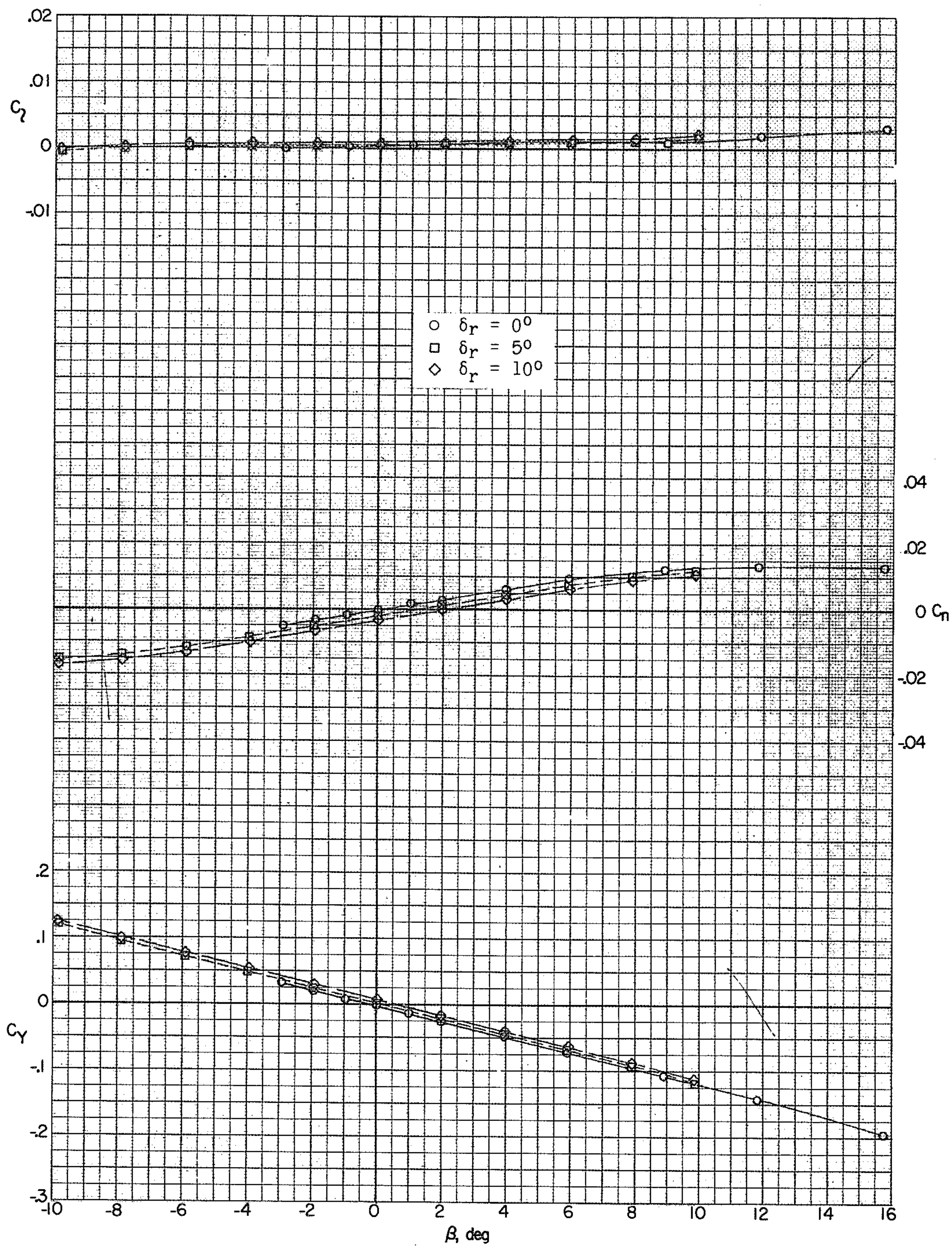

(g) $M = 2.16$; $\alpha = 0.4^{\circ}$.

Figure 20.- Continued.

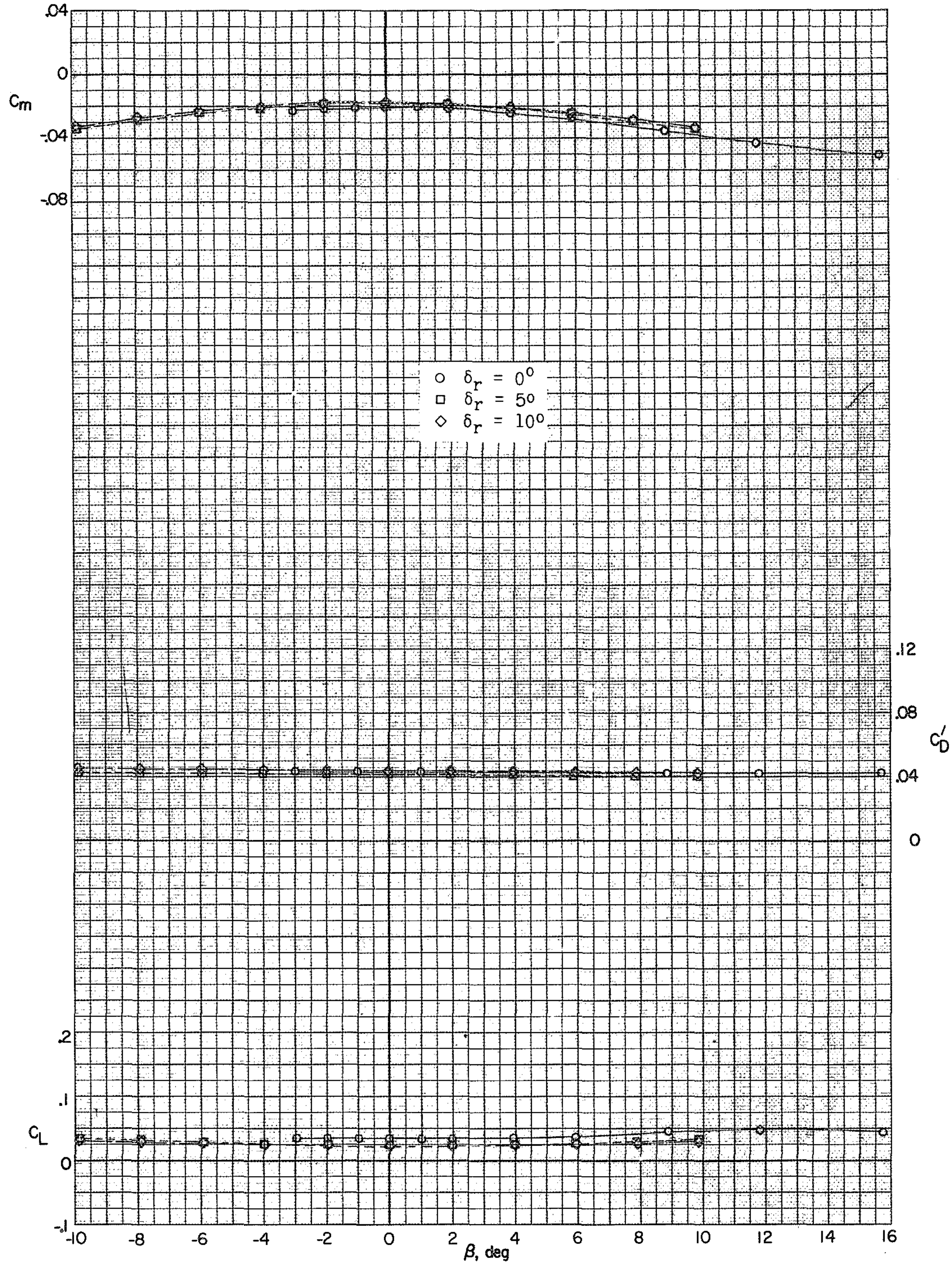

(g) Concluded.

Figure 20.- Continued.

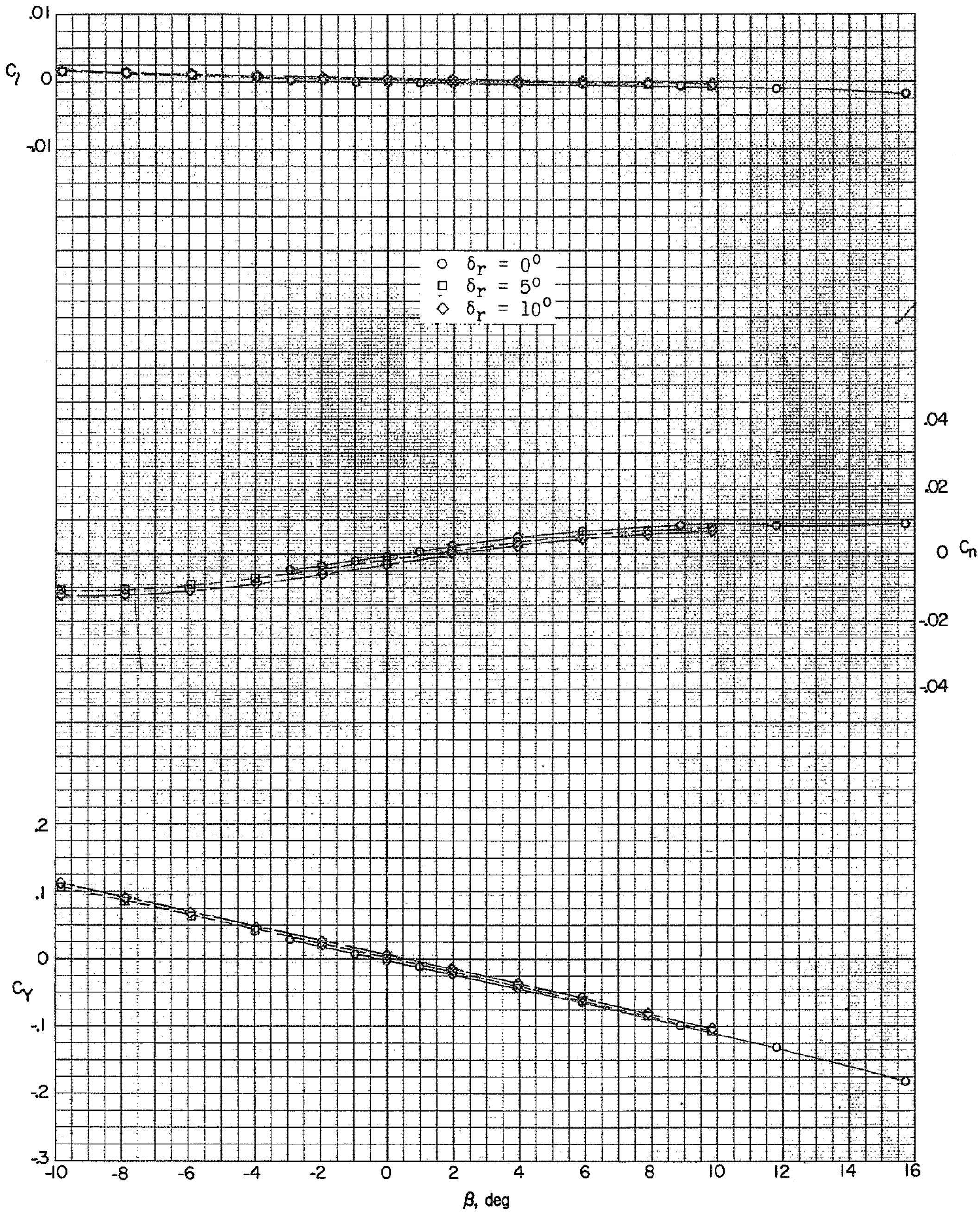

(h) $M = 2.16$; $\alpha = 6.5^\circ$.

Figure 20.- Continued.

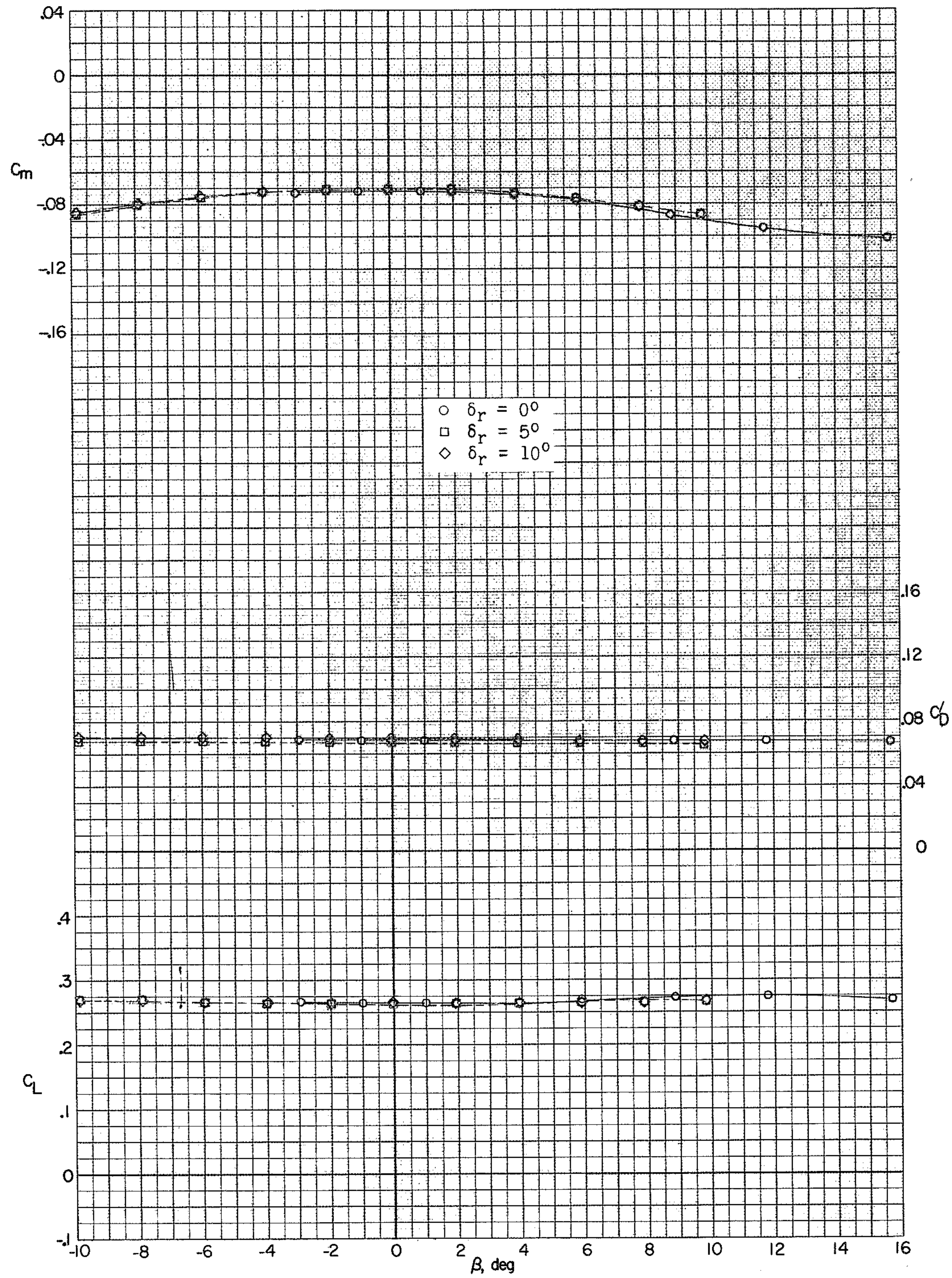

(h) Concluded.

Figure 20.- Continued.

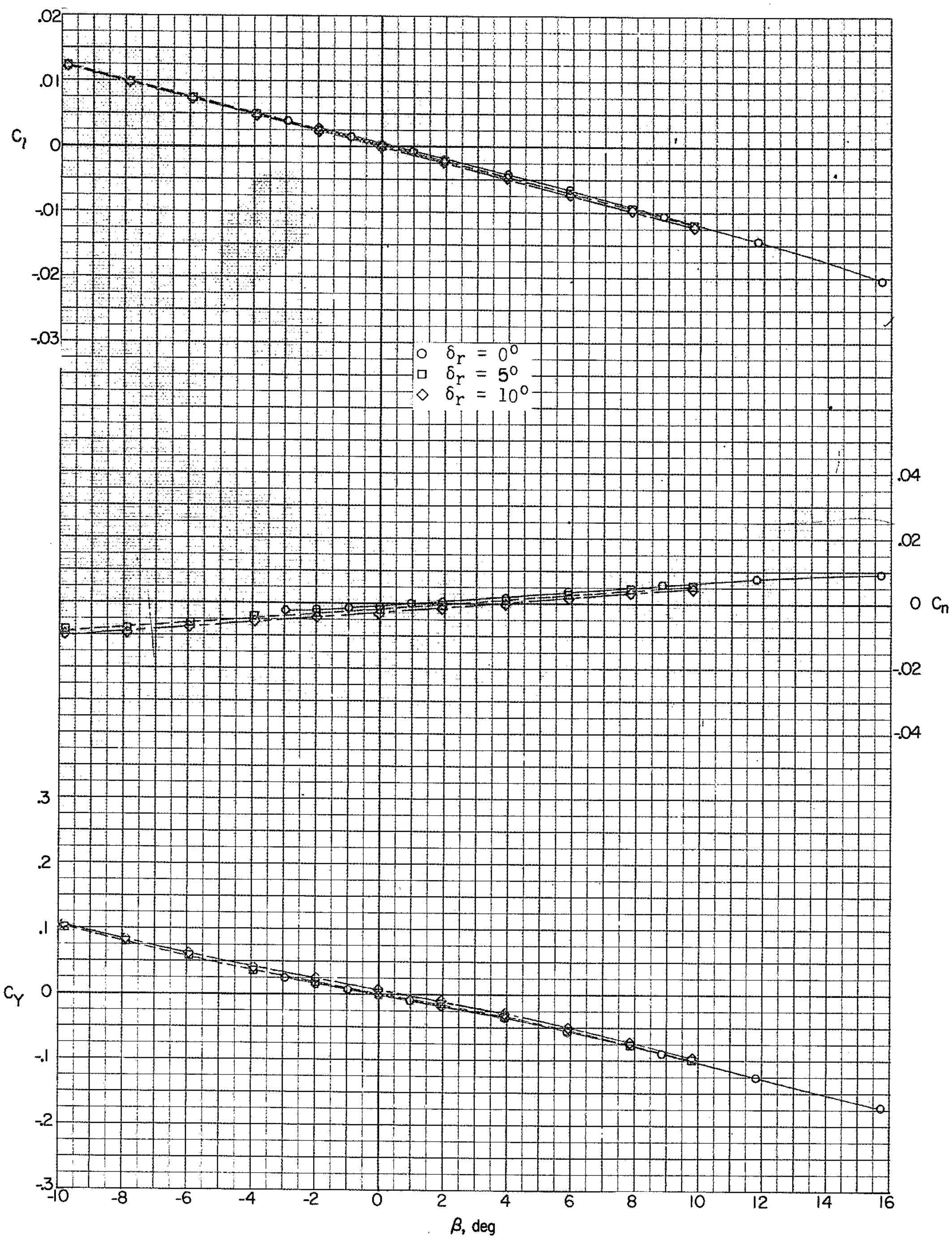

(i) $M = 2.16$; $\alpha = 16.9^\circ$.

Figure 20.- Continued.

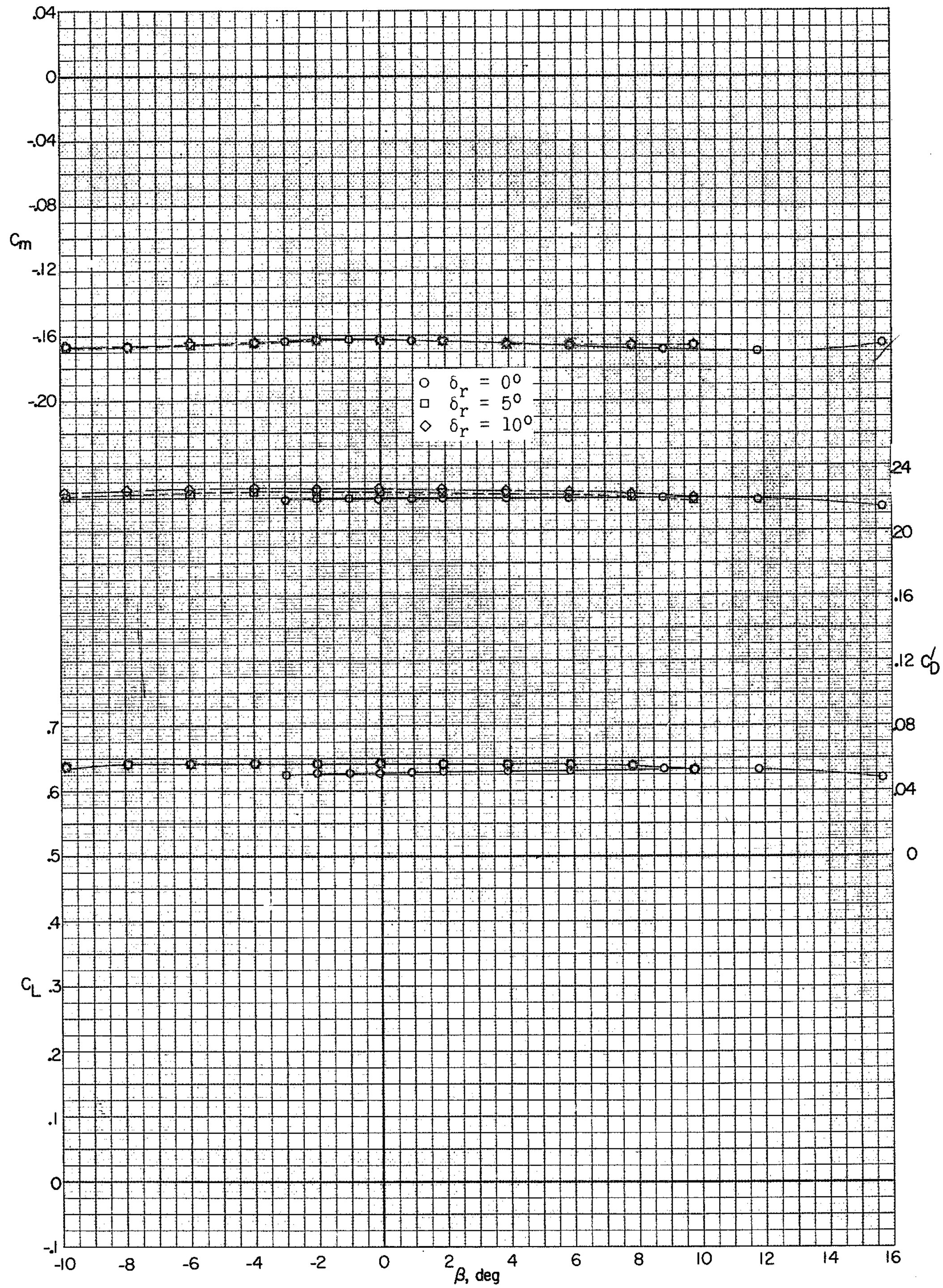

(i) Concluded.

Figure 20.- Concluded.

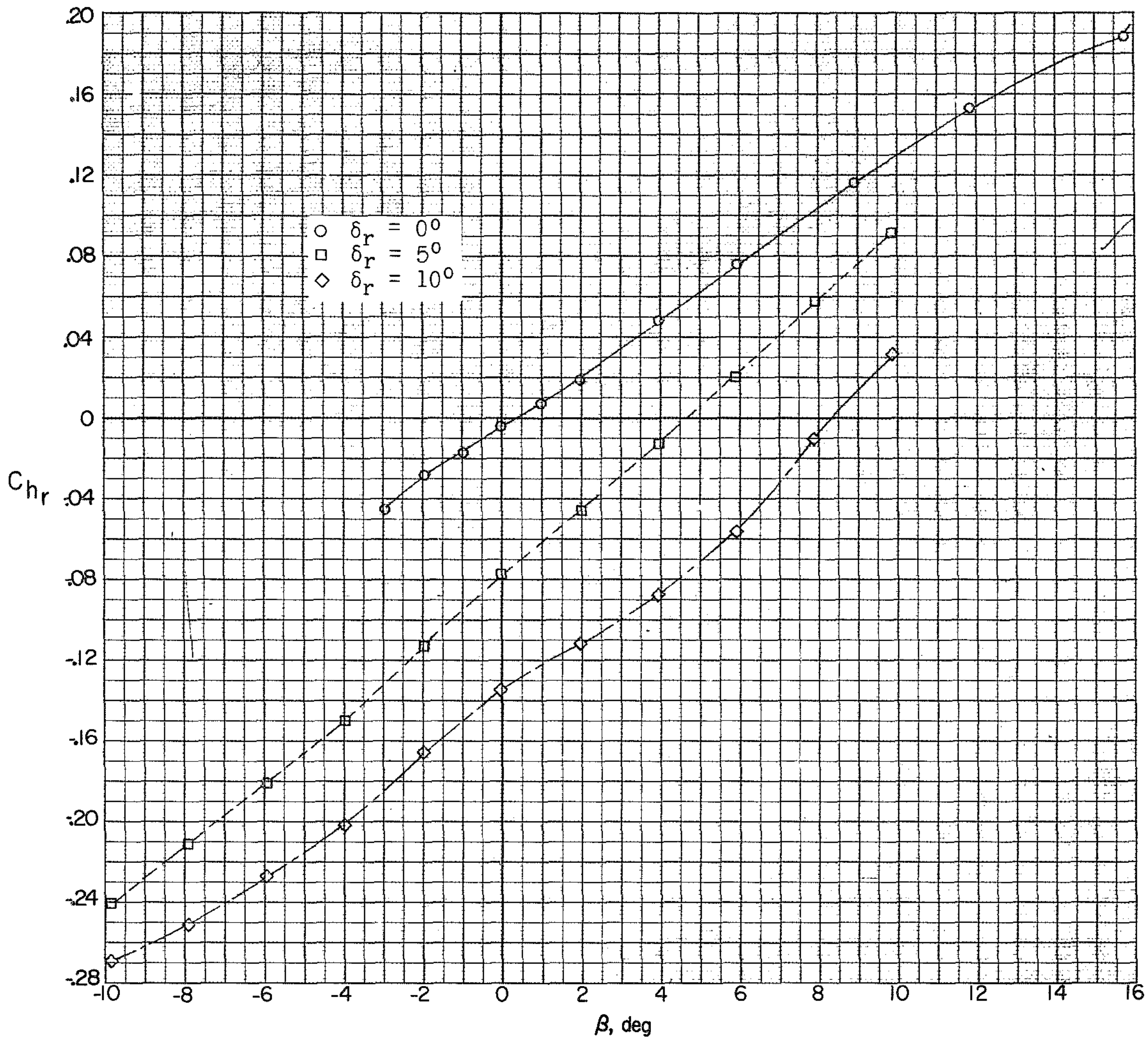

(a) $M = 1.57$; $\alpha = 0.4^\circ$.

Figure 21.- Effect of rudder deflection on rudder hinge-moment coefficient in sideslip. (Flagged symbols denote wall-reflected shock waves striking the tail.)

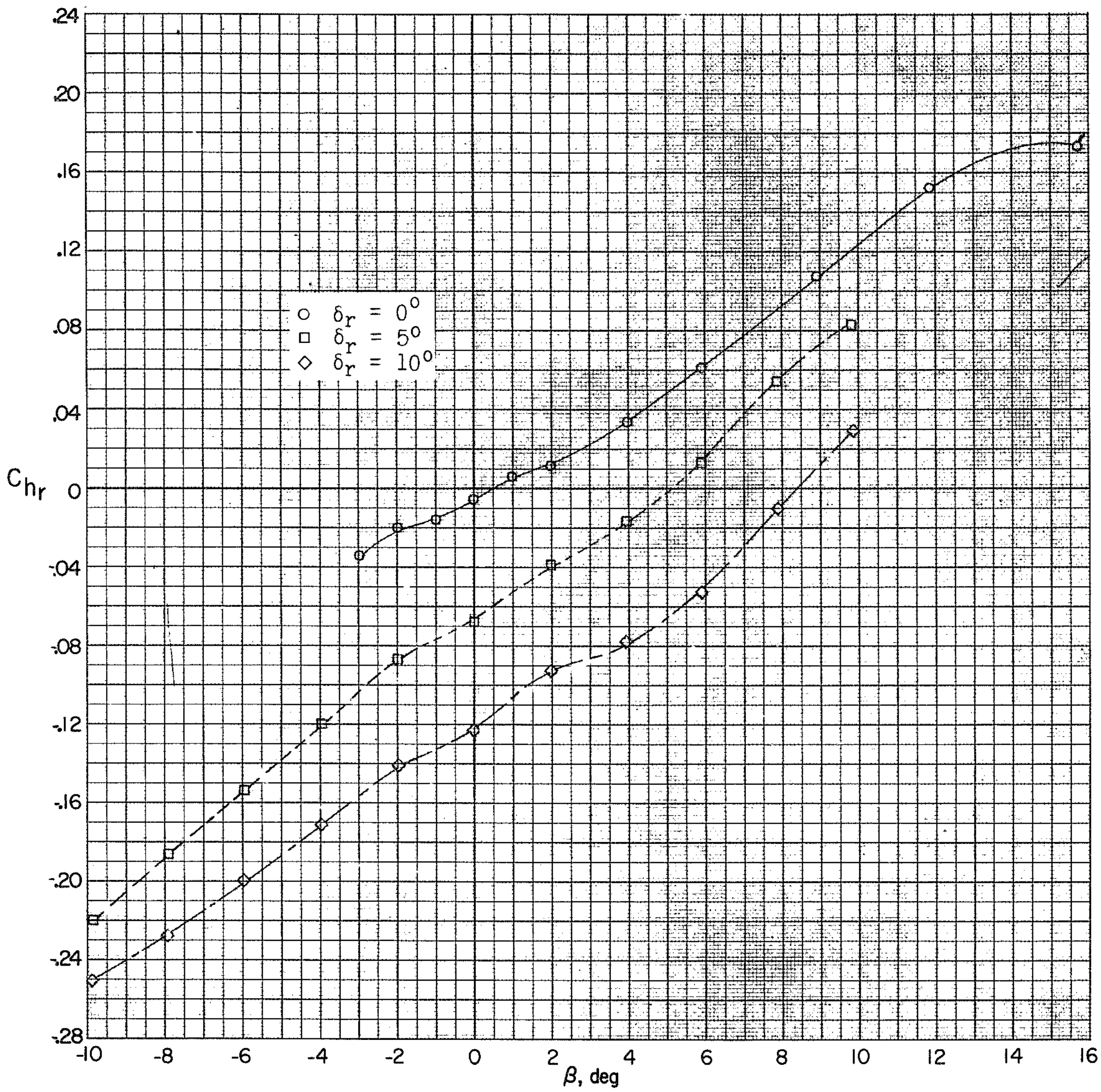

(b) $M = 1.57$; $\alpha = 6.7^o$.

Figure 21.- Continued.

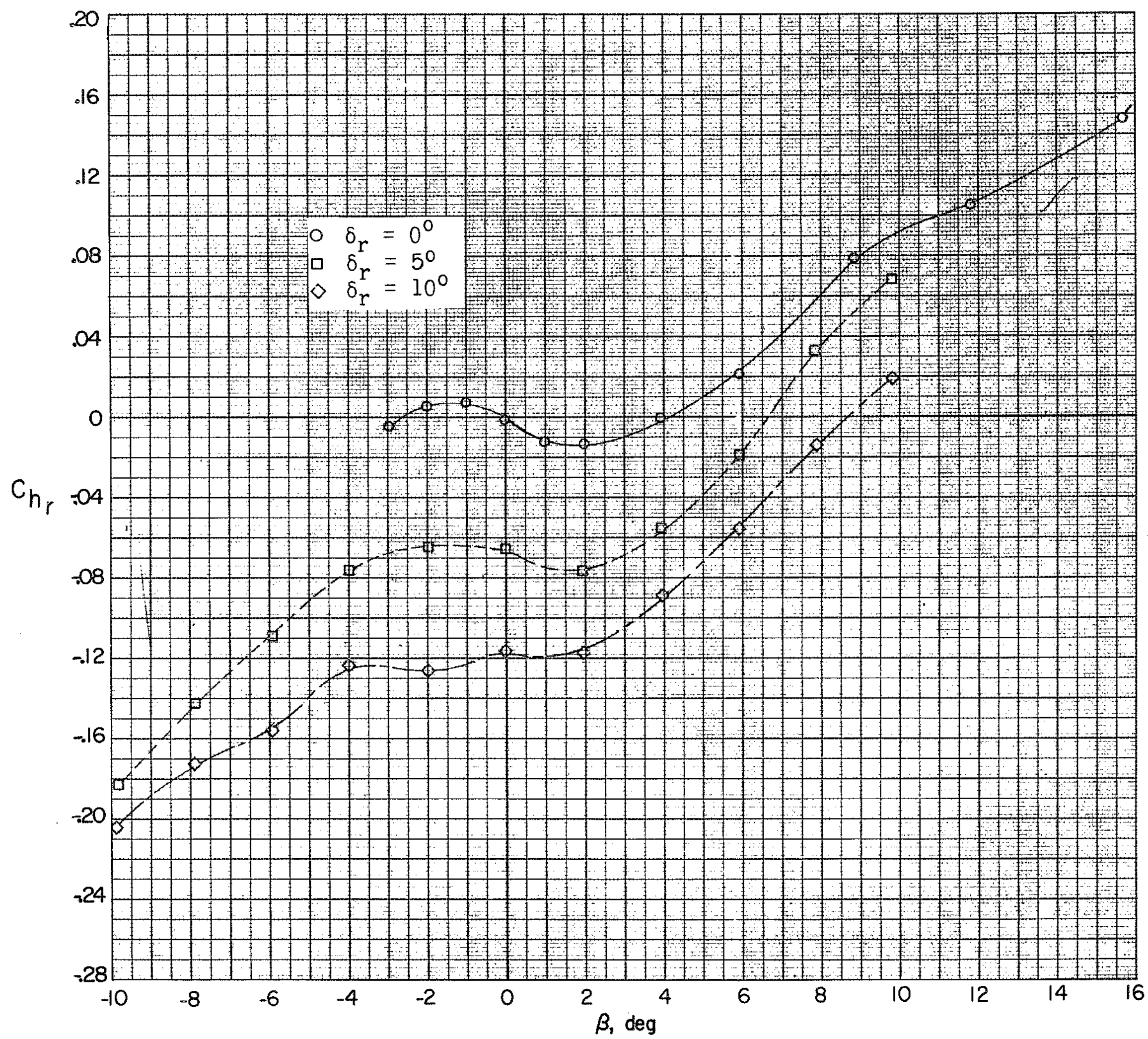

(c) M = 1.57; $\alpha = 17.4^o$.

Figure 21.- Continued.

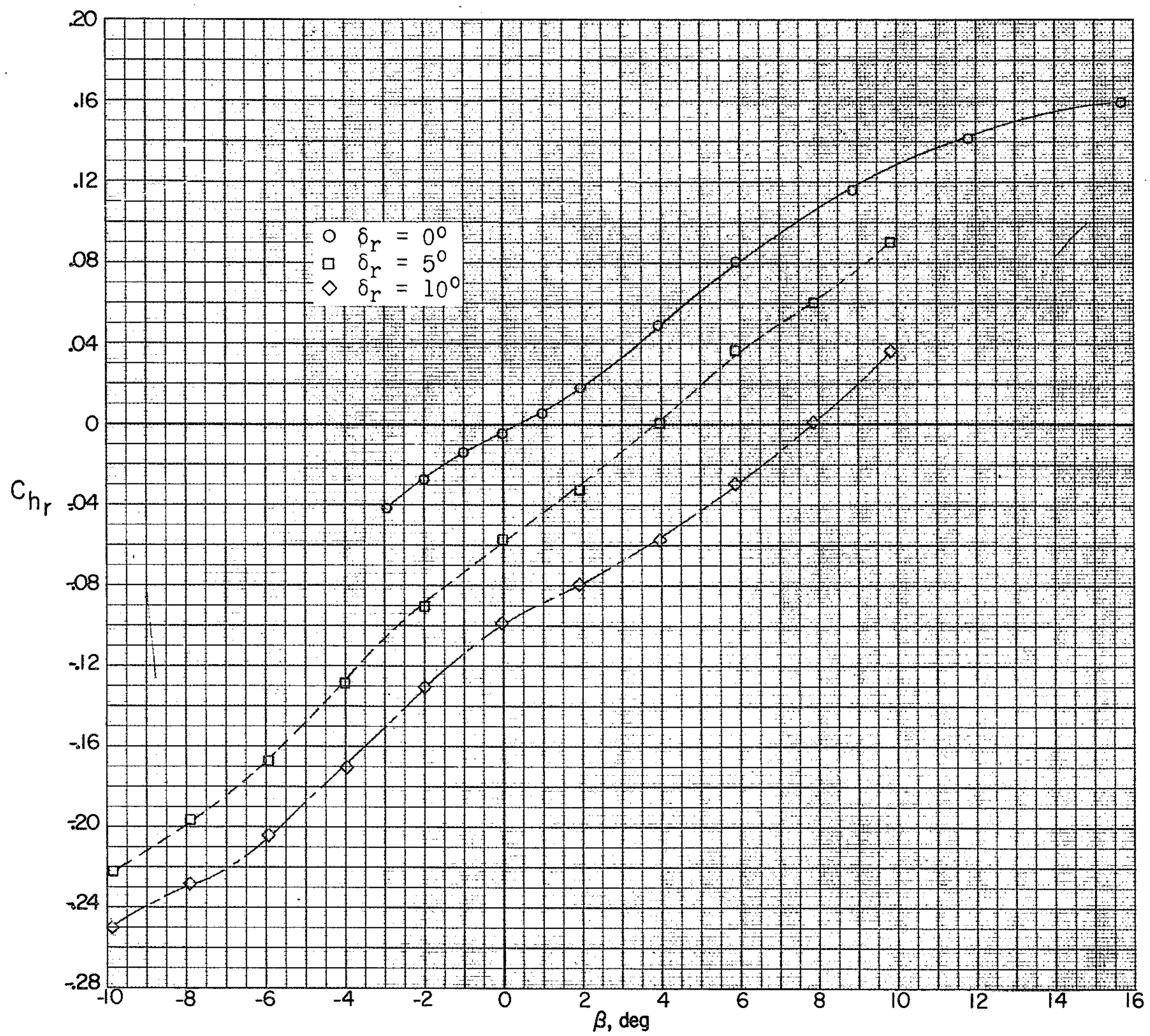

(d) $M = 1.87$; $\alpha = 0.4^\circ$.

Figure 21.- Continued.

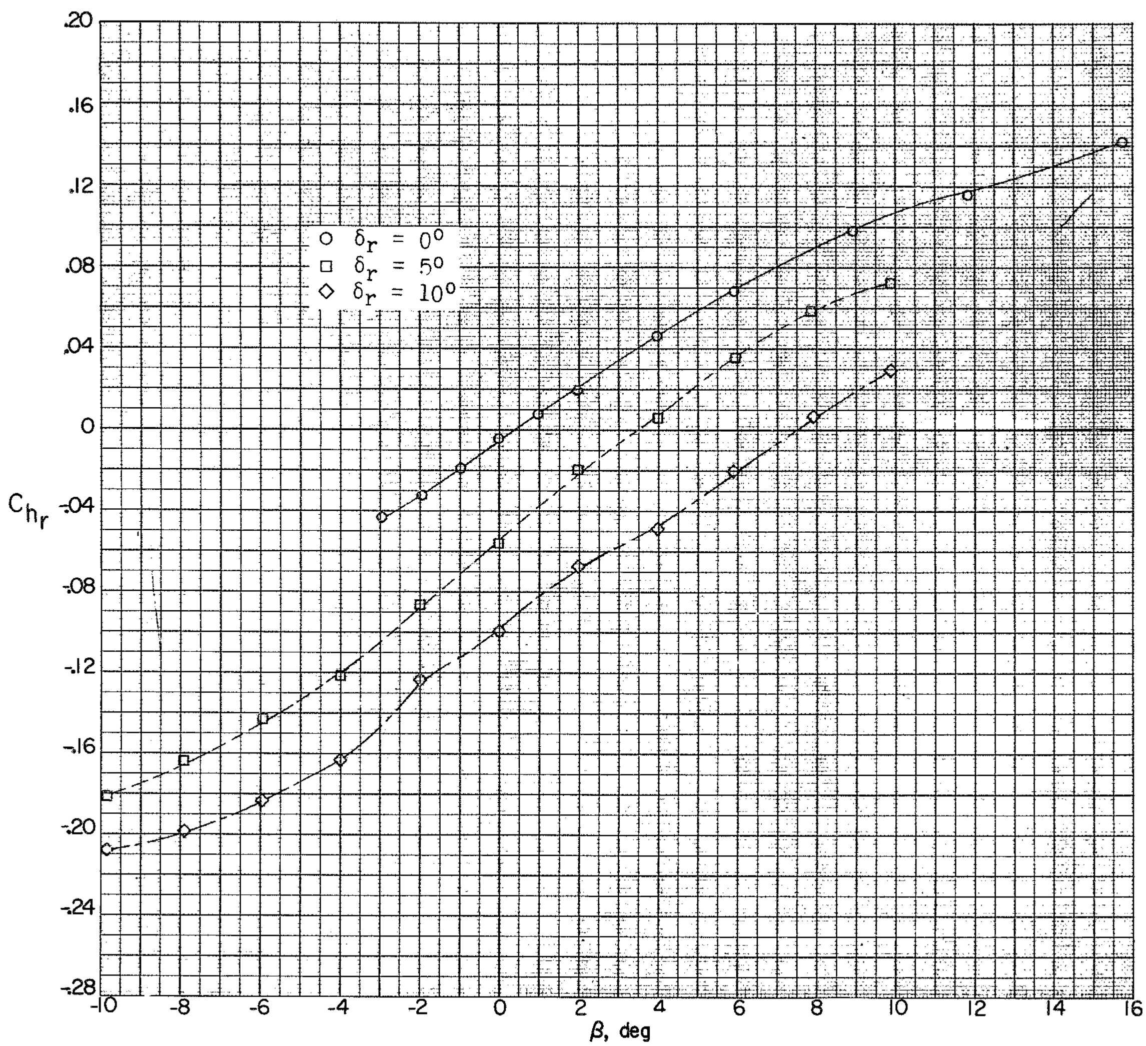

(e) $M = 1.87$; $\alpha = 6.6^\circ$.

Figure 21.- Continued.

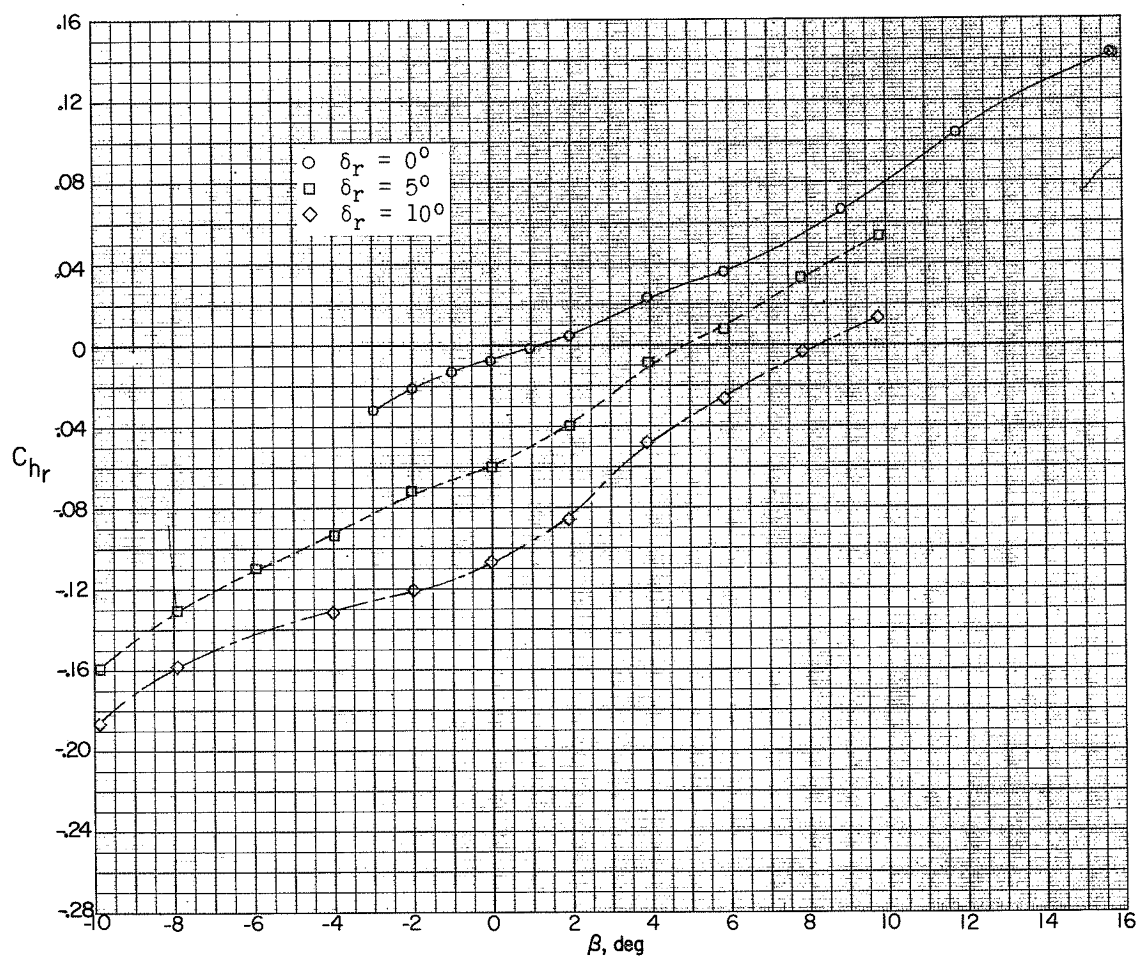

(f) $M = 1.87$; $\alpha = 17.1^\circ$.

Figure 21.- Continued.

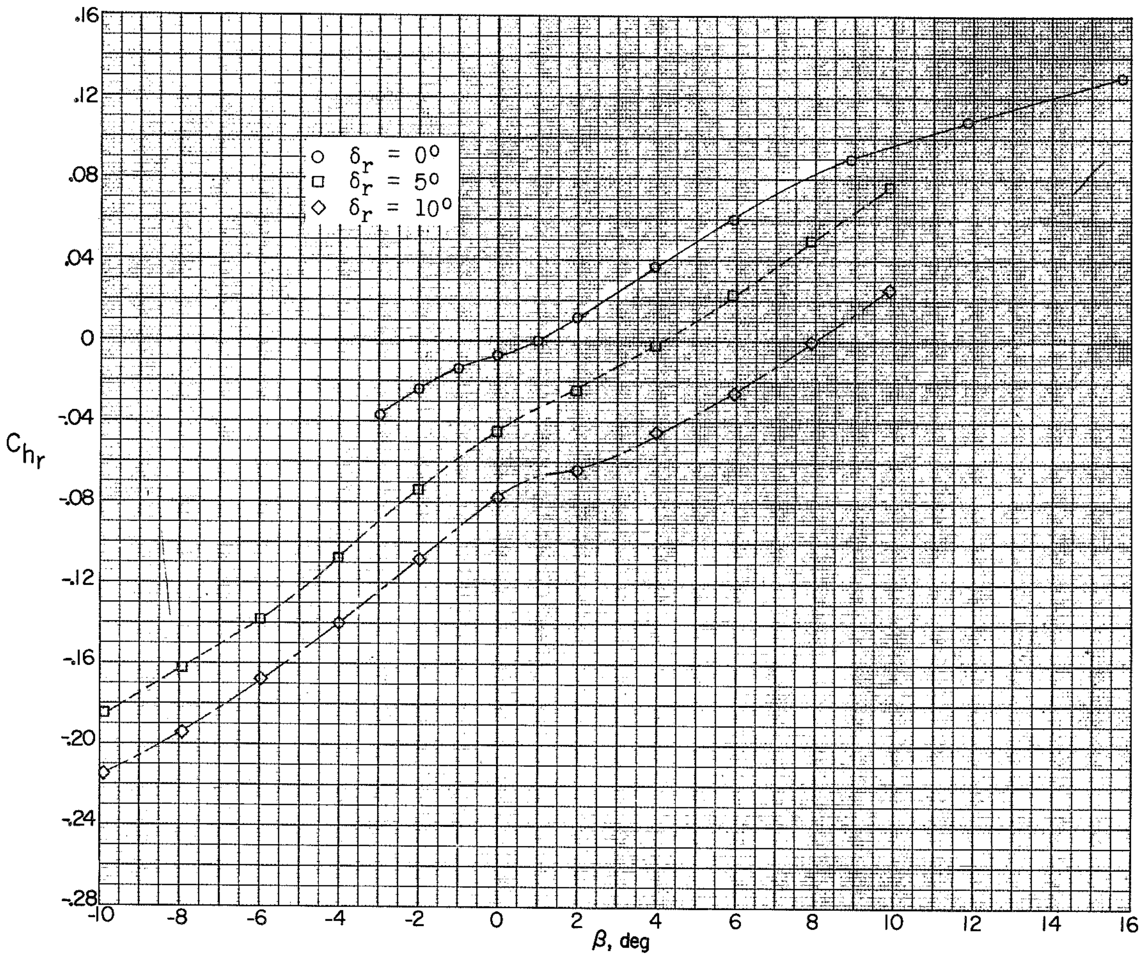

(g) $M = 2.16$; $\alpha = 0.4°$.

Figure 21.- Continued.

[redacted]

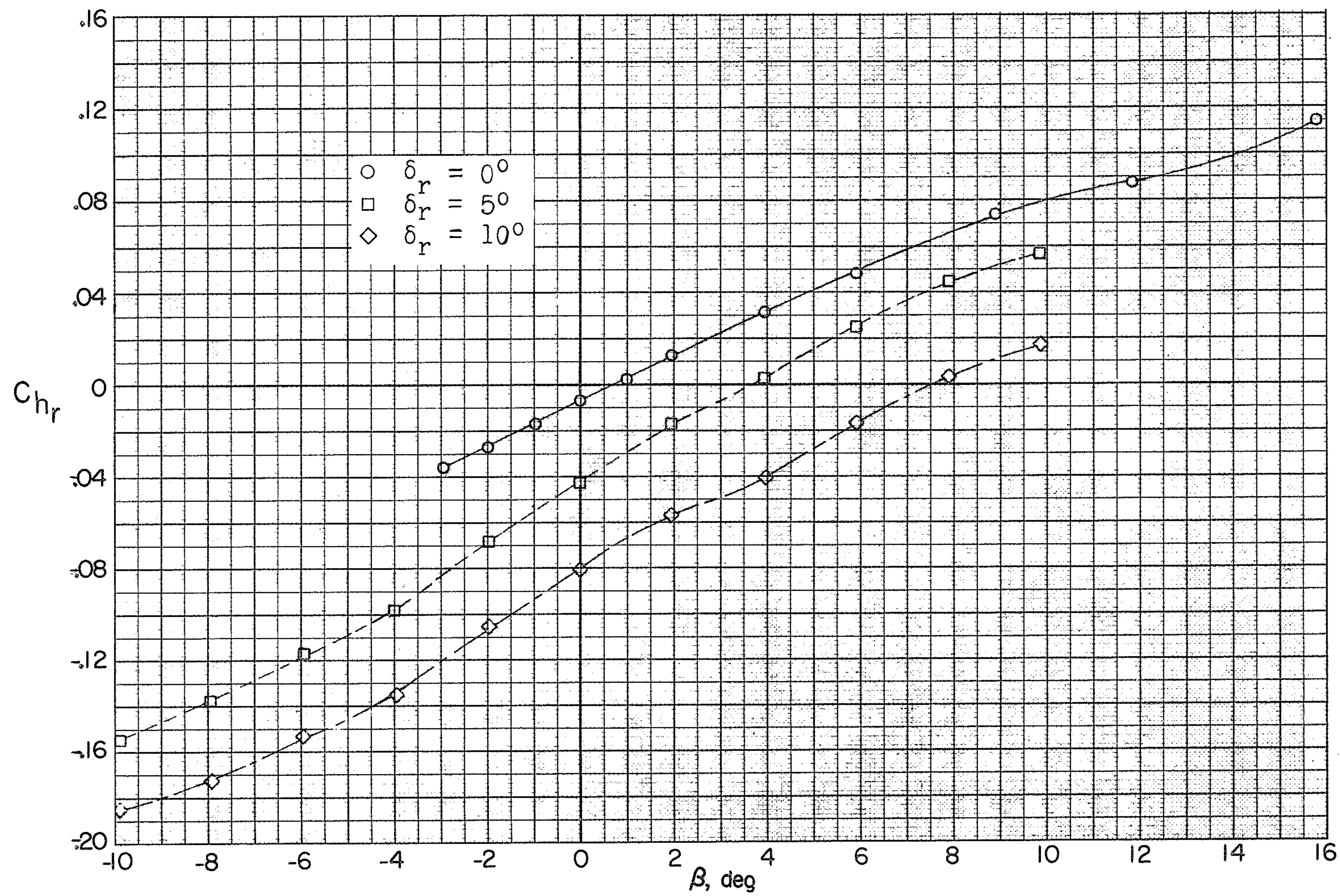

(h) $M = 2.16$; $\alpha = 6.5^{\circ}$.

Figure 21.- Continued.

[redacted]

[redacted]

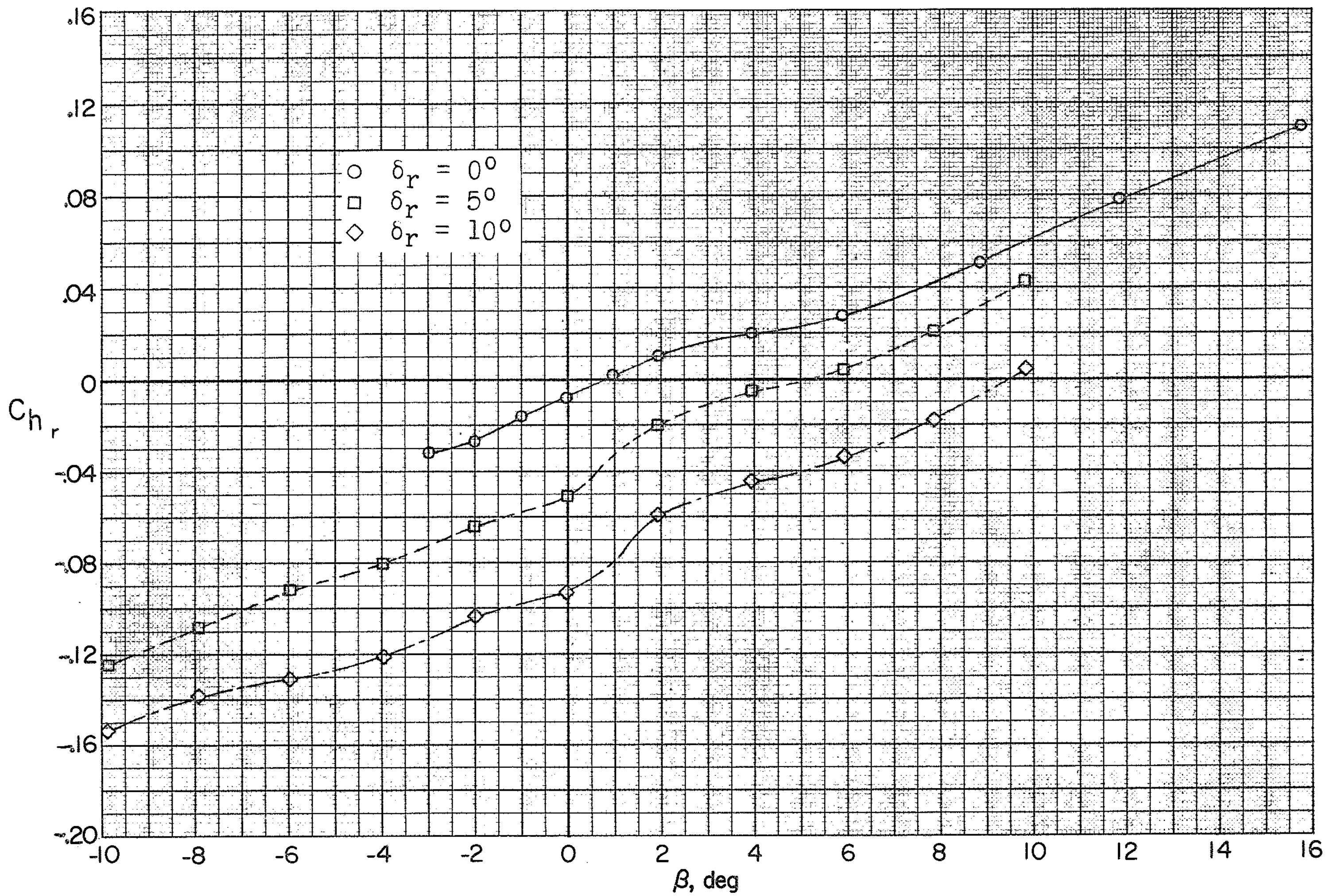

(i) $M = 2.16$; $\alpha = 16.9^\circ$.

Figure 21.- Concluded.

[redacted]

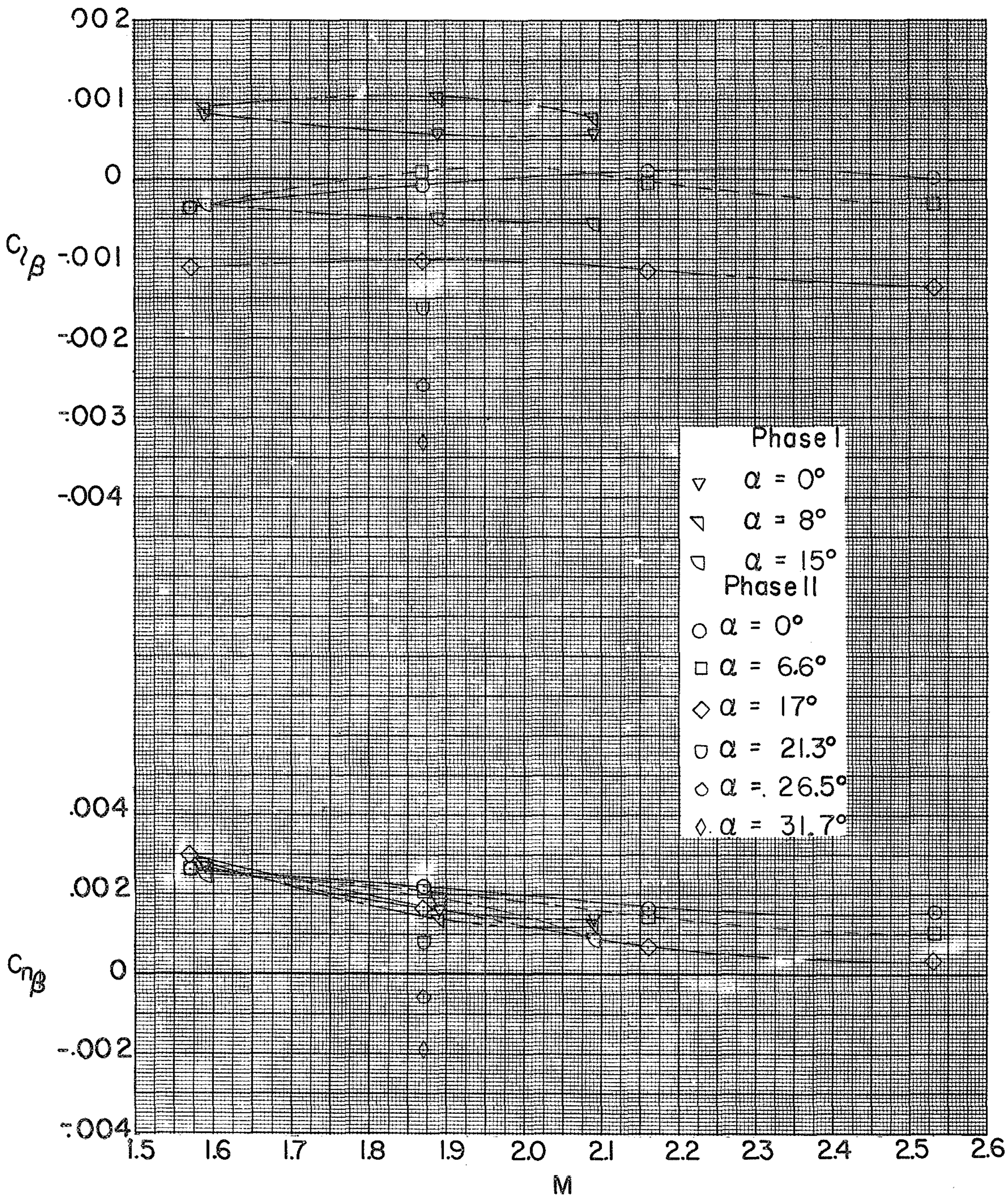

Figure 22.- Comparison of directional stability derivatives between results of phase I (ref. 1) and phase II tests.

INVESTIGATION OF DRAG AND STATIC LONGITUDINAL AND LATERAL STABILITY AND CONTROL CHARACTERISTICS OF 1/20-SCALE MODEL OF McDONNELL F4H-1 AIRPLANE AT MACH NUMBERS OF 1.57, 1.87, 2.16, AND 2.53

PHASE II MODEL

TED NO. NACA AD 3115

By Melvin M. Carmel and Kenneth L. Turner

ABSTRACT

The second phase in a series of investigations of the drag and static longitudinal and lateral stability and control characteristics of a 1/20-scale model of the McDonnell F4H-1 airplane at Mach numbers of 1.57, 1.87, 2.16, and 2.53 has been conducted in the Langley Unitary Plan wind tunnel. The model had a wing with a 45° sweepback of the quarter-chord line, aspect ratio of 2.821, a taper ratio of 0.167. The model was modified to include a wing tip dihedral of 12°, a larger vertical fin and rudder, and a revised duct. This is a data report with only minimum analysis.

INDEX HEADINGS

Stability, Longitudinal - Static	1.8.1.1.1
Stability, Lateral - Static	1.8.1.1.2
Stability, Directional - Static	1.8.1.1.3
Control, Longitudinal	1.8.2.1
Control, Directional	1.8.2.3